Titre: Title:	Controlling Morphology and Resistivity in Multiphase Polymer Blends with Poly(ether-b-amide)
Auteur: Author:	Jun Wang
Date:	2016
Type:	Mémoire ou thèse / Dissertation or Thesis
Référence: Citation:	Wang, J. (2016). Controlling Morphology and Resistivity in Multiphase Polymer Blends with Poly(ether-b-amide) [Thèse de doctorat, École Polytechnique de Montréal]. PolyPublie. https://publications.polymtl.ca/2067/

UNIVERSITÉ DE MONTRÉAL

CONTROLLING MORPHOLOGY AND RESISTIVITY IN MULTIPHASE POLYMER BLENDS WITH POLY(ETHER-B-AMIDE)

JUN WANG

DÉPARTEMENT DE GÉNIE CHIMIQUE

ÉCOLE POLYTECHNIQUE DE MONTRÉAL

THÈSE PRÉSENTÉE EN VUE DE L'OBTENTION

DU DIPLÔME DE PHILOSOPHIAE DOCTOR

(GÉNIE CHIMIQUE)

MARS 2016

UNIVERSITÉ DE MONTRÉAL

ÉCOLE POLYTECHNIQUE DE MONTRÉAL

Cette thèse initulée:

CONTROLLING MORPHOLOGY AND RESISTIVITY IN MULTIPHASE POLYMER BLENDS WITH POLY(ETHER-B-AMIDE)

présentée par : WANG Jun

en vue de l'obtention du diplôme de : Philosophiae Doctor

a été dûment acceptée par le jury d'examen constitué de :

M. TAVARES Jason-Robert, Ph. D., président

M. FAVIS Basil, Ph. D., membre et directeur de recherche

Mme HEUZEY Marie-Claude, Ph. D., membre

Mme DEMARQUETTE Nicole Raymonde, Ph. D, membre

DEDICATION

To my families

ACKNOWLEDGEMENTS

First of all, I would like to thank my research supervisor, Prof. Basil D. Favis, for his continuous support, guidance, and understanding both in work and in life. He is a supervisor who not only focuses on research but also helps me to develop in all aspects to become a qualified independent researcher. His door has always remained open whenever I have a question and whatever the question is. Working with him is one of the most important periods in my life.

I would like to thank the persons from our industrial collaborator Arkema: Dr. Alejandra Reyna-Valencia, Dr. Eric Gamache, Dr. Frederic Malet, Ms. Laure Berdin Sguerra, Dr. Richard Chaigneau, Dr. Damien Rauline, Dr. Yves Deyrail and Dr. Quentin Pineau. They helped me on many aspects of the project and their hospitality during my visit to Arkema is also acknowledged.

I want to give my thanks to the current and previous members of our research group, Ebrahim, Ali, Vahid, Nima, Sepehr, Ata, Dr. Pierre Sarazin and Dr. Nick Virgilio, for their help and the useful discussions we had.

I would like to thank Prof. Pierre Carreau for teaching me the "well-known" Transport Phenomena course. It forced me to sit down and read a textbook again and again – something that I had not done for years.

Thanks to Prof. Daniel Therriault, Michael D. Buschmann and Frederic Sirois for giving me access to their lab facilities.

I also want to thank the current and previous technicians, research assistants and administrative staff in the Department of Chemical Engineering, in particular, Melina Hamdine, Guillaume Lessard, Claire Cerclé, Gino Robin, Martine Lamarche, Ricardo Villanueva Vazquez, Robert Delisle and Julie Tremblay, for their help during my PhD study. Thanks to Sylvie St-Amour from FPInnovations for her assistance on mercury intrusion porosimetry.

Finally and most importantly, I want to give my thanks to my families. I want to thank my parents and my two older sisters for having always been so supportive and allowing me to do whatever I want to; I owe them everything. I want to thank my little boy Bryan for the happiness he has brought to me. Thanks to my mother-in-law for helping us to take care of Bryan. Lastly, I want to give my special thanks to my lovely wife, Xiaoyan; for over ten years, she has always been there for me. I'm so lucky to have her accompany in my life.

RÉSUMÉ

Mélanger des polymères conducteurs avec des polymères conventionnels est une méthode efficace pour produire de nouveaux matériaux dotés de propriétés électriques spécifiques. Comparés à des mélanges binaires, des systèmes de mélanges de polymères ternaires et quaternaires doivent présenter un seuil de percolation bien plus bas si un des composants est encapsulé par d'autres phases continue/percolée, avec un effet plus marqué si localisé à une interface continue/percolée. Cependant, la majorité des travaux publiés s'est concentré à l'examen du cas où la phase conductrice est située au cœur du système en raison de tensions interfaciales intrinsèques élevées avec d'autres polymères. Assembler un composant polymère conducteur à une interface continue directement par l'intermédiaire de mélanges à l'état fondu a rarement été rapporté dans la littérature. Par ailleurs, des études sur le développement de la morphologie d'une phase intermédiaire partiellement ou complètement mouillée dans des systèmes ternaires et quaternaires sont encore très limitées.

Dans cette thèse, des mélanges de polymères destinés à des applications antistatiques avec un copolymère PEBA conducteur ionique (composé de blocs alternés PEO et PA) au sein de systèmes binaires, ternaires et quaternaires ont été étudiés.

Dans un premier temps, deux mélanges binaires, LDPE/PEBA et PS/PEBA, avec des tensions interfaciales considérablement distinctes ont été préparés. La tension interfaciale du système initial a été évaluée à 8.0 mN/m, et le développement de la morphologie du PEBA pour ce système suit une coalescence de deux gouttes observée typiquement au sein de systèmes de tension interfaciale élevée. Le second système possède, de façon inattendue, une tension interfaciale de 1.6 mN/m, vraisemblablement en raison de la présence de liaisons hydrogène-π entre le PS et le bloc PEO. Une miscibilité partielle entre le PS et le PEBA (bloc PEO) est aussi confirmée par le déplacement de Tg pour le PS dans les mélanges. Bien qu'une continuité plus élevée soit observée à des fractions volumiques plus faibles en PS/PEBA que en LDPE/PEBA, la résistivité surfacique du PS/PEBA est plus élevée que celle du LDPE/PEBA sur une large plage de compositions. Ce résultat a été attribué à la miscibilité partielle et/ou la constriction importante au sein de la morphologie d'instabilité capillaire gelée lorsque le PEBA est mélangé avec le PS, ce qui influence le transfert de charge au sein de la phase PEBA. Un modèle conceptuel du

transport de charge dans le copolymère PEBA a également été proposé basé sur le phénomène de migration des protons dans les domaines PEO.

Dans la seconde partie de ce travail, un polymère conducteur ionique (PEBA) a été directement assemblé à l'interface continue de deux autres polymères grâce au procédé de mélangeage à l'état fondu. Deux mélanges ternaires de LDPE/PEBA/PET et LDPE/PEBA/PVDF, ont été préparés démontrant respectivement un mouillage partiel et un mouillage complet. Une transition novatrice de morphologie de mouillage partiel à mouillage complet a été identifiée au sein du système LDPE/PEBA/PET. Une analyse thermodynamique indique que le LDPE/PEBA/PET est un système faiblement partiellement mouillé, et le phénomène de transition a été attribué à l'effet de coalescence dominant par rapport au démouillage avec une concentration en augmentation de PEBA. Dans le cas d'un système LDPE/PEBA/PVDF complètement mouillé, de fines couches intactes de PEBA (~ 100 nm) ont été observées pour des concentrations de PEBA aussi faibles que 3%. Il apparaît clairement qu'une concentration minimale est requise afin de former une interface mouillée, et que cette concentration dépend de la valeur du coefficient d'étalement. L'auto-assemblage de PEBA à l'interface continue réduit considérablement le seuil de percolation dans des mélanges ternaires par rapport à des mélanges binaires. Dans le cas d'application antistatiques requérant une résistivité surfacique plus faible que 1013 Ω/sq, 20% de PEBA est nécessaire dans des mélange binaires conventionnels ; cette valeur se réduit à 10% pour les mélanges ternaires LDPE/PEBA/PET, et jusqu'à 1% pour le système LDPE/PEBA/PVDF.

La troisième partie de ce projet se consacre au contrôle de la localisation du PEBA dans des mélanges de polymères polyphasés à structure hiérarchisée. Il a été montré que lorsque des polymères conducteurs sont mélangés avec des polyoléfines et/ou du PS dans des mélanges ternaires, ils ont tendance à être situés au cœur en raison des tensions interfaciales élevées avec ces polymères. Néanmoins, mélanger des polymères conducteurs avec des polymères de grande consommation tels que les polyoléfines et le PS peut présenter des gains de coûts conséquents. Pour cette raison, un mélange ternaire de LDPE/PS/PEBA avec PEBA comme phase cœur a été choisi comme premier cas d'étude de cette partie du travail. Afin de contrôler la localisation du PEBA au sein de systèmes multiphasiques possédant une concentration élevée en LDPE/PS (70–90%), un quatrième composant ou un modificateur interfacial a été ajouté. Dans les deux cas, le PEBA a été localisé avec succès sur une interface continue, et a formé des structures percolatées

dans les systèmes ternaires et quaternaires hiérarchiquement ordonnés. Ceci a permis une réduction significative de la résistivité surfacique d'un facteur de l'ordre de 2 à 4 en comparaison avec les mélanges ternaires initiaux de LDPE/PS/PEBA où le PEBA était situé au cœur.

Finalement, comme présenté dans l'annexe, afin de démontrer une approche généralisée aux structures hiérarchiques dans les mélanges ternaires, une nouvelle stratégie a été développée permettant de générer des polymères hiérarchiquement poreux où la taille des pores est contrôlée grâce à un système de mélange ternaire A/B/C-B-C.

ABSTRACT

Blending conductive polymers with conventional polymers has been an effective approach to produce new materials with tailored electrical properties. Compared to binary blends, ternary and quaternary polymer blend systems are expected to have a much lower percolation threshold if a component is encapsulated by other continuous/percolated phases, with a more dramatic influence when it is located at a continuous/percolated interface. However, almost all the published work has examined the case where the conductive phase is situated in the core of the system owing to its inherent high interfacial tensions with other polymers. Assembling a conductive polymeric component at a continuous interface directly through melt blending has rarely been reported. Also, studies on the morphology development of a partially wet or completely wet intermediate phase in ternary and quaternary systems are still very limited.

In this dissertation, polymer blends destined for antistatic applications with an ionically conductive PEBA copolymer (comprised of alternating PEO and PA blocks) in binary, ternary and quaternary systems were studied. In the first part, two binary blends, LDPE/PEBA and PS/PEBA, with significantly different interfacial tensions were prepared. The interfacial tension for the former system was determined to be 8.0 mN/m and the morphology development for PEBA in this system follows a droplet-droplet coalescence mechanism typically observed in high interfacial tension systems. The latter system possesses, unexpectedly, a much lower interfacial tension of 1.6 mN/m, possibly owing to the presence of π-hydrogen bonding between PS and the PEO block. Partial miscibility between PS and PEBA (the PEO block) is also confirmed by the shift of Tg for PS in the blends. Although a higher continuity is observed at lower volume fractions in PS/PEBA than in LDPE/PEBA, the surface resistivity for PS/PEBA is surprisingly higher than that of LDPE/PEBA over a wide range of compositions. This result was attributed to the partial miscibility and/or the significant constriction in the frozen capillary instability morphology when PEBA is blended with PS, which influences the charge transfer in the PEBA phase. A conceptual model for charge transport in the PEBA copolymer based on the migration of protons in the PEO domains is also proposed.

In the second part of this work, we assembled an ionically conductive polymer (PEBA) at the continuous interface of two other polymers directly through melt blending. Two ternary blends of LDPE/PEBA/PET and LDPE/PEBA/PVDF were prepared which demonstrate partial wetting and

complete wetting respectively. A novel morphology transition from partial wetting to complete wetting was identified in the LDPE/PEBA/PET system. Thermodynamic analysis indicates that LDPE/PEBA/PET is a weak partial wetting system and the transition phenomenon was attributed to the dominant effect of coalescence over dewetting with increasing PEBA concentration. In the case of the completely wet LDPE/PEBA/PVDF system, thin intact PEBA layers (~ 100 nm) were observed at PEBA concentrations as low as 3%. It appears clear that a minimum concentration is required to form a completely wet interface and that this concentration depends on the value of the spreading coefficient. The self-assembling of PEBA at the continuous interface dramatically reduces its percolation threshold in the ternary blends as compared to binary blends. For antistatic applications requiring a surface resistivity lower than 10^{13} Ω/sq, 20% of PEBA is needed in the conventional binary blends; the value is reduced to 10% for LDPE/PEBA/PET, and to as low as 1% for the LDPE/PEBA/PVDF system. The third part of the project focuses on controlling the localization of PEBA in hierarchically ordered multiphase polymer blends. It has been shown that when conductive polymers are blended with polyolefins and/or PS in ternary blends, they tend to be located in the core due to its high interfacial tensions with these polymers. Nevertheless, blending conductive polymers with commodity polymers such as polyolefins and PS can present significant potential cost advantages. Thus, we started this part of the work with a ternary blend of LDPE/PS/PEBA where PEBA is the core phase. In order to control the localization of PEBA in the multiphase systems with high LDPE/PS content (70–90%), either a fourth component or an interfacial modifier was added. In both cases, PEBA was successfully localized to a continuous interface and formed percolated structures in the hierarchically ordered ternary and quaternary systems. This led to a significant reduction of 2–4 orders of magnitude in surface resistivity as compared to the initial ternary blends of LDPE/PS/PEBA where PEBA was located in the core.

Finally, as shown in the Appendix, in order to demonstrate a generalized approach to hierarchical structures in ternary blends, we developed a new strategy to generate hierarchically porous polymers with controllable pore size through a ternary A/B/C-B-C blend system. PLA/HDPE/SEBS was used as a model system.

TABLE OF CONTENTS

DEDICATION iii

ACKNOWLEDGEMENTS iv

ABSTRACT viii

TABLE OF CONTENTS x

LIST OF TABLES xv

LIST OF FIGURES xvi

LIST OF SYMBOLS AND ABBREVIATIONS xxiv

LIST OF APPENDICES xxvii

CHAPTER 1 INTRODUCTION 1

CHAPTER 2 LITERATURE REVIEW AND OBJECTIVES 4

2.1 Conductive Polymer Systems 4

2.1.1 Conductive Polymer Composites 4

2.1.2 Conjugated Polymers 5

2.1.3 Ionically Conductive Polymers 6

2.1.4 Redox Polymers 7

2.2 Conductive Polymer Systems for Antistatic Applications 8

2.2.1 Static Electricity 8

2.2.2 Classification of Antistatic Additives 10

2.3 Poly(ether-b-amide) (PEBA) Copolymers 13

2.3.1 Chemical Structure and Synthesis 13

2.3.2 Solid-state Structures of PEBA 15

2.4 Ion Transport in Ionically Conductive Polymers 16

2.4.1 Ion Transport in Block Copolymer Electrolytes 16

2.4.2 Charge Dissipation Mechanism in PEBA Copolymers....18
2.5 Control of Morphology in Immiscible Polymer Blends....19
2.5.1 Basic Thermodynamics in Polymer Blends....19
2.5.2 Morphologies of Immiscible Binary Polymer Blends....20
2.5.2.1 Morphology Development in Binary Polymer Blends....21
2.5.2.2 Factors Controlling the Morphology Development....24
2.5.3 Morphologies of Multiphase Polymer Blend Systems....25
2.5.3.1 Models for Morphology Prediction in Multiphase Systems....25
2.5.3.2 Other Factors Affecting the Morphology in Multiphase Polymer Systems....31
2.5.3.3 Controlling Phase Localization in Multiphase Polymer Blends....32
2.6 Conductive Polymer Blends with Multiple Percolation....33
2.7 Conductive Polymer Composites: Controlling the Localization of the Fillers....35
2.8 Summary of Literature Review and Objectives....38
CHAPTER 3 ORGANIZATION OF ARTICLES....39
CHAPTER 4 ARTICLE 1: CONTINUITY, MORPHOLOGY AND SURFACE RESISTIVITY IN BINARY BLENDS OF POLY(ETHER-BLOCK-AMIDE) WITH POLYETHYLENE AND POLYSTYRENE....41
4.1 Abstract....41
4.2 Introduction....42
4.3 Materials and experimental....44
4.3.1 Materials....44
4.3.2 Rheology....45
4.3.3 Small angle X-ray scattering (SAXS)....45
4.3.4 Interfacial tension measurement....46
4.3.5 Differential scanning calorimetry (DSC)....46

4.3.6 Melt blending 47
4.3.7 Selective extraction 47
4.3.8 Continuity 47
4.3.9 Morphology and phase size 48
4.3.10 Surface resistivity preparation and measurement 48
4.4 Results and discussion 49
4.4.1 Rheological properties 49
4.4.2 Interfacial tension 51
4.4.3 Small-angle X-ray scattering (SAXS)/Solid state structure 51
4.4.4 Miscibility 53
4.4.5 Continuity and morphology 57
4.4.6 Surface resistivity and charge dissipation mechanism 63
4.5 Conclusion 68
4.6 Acknowledgment 69
4.7 References 69
CHAPTER 5 ARTICLE 2: ASSEMBLING CONDUCTIVE PEBA COPOLYMER AT THE CONTINUOUS INTERFACE IN TERNARY POLYMER SYSTEMS 74
5.1 Abstract 74
5.2 Introduction 75
5.3 Materials and experimental 78
5.3.1 Materials 78
5.3.2 Rheology 79
5.3.3 Interfacial tension measurement 79
5.3.4 Melt blending 80
5.3.5 Morphology characterization, image analysis and selective extraction 80

5.3.6 Resistivity measurement 81
5.4 Results and discussion 82
5.4.1 Rheology 82
5.4.2 Ternary blends 83
5.4.3 Transition from partial to complete wetting in LDPE/PEBA/PET 92
5.4.4 Minimum threshold concentration for complete wetting in LDPE/PEBA/PVDF 97
5.5 Conclusion 98
5.6 Acknowledgment 99
5.7 References 99
5.8 Supporting Information 102
5.8.1 Interface coverage 102
5.8.2 Volume resistivity of the blends 103
5.8.3 In-situ measurement of the Neumann angle for LDPE/PEBA/PET 104
5.8.4 References 105
CHAPTER 6 ARTICLE 3: CONTROLLING THE HIERARCHICAL STRUCTURING OF CONDUCTIVE PEBA IN TERNARY AND QUATERNARY BLENDS 106
6.1 Abstract 106
6.2 Introduction 107
6.3 Experimental 110
6.3.1 Materials 110
6.3.2 Interfacial tension measurement 110
6.3.3 Melt blending 111
6.3.4 Morphology characterization and image analysis 111
6.3.5 Selective extraction and continuity 112
6.3.6 Surface resistivity: preparation and measurement 112

6.4 Results and Discussion 113

6.4.1 Morphology of LDPE/PS/PEBA ternary blends 113

6.4.2 Structuring PEBA at the continuous interface in quaternary blends 115

6.4.3 Surface resistivity: ternary and quaternary blends 120

6.4.4 Structuring PEBA at the continuous interface of a ternary blend by interfacial modification 123

6.5 Conclusion 130

6.6 Acknowledgment 131

6.7 References 131

6.8 Supporting Information 135

6.8.1 Effect of formulation on morphology and surface resistivity 135

CHAPTER 7 GENERAL DISCUSSION 138

CHAPTER 8 CONCLUSION AND RECOMMENDATIONS 141

8.1 Conclusion 141

8.2 Recommendations for future work 142

BIBLIOGRAPHY 144

APPENDIX ARTICLE 4: HIERARCHICALLY POROUS POLYMERIC MATERIALS FROM TERNARY POLYMER BLENDS 155

LIST OF TABLES

Table 2.1: Commercially available PEBA copolymers and their composition (taken from Ref. [55]). 14

Table 4.1: Characteristics of the materials used 45

Table 4.2: Interfacial tension between different polymers 51

Table 4.3: Structural parameters for the PEBA copolymer 53

Table 5.1: Characteristics of the polymers used 79

Table 5.2: Interfacial tensions, spreading coefficients and predicted morphologies (PEBA is the minor phase) 83

Table 5.3: The distribution of PEBA and the interfacial area in the ternary blends 88

Table 6.1: Characteristics of the materials used* 110

Table 6.2: Interfacial tension and spreading coefficient for LDPE/PS/PEBA (200°C) 115

Table 6.3: Interfacial tensions and spreading coefficients in LDPE/PS/PEBA/PET (250°C) and LDPE/PS/PEBA/PVDF (200°C)* 116

Table 6.4: Interfacial tensions and spreading coefficients of the EAM modified LDPE/PS/PEBA (200°C) 124

Table 7.1: Different wetting behaviours at different interfaces in the ternary PE/PP/PS blend .. 139

Table A1: Interfacial tensions between different polymers at 200°C (PE/SEBS at 195°C) 159

Table A2: Continuity of the ternary blends with different volume fractions. 173

LIST OF FIGURES

Figure 1.1: Examples of advanced structures developed in multi-phase polymer blends. a) tri-continuous structures in PE/PS/PMMA ternary blends (PMMA extracted) (taken from Ref. [10]); b) PS forms completely wet layer at the interface of HDPE/PMMA with a high continuity (about 70%) achieved at 3% (taken from Ref. [11]); c) PS self-assembles into close-packed droplet array at the PE/PP interface (taken from Ref. [28]); d-e) tune the morphology of PS at the interface of PA/PC from partially wet droplets to completely wet layers by adding PS-g-MA (taken from Ref. [13]); f) confine CNTs within thin EMAA layers formed at the PP/PA interface to reduce the percolation threshold (taken from Ref. [23]). 3

Figure 2.1: Development of conductive pathways in polymer composite systems as a function of filler concentration (taken from Ref. [34]). 4

Figure 2.2: Structures and conductivities of some conjugated conductive polymers (taken from Ref. [33]). 6

Figure 2.3: Schematic of conductive mechanism in polyactylene with an oxidative dopant (taken from Ref. [37]). 6

Figure 2.4: Ion transport in PEO: a) Lateral migration of the cation through C-O bond rotation along the AB line; b) the transfer of the cation between PEO chain segments by oxygen ligand replacement (taken from Ref. [32]). 7

Figure 2.5: Schematic for the measurement of the surface resistivity. U and I are the applied voltage and measured current; g, D_0, D_1 *and* D_2 are the geometry parameters of the measuring setup. 9

Figure 2.6: Charge dissipation mechanism of migrating antistats (adapted from Ref. [1]). 11

Figure 2.7: Schematic of dissipative networks developed in the IDP/host polymer binary blend (taken from Ref. [1]). 12

Figure 2.8: Schematic of the general chemical structure of a PEBA copolymer (adapted from [56]). 13

Figure 2.9: Synthesis of ester-linked PEBA copolymers through the two-step thermal polymerization (taken from Ref. [55]). 15

Figure 2.10: a) Schematic representation of PEBA solid-state structures; b) TEM image of a poly(ether-b-amide) copolymer with a polyamide/polyether weight ratio of 23/77 (taken from Ref. [5, 55]). 15

Figure 2.11: Theoretical morphology factor f_{ideal} of polyelectrolytes with different morphologies. The blue region represents the conducting phase (taken from Ref. [62]). 17

Figure 2.12: Schematic representation of ion transport in the PS-PEO-PS electrolytes (taken from Ref. [45]). 18

Figure 2.13: Electrostatic dissipation mechanism via hydrogen-bondings between PEO/water and amide/water. The partial ionization of water molecules generates protons for charge dissipation (taken from Ref. [8]). 19

Figure 2.14: Three typical states of miscibility in a binary system: (A) completely immiscible; (B) completely miscible; and (C) partially miscible (taken from Ref. [67]).....20

Figure 2.15: Schematic presentation of morphology development in binary polymer blends (taken from Ref. [10]). 21

Figure 2.16: Schematic representation of flow-induced coalescence of two droplets in a Newtonian system. The two droplets are brought close to each other and rotate in the flow filed; the film in-between thins and finally raptures; the two droplets contact and emerge into one (taken from Ref. [77]). 23

Figure 2.17: Mechanism for morphology development in systems of low interfacial tension (a) and high interfacial tension (b) (taken from Ref.[74]). 24

Figure 2.18: Possible morphologies in a ternary blend of A/B/C as predicted by Harkins' spreading theory (A is the minor phase). (a)-(c): complete wetting, one phase fully separate the rest two; (d) partial wetting, three phase contact (taken from [28]). 26

Figure 2.19: Three-dimensional schematic representation of the multiple percolated structures in the ternary HDPE/PS/PMMA system: thin PS layer is at the HDPE/PMMA interface (taken from Ref. [11]). 27

Figure 2.20: (a) Different morphology evolution patterns in PA6/SEBS/PC and PA6/PS/PC after adding SEBS-MA and PS-MA respectively (which gradually replace SEBS and PS in the two systems) as interfacial modifiers (taken from Ref. [13]). (b) Morphologies of the annealed HDPE/PS/PP and PP/PS/PCL blends (taken from Ref. [93]). PS droplets appear more spherical in the former and more extended along the PP/PCL interface in the latter. ..28

Figure 2.21: (a) Four sets of spreading coefficients of the quaternary HDPE/PP/PS/PMMA blend. (b) AFM image of the HDPE/PP/PS/PMMA (45/45/5/5) blend after 30 min of annealing; the lines of three phase contact for HDPE/PS/PP and PP/PS/PMMA are indicated by arrows (taken from Ref. [94]). (c) TEM image of PBT/PS/SAN/PC (taken from Ref. [89]). 29

Figure 2.22: Three possible morphologies of a ternary system with a matrix A and two dispersed phases B and C (taken from Ref. [95]). B+C: phase B and phase C are separated by the matrix A; B/C: phase C is encapsulated by phase B in the matrix A; C/B: phase B is encapsulated by phase C in the matrix A. 31

Figure 2.23: Effect of molecular weight on the morphology in ternary HDPE/PS/PMMA blends. (a) and (b): PMMA is encapsulated by PS (PMMA was extracted); (c) PS is engulfed by PMMA (PS was extracted) (taken from Ref. [91]). 32

Figure 2.24: Morphology of the ternary blend of HDPE/PP/PS (70/20/10): (a) without SEB; (b) with 1% SEB. Polymer phases: A–HDPE, B–PP, and C–PS (taken from Ref. [95]). 33

Figure 2.25: The localization of solid particles in polymer blends predicted by Young's Equation. (a): within Phase 2 when $\omega > 1$; (b) at the interface when $-1 < \omega < 1$; (c) within Phase 1 when $\omega < -1$ (taken from Ref. [106]). 35

Figure 2.26: Effect of selective localization on the resistivity in the PE/PS/CB (45/55/X) blends as compared to the PE/CB blends (left image): PE/CB (◊); CB in PE phase in the PE/PS/CB system (□); CB at the interface of the PE/PS in PE/PS/CB system (○). Optical micrograph of PE/PS/CB (45/55/1) where CB is confined at the PE/PS interface (right image) (taken from Ref. [18]). 36

Figure 2.27: Schematic representation of confining CNT at the interface by a completely wet A/B/C system. B forms a thin layer at the percolated/continuous A/C interface. CNT has the

highest affinity with the B phase among the three components in the ternary blend (taken from [22]) 37

Figure 4.1: (a) Complex viscosity and (b) storage modulus (filled symbols)/loss modulus (open symbols) of the raw materials. 50

Figure 4.2: SAXS intensity as a function of the magnitude of the scattering vector *q*. The two arrows indicate the two peaks detected. 52

Figure 4.3: (a) The glass transition temperatures of PS and PEBA in the PS/PEBA blends; (b) crystallization behaviour of PEBA, PS and the PS/PEB blends during cooling. Dashed line indicates Tg of PS 56

Figure 4.4: Continuity of PEBA in LDPE/PEBA and PS/PEBA blends. 58

Figure 4.5: Morphology of the LDPE/PEBA and PS/PEBA blends with different volume fractions. LDPE/PEBA: (a) 90/10; (b) 80/20; (c) 70/30. PS/PEBA: (d) 90/10; (e) 80/20; (f) 70/30. PEBA was extracted. Circles indicate signs of connections between the PEBA domains. 59

Figure 4.6: Morphology of the PEBA phase in the PS/PEBA and LDPE/PEBA blends with different compositions after LDPE and PS are selectively dissolved. 61

Figure 4.7: PEBA phase size in different blends obtained from IA (PEBA volume fraction ≤ 20%) and MIP (PEBA volume fraction > 20%). The dashed line for LDPE/PEBA system indicates the approximate concentration limit for droplets (left side) and fibers (right side). For PS/PEBA the phase size indicates a fiber diameter at all concentrations. 62

Figure 4.8: Schematic illustration of continuity development by frozen capillary instability in PS/PEBA up to 10% concentration. 63

Figure 4.9: Surface resistivity in the LDPE/PEBA and PS/PEBA blends as a function of PEBA composition. The horizontal dashed line indicate the surface resistivity of pure PEBA. 65

Figure 4.10: Effect of water content on surface resistivity for pure PEBA and its binary blends with LDPE and PS..... 66

Figure 4.11: Schematic representation of the charge dissipation mechanism in the PEBA binary blend. 68

Figure 5.1: Partial and complete wetting morphologies in ternary blends of A/B/C predicted by Harkins' spreading theory (B: the minor phase at interface) 77

Figure 5.2: Complex viscosities of the neat polymers at 200 and 250°C. The dashed line indicates the processing shear rate of 25 s^{-1}. 82

Figure 5.3: SEM images of cryo-microtomed LDPE/PEBA/PET blends with increasing PEBA composition. The right column shows the effect of phosphotungstic acid staining at a higher magnification (the white phase is PEBA). Photo (d) presents the observed two typical morphologies (layer and droplets) in different spots as separated by the line. 85

Figure 5.4: SEM images of cryo-fractured LDPE/PEBA/PET blends (the white domains are PEBA stained by phosphotungstic acid) 86

Figure 5.5: SEM images of cryo-fractured LDPE/PEBA/PVDF blends at different PEBA compositions (the white domains are PEBA stained by phosphotungstic acid). 87

Figure 5.6: Domain thickness of PEBA at the interface in the ternary blends. Filled symbols: measured directly from SEM images; open symbols: calculated based on the amount of PEBA at the interface and the interfacial area. 89

Figure 5.7: Surface resistivity of the binary and ternary blends. The dashed lines indicate the boundary of the two stages (steep reduction and gradual reduction) and the dotted line shows the surface resistivity of neat PEBA. 91

Figure 5.8: Morphology of the blends (PEBA is stained by phosphotungstic acid) after annealing for 10 min. (a) and (b): LDPE/PEBA/PET 50/3/47 and 50/10/40 at 260°C; (c) and (d): LDPE/PEBA/PVDF 50/3/47 and 50/10/40 at 200°C. Scale bar: 10 μm.....93

Figure 5.9: Schematic of the Neumann triangle: the equilibrium profile of a liquid B situated at the interface of liquids A and C. 94

Figure 5.10: Schematic of the transition from partial wetting to complete wetting in weak partial wetting systems (Plane direction: perpendicular to the interface for top images and along the interface for lower images). 95

Figure 5.11: Morphology of cryo-fractured LDPE/PEBA/PET (50/35/15) annealed at 250°C for 10 min (PEBA is stained by phosphotungstic acid). 96

Figure 5.12: An example of an LDPE/PEBA/PET cryo-fractured sample for interface coverage calculation 103

Figure 5.13: Interface coverage by PEBA at the LDPE/PET interface in LDPE/PEBA/PET blends 103

Figure 5.14: Volume resistivity of the blends. 103

Figure 5.15: Geometrical parameters of the LDPE/PEBA/PET (50/3/47) blend for determining the Neumann angle θ. 104

Figure 6.1: Possible morphologies in ternary blends of A/B/C predicted by Harkins' spreading theory (C is the minor phase). 108

Figure 6.2: Morphology of LDPE/PS/PEBA with a volume fraction of 75/20/5 (PEBA extracted). 113

Figure 6.3: Morphology evolution in LDPE/PS/PEBA (50/X/Y) as the volume fraction of PEBA increases. Scale bar: 10 µm. 114

Figure 6.4: Morphology of the quaternary blends of LDPE/PS/PEBA/PET at different compositions (the white phase is PEBA stained by phosphotungstic acid). Cryo-microtomed samples: (a) 50/20/10/20 and (b) 50/22.5/5/22.5; cryo-fractured samples: (c) 50/22.5/5/22.5 and (d) 50/23.5/3/23.5. 118

Figure 6.5: Morphology of the LDPE/PS/PEBA/PET quaternary blends at different compositions (the white phase is PEBA stained by phosphotungstic acid). Cryo-microtomed samples: (a) 50/20/10/20; cryo-fractured samples: (b) 50/20/10/20; (c) 50/22.5/5/22.5 and (d) 50/23.5/3/23.5.....119

Figure 6.6: Surface resistivity of the binary, ternary blends and quaternary blends with PEBA. The horizontal dashed line shows the surface resistivity of pure PEBA. 121

Figure 6.7: Schmatics of morphology and surface resistivity evolution in LDPE/PEBA, LDPE/PS/PEBA, LDPE/PS/PEBA/PET and LDPE/PS/PEBA/PVDF. 122

Figure 6.8: Morphology of the ternary LDPE/PS/PEBA (50/40/10) blends (microtomed surface and PEBA extracted). Without interfacial modification and annealed at 200°C for (a) 0 min

and (b) 30 min. Modified with EAM and annealed at 200°C for (c) 0 min, (d) 10 min and (e) 30 min. Scale bar: 10 μm. 125

Figure 6.9: Surface resistivity of LDPE/PS/PEBA 50/40/10 with and without modification by EAM after annealing at 200°C for different periods of time. 127

Figure 6.10: Detailed morphology of LDPE/PS/PEBA (50/40/10) with EAM after 30 min of annealing at 200°C (the white phase is PEBA which is stained by phosphotungstic acid). (a) and (b) are cryo-microtomed samples; (c)–(f) are cryo-fractured samples at different magnifications. 128

Figure 6.11: Schematic comparison of the morphology after annealing between the PE/PP/PS (modified with SEB) system from previous work (a) [19] and the PE/PS/PEBA (modified with EAM) system in this study (b). 129

Figure 6.12: Morphology of the quaternary LDPE/PS/PEBA/PET blends with different formations characterized by SEM (the white phase is PEBA which is stained by phosphotungstic acid). (a) and (b): LDPE/PS/PEBA/PET (50/10/10/30) at low and high magnifications; (c): LDPE/PS/PEBA/PET (50/20/10/20); (d) LDPE/PS/PEBA/PET (50/30/10/10). 136

Figure 6.13: The proportions of PEBA in PS, PET and at the interface of PS/PET in the quaternary LDPE/PS/PEBA/PET blends (the small amount of PEBA in LDPE is neglected). 137

Figure 7.1: Two scenarios of effect of interfacial modification on phase localization in ternary polymer blends (Phase 3: the minor component). Case (a): change from partial wetting to complete wetting, has already demonstrated in literature. Case (b): change from complete wetting to another complete wetting, has not been reported. 140

Figure A1: Complex viscosity and elastic modulus as a function of angular frequency at 200°C. 160

Figure A2: SEM and MIP results: a) ~ c): PLA/HDPE/SEBS (50/45/5, 50/35/15, 50/25/25, SEBS extracted by cyclohexane); d) PLA/HDPE/SEBS (50/25/25, PLA and SEBS extracted by chloroform); e) PLA/HDPE (50/50, PLA extracted by chloroform); f) HDPE/SEBS (50/50, SEBS extracted by cyclohexane); g) Mercury Intrusion Porosimetry (MIP) results. 163

Figure A3: AFM phase images: a, b, c) HDPE/PLA/SEBS (25/50/25) at different magnifications; d) pure SEBS; e) HDPE/SEBS (50/50); f) PLA/SEBS (50/50). Scale bar: 1μm. 165

Figure A4: Pore size evolution for the ternary blend (PLA/HDPE/SEBS 50/25/25) annealed at 200°C for a period of 60 min (data obtained after extracting PLA and SEBS from the blends). 167

Figure A5: Morphology of the annealed (at 220°C for 60 min) ternary blends PLA/HDPE/SEBS with volume fractions: a) 50/25/25, b) 50/40/10, and c) 60/32/8. 169

Figure A6: Pore size distribution (MIP results) of the blends PLA/HDPE/SEBS with different volume fractions after anealed at 220°C for 60 min (the smaller pore size region is further shown in the inserted image). 169

Figure A7: Time sweep measurements performed at 0.1 Hz 173

Figure A8: Morphology evolution of PLA/HDPE/SEBS 50/25/25 during annealing at 200°C (PLA and SEBS extracted). 174

LIST OF SYMBOLS AND ABBREVIATIONS

English Letters:

a	molecular length
A	area
e	film thickness
G	Gibbs free energy
H	enthalpy
k	numerical dissipation factor
m	weight
n	number of moles
P	perimeter
q	scattering vector
R	radius
S	entropy
Ca	capillary number
Tg	glass transition temperature
Tm	melting temperature
Mn	number average molecular weight
Mw	weight average molecular weight

Greek Letters:

α_0	initial distortion amplitude
β	constriction factor
ε	volume fraction
η	viscosity

$\dot{\gamma}$	shear rate
σ	conductivity
γ	interfacial tension
τ	shear stress/tortuosity
ω	wetting parameter
λ	spreading coeffcient
θ	Neumann angle (contact angle)
μ	chemical potential
v	dewetting speed

List of Abbreviations:

ABS	acrylonitrile-butadiene-styrene copolymer
AFM	atomic force microscope
CB	carbon black
CNT	carbon nanotubes
EAM	ethylene–acrylic ester–maleic anhydride random terpolymer
EMAA	poly(ethylene-co-methacrylic acid)
ESD	electrostatic discharge
HDPE	high-density polyethylene
ICP	inherently conductive polymer
IDP	inherently dissipative polymer
LDPE	low-density polyethylene
MA	maleic anhydride
PA	polyamide
PANI	polyaniline

PBT	polybutylene terephthalate
PC	polycarbonate
PE	polyethylene
PEBA	Poly(ether-b-amide)
PEO	poly(ethylene oxide)
PET	polyethylene terephthalate
PMMA	poly(methyl methacrylate)
PP	polypropylene
PPO	poly(propylene oxide)
PTCNQ	poly(tetracyanoquinodimethane)
PTMO	poly(tetramethylene oxide)
PPV	polyparaphenylene vinylene
PPY	polypyrrole
PS	polystyrene
PT	polythiophene
PTTF	poly(tetrathiafulvalene)
PVDF	polyvinylidene fluoride
PVF(c)	poly(vinylferrocene)
SAXS	small angle X-ray scattering
SAN	poly(styrene-co-acrylonitrile)
SEBS	styrene-ethylene/butylene-styrene triblock copolymer
SEB	styrene-(ethylene-butylene) diblock copolymer
SEM	scanning electron microscope
STEM	scanning transmission electron microscope

LIST OF APPENDICES

APPENDIX ARTICLE 4: HIERARCHICALLY POROUS POLYMERIC MATERIALS FROM TERNARY POLYMER BLENDS……...155

CHAPTER 1 INTRODUCTION

More than two thousand years ago, the Greek scientist Thales of Miletus discovered that amber attracts small dust particles when rubbed with animal fur – a phenomenon of static electricity. In modern society, static electricity has emerged as a common problem in many areas associated with the usage of polymeric materials which themselves are electrical insulators in most cases. Electrical charge accumulation and uncontrolled electrostatic discharge (ESD) on a polymer surface can cause issues such as dust adsorption, damage to electronic components and even initiating explosion, which are encountered in many industrial sectors, including electronics, medicine and pharmacy, automotive, aerospace, mining, etc. [1-3]. To avoid static charge accumulation while maintaining the nonconductive nature, the surface resistivity of the polymeric parts generally needs to be reduced to the range of 10^9–10^{13} Ω/sq (technically termed as antistatic materials). However, most conventional polymers fail to meet this criterion.

Many additives have been developed and added to conventional polymers to tailor the surface resistivity according to different applications. Among them, conductive polymers are particularly effective in providing long-term and reliable ESD protection, and they also bear the colorable and non-sloughing features which are desired for many applications [1, 4]. After blending with the host polymers (e.g., PE, PP, PET, PS, etc.), conductive polymers can develop three-dimensional conductive pathways throughout the blend for charge dissipation. Ionically conductive poly(ether-b-amide) (PEBA) copolymers take a major share in this antistat category and the commercial products include Arkema Pebax®, BASF Irgastat® P and Sanyo Pelestat®. These copolymers also display very good processibility, thermal stability and mechanical properties [5]. The final product with PEBA for antistatic applications is typically a binary polymer system (comprised of a host polymer and a conductive polymer) requiring high composition (10–25%) for the polymeric antistat to develop electrical percolation in the host polymer, which increases the cost and may also deteriorate certain physical properties (e.g., mechanical performance, clarity, etc.). Meanwhile, despite the commercial success for PEBA, very limited work has been published to study the effect of PEBA continuity/morphology on surface resistivity of the blends, particularly in multiphase systems [6, 7]. Furthermore, the studies on the charge dissipation mechanism in these copolymers are also very limited [8, 9].

The study of morphology in multiphase polymer blends has been attracting increasing attention over the past 15 years [10-14]. Different from the binary blends where dispersed phase/matrix and co-continuous morphologies are observed, complex structures can be obtained in multiphase polymer systems (Fig. 1.1). The multi-percolated structures generated from multiphase polymer blends are of particular interest in terms of reducing the percolation threshold of PEBA and achieving the required surface resistivity for antistatic applications at low PEBA compositions. Previous studies with other conductive polymers have shown that much higher conductivity can be obtained in these systems as compared to in traditional binary blends [15-17]. However, in almost all the work published on the melt processing of conductive polymer blends, the conductive component is situated in the core and encapsulated by other polymers (rather than at the interface) [6, 15-17]. In this context, the well documented studies on conductive composites demonstrate the significant advantage of placing the conductive inorganic fillers (e.g., carbon black, carbon nanotube, etc.) at the interface for improved electrical conductivity [18-23]. These results point to the great potential to significantly lower the electrical percolation threshold by confining PEBA at the interface of the host polymers. In practice, it is desirable to obtain the structures through melt blending since it is a cost-effective technique widely used in industry.

In ternary polymer blends with two major phases A and C and a minor phase B located at the interface of A/C, the phase B can adapt to either layer (B completely wets the A/C interface; e.g., Fig. 1.1b: PS layer at HDPE/PMMA interface) or droplet (B partially wets the A/C interface; e.g., PS droplets at the PE/PP interface as shown in Fig. 1.1c) morphology depending on the spreading coefficients [24, 25]. The former scenario has attracted much research effort due to its ability to develop percolation at very low concentrations [11, 23, 26, 27]. However, some important questions, for example, whether there exists a minimum layer thickness to achieve full segregation and what factors may control this thickness, have been barely investigated [27]. In the latter scenario, some studies indicate the droplets are discrete at the interface [28, 29]. Other studies reported on the transformation from partial wetting to complete wetting by adding an interfacial modifier (Figs. 1.1d and e) [12, 13]. To date, it is still not clear how the morphology of the intermediate phase evolves during processing. Understanding these questions will benefit the advanced applications of these complex but well-controllable structures.

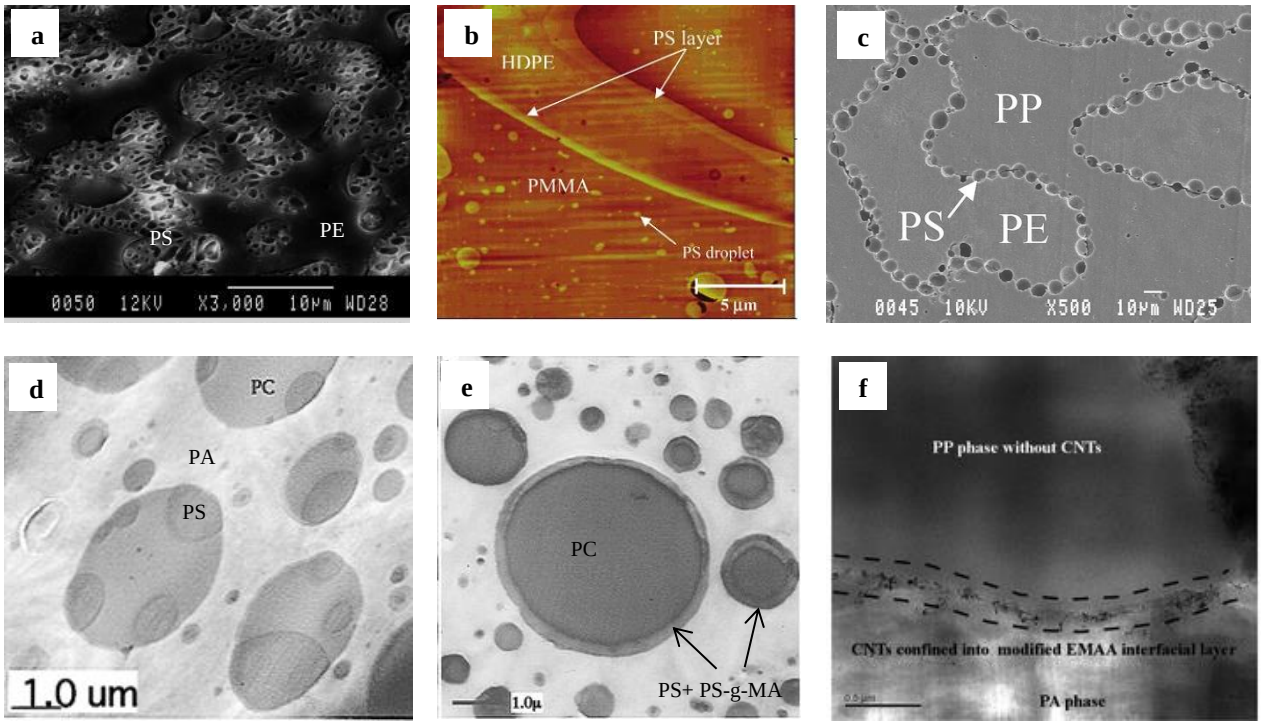

Figure 1.1: Examples of advanced structures developed in multi-phase polymer blends. a) tri-continuous structures in PE/PS/PMMA ternary blends (PMMA extracted) (taken from Ref. [10]); b) PS forms completely wet layer at the interface of HDPE/PMMA with a high continuity (about 70%) achieved at 3% (taken from Ref. [11]); c) PS self-assembles into close-packed droplet array at the PE/PP interface (taken from Ref. [28]); d-e) tune the morphology of PS at the interface of PA/PC from partially wet droplets to completely wet layers by adding PS-g-MA (taken from Ref. [13]); f) confine CNTs within thin EMAA layers formed at the PP/PA interface to reduce the percolation threshold (taken from Ref. [23]).

CHAPTER 2 LITERATURE REVIEW AND OBJECTIVES

2.1 Conductive Polymer Systems

According to the range of electrical conductivity, solid materials can be divided into three groups: conductors, semiconductors and insulators [30]. Although polymers are traditionally used as insulators, conductive polymer systems have also been developed which can be classified into four types: 1) conductive polymer composites; 2) conjugated polymers; 3) ionically conductive polymers; and 4) redox polymers. The electrical conductivity in these systems can arise from the flow of electrons (electronically conductive polymers) and/or from the net motion of charged ions (ionically conductive polymers) [31, 32].

2.1.1 Conductive Polymer Composites

The most widely used conductive polymers are polymer composites where electrical conductivity is imparted by adding conductive fillers (such as carbon and metal particles) to the insulating polymer matrix [33]. Generally, the development of conductive pathways in these systems can be divided into three regions as a function of filler content (Fig. 2.1). At low filler loading, the fillers remain discrete and the conductivity of the composite shows little improvement as compared to the pure polymer (region A). After exceeding a critical point (percolation threshold), the conductive network develops through filler contact and the conductivity increases steeply (region B). Further increasing the filler amount leads to a slight monotonic increment approaching the intrinsic conductivity of the filler (region C).

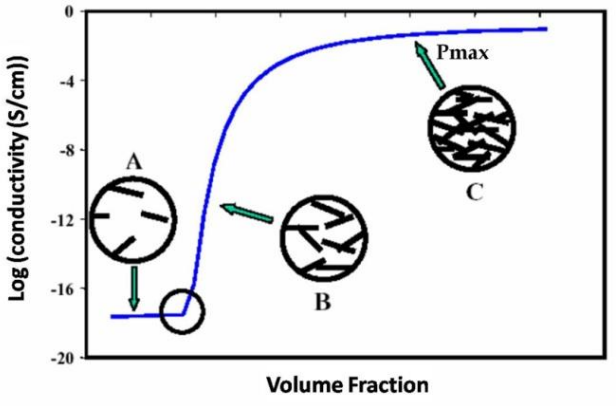

Figure 2.1: Development of conductive pathways in polymer composite systems as a function of filler concentration (taken from Ref. [34]).

2.1.2 Conjugated Polymers

Conjugated polymers are characterized by alternating single and double bonds which results in an extended π electron system. The interest in conjugated conductive polymers started in the 1970s when the conductivity of polyacetylene films was dramatically improved after it was exposed to iodine vapor [35, 36]. Following this work, a variety of conjugated polymers have been synthesized, including, polypyrrole (PPY), polythiophene (PT), polyaniline (PANI), polyparaphenylene vinylene (PPV), etc. Fig. 2.2 shows the structures of some of the conjugated conductive polymers and their conductivities. These polymers are inherently conducting due to the conjugated π electron system and thus are also referred to as inherently conductive polymers (ICPs). However, their original conductivities are very low (e.g., polyacetylene from *cis*-isomers has a conductivity of 10^{-9} S/cm at 273K [35]), but can be increased by oxidation (p-doping) and/or, reduction (n-doping) to generate mobile charge carriers. For example, in the well-known work on polyacetylene from Shirakawa, MacDiarmid and Heeger, the conductivity of polyacetylene (from *trans*-isomers) was increased from 3.3×10^{-6} to 30 S/cm by iodine doping [35]. The mechanism of this process is briefly presented in Fig. 2.3 by using oxidation as an example [37]. After doping, an electron is removed from the π system which leads to the delocalization of a radical ion (polaron) as shown in Fig. 2.3a. Further oxidation and radical recombination yields two charged carriers on the chain (Fig. 2.3b). Meanwhile, a number of neutral defects also exist in the synthesized polyacetylene (solitons) and charged soltions can be generated after oxidation (Fig. 2.3b). These delocalized charges are mobile (but not the dopant ions) along the polymer chain and also capable of traveling to other chains through hopping which make current conduction through the bulk possible. Due to the intrinsic conjugated structures on the backbone, unfunctionalized conjugated polymers are usually insoluble, infusible and brittle, which limit their wide applications [32].

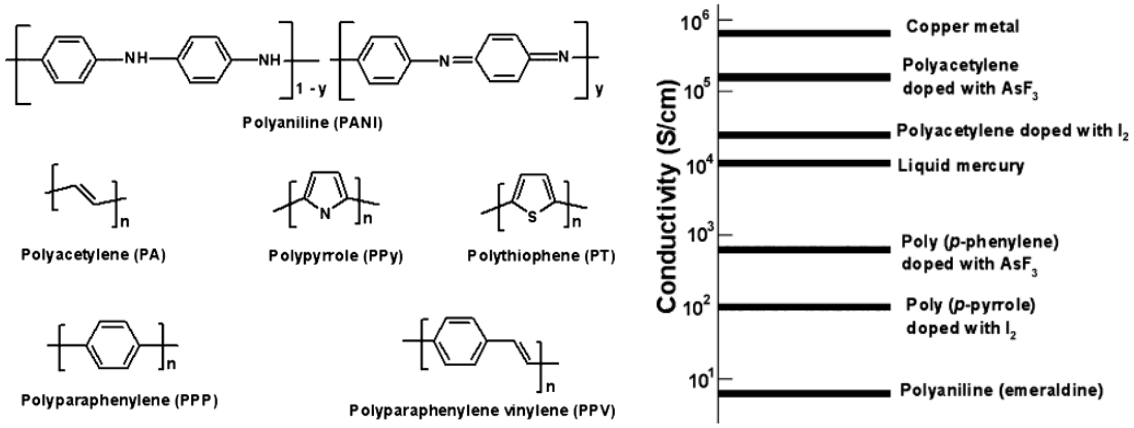

Figure 2.2: Structures and conductivities of some conjugated conductive polymers (taken from Ref. [33]).

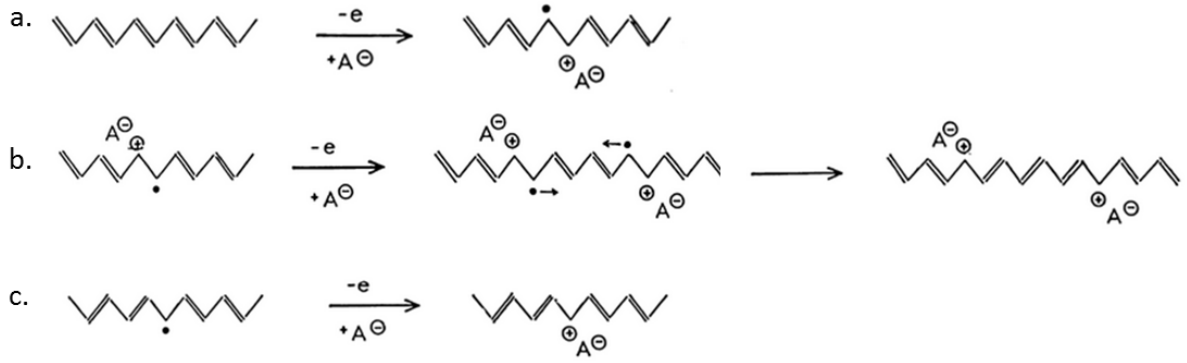

Figure 2.3: Schematic of conductive mechanism in polyactylene with an oxidative dopant (taken from Ref. [37]).

2.1.3 Ionically Conductive Polymers

Ionic conductivity is generally restricted to salt solutions (with polar solvent) or molten salts. The ion transportation in solid polymers without a solvent was only recognized a few decades ago in the 1970–80s [38-41]. The macromolecule acts as a solvent to partially disassociate the salt, resulting in a complex system with electrolyte behaviour. Thus, ionically conductive polymers are also known as polymer electrolytes [31, 32, 41]. It is generally accepted that the conductivity originates from ion migration between coordination sites generated by the local segmental motion of the polymer chains [31, 42-44] (Fig. 2.4). Therefore, ionically conductive polymers are expected to bear electron-donating atoms or groups to coordinate with cations and low bond rotation barriers (flexible bonds and weak inter-chain interactions) to facilitate segmental motion

[32]. Poly(ethylene oxide) (PEO) (as well as its copolymers) remains the most extensively studied ionically conductive polymer, particularly as solid polymer electrolytes in lithium batteries, due to the high dielectric constant and strong solvating ability for lithium ions [31, 38, 43, 45].

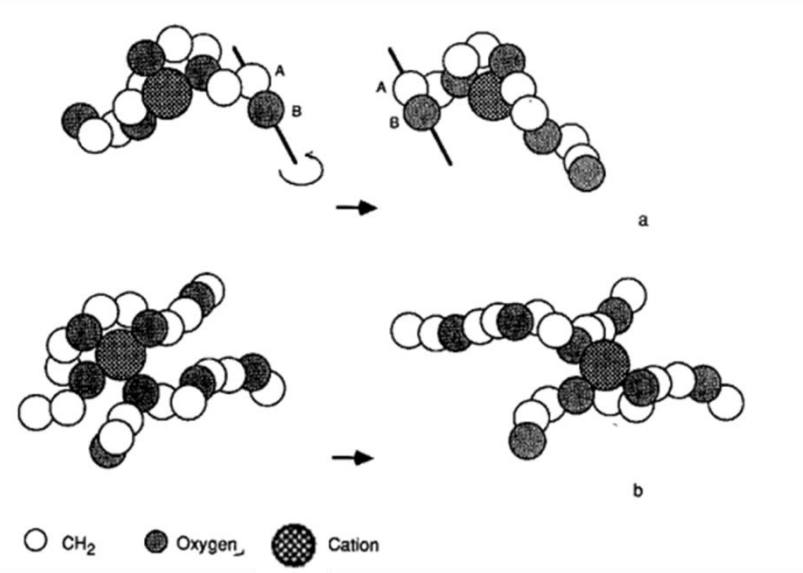

Figure 2.4: Ion transport in PEO: a) Lateral migration of the cation through C-O bond rotation along the AB line; b) the transfer of the cation between PEO chain segments by oxygen ligand replacement (taken from Ref. [32]).

Generally, ionically conductive polymers are highly processable. However, with the ionic conduction mechanism (dissociation of opposite ionic charges and ion migration through slow polymer chain motion), these polymers normally show very low intrinsic conductivity in the absence of water (in the order of 10^{-14} S/cm) [47]. The conductivity can be increased to ~ 10^{-4} S/cm (at room temperature) by doping (most frequently using lithium salts) and controlling crystallinity/chain mobility of the polymers [48, 49].

2.1.4 Redox Polymers

These polymer systems contain a large number of electrostatically and spatially localized redox centers which can be either incorporated into the backbone or associated with the pendant groups of the chain [50]. Conductivity in such systems is realized by the electron hopping between adjacent redox sites overcoming the insulating barrier [33]. Note that the difference in

electroactivity of the redox centers in these polymers as compared to the previous conjugated polymers is that the process in the former case is highly localized, while a reorganization of the bonds along the macromolecule chain occurs in conjugated polymers. Poly(tetracyanoquinodimethane) (PTCNQ), poly(tetrathiafulvalene) (PTTF) and poly(vinylferrocene) (PVF or PVFc) are among those that belong to this category [50].

2.2 Conductive Polymer Systems for Antistatic Applications

2.2.1 Static Electricity

Static electricity is a phenomenon referred to the imbalance of positive and negative charges within or on the surface of an object. Friction, conduction and induction are the three ways to impart net static charges. A locally excess amount of static charge q_0 inside/on any material will decay with time t exponentially due to the presence of the self-field of the charge [51]:

$$q = q_0 e^{-t/\tau}$$

where q is the charge concentration after a period of decaying time t and τ is the charge relaxation time. For conductors, τ is so small that it is even difficult to measure (e.g., τ_{copper} is in the order of 10^{-18} s). But for conventional polymers which normally have high resistivities, τ can be very large. Consequently, charges generated on/in polymeric materials may be retained for long periods of time, in some cases for years. The long lifetime of the charge accumulated on a polymer surface can cause many problems, such as damage to electronic devices, contamination in clean rooms or to medical devices and pharmaceuticals, initiating explosion, etc. [4].

Compared to the bulk, the surface of an object is more vulnerable to the charging effect. Thus, surface resistivity is one of the key criteria to evaluate the charge dissipation ability of a material. Fig. 2.5 shows the schematic to measure the surface resistivity (ρ_s) as per ASTM D257 Standard. Two electrodes are attached on the surface of a material as schematically shown. After applying a voltage of U, the electrical current can penetrate into the material from anode to cathode (see Fig. 2.5). Studies carried out by Arkema (unpublished data) have found that the current can penetrate to a depth of about 150 μm. Thus, surface resistivity should be mostly related to the characteristics of a region near the material surface (with a depth of hundreds of microns). It

should be noted that the real unit for surface resistivity is Ω. However, in the literature, Ω/sq (ohm per square) is commonly used to make it distinguished from surface resistance (which also bears the unit Ω).

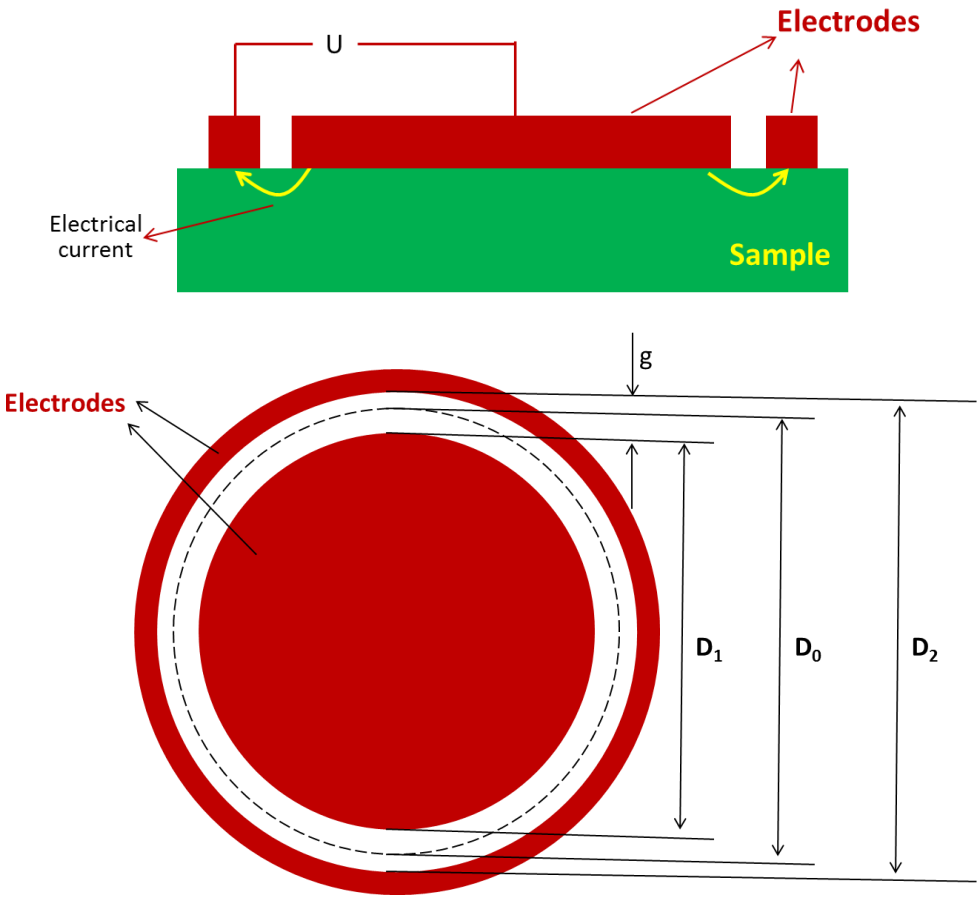

$$\rho_s = \frac{\pi D_0}{g} \times \frac{U}{I}$$

Figure 2.5: Schematic for the measurement of the surface resistivity. *U* and *I* are the applied voltage and measured current; *g*, D_0, D_1 *and* D_2 are the geometry parameters of the measuring setup.

2.2.2 Classification of Antistatic Additives

In order to avoid static charge accumulation, the surface resistivity of the material generally needs to be reduced to 10^9–10^{13} Ω/sq (antistatic materials) [4, 52]. Most conventional polymers fail to meet this criterion with typical surface resistivities > 10^{14} Ω/sq. Many additives have been developed to tailor the surface resistivity of polymeric materials and can be divided into three main categories: migrating antistats; conductive fillers and inherently dissipative/conductive polymers.

1) Migrating Antistats

Migrating antistats are typically low molecular weight surfactants with a non-polar chain and a polar hydrophilic head [1]. They can be either directly sprayed or coated on the article surface or mixed with polymers during processing. In the latter scenario, the antistats gradually diffuse or "bloom" to the polymer surface over time, which creates a thin hydrophilic layer attracting moisture and thus imparts a charge dissipative capacity to the surface. The charge dissipation mechanism in this case is schematically shown in Fig. 2.6. Although migrating antistats are widely used due to their low cost and effectiveness (they reduce the surface resistivity to 10^{10} to 10^{12} Ω/sq), they also possess some significant weaknesses [4]. Firstly, they only provide short-term protection since the additives are wiped away from the surface with the lapse of time and static charges can appear again (Fig. 2.6). Furthermore, the antistats rely on absorbing moisture to dissipate charges and thus the antistatic performances can vary significantly with humidity in environment. Thirdly, they cannot confer immediate antistatic properties to the host polymer since it takes time for the chemicals to migrate to the surface. And lastly, the enrichment effect on the material surface also limits their applications in many areas, such as packaging for pharmaceuticals and food, cleanroom applications, etc.

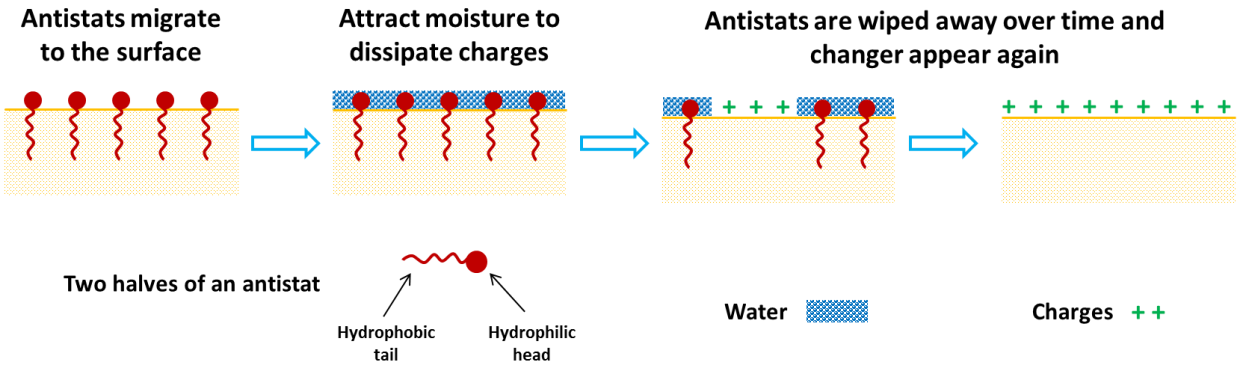

Figure 2.6: Charge dissipation mechanism of migrating antistats (adapted from Ref. [1]).

2) Conductive Fillers

Conductive fillers used for static control applications include carbon materials (carbon back, carbon nanotube, graphite, graphene, etc.) and metal particles. The conductivity/resistivity of the polymer/filler composite can be tailored by the concentration of the conductive filler (Fig. 2.1), viscoelasticity of the polymer and processing conditions [18]. Polymer/carbon back composites are the most commonly seen in antistatic applications due to their versatility, low cost and permanent conductivity. However, the shedding of the carbon particles (known as "sloughing") from the composite has been one major disadvantage which limit their applications in certain areas (e.g., clean room, pharmaceutical industry, etc.). In this context, the use of carbon nanotubes, which are non-sloughing, continues to grow and require less concentration to percolate due to their high aspect ratio [1, 53]. One common problem to all the polymer/conductive filler systems is that the conductivity/resistivity varies significantly from the insulating region to the conductive region around the percolation threshold, which makes it very difficult to precisely control the resistivity in the antistatic range.

3) Inherently Dissipative/Conductive Polymers

Inherently dissipative and conductive polymers (IDPs and ICPs) represent a new class of additives for static control applications, which confer the host material immediate and permanent antistatic properties through the formation of 3D dissipative/conductive pathways (Fig. 2.7). The development of polymeric conductive networks follows the general mechanism of morphological evolution in binary polymer blends (see Fig. 2.15). There is currently no clear definition in the literature for "inherently dissipative polymers".

Technically, they refer to polymers offering a comparable charge dissipation capacity to migrating antistats with a typical surface resistivity from 10^8 to 10^{12} Ω/sq (e.g., Arkema Pebax®, DuPont Entira™ Antistat, BASF Irgastat®, Sanyo PELESTAT®, etc.). These polymers normally contain PEO blocks (although not always) for charge dissipation [1], and thus most of them are actually ionically conductive polymers. The ICPs have much higher conductivities which are along the lines of metals (as high as 10^5 S/cm; e.g., polyaniline, polypyrrole, polythiophene, etc.) [32]. As discussed previously, the key chemical structure in ICPs is the alternating single (C–C) and double (C=C) bonds (conjugation), which allows the electrons to be more easily delocalized and transfer between different atoms [54]. Despite the wide range of conductivities/resistivities obtained for conventional polymers after blending with ICPs [15, 16], IDPs have achieved much more success for antistatic applications due to their good processibility and stability, high mechanical performances and low cost [1, 4, 5]. Other advances of using IDPs for static control over other additives include: 1) they are colourable and non-sloughing; 2) provide permanent and immediate antistatic capacity with precisely controlled resistivity; 3) much less vulnerable to environmental humidity (than migrating antistats) [1, 4].

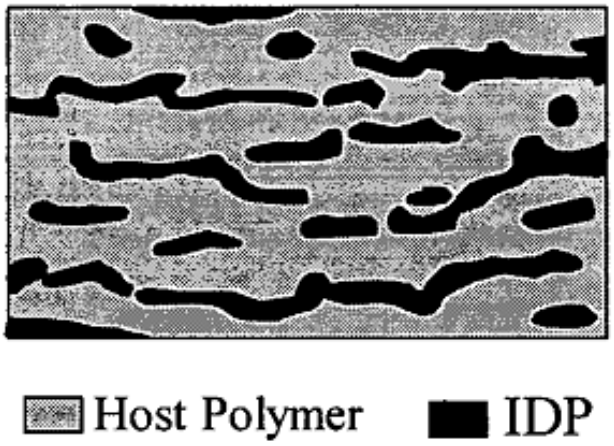

Figure 2.7: Schematic of dissipative networks developed in the IDP/host polymer binary blend (taken from Ref. [1]).

2.3 Poly(ether-b-amide) (PEBA) Copolymers

Poly(ether-b-amide) (PEBA) is a class of segmented copolymers comprised of hard polyamide blocks and soft polyether blocks with a low glass transition temperature [55]. The hydrogen bonds between the amide groups of the semi-crystallized polyamide result in physical crosslinks which provide mechanical strength to the copolymer, while the flexible polyether blocks impart elastomeric properties. Above the melting temperature of the polyamide, the physical crosslinks are destroyed and the materials are transformed to common thermoplastics.

2.3.1 Chemical Structure and Synthesis

The general chemical structure of PEBA is schematically shown in Fig. 2.8. The polyamide segments in PEBA copolymers are mostly based on polyamide 6 and 12. The flexible polyether blocks are prepared from alkylene oxide oligomers, including poly(tetramethylene oxide) (PTMO), poly(ethylene oxide) (PEO, also called PEG), and poly(propylene oxide) (PPO, also called PPG).

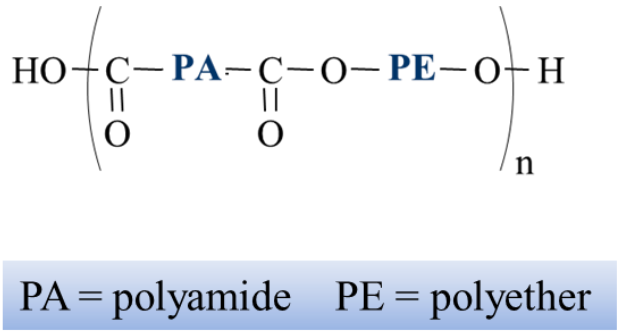

Figure 2.8: Schematic of the general chemical structure of a PEBA copolymer (adapted from [56]).

Table 2.1 lists the main PEBA copolymers commercially available on the market and their composition. The use of different types of polyethers affects the physical properties of the final PEBA copolymers [55]. For example, when PEO is introduced, the hydrophilicity of the copolymer will be improved, and breathability and antistatic capacity will also be conferred.

Table 2.1: Commercially available PEBA copolymers and their composition (taken from Ref. [55]).

Trade name	Hard segment	Soft segment
PEBAX®	PA12 PA6	PTMO PEO
PLATAMID®	Copolyamide	PEO
VESTAMID® E	PA12	PTMO
GRILAMID® ELY	PA12	PTMO
PELESTAT®	PA12 PA6	BEO
PAE	Copolyamide	PPO

PEBA copolymers can be synthesized through different approaches. Only the typical thermal polymerization method with ester links will be briefly introduced since it represents how the specific PEBA (Pebax® from Arkema) used in this project is produced [55]. These PEBA copolymers consist of linear chains of polyamide and polyether blocks with molecular weights of about 400–3000 g/mol and 500–5000 g/mol respectively [56]. The polymerization process is carried out in two steps. Firstly, the α,ω-dicarboxylic acid terminated polyamide block is synthesized from the reaction of lactam(s), aminoacid(s) and/or diacid and diamine with a chain-terminating diacid. The average molecular weight of the resulted polyamide block is controlled by the molar ratio between the chain-terminating agent and the reactant monomers. This step is usually carried out under pressure at high temperatures. In the second step, a commercially available α,ω-dihydroxy terminated polyether reacts with the previously synthesized polyamide block to produce the designated PEBA copolymer in the presence of catalyst. A lower temperature and vacuum are used to minimize the degradation of the polyether and drive the reaction towards ester formation respectively. The two-step process is schematically shown in Fig. 2.9.

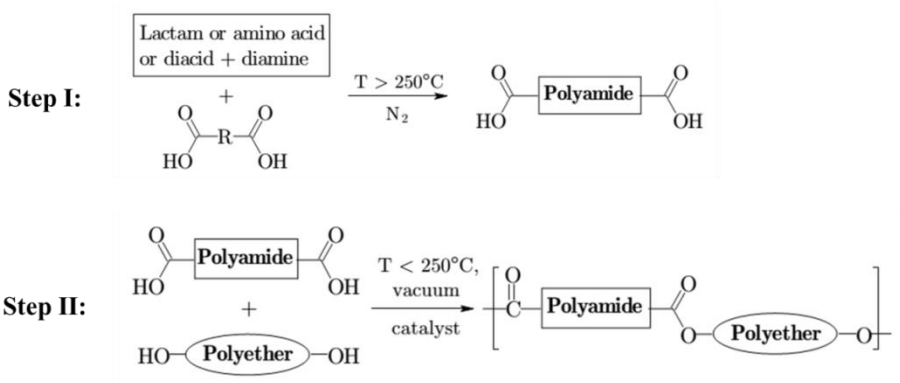

Figure 2.9: Synthesis of ester-linked PEBA copolymers through the two-step thermal polymerization (taken from Ref. [55]).

2.3.2 Solid-state Structures of PEBA

PEBA copolymers present a micro-phase separated morphology in the solid-state due to the thermodynamic incompatibility between the polyamide and polyether components (macro-phase separation is prevented by the covalent bonds between the two blocks) (Fig. 2.10). The polyamide segments crystallize into lamellar structures independently of the polyamide/polyether composition [56-59]. Barbi et al. studied solvent-cast PEBA films of various grades (polyether weight ratio varies from 53 to 80%) by SAXS [59]. They found that the layer thickness of polyamide lamellae is on the order of 6 nm and the long period ranges from 12 to 18 nm. For the rigid grades (the weight ratio of polyamide/polyether > 1), the lamellar structures can organize into spherulitic superstructures with a radius of a few microns [5].

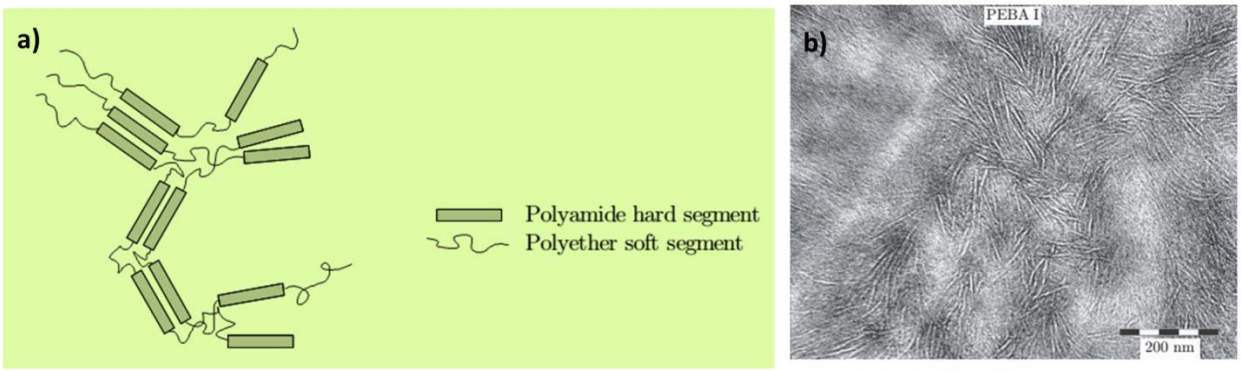

Figure 2.10: a) Schematic representation of PEBA solid-state structures; b) TEM image of a poly(ether-b-amide) copolymer with a polyamide/polyether weight ratio of 23/77 (taken from Ref. [5, 55]).

2.4 Ion Transport in Ionically Conductive Polymers

2.4.1 Ion Transport in Block Copolymer Electrolytes

High ionic conductivity in PEO requires rapid segmental motion to accelerate ion transport, which, on the other hand, tends to decrease the rigidity of the polymer [42]. The use of PEO containing block copolymers has been shown to be a possible solution to decouple the electrical and mechanical properties, where the PEO block provides ionic conductivity and the other component(s) imparts desired mechanical properties [60]. These copolymer systems are characterized by a micro-phase separated morphology due to the thermodynamic immiscibility between the polymer blocks. The shape of the PEO microdomains can be spheres, cylinders, bicontinuous (gyroid) or lamellae, which is mainly controlled by the Flory-Huggins interaction parameter, overall degree of polymerization and the composition fraction [61, 62].

1) Effect of Morphology

The ionic conductivity of a block copolymer electrolyte (σ) may be expressed as follows:

$$\sigma = f \phi_c \sigma_0$$

where f is the morphology factor; ϕ_c and σ_0 are the volume fraction and intrinsic conductivity of the conducting phase, respectively. According to the work of Sax and Ottino, f can be calculated based on the morphology of the polymer electrolyte as shown in Fig. 2.11 (termed as f_{ideal}) [63]. For a spherical morphology, f_{ideal} equals 0 since no conductive pathways exist in the system. In the case of a cylindrical morphology, one-third of the grains will statistically contribute to ion transport in a certain direction and thus f_{ideal} takes a value of 1/3. Similarly, f_{ideal} equals 2/3 in a lamellar morphology and 1 in a gyroid morphology. Villaluenga *et al*. found that adding 2 wt% nanoparticles into lithium/polystyrene-b-poly(ethylene oxide) electrolytes resulted in an unexpected increase in conductivity [62]. Examination of the solid state structures by SAXS and STEM confirmed a morphology transition from lamella to gyroid and thus resulted in a conductivity increase. The morphology factor f was determined to be 0.94 ± 0.28 in the sample of gyroid morphology, very close to the theoretical value (f_{ideal}). Cheng et al. studied the effect of crystalline structures on ion transport in polymer electrolytes with lamellar morphology [43]. They designed a model system comprised of single PEO crystals with controlled crystal structure and size, crystallinity, and orientation. It was found that, at low ion content, the conductivity

along the lamellar plane direction can be 2000 times higher than that in the direction perpendicular to the plane due to tortuosity effects, indicating the ion transport in the system is confined within the chain fold region and is directed by the lamellar structures. However, Chintapalli *et al*. reported on the influence of grain size on the ionic conductivity of a block copolymer electrolyte. Surprisingly, the conductivity was decreased by a factor of 5.2 as the grain size increased from 13 to 88 nm. Results from another study also suggests that long-rang order hinders ion conductivity since ionic conductivity may be blocked by the boundaries of large grains [64].

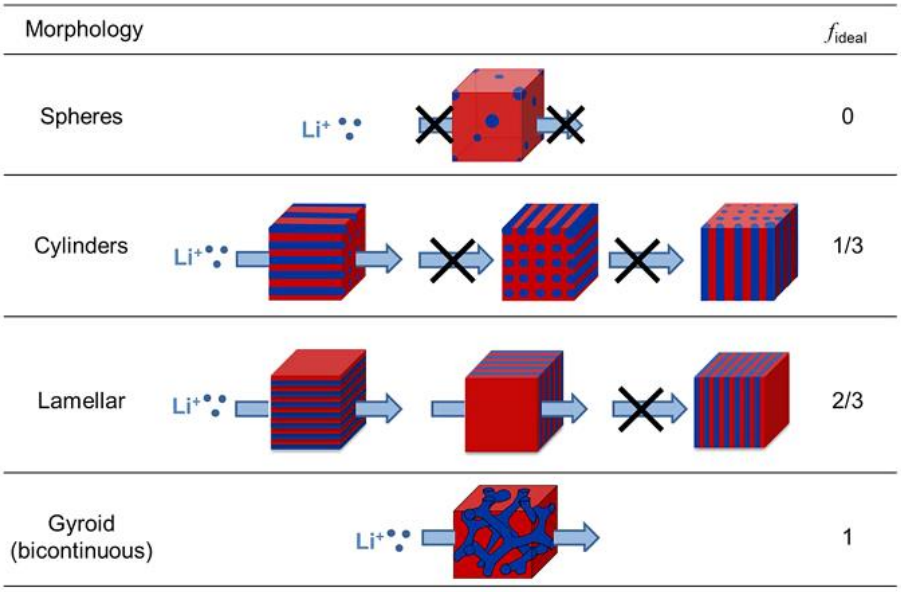

Figure 2.11: Theoretical morphology factor f_{ideal} of polyelectrolytes with different morphologies. The blue region represents the conducting phase (taken from Ref. [62]).

2) Effect of Chain Mobility

It is generally believed that ion transport is mainly restricted within the amorphous region of a polymer electrolyte and thus should be enhanced by increasing the chain mobility. Methods to reduce the crystallinity of PEO by adding plasticizer and inorganic particles have been shown to be effective to increase the conductivity [65]. Decreasing the molecular weight is also expected to increase the ionic conductivity, which has been reported in PEO homopolymer/lithium salt complex systems [66]. However, an opposite tendency was reported in the case of block

copolymers containing PEO [45, 60, 64]. Bouchet et al. modeled the conductivity (σ) of the PS-PEO-PS electrolytes using the following equation [45]:

$$\sigma = \frac{\sigma^0 \varepsilon}{\tau}$$

where σ^0 and ε are the conductivity and volume fraction of the PEO phase (a complex of pure PEO and doped lithium slat) respectively; and τ is the tortuosity of the PEO network. They proposed that a "dead zone" of 1.6 nm independent of PEO molecular weight exists at the interface of PS/PEO where the PEO chain mobility is impeded by the covalently bonded hard PS domain (Fig. 2.12). That portion of the PEO chains does not contribute to the ion transport in the system. Similar results were also obtained in another study where the interfacial zone was estimated to be around 5 nm [64]. The argument explains the unexpected behavior in copolymer electrolytes that ionic conductivity increases with increasing PEO molecular weight, since a relatively larger portion of PEO would contribute to ion conduction as the PEO molecular weight increases [45].

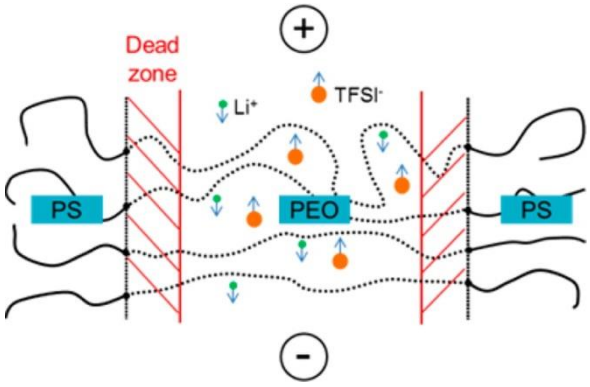

Figure 2.12: Schematic representation of ion transport in the PS-PEO-PS electrolytes (taken from Ref. [45]).

2.4.2 Charge Dissipation Mechanism in PEBA Copolymers

PEBA copolymers have been widely used for antistatic applications [4, 55]. However, the charge transportation mechanism in such copolymers has not been well understood. Young and Lin studied the electrostatic dissipating properties of copolymers consisting of PEO blocks and amide groups [8]. They proposed that the PEO blocks absorb water through hydrogen bonding and the

partially ionized water molecules generate protons serving as the medium for charge transfer (Fig. 2.13). It was also demonstrated in the study that hydrogen bonding between the amide group and the water molecule is also important to obtain low surface resistivity.

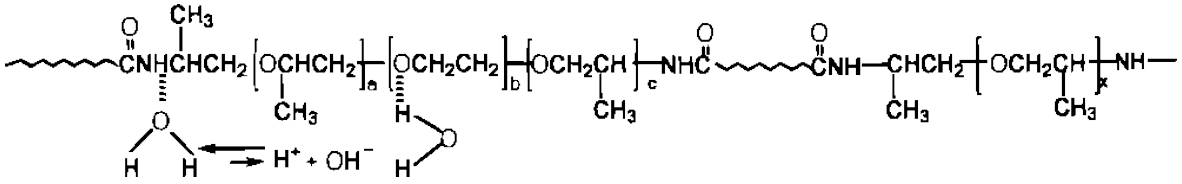

Figure 2.13: Electrostatic dissipation mechanism via hydrogen-bondings between PEO/water and amide/water. The partial ionization of water molecules generates protons for charge dissipation (taken from Ref. [8]).

2.5 Control of Morphology in Immiscible Polymer Blends

2.5.1 Basic Thermodynamics in Polymer Blends

The miscibility of a polymer blend is determined by the free energy of mixing (ΔG_{mix}) defined as:

$$\Delta G_{mix} = \Delta H_{mix} - T\Delta S_{mix}$$

where ΔH_{mix} and ΔS_{mix} are the enthalpy and entropy change on mixing respectively [67]. Fig. 2.14 shows the three states of miscibility in binary systems. Case A represents an immiscible system since the free energy of mixing is positive in the whole composition range. Case B is an example where complete miscibility is achieved at any composition for the two components. In Case C, however, although ΔG_{mix} is negative in all proportions, phase separation will occur over the composition range between the two minima to achieve a lower free energy (at the minima of the curve). Case C represents a system with partial miscibility. Therefore, complete miscibility in a polymer blend system requires: (1) $\Delta G_{mix} < 0$; (2) $\frac{\partial^2 \Delta G_{mix}}{\partial \varphi^2} > 0$.

In polymer blends, immiscibility is the most common scenario since ΔH_{mix} is normally positive (lack of specific interactions) and ΔS_{mix} is very small (high molecular weight of the components). In many cases, immiscibility is actually desirable since the final product is ideally a polymer-

polymer mixture which synergistically combines the characteristic properties of each component [67].

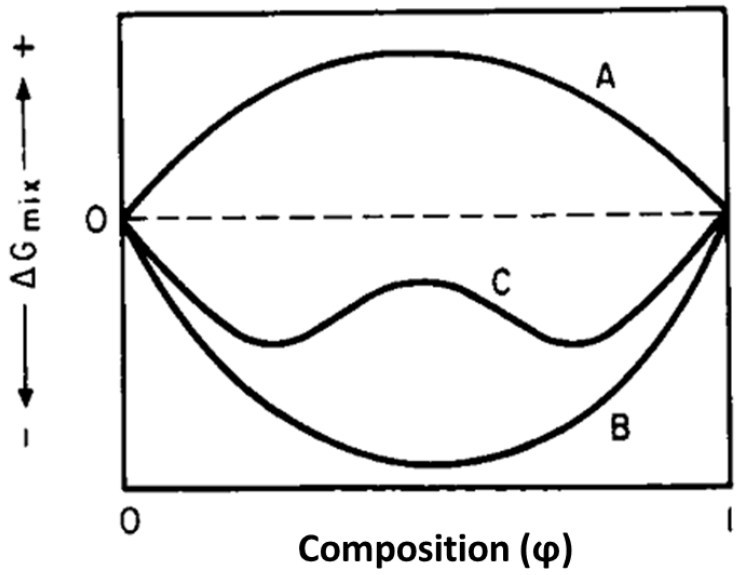

Figure 2.14: Three typical states of miscibility in a binary system: (A) completely immiscible; (B) completely miscible; and (C) partially miscible (taken from Ref. [67]).

2.5.2 Morphologies of Immiscible Binary Polymer Blends

In immiscible binary polymer blends, when a minor phase is added to a matrix, a type of dispersed phase (e.g., droplets, fibers or lamellar structures)/matrix morphology can be obtained [68]. As the composition of the minor phase increases, more dispersed domains are present in the system and after a crucial concentration (percolation threshold), percolated structures can be developed. Further increasing the composition results in the so-called co-continuous morphology which is characterized by each component being interconnected throughout the blend (100% continuity for each phase). Fig. 2.15 schematically shows the morphology development in binary polymer blends. The transition from dispersed phase/matrix morphology to co-continuous morphology is affected by many factors, including interfacial tension, viscosity (ratio), elasticity and shear stress, and the final morphology is a balance between phase deformation-disintegration and coalescence [69].

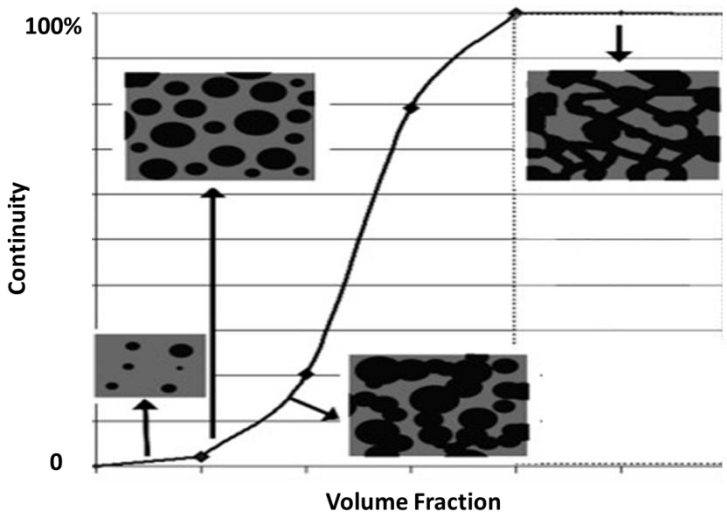

Figure 2.15: Schematic presentation of morphology development in binary polymer blends (taken from Ref. [10]).

2.5.2.1 Morphology Development in Binary Polymer Blends

The morphology in binary polymer blends develops through the coalescence of the dispersed phase [70]. The shape of the dispersed phase (droplets, fibers, etc.) depends on the deformability of the dispersed phase as well as its stability after deformation [69]. The deformability of the dispersed phase can be characterized by the capillary number (*Ca*) as developed by Taylor [71, 72]:

$$Ca = \frac{\eta_m \dot{\gamma} R}{\sigma}$$

where η_m is the matrix viscosity, σ is the interfacial tension, $\dot{\gamma}$ is the shear rate, and R is the radius of the dispersed phase. *Ca* is the ratio between the deforming stress ($\eta_m \dot{\gamma}$) imposed by the flow and the interfacial forces (σ/R). If *Ca* is small (e.g., in the case of high interfacial tension), the interfacial forces dominate and a steady droplet morphology develops. Upon exceeding a critical value, the dispersed phase can be deformed and finally breaks. The stability of a deformed thread (known as capillary instability) can be estimated by the time of breakup (t_b) from Tomotika's equation [73]:

$$t_b = \frac{2\eta_m R_0}{\Omega_m \sigma} \ln\left(\frac{0.82 R_0}{\alpha_0}\right)$$

where Ω_m is a tabulated function related to the viscosity ratio, R_0 is the initial radius of the thread and α_0 is the initial distortion amplitude. For polymer blends with a low interfacial tension, the dispersed phase will present as a stable thread-like morphology owing to the much longer thread lifetime as compared to droplet lifetime [74-76].

The flow-induced coalescence of two droplets in a Newtonian system can be divided into three steps: (i) the two droplets approach each other due to the flow field; (ii) the matrix film between the droplets is drained to a critical thickness; and (iii) the film ruptures and the coalescence of the droplets occurs [77] (Fig. 2.16). The coalescence in polymer blend systems, however, is less understood. Fortelný and Kovář reported that coalescence is significantly decreased if the matrix viscosity is above a critical value and if the volume fraction of the dispersed phase is below a critical value [78]. However, Sundararaj and Macosko showed that significant coalescence occurred in a system with high matrix viscosity and a low dispersed phase concentration (as compared to the work from Fortelný and Kovář) [77]. They also argued that interfacial modification (compatibilization) suppresses coalescence by stabilizing the interface instead of through decreasing the interfacial tension. Tokita derived an expression for the particle size of the dispersed phase by considering both the breakup and coalescence processes in dynamic state [79]. At equilibrium, the particle size of the dispersed phase (D_e) can be expressed as:

$$D_e \approx \frac{24 P_r \gamma_{12}}{\pi \tau}\left(\varphi + \frac{4 P_r E_{DK}}{\pi \tau}\varphi^2\right)$$

where P_r is the probability that a collision leads to coalescence; γ_{12} is the interfacial tension; τ is the shear stress; ϕ is the volume ratio of the dispersed phase; E_{DK} is the bulk breaking energy. The model predicts that the particle size of the dispersed phase is reduced by increasing the shear stress, and by decreasing the interfacial tension and the composition of the dispersed phase. The dependence of phase size on composition was further confirmed in a later study with different polymer blend systems [80]. However, the influence of shear stress in the theory was considered to be overestimated.

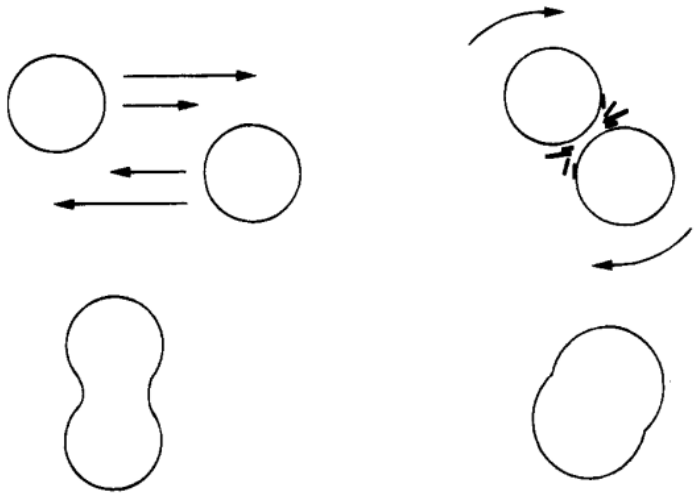

Figure 2.16: Schematic representation of flow-induced coalescence of two droplets in a Newtonian system. The two droplets are brought close to each other and rotate in the flow filed; the film in-between thins and finally raptures; the two droplets contact and emerge into one (taken from Ref. [77]).

Li et al. systematically examined the effect of interface type on polymer blend morphology and proposed different mechanisms for the formation of the co-continuous morphology [74]. In compatible binary blends, such as high-density polyethylene (HDPE)/styrene-(ethylene/butylene)-styrene (SEBS), the dispersed phase is readily deformed into a stable thread during melt mixing owing to the very low interfacial tension (0.7 ~ 1.0 mN/m) (Fig. 2.17a). Thus the continuity is developed mainly through a thread-thread coalescence mechanism. This type of system is expected to be characterized by full continuity achieved at a low phase concentration, a wide composition range for maintaining the co-continuous region and little phase size change with increasing phase concentration. For incompatible binary blends, such as HDPE/PS with an interfacial tension of 5.6 mN/m, the droplet lifetime is much longer than the thread lifetime (Fig. 2.17b). So the dispersed phase demonstrates a droplet morphology at low concentrations and the continuity develops by a droplet-droplet coalescence mechanism. The main features for this system would include full continuity at high phase concentration, a narrow composition range for the co-continuous region and significant phase size change with increasing phase concentration.

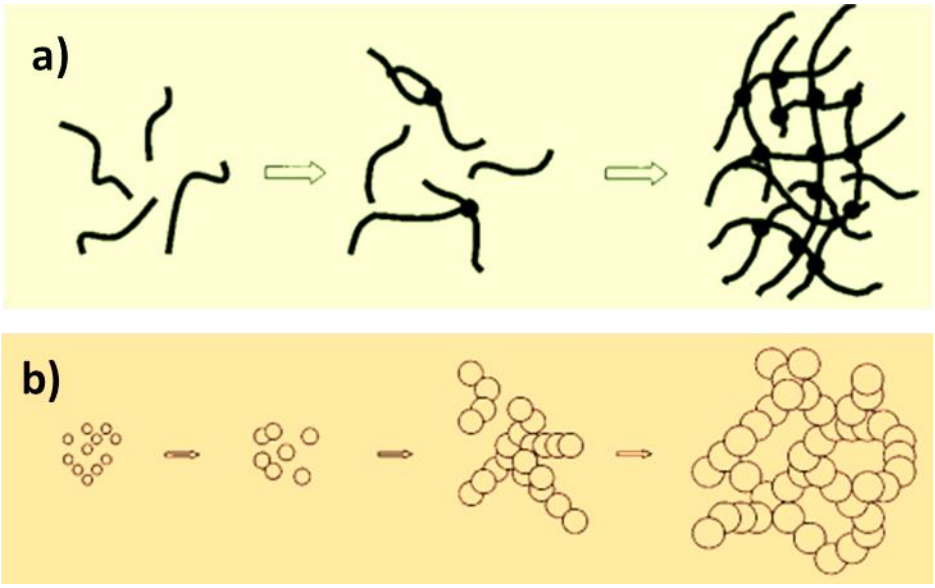

Figure 2.17: Mechanism for morphology development in systems of low interfacial tension (a) and high interfacial tension (b) (taken from Ref.[74]).

2.5.2.2 Factors Controlling the Morphology Development

The understanding related to controlling the morphology in binary immiscible polymer blends by different parameters has been well advanced in the past few decades. **Interfacial tension** is probably the most important factor in controlling the morphology in polymer blends. As discussed above, a low interfacial tension tends to result in fibrous domains of fine phase size and the co-continuous morphology forms at low concentrations owing to the thread-thread coalescence mechanism [74, 75, 81]. However, in high interfacial tension systems, the morphology of the minor phase is dominated by spherical droplets and the co-continuity is attained by droplet-droplet coalescence which leads to a high percolation threshold. **Viscosity (ratio)** is another important parameter to control the continuity. According to the estimation of thread breakup time from Elemans et al. [82], high matrix viscosity and viscosity ratio (giving a small value of the Tomotika function Ω) tend to stabilize the fibrous structure formed during melt blending with long thread breakup time, and thus lead to a higher continuity. Note that the viscosity ratio is defined as the ratio of the viscosity of the dispersed phase to the viscosity of the matrix. This tendency is consistent well with the results reported by Omonov et al. where the continuity of different blends of polypropylene/polystyrene is examined [83]. In highly compatible systems, however, the viscosity effect on continuity was found to be diminished [75].

A classic work on the **elasticity** effect was carried out by Van Oene and an effective interfacial tension was proposed by taking the second normal stress of the components into account [84]. The work showed that the phase with higher elasticity tends to encapsulate the one with lower elasticity. Bourry and Favis also found that models based on storage modulus and tanδ were able to predict the phase inversion well in a PE/PS blend system [85]. The role of **shear stress** on the dispersed phase size in Newtonian systems is described in Taylor's theory [71, 72] where the phase size is inversely proportional to the shear stress. However, in polymer blend systems, little effect on the phase size was observed by changing the shear stress by a factor of two to three [77, 86]. In another study, increasing shear stress was shown to be effective to change the spherical dispersed phase to fibrous structures [87].

2.5.3 Morphologies of Multiphase Polymer Blend Systems

2.5.3.1 Models for Morphology Prediction in Multiphase Systems

1) Harkins' Spreading Theory

In the 1920s, Harkins and Feldman proposed a model to predict spreading or non-spreading of a liquid *b* drop on a liquid *a* surface which simply considers the free energy decrease λ (*i.e.*, the spreading coefficient) [24]:

$$\lambda = \gamma_a - (\gamma_b + \gamma_{ab})$$

where γ_a, γ_b, and γ_{ab} represent the surface free energy of phase *a*, surface free energy of phase *b* and the free energy of the *a*/*b* interface. Clearly, phase *b* will spread on phase *a* if $S > 0$. Later, Torza and Mason used a similar concept to predict the equilibrium configuration when two immiscible liquid droplets are brought into contact in a third liquid matrix based on the interfacial tensions of the three components [25, 88]. It should be mentioned that although their model uses interfacial tension, it yields the same results as using the concept of minimizing surface free energy [25]. Hobbs *et al*. first applied Harkins' equation (directly based on interfacial tension) to predict the morphology in multiphase polymer blends [89]. In a ternary blend system, as schematically shown in Fig. 2.18, the model defines three spreading coefficients based on the three interfacial tensions of different polymer pairs. If one spreading coefficient is positive, complete wetting (two phase contact) tends to occur where A is exclusively located within either C or B, or forms a layer fully separating the B/C interface (Fig. 2.18a–c). In the case of three

negative spreading coefficients, phase A will preferentially arrange into droplets and partially wet (three phase contact) the B/C interface (Fig. 2.18d). Harkins' spreading theory has been the most widely used model to predict the morphologies in ternary polymer blends and normally presents good agreement with the experimental results [11, 12, 14, 27, 28, 90-92].

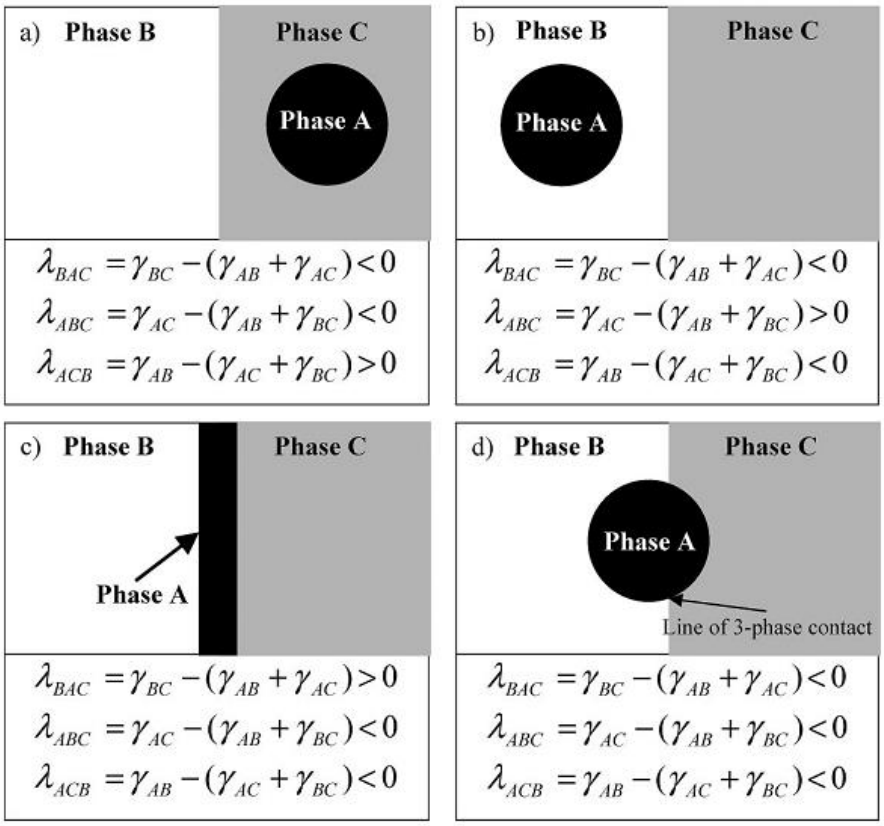

Figure 2.18: Possible morphologies in a ternary blend of A/B/C as predicted by Harkins' spreading theory (A is the minor phase). (a)-(c): complete wetting, one phase fully separate the rest two; (d) partial wetting, three phase contact (taken from [28]).

In all types of morphologies shown in Fig. 2.18, case (c) is of particular interest in reducing the percolation threshold. Zhang et al. studied HDPE/PS/PMMA ternary blends where PS formed thin layers and completely wet the HDPE/PMMA interface (Fig. 2.19) [11]. In that system, almost 70% of continuity was obtained for PS at a volume fraction of only 3%. In another study, it was reported that the minimum PS layer thickness to completely segregate PMMA from HDPE is close to two times of the radius of gyration of PS (about 40 nm) [27].

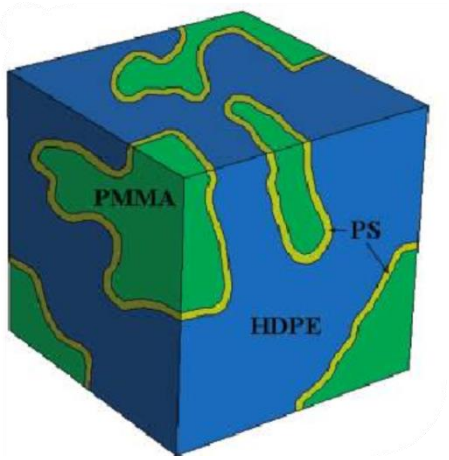

Figure 2.19: Three-dimensional schematic representation of the multiple percolated structures in the ternary HDPE/PS/PMMA system: thin PS layer is at the HDPE/PMMA interface (taken from Ref. [11]).

In addition to the four morphological states presented in Fig. 2.18, some studies also indicate the possible existence of a boundary region between partial wetting and complete wetting. Horiuchi *et al*. studied two ternary systems PA6/SEBS/PC and PA6/PS/PC compatibilized by SEBA-g-MA (maleated SEBS) and PS-g-MA (maleated PS) through interfacial reaction [13]. They found that the encapsulation of PC by SEBS in the PA6 matrix was facilitated by gradually substituting SEBS with SEBA-MA, but a full encapsulation was achieved when only SEBS-MA was used alone (Fig. 2.20a). However, in the case of the PA6/PS/PC system, PC can be fully engulfed even when the weight ratio of PS/PS-MA is 7/3. They attributed the results to the difference in the interfacial reactivity of the two systems. A similar partial encapsulation phenomenon was also reported by Wilkinson et al. in the PP/PA6/(SEBS/SEBS-MA) system [12]. The dispersed PA6 phase is partially engulfed by SEBS/SEBS-MA (75/25), resulting in an "acorn-type" morphology. It was argued that the system was in the intermediate region between partial wetting and complete wetting (the spreading coefficient is approximately 0), and therefore the interface of PP/PA6 was only partially separated. Virgilio reported the morphology of two partially wet ternary blends of HDPE/PS/PP ($\lambda_{HDPE/PS/PP} = -6.5 \pm 1.3$ mN/m) and PP/PS/PCL ($\lambda_{PP/PS/PCL} = -0.1 \pm 1.8$ mN/m) with annealing (Fig. 2.20b) [93]. It appears that the shape of the PS droplets depends on the value of the spreading coefficient. When the coefficient is closer to 0 (e.g., in PP/PS/PCL system), the PS droplets are more extended at the interface. In the classic work of

Harkins and Feldman, a monomolecular layer seemed to form only with a high positive spreading coefficient, while a thick permanent sheet was observed for systems with low positive spreading coefficients [24]. These results imply the spreading of the intermediate phase would be greatly influenced by the value of the spreading coefficient.

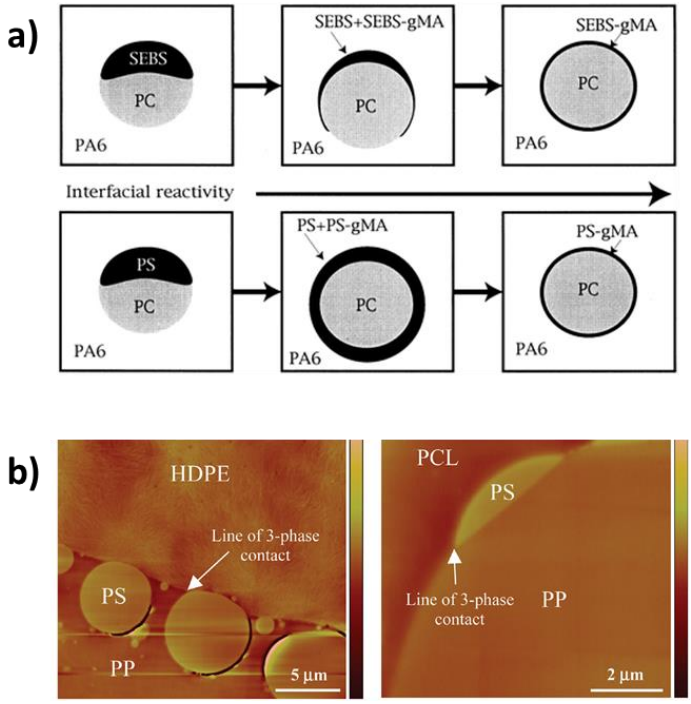

Figure 2.20: (a) Different morphology evolution patterns in PA6/SEBS/PC and PA6/PS/PC after adding SEBS-MA and PS-MA respectively (which gradually replace SEBS and PS in the two systems) as interfacial modifiers (taken from Ref. [13]). (b) Morphologies of the annealed HDPE/PS/PP and PP/PS/PCL blends (taken from Ref. [93]). PS droplets appear more spherical in the former and more extended along the PP/PCL interface in the latter.

The morphology predication is more complicated for systems with more than three components. In quaternary blends, for example, there are four sets of spreading coefficients related to the four possible ternary system combinations. Virgilio and Favis showed in the HDPE/PP/PS/PMMA system that the morphology configuration respects all four sets of spreading coefficients (Figs. 2.21a and b) [94]. The spreading coefficients predict complete wetting for HDPE/PS/PMMA and HDPE/PP/PMMA, indicating the interface of HDPE/PMMA in the two cases tends to be separated by PS and PP respectively. PP/PS/PMMA and HDPE/PP/PS are partially wet systems, and thus lines of three phase contact are expected in both systems. All those morphological

features predicted in the ternary systems are observed in the quaternary HDPE/PP/PS/PMMA blend. In another study, Hobbs *et al*. showed that although both polycarbonate (PC) and poly(styrene-co-acrylonitrile) (SAN) tend to completely segregate the PS from polybutylene terephthalate (PBT) due to the positive spreading coefficients ($\lambda_{PBT/PC/PS}$ = 0.73 mN/m and $\lambda_{PBT/SAN/PS}$ = 1.8 mN/m), in the PBT/PC/SAN/PS quaternary blend, neither PC nor SAN was found to fully engulf the PS phase (Fig. 2.21c) [89]. Instead, PC and SAN form alternating domains surrounding PS within the PBT matrix. The resulting morphology was attributed to the competition between PC and SAN to completely wet the PS phase. However, the observation could also indicate that the morphology of quaternary blends may not necessarily respect all the four sets of spreading coefficients.

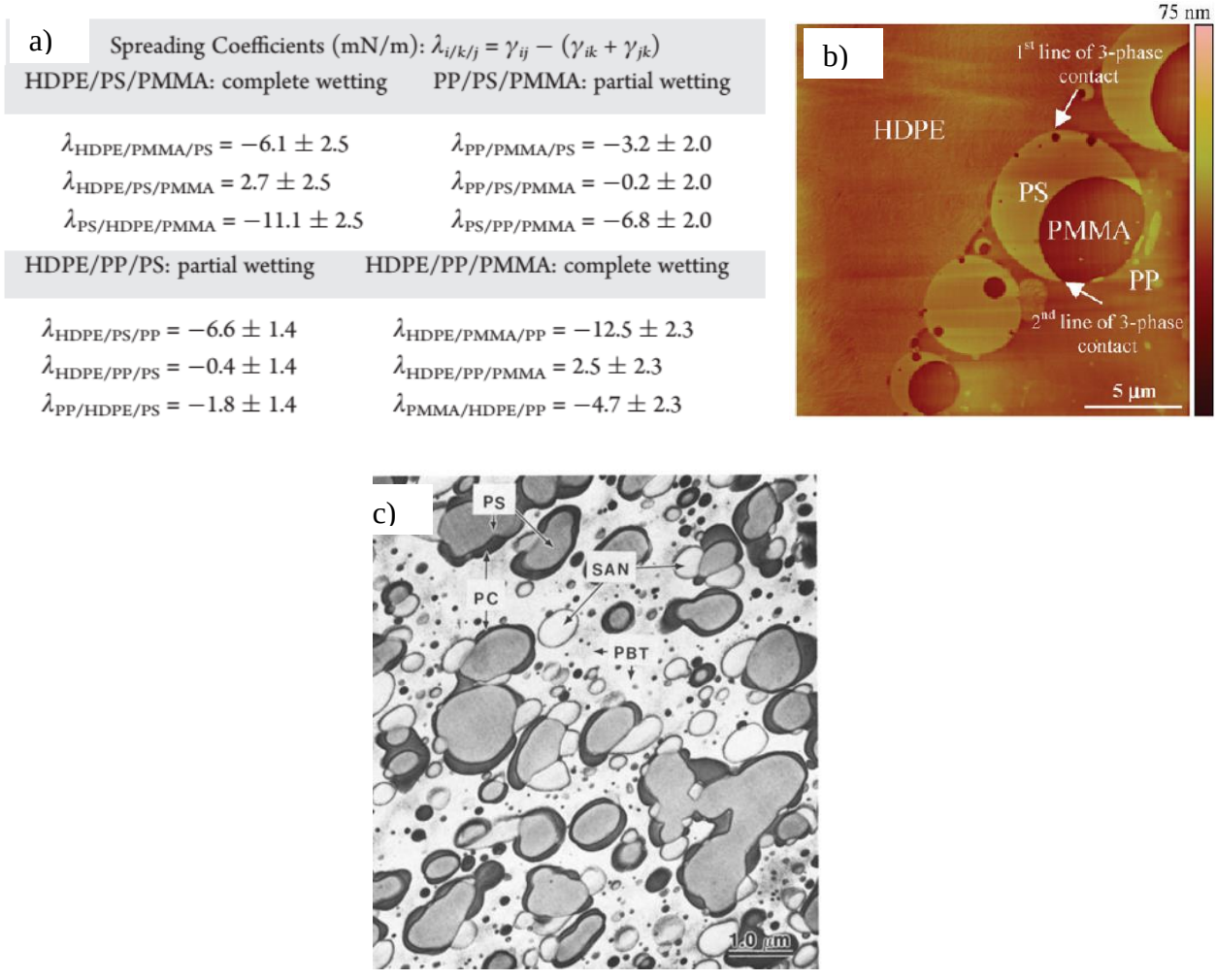

Figure 2.21: (a) Four sets of spreading coefficients of the quaternary HDPE/PP/PS/PMMA blend. (b) AFM image of the HDPE/PP/PS/PMMA (45/45/5/5) blend after 30 min of annealing; the

lines of three phase contact for HDPE/PS/PP and PP/PS/PMMA are indicated by arrows (taken from Ref. [94]). (c) TEM image of PBT/PS/SAN/PC (taken from Ref. [89]).

2) Lowest Free Energy Model

Guo *et al*. argued that the morphology in multiphase polymer blends depends on both the interfacial tension and interfacial area; the most stable morphology would be the case that has the lowest free energy [95]. The model considers three possible structures for a system comprised of a matrix A and two dispersed phases B and C (Fig. 2.22): (1) B and C are separated by A (B+C); (2) C is encapsulated by B (B/C); and (3) B is engulfed by C (C/B). For any multiphase polymer system, the Gibbs free energy *G* can be written as:

$$G = \sum_i n_i \mu_i + \sum_{i \neq j} A_i \gamma_{ij}$$

where n_i and μ_i are the number of moles and chemical potential of phase *i respectively*; *A* is the interfacial area; γ is the interfacial tension between phase *i* and *j*. As the first term is the same for all possible morphologies, only the second term (interfacial free energy) in the equation is considered. The interfacial free energy of the possible morphologies shown in Fig. 2.22 can be calculated using the following equations:

$$\left(\Sigma A_i \gamma_{ij}\right)_{B+C} = (4\pi)^{1/3}\left[n_B^{1/3} x^{2/3} \gamma_{AB} + n_C^{1/3} \gamma_{AC}\right](3V_C)^{2/3}$$

$$\left(\Sigma A_i \gamma_{ij}\right)_{B/C} = (4\pi)^{1/3}\left[n_B^{1/3}(1+x)^{2/3} \gamma_{AB} + n_C^{1/3} \gamma_{BC}\right] \times (3V_C)^{2/3}$$

$$\left(\Sigma A_i \gamma_{ij}\right)_{C/B} = (4\pi)^{1/3}\left[n_B^{1/3} x^{2/3} \gamma_{BC} + n_C^{1/3}(1+x)^{2/3} \gamma_{AC}\right] \times (3V_C)^{2/3}$$

where *x* is the volume ratio of phase B to phase C; n_B and n_C are the number of particles for phase B and phase C. This model has also been extended to quaternary systems [96]. The authors claimed that the morphology predicted by the model agrees with the experimental results in the blends of HDPE/PP/PS and HDPE/PS/PMMA. Although this model has also been used in many other studies [14, 92], one limitation is that it does not account for the case of partial wetting which is clearly demonstrated in many polymer blend systems [29, 89, 93].

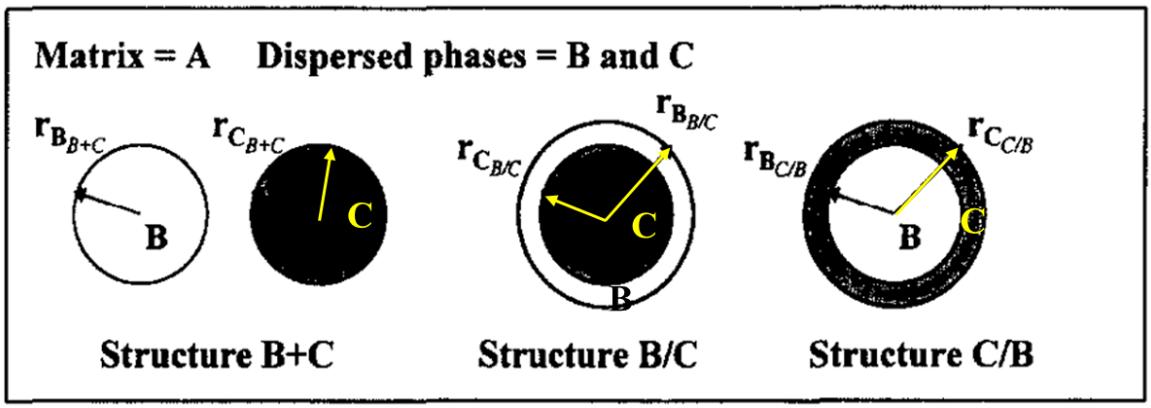

Figure 2.22: Three possible morphologies of a ternary system with a matrix A and two dispersed phases B and C (taken from Ref. [95]). B+C: phase B and phase C are separated by the matrix A; B/C: phase C is encapsulated by phase B in the matrix A; C/B: phase B is encapsulated by phase C in the matrix A.

2.5.3.2 Other Factors Affecting the Morphology in Multiphase Polymer Systems

The general good agreement between the experimental results and theoretical prediction from the two models discussed above implies that the morphology in multiphase polymer blends is dominated by the thermodynamics of the system. However, the effect of kinetic factors, such as the viscoelasticity of the component, has also been studied.

Le Corroller and Favis showed in the PE/PP/PS partial wetting system that much more PS droplets were present at the PE/PP interface when the PE phase possesses a higher viscosity [97]. The phenomenon was explained by the higher PE/PP interface mobility during annealing when low-viscosity PE was used, which facilitated the PS droplet disengagement from the interface. However, this tendency was only observed when the thermodynamic forces to drive PS to the interface is low ($\lambda_{PE/PP/PS}$ is close to zero in PE/PP/PS; note that if $\lambda_{PE/PP/PS} > 0$, PS would tend to be encapsulated by PP rather than be located at the interface). In the PE/PP/PC ternary system, the viscosity effect appears to vanish owing to the strong driving force for PC to migrate to the PE/PP interface (all the three spreading coefficients are less than –1 mN/m). Nemirovski *et al.* studied several immiscible ternary blends and argued that the spreading of the intermediate phase in completely wet systems should be facilitated by a low engulfing-to-engulfed viscosity ratio [98]. Other studies however, found little influence of viscosity on the polymer blend morphology [99, 100].

The effect of elasticity on the morphology of multiphase polymer blends was also reported. In HDPE/PS/PMMA blends, it is thermodynamically predicted that PS tends to fully engulf PMMA in the HDPE matrix. However, Reignier *et al*. obtained different wetting behaviours of either PS encapsulating PMMA or PMMA encapsulating PS depending on the molecular weight of the components (Fig. 2.23) [91]. Upon annealing, the morphology resumed the situation that PMMA is encapsulated by PS in all cases. The authors further developed a conceptual model by considering the elasticity contribution on interfacial tension in the dynamic mixing state (dynamic interfacial tension defined by Van Oene [84]), which was able to account for all the observed morphologies.

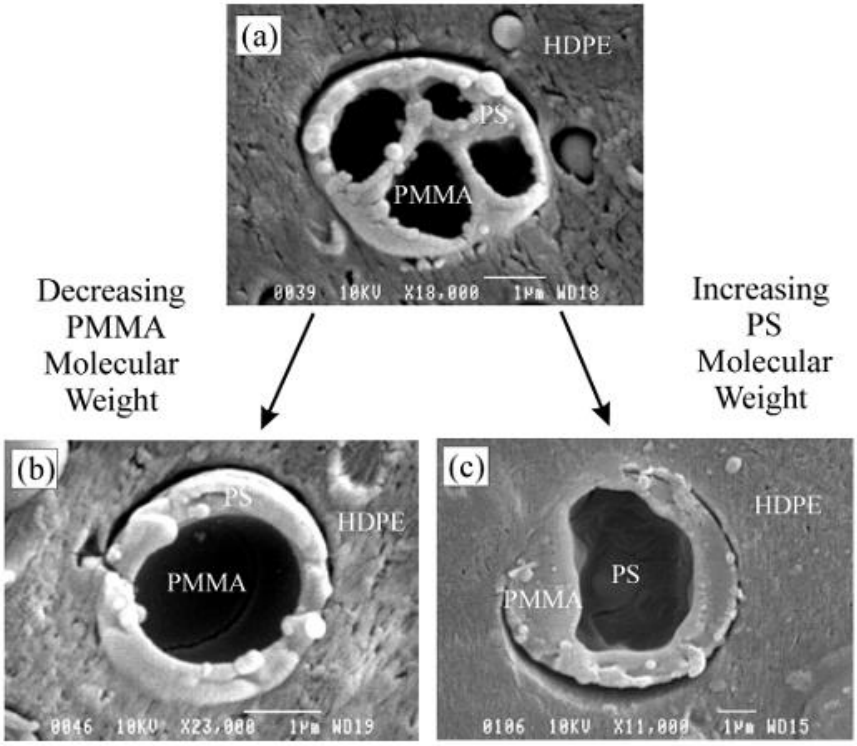

Figure 2.23: Effect of molecular weight on the morphology in ternary HDPE/PS/PMMA blends. (a) and (b): PMMA is encapsulated by PS (PMMA was extracted); (c) PS is engulfed by PMMA (PS was extracted) (taken from Ref. [91]).

2.5.3.3 Controlling Phase Localization in Multiphase Polymer Blends

In multiphase polymer blends, the phases arrange in a certain order determined mainly by interfacial tension. Therefore, the phase location in multiphase polymer systems can be tuned by controlling the interfacial tension between the components (the new morphology can be predicted

using the models discussed in Section 2.5.2.1 with the modified interfacial tension). Guo *et al*. studied the effect of interfacial modification on the morphology of a HDPE/PP/PS (70/20/10) ternary system [95]. Before modification, the PS phase is primarily located within the PP phase (Fig. 2.24a). By adding 1% SEB, the PS droplets were exclusively excluded from the PP phase (drawn to the HDPE phase and the HDPE/PP interface) due to the reduction of the HDPE/PS interfacial tension (Fig. 2.24b). Virgilio *et al*. studied a similar SEB modified HDPE/PP/PS system with annealing and they demonstrated that, by varying the interfacial tension through interfacial modification, it is possible to localize the PS droplets at the HDPE/PP interface towards the PP side, at the HDPE/PP interface toward the HDPE side, or completely within the HDPE phase [28].

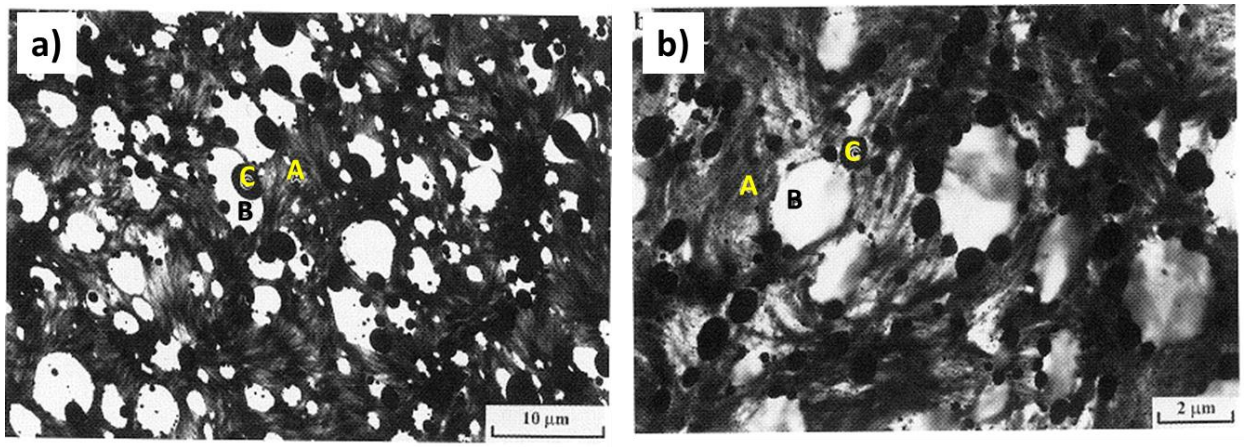

Figure 2.24: Morphology of the ternary blend of HDPE/PP/PS (70/20/10): (a) without SEB; (b) with 1% SEB. Polymer phases: A–HDPE, B–PP, and C–PS (taken from Ref. [95]).

2.6 Conductive Polymer Blends with Multiple Percolation

Multiple percolation refers to hierarchical structures where connected pathways are found within another level of connected pathways [101]. In conductive systems with n (n > 1) levels of percolation and where the conductive phase is located at the last level, the percolation threshold (φ) may be expressed as:

$$\varphi = \varphi_c \cdot \varphi_{n-1} \cdot \varphi_{n-2} \cdots \varphi_2 \cdot \varphi_1$$

where φ_c is the percolation threshold of the conductive phase in phase (*n-1*), and φ_{i-1} is the percolation threshold of the conductive phase (*i-1*) in phase (*i-2*). Since φ_{i-1}< 1, the percolation

threshold of the conductive phase will theoretically decrease with an increasing number of components present in the system as long as the hierarchical structures are preserved.

Zilberman et al. reported a PS/PA/PANI ternary system with double percolation structures where percolated PANI is located within the percolated PA phase in the PS matrix [16]. Segregation of PANI from PS resulted in a higher effective composition (as compared to the nominal PANI composition in the blends) for PANI to develop conductive pathways in the PA phase. At an appropriate PA composition, a conductivity as high as 10^{-4} S/cm was achieved with 10% of PANI in the ternary blends, while the conductivity obtained in the related binary blends of PS/PANI and PA/PANI were much lower (10^{-14} S/cm and 10^{-11} S/cm respectively). Ravati and Favis studied a series of hierarchically ordered multi-percolated polymer blends with PANI [15]. Complete wetting was obtained in all cases and the PANI phase was always located in the core of the system. By increasing the number of the components from 3 to 5, the conductivity was significantly increased from 10^{-11} to 10^{-6} S/cm with 5% PANI.

Kobayashi and coworkers reported several ternary polymer blend systems with ionic conductive poly(ether esteramide) (PEEA) for antistatic applications [6, 52, 102-104]. In the PET/PEEA/ionomer blends (ionomer: poly(ethylene-co-methacrylic acid) neutralized by lithium, magnesium, zinc or sodium), it was found that the ionomer was encapsulated by PEEA in the PET matrix [6, 52]. The antistatic performances were improved (characterized by lower surface/volume resistivity and faster surface charge decay) in the ternary systems as compared to the binary blends of PET/PEEA. The result was attributed to the increase in the surface area of PEEA due to the encapsulation of the ionomer by PEEA. In the following studies, they found that adding poly(ethylene glycol) bis(2-ethylhexanoate) (PEG-EH) to the poly(trimethylene terephthalate) (PTT)/PEEA blends improved the static decay performance [104]. Since PEG-EH is miscible with PEEA, after blending, it goes to the PEEA phase and decreases the Tg of PEEA (acts as a plasticizer), and thus enhances ion mobility in the PEEA domains. However, when polycarbonate (PC) is introduced to the PTT/PEEA system, the miscibility between PC and PEEA results in a higher Tg for PEEA and a consequent lower chain mobility, which leads to reduced static decay performances for the blends [103].

2.7 Conductive Polymer Composites: Controlling the Localization of the Fillers

A general discussion on conductive polymer composite systems has been provided in Section 2.1.1. In this part, we will review the recent progress on controlling the conductivity/resistivity of the composite systems by selective localization of conductive fillers in polymer blends.

At thermodynamic equilibrium, the localization of solid particles in a polymer blend system can be predicted by Young's Equation (or the wetting parameter ω) defined as follows [105]:

$$\omega = \frac{\gamma_{1s} - \gamma_{2s}}{\gamma_{12}}$$

where γ_{1s} and γ_{2s} are the interfacial tensions of polymer 1/solid particle and polymer 2/solid particle respectively; γ_{12} is the interfacial tension of polymer 1/polymer 2. Fig. 2.25 presents the three possible localizations of the solid particle depending on the value of ω: (a) within Phase 2, (b) at the interface of Phase 1 and Phase 2, and (c) within Phase 1.

Figure 2.25: The localization of solid particles in polymer blends predicted by Young's Equation. (a): within Phase 2 when $\omega > 1$; (b) at the interface when $-1 < \omega < 1$; (c) within Phase 1 when $\omega < -1$ (taken from Ref. [106]).

Many studies have shown that the percolation threshold can be significantly reduced by confining the conductive filler within one phase, or more preferentially at the interface, of a co-continuous polymer blend system. Gubbels et al. reported on the localization of carbon black (CB) both within the PE phase and at the interface of the PE/PS binary blend [18]. They first mixed carbon black with PS which has less affinity with the filler and then added the PE phase. During melt blending, the carbon black is thermodynamically driven to the PE phase by accumulating at and finally crossing the interface. By controlling the mixing time, the carbon black can be confined at the interface or within the PE phase. They showed that the percolation threshold can be reduced

to 3 wt% or 0.4 wt% when the carbon black is localized within the PE phase, or at the interface, in the binary blend while 5 wt% of the conductive filler is needed for percolation when it is dispersed only in a PE matrix (Fig. 2.26). However, despite the very low percolation threshold, the localization of the carbon black at the interface was achieved by kinetic control and the morphology is thus not stable. In a later study, the carbon black was oxidized by HNO_3 in an attempt to thermodynamically confine the particles at the interface [19]. But only limited success was achieved which was attributed to the nonuniformity of the particle surface properties after modification.

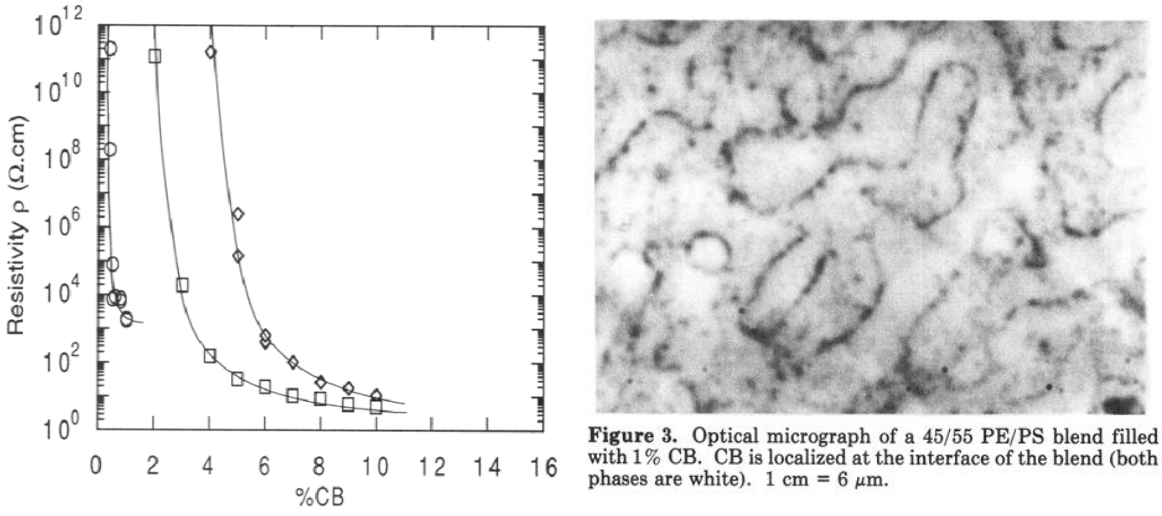

Figure 2.26: Effect of selective localization on the resistivity in the PE/PS/CB (45/55/X) blends as compared to the PE/CB blends (left image): PE/CB (◊); CB in PE phase in the PE/PS/CB system (□); CB at the interface of the PE/PS in PE/PS/CB system (○). Optical micrograph of PE/PS/CB (45/55/1) where CB is confined at the PE/PS interface (right image) (taken from Ref. [18]).

Carbon nanotubes (CNTs) can present an even lower percolation threshold owing to their higher aspect ratio. However, the high aspect ratio also makes the selective localization of CNTs at the interface of polymer blends a great challenge since even a minor surface energy difference between the polymers can drive the particles to one of the phases [107]. Recently, some studies have utilized the complete wetting morphology in ternary blends (Fig. 2.18c) to circumvent the challenge of localizing high aspect ratio materials at the polymer interface. A general schematic representation of this approach is presented in Fig. 2.27. Zhao et al. grafted PMMA onto carbon nanotubes (CNTs) and added them to a ternary blend of PS/PMMA/PVDF (70/10/20) where

PMMA forms a layer of ~ 1 μm thickness and completely engulfs the PVD phase [26]. The surface modification of CNTs led to the thermodynamic localization of the CNTs in the thin PMMA layer and the CNT conductive pathways were thus constructed within an environment similar to the polymer interface. With this approach, a percolation threshold as low as 0.3 wt% for CNTs was obtained. Cohen et al. used a similar method to confine CNTs within the modified poly(ethylene-co-methacrylic acid) (mEMAA) phase which was situated between the co-continuous PA and PP phases [23]. The volume resistivity in this case was shown to be much lower than that of the PA/PP/carbon nanotube system where the CNTs are confined within the PA phase. They also suggested that using a low-viscosity EMAA facilitates the formation of the continuous EMAA intermediate phase between PA and PP. Chen et al. localized CNTs at the interface of polycarbonate/acrylonitrile-butadiene-styrene (PC/ABS) by introducing a compatibilizer (maleic anhydride grafted ABS, MA-g-ABS) for PC and ABS, which, at the same time, shows the strongest interaction with the CNTs [22]. Using this strategy, CNTs can be driven to the interface of PC and ABS and an ultra-low percolation threshold of 0.05 wt% was obtained in their system, significantly lower than the value of 0.25 wt% when CNTs were located within PC or ABS. These studies demonstrate the significance of reducing the percolation threshold by confining the conductive component at the percolated polymer interface.

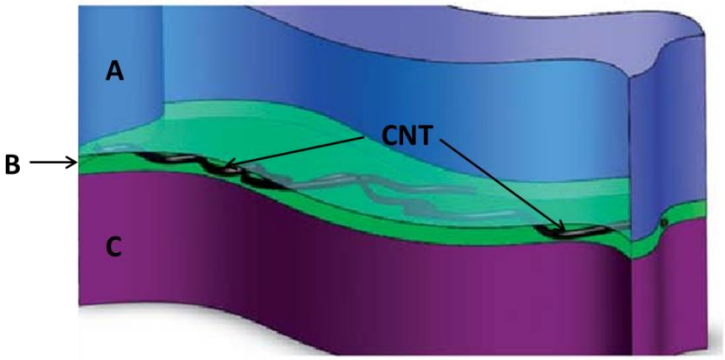

Figure 2.27: Schematic representation of confining CNT at the interface by a completely wet A/B/C system. B forms a thin layer at the percolated/continuous A/C interface. CNT has the highest affinity with the B phase among the three components in the ternary blend (taken from [22])

2.8 Summary of Literature Review and Objectives

Previous studies with conductive polymers have shown that much lower resistivity can be obtained in multiphase polymer systems as compared to traditional binary blends [15-17]. However, in almost all the work published on the melt processing of conductive polymer blends, the conductive component is situated in the core and is encapsulated by other polymers [6, 15-17]. This can limit its capacity to reduce resistivity as compared to situating it at the interface. Meanwhile, in a ternary polymer system, the intermediate phase at the interface can adopt either a complete layer or a droplet morphology depending on the spreading coefficients [24, 25]. To date, very little work has been reported on the morphology development of the intermediate phase and its influence on resistivity in melt polymer blends.

Considering all the aforementioned contents, the objectives of this work are presented as follows:

Main objective

Reduce the electrical percolation threshold of PEBA for antistatic applications through the control of morphology in multiphase polymer blend systems.

Specific objective

1. Study the effect of continuity and morphology on the surface resistivity of the PEBA binary blends. Identify the key parameter(s) to control the surface resistivity of the blends.
2. Assemble PEBA at the continuous interface in completely and partially wet ternary polymer blends and study the morphology development and its effect on the surface resistivity.
3. Develop strategies to control the localization of PEBA (in the core or at the interface) in multiphase polymer systems and investigate its influence on the morphology and surface resistivity of the systems.

CHAPTER 3 ORGANIZATION OF ARTICLES

Based on the specific objectives and the results obtained during the project, four articles are prepared and will be presented in CHAPTER 4–6 as well as in APPENDIX.

CHAPTER 4 presents the first article entitled “Continuity, Morphology and Surface Resistivity in Binary Blends of Poly(ether-block-amide) with Polyethylene and Polystyrene”. In that paper, we prepared two binary blend systems of LDPE/PEBA and PS/PEBA with distinct interfacial tensions and examined the effect of continuity, morphology and other possible factors on the surface resistivity of the blends. A frozen capillary instability morphology was observed in the PS/PEBA blends. Finally, the charge dissipation mechanism in PEBA was also discussed.

The second article is entitled “Assembling Conductive PEBA Copolymer at the Continuous Interface in Ternary Polymer Systems: Morphology and Resistivity”. In the study, the PEBA copolymer was thermodynamically assembled at the continuous interface in two systems demonstrating partial wetting (LDPE/PEBA/PET) and complete wetting (LDPE/PEBA/PVDF) respectively. The spreading coefficients of the two systems were determined and used to predict the morphology of PEBA at the interface. We observed a novel morphology transition from partial wetting to complete wetting in the LDPE/PEBA/PET system and proposed a model to explain this phenomenon. The formation of complete layers in completely wet systems was also discussed. These results are presented in CHAPTER 5.

The third article entitled “Controlling the Hierarchical Structuring of Conductive PEBA in Ternary and Quaternary Blends” is presented in CHAPTER 6. As demonstrated in the second article, confining conductive polymers at the continuous interface possesses a great advantage in reducing the percolation threshold. Thus, in the third part of the project, we examined approaches to control the localization of PEBA in multi-percolated polymer blend systems, in particular, with high commodity polymer content (70–90%). Starting with ternary LDPE/PS/PEBA blends where PEBA is located in the core, we demonstrated two strategies to move the PEBA phase to the continuous interface: adding a fourth component which forms a continuous phase (quaternary blends) or introducing a small amount of interfacial modifier. The PEBA localization, morphology development and surface resistivity of the blends were studied in these two scenarios.

Finally, in the APPENDIX, the fourth article entitled “Hierarchically Porous Polymeric Materials from Ternary Polymer Blends” is presented. Utilizing the hierarchical structures in co-continuous

ternary polymer blends, we reported a new strategy to generate hierarchically porous polymers with controllable pore size through an A/B/C-B-C system. PLA/HDPE/SEBS was used as a model system where SEBS forms very fine structures located within the HDPE phase owing to the low interfacial tension between SEBS and HDPE. Hierarchically porous polymeric materials were thus generated by selectively removing the PLA and SEBS phases. Annealing and compositional variation were further employed to control the pore size independently.

CHAPTER 4 ARTICLE 1: CONTINUITY, MORPHOLOGY AND SURFACE RESISTIVITY IN BINARY BLENDS OF POLY(ETHER-BLOCK-AMIDE) WITH POLYETHYLENE AND POLYSTYRENE*

Jun Wang [a], Alejandra Reyna-Valencia [b], Basil D. Favis [a]

[a] *CREPEC, Department of Chemical Engineering, École Polytechnique de Montréal, Montréal, Québec, H3T 1J4, Canada*

[b] *Laboratoire d'étude des matériaux (LEM), Arkema-CERDATO, Serquigny, 27470, France*

4.1 Abstract

Binary blends of low-density polyethylene (LDPE)/poly(ether-block-amide) (PEBA) and polystyrene (PS)/PEBA were prepared by melt blending. The interfacial tension of the blends was measured by the breaking thread method with a value of 8.0 mN/m for LDPE/PEBA and 1.6 mN/m for PS/PEBA. The modulated DSC results show a partial miscibility between PS and PEBA at low PEBA concentrations. The continuity development in the LDPE/PEBA blend follows a droplet-droplet coalescence mechanism typically present in the high interfacial systems. However, in the case of the low interfacial tension PS/PEBA blend, a frozen capillary instability morphology was observed for the first time and a new continuity development mechanism was proposed. The continuity and morphology of the blends, and their effect on surface resistivity was examined. Our results indicate that although the continuity is crucial to controlling surface resistivity, other factors, such as the morphology (tortuosity and constriction) and interfacial properties also play an important role. A conceptual model to describe the charge dissipation is presented.

Key words: *inherently dissipative polymers, poly(ether-block-amide), antistatic polymer blends, partial miscibility, continuity, morphology, phase size, interfacial properties, surface resistivity, charge dissipation.*

---

* Submitted to *Polymer*.

4.2 Introduction

The electrostatic properties of polymers and particularly surface charge accumulation can have a significant impact on a wide range of application fields including electronics, packaging and automotive. Static electricity and uncontrolled electrostatic discharge can cause many problems including dust attraction, damage to sensitive electronic components and the potential to initiate explosion. In order to be classified as an antistatic material and avoid static charge accumulation, while maintaining the nonconductive nature of the object, the surface resistivity of the polymeric parts generally needs to be reduced to the range of 10^9 ~ 10^{13} Ω/sq [1]. However, most conventional polymers fail to meet this criterion. A number of additives have been developed and added to polymers to tailor the surface resistivity according to different applications. These additives can be divided into three main categories: 1) migrating antistats, usually composed of an amphiphilic surfactant; 2) conductive fillers, such as carbon black and metal powders and; 3) inherently dissipative/conductive polymers (IDPs/ICPs) [2]. IDPs have been particularly effective in providing a precise control on resisitivity and avoiding issues related to long term performance and discoloration. They also display very good processibility, thermal stability and mechanical properties as compared to ICPs.

Poly(ether-block-amide) copolymers (PEBAs) are segmented block copolymers consisting of hard polyamide (PA) blocks and soft polyether blocks [3]. Varying the polyamide/polyether ratio, the physical and mechanical properties can be tailored [4]. When the polyether block is polyethylene oxide (PEO), an inherent charge dissipative capacity is conferred to the copolymer, as in the above-mentioned IDPs. PEBAs represent a main category of IDPs for antistatic applications [3]. When PEBA is blended with a matrix material at the appropriate concentration, it can form a continuous three-dimensional (3D) percolated network thus allowing for charge dissipation. The antistatic properties of the blend clearly depend on the morphology and continuity of the IDP phase.

Continuity development in immiscible binary polymer blends has received significant attention over the last 15 years. When a minor phase is added to an immiscible polymer matrix, dispersed droplets, fibers or lamellar morphologies can be obtained [5]. As the composition of the minor phase increases, the so-called co-continuous morphology develops where both components are fully interconnected throughout the blend. The transition from a dispersed phase/matrix to a co-

continuous morphology is affected by many factors, including interfacial tension, viscosity (ratio), elasticity and shear stress. The final morphology is a balance between phase deformation/disintegration and coalescence [6]. Li *et al*. studied the effect of the interface type on continuous morphology development by considering the lifetime of droplets and threads during melt processing [7]. For a low interfacial tension system (Type I), the lifetime of threads is much longer than droplets and the onset of percolation effects occur at low concentration owing to a thread-thread coalescence mechanism. In a higher interfacial tension system (Type II), the morphology of the minor phase is dominated by spherical droplets and the co-continuity is attained by droplet-droplet coalescence which leads to a high percolation threshold. Other factors such as viscosity ratio and elasticity on co-continuus morphology formation have also been examined [8-12].

The percolated/continuous structure in immiscible polymer blends can be utilized to enhance the properties of conductive polymeric materials. By controlling the composition of the conductive phase in the non-conductive matrix, a series of materials with tailored conductivity can be obtained [13, 14]. The concept has been demonstrated in the early development of conducting polymer blends, typically with polyaniline (PANI). For example, Ikkala et al. blended conducting PANI with various host polymers (PE, polypropylene, PS and polyvinyl chloride) and found that a wide scope of conductivity from 1×10^{-11} to 1×10^{-1} S/cm can be obtained by varying the PANI content. [13] The absolute conductivity values as a function of PANI content in different blends may vary depending on the rheological properties of the matrix polymers and processing conditions.

PEBA copolymers, in particular, have been used for antistatic applications with various host polymers [15-17]. However, very little research has been done to understand the charge dissipative mechanism of the pure material and the effect of PEBA morphology on the antistatic performance after blending with another polymer [1, 18-21]. Wang et al. studied blends of high impact polystyrene (HIPS) and NaSCN doped PEBA and showed that the antistatic ability of the blends originates from the formation of 2D/3D ion-conductive channels of the PEBA phase as its concentration increases [18]. They suggested that the ionic conductivity of the blends depends on both the dynamic motions of the PEO chain motions and the directional migration of charge carriers. The surface resistivity of the blends did not change until reaching 10% of PEBA and they attributed this percolation threshold to a viscosity effect. In another study, a series of PEBA

with different compositions of polyamide and polyether were synthesized and the surface resistivity results showed that the copolymers with higher molecular weight and/or higher composition of the polyether block present better antistatic properties [20]. Fu and coworkers reported on PEBA/poly(acrylonitrile-co-butadiene-co-styrene) antistatic polymer blends and the effect of relatively humidity on the surface resistivity was examined [21]. Strategies to improve the conductivity of IDPs have also been reported where ions are introduced to the system, for example, through chemical fixation of ionic liquids [22], blending with ionomers [1] and doping with salt [18].

No effort to date has been carried out to establish the relationship between the phase continuity of PEBA and the resistivity of the blends. Furthermore, the effect of water content on resistivity and the charge dissipative mechanism in PEBAs are not well understood. PEO is known as an ionic conductive polymer whose conductivity is heavily determined by the chain mobility [23]. When the PEBA copolymer is blended with different host polymers, there are possibilities that some specific interaction (interaction between PEO blocks and the host polymer) exists and (partial) miscibility happens in certain systems, which may change the intrinsic conductivity of the PEBA. Kobayashi *et al*. reported that when polycarbonate (PC) was introduced to a poly(trimethylene terephthalate)/PEBA system, the static decay performances of the blends were reduced [24]. The result was attributed to the miscibility between PC and PEBA, which decreased the chain mobility of PEBA (due to higher Tg) for charge transport.

This study aims to compare two PEBA binary blends of significantly different interfacial tension. The effects of continuity, morphology and interfacial properties on the surface resistivity will be examined. The overall charge dissipative mechanism of the PEBA will also be considered.

4.3 Materials and experimental

4.3.1 Materials

The polyethylene (PE) used in this work is LDPE 1008 from Total. The Pebax® MV1074 is supplied by Arkema and it is a segmented PEBA block copolymer with alternating polyethylene oxide (PEO) (55 wt%) and polyamide 12 (PA12) (45 wt%) blocks. There are 10–20 blocks of each constituent in the copolymer [25]. Polystyrene 615APR was purchased from Dow Chemical.

The additional characteristics of the polymers are provided in Table 4.1. All the materials were dried at 60°C in a vacuum oven for 48 h before use.

Table 4.1: Characteristics of the materials used

Polymers	Mn (g/mol)	Mw (g/mol)	Tm/Tg [d]	Complex viscosity at 25 s^{-1} at 200°C (Pa·s)
PEBA	66100a	134000a	Tm (PA) = 158°C, Tm (PEO) = 9.8°C, Tg = - 55.5°C	210
PS	140900b	289800b	Tg = 98.9°C	1180
LDPE	–	135,000–140,000c	Tm = 111.0°C	1300

[a] GPC data. [b] GPC data obtained from Ref. [26]. [c] Obtained from supplier. [d] Measured by DSC.

4.3.2 Rheology

The disk-shaped samples of the neat polymers were prepared from compression molding and a MCR 501 rheometer was used to examine the rheological properties, all under nitrogen atmosphere. The test was performed with a parallel-plate configuration and a 1 mm gap. The linear viscoelasticity region was first determined by strain sweeps. The oscillation mode (frequency: 1 Hz) was used to evaluate the thermal stability of the raw materials at 200°C for 40 min and little variation was obtained for the complex viscosity (within 3% for all the materials). The frequency sweep was then carried out within the linear viscoelasticity region for all the samples.

4.3.3 Small angle X-ray scattering (SAXS)

The SAXS tests were performed on a Bruker AXS Nanostar system, equipped with a Microfocus Copper Anode (wavelength λ = 0.154 nm) at 45 kV/0.65 mA. A VANTEC 2000 2D detector at a distance of 68.0 cm from the samples was used. Before measurements, the distance was calibrated with a Silver Behenate standard. The samples were characterized with a collection

exposure time of 1000s. The background was subtracted using the Primus GNOM 3.0 program from ATSAS 2.3 software. The approximate peak maxima were determined by Peak software and used to calculate the d-spacing from Bragg's law.

4.3.4 Interfacial tension measurement

The interfacial tensions of PE/PEBA and PS/PEBA were determined by the breaking thread method on an optical microscope (Optiphot-2) with a hot stage. In the case of PE/PEBA, the thread of PEBA was sandwiched by the PE films. In the case of PS/PEBA, PS was used as the thread and PEBA as films. A slow heating rate of 5 °C/min was first applied to increase the temperature of the system to 100°C to reduce the residual stress, followed by a high heating rate of 20–50°C/min to the test temperature of 200°C. The evolution of capillary instabilities along the thread was recorded and the interfacial tension was calculated based on the following equation:

$$\gamma = \frac{q\eta_m D_0}{\Omega_m}$$

where γ is the interfacial tension, q is the growth rate of the distortion, η_m is the matrix viscosity, D_0 is the original thread diameter, and Ω_m is a tabulated function. The test was performed under a N_2 environment to minimize thermal degradation. More details about this technique are reported elsewhere [8, 27].

4.3.5 Differential scanning calorimetry (DSC)

The DSC Q1000 machine (TA Instruments) was used to characterize the thermal behaviours of the samples including the glass transition temperature (Tg) and crystallization. The samples were first maintained at 200°C for 5 min to eliminate the thermal history. For determination of the Tg, the modulated DSC mode was used owing to its high sensitivity for the second-order phase transition and the second heating run was recorded from –90°C to 200°C with a heating rate of 2°C/min. An oscillation period of 60 s and an oscillation amplitude of ±1.27°C were employed in the test. The Tgs were then obtained from the reversible heat flux curves. The crystallization studies were carried out under the standard DSC mode with a cooling rate of 10°C/min. The cell constant and melting peak temperature were calibrated with an empty pan and a standard indium

sample. A standard sapphire sample was used to calibrate the heat capacity. Three repeats were carried out for each sample and errors in the measured Tgs are within ± 0.3°C for PS and ± 0.5°C for PEBA.

4.3.6 Melt blending

The blend samples were prepared in a Brabender internal mixer (Plasti-Corder DDR501) with roller blades at a speed of 50 RPM. The processing was carried out under a N2 blanket at 200°C for 7 min. With the fill factor set at 0.7, the total volume of each blend was 21 mL. For the continuity and morphology examination, the blend samples were quickly collected from the internal mixer after processing and immediately quenched in liquid nitrogen to freeze-in the morphology.

4.3.7 Selective extraction

Selective extraction was performed for different samples to either determine the continuity or improve the contrast for morphology analysis. Formic acid was used to dissolve PEBA at 50°C. For the matrix dissolution experiments, 1 g of the PS/PEBA blend was immersed in 50 mL THF in a centrifuge tube and kept for 2 days under constant shaking. The suspension was then centrifuged at 3000 rpm for 5 min and the solution was then refreshed. The process repeated for four times which was enough to remove the PS phase according to our previous study [7]. In order to extract the LDPE phase, 1 g of the LDPE/PEBA blend was placed in 250 mL of slightly boiled cyclohexane for one week. The solutions were then filtered and the filtrate was washed with hot cyclohexane several times. The resulting PEBA samples were dried for further analysis.

4.3.8 Continuity

In order to determine the continuity of PEBA, selective extraction was performed on the blend samples of 0.5 cm^3 cubes. The weight of the sample was monitored after extraction and drying (at 65°C under vacuum) until a constant value was reached. The continuity of the PEBA phase was calculated from the following equation:

$$\text{Continuity (\%) } of \text{ PEBA} = \frac{m_1 - m_2}{m_0} \times 100\%$$

where m_1 and m_2 is the mass of the sample before and after selective extraction of PEBA, respectively. m_0 represents the original mass of PEBA in the sample.

4.3.9 Morphology and phase size

A Leica microtome (RM2165) equipped with an LN21 cooling system was used to cut the samples for morphology analysis on a JEOL JSM 840 scanning electron microscope (SEM). Prior to SEM analysis, the target phase was selectively extracted to improve the contrast and a gold layer was deposited on the sample with plasma sputtering. A voltage of 2–5 kV was used for SEM observations.

The SEM images were used to measure the number average diameter (Dn) and volume average diameter (Dv) of the PEBA domains at low concentrations (20%). In the LDPE/PEBA blends, the values represent mainly PEBA droplet diameters, while in the case of PS/PEBA, they are the diameters of PEBA fibers. The PEBA phase images were analyzed with a digitizing table from Wacom and SigmaScan v.5 software. The Saltikov correction was performed for the diameter calculation to correct for polydispersity effects and for the fact that the PEBA domains are randomly cut during microtoming [28]. At least 500 droplets from two parallel samples were used to perform the calculations. The PEBA phase sizes with high PEBA concentrations (30%) were examined by mercury intrusion porosimetry (MIP) (AutoPore IV 9500) after extracting the PEBA phase. A contact angle of 140° and a surface tension of 0.485 N/m were applied for the calculation. The area and volume median diameters represent the pore diameters where half of the pore surface and volume is occupied by mercury correspondingly (also termed as Dn and Dv respectively). With three repeats performed for each sample, the experimental error is within 10% in all cases. More information on the MIP test can be found in a previous publication [29].

4.3.10 Surface resistivity preparation and measurement

The blend samples were taken from the Brabender roller blades immediately after processing and quickly transferred to a mold (64 mm × 64 mm × 1mm) for compression molding at 180°C (the mold was preheated at the same temperature). In order to minimize the morphology change, the pressure was increased to 150–200 psi slowly. Note that the reading essentially indicates the pressure exerted on the mold rather than on the sample directly. Afterwards, the sample was quickly cooled down on a cold press. The whole procedure (from termination of blending to

cooling the sample down) was timed to be within 2.5 min. A N_2 flow was used to purge the system during the whole process. Preliminary tests were performed to optimize the pressing conditions by comparing the morphology of the samples before and after hot pressing. With the procedure used here, the morphologies in the blends were well preserved after compression molding. Before the surface resistivity test, all the samples were stored in an environment of 50% RH at room temperature for one week (unless specified) to obtain a constant moisture content. The water content was confirmed using Karl Fisher titration by heating the sample at 170°C for 10 min.

The surface resistivity test was performed on the Keithley Model 6517B Electrometer equipped with the 8009 Resistivity Test Fixture. The surface resistivity was obtained under a DC voltage of 40V after a bias time of 60 s. This setup measures the surface resistivity according to the ASTM D257 Standard. Tow electrodes are attached on the same side of the surface of the sample. The electrical current transports from anode to cathode by penetrating into the sample in between the electrodes. Studies have shown that the current can penetrate to a depth of about 150 μm (Arkema unpublished data). The skins of selected samples were also rubbed out (at least 20 μm) by a polisher (Metaserv 2000) and no significant differences on surface resistivity were observed after the process, indicating the morphologies throughout the samples are uniform.

4.4 Results and discussion

4.4.1 Rheological properties

The rheological properties of the polymers are shown in Fig. 4.1. It can be seen from the figure that the viscosity of PEBA is significantly lower than that of LDPE and PS within the whole range of shear rate examined (Fig. 4.1a). PS also has a lower viscosity than LDPE at low shear rate, but they become very close at high shear rate (angular frequency > 10 rad/s). It should be mentioned that 50 RPM was used for all the blends and the shear rate in our processing is estimated to be around 25 s^{-1} [30]. In this region, LDPE and PS have very close viscosities. The storage and loss modulus of the polymers are also presented in Fig. 4.1b and they follow the same trend as the viscosity. The results indicate that although viscosity and elasticity can potentially be two very important factors in morphology development, they are not expected to be a significant concern in the current system when comparing the morphology of the LDPE/PEBA and PS/PEBA binary blends.

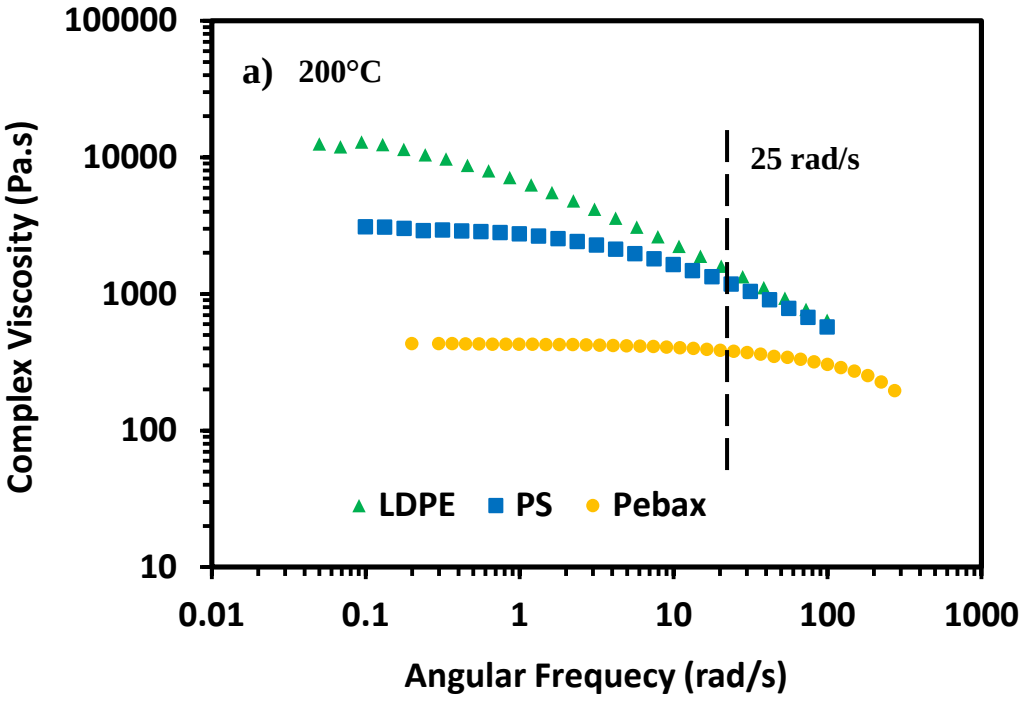

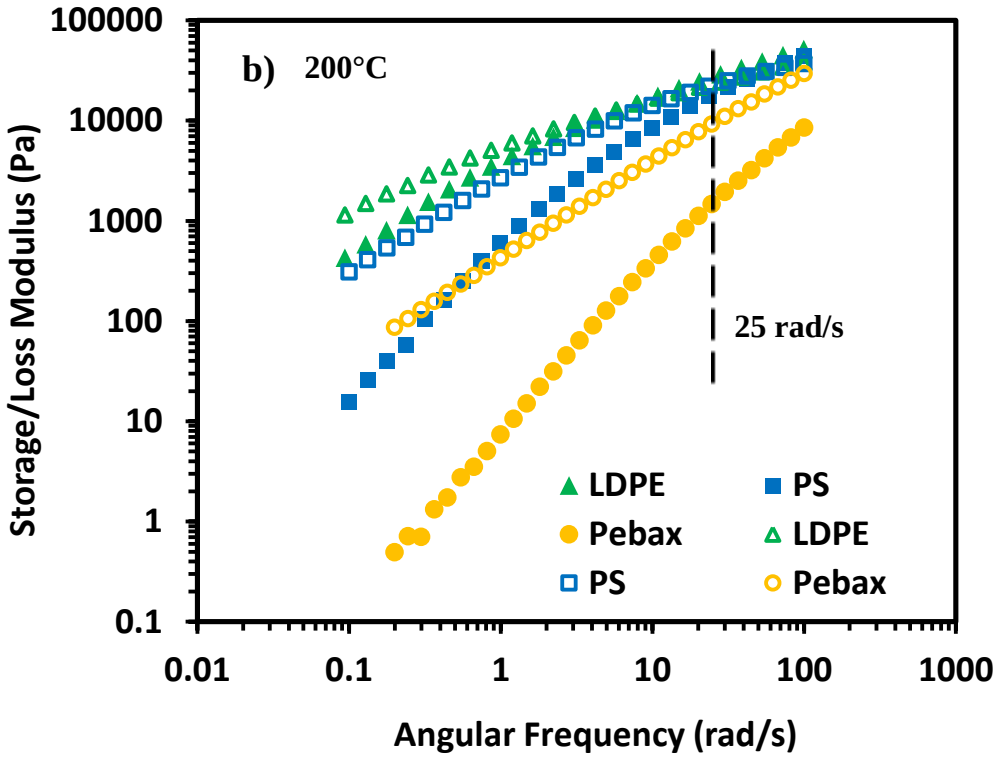

Figure 4.1: (a) Complex viscosity and (b) storage modulus (filled symbols)/loss modulus (open symbols) of the raw materials.

4.4.2 Interfacial tension

The interfacial tension of PE/PEBA and PS/PEBA were measured directly by the breaking thread method and are shown in Table 4.2. It can be seen from the interfacial tension data that PE/PEBA is a highly incompatible system with an interfacial tension of 8.0 mN/m. On the other hand, PS/PEBA has an unexpected low interfacial tension with a value of 1.6 mN/m, indicating a much higher compatibility between the two polymers. The PEBA used in this study is a segmented block copolymer with alternating PEO and PA-12 blocks. Previous work has shown that PS and PA are highly incompatible and their interfacial tension is over 7 mN/m [31, 32]. Clearly the low interfacial tension between PS and PEBA originates from the presence of the PEO block in Pebax. The literature also reports a low interfacial tension of 1 mN/m between PS and PEO [33]. However, these systems have been reported to be immiscible both in solution and bulk [34, 35].

Table 4.2: Interfacial tension between different polymers

Polymer pairs	Interfacial tension γ (mN/m)
PE/PEBA	8.0 ± 1.4 (200°C)
PS/PEBA	1.6 ± 0.2 (200°C)
PS/PA	7.6 (230°C) [31], 7.3 (240°C) [32]
PS/PEO	1.0 (170°C) [33]

4.4.3 Small-angle X-ray scattering (SAXS)/Solid state structure

Since the charge dissipative mechanism is closely related to the solid state structure, it is important to consider the X-ray diffraction of the PEBA copolymer used in this work. Significant research has been carried out to understand the solid-state microstructure of PEBA copolymers[4]. It has been shown that, with different techniques, these copolymers typically possess a microphase separated solid-state microstructure and that the PA segments crystallize in lamellar structures. However, the structural information for the particular PEBA copolymer (MV1074) used in this work is still not clear. The SAXS analysis was thus performed for the copolymer after compression moulding. The $I(q)$ is shown in Fig. 4.2, where I is the scattered intensity and q is the scattering vector modulus ($q = 4\pi sin\theta/\lambda$). Two peaks were detected on the $I(q)$ curve of the

PEBA sample. The long period *d* is determined to be 11.5 nm from the first scattering peak q^* ($d = 2\pi/ q^*$) and a lamellar morphology can be identified since the second peak is present at the position of $2q^*$ (Table 4.3). The layer thicknesses of PA12 and PEO in the lamella structure of the PEBA are estimated to be 5.2 nm and 6.3 nm respectively based on the weight ratio (the densities of PA12 and PEO are close, Table 4.3). A similar estimation was performed on PS-PEO-PS triblock copolymer electrolytes to determine the dimension of the PEO domain and the results corresponds well with the conductivity data [36]. Besides, the domain volume fraction was found to be close to the weight ratio for different PEBA grades by applying a lamellar 1D model [37]. The above results correspond well with the structures of other PEBA grades from previous studies [4, 37]. Barbi et al. studied the solid-state microstructures on the solvent casting films from various PEBAs and found that the copolymers show lamellar nanostructures with the approximate layer thicknesses of 6 nm and long periods ranging from 12 to 18 nm [37].

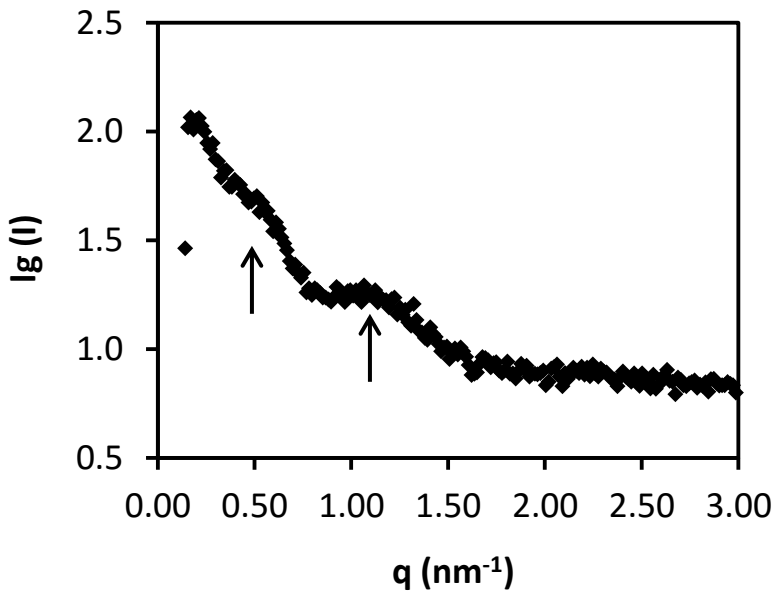

Figure 4.2: SAXS intensity as a function of the magnitude of the scattering vector *q*. The two arrows indicate the two peaks detected.

The grain size was inferred to be about 25 nm by using the Scherrer equation which is approximately the size of two times of the long period, indicating that the lamellar structure within the PEBA sample is not well defined. This actually could be considered as an advantage

for the PEBA to dissipate charge since it has been previously shown in PS-PEO block copolymers that the conductivity increases by a factor of 5.2 as the grain size decreases from 88 nm to 13 nm [38].

Table 4.3: Structural parameters for the PEBA copolymer

q values of first peak/second peak (nm^{-1})	**0.55/1.17**
Long period (nm)	11.5
Density of PA12 (g/cm^3)	1.01 ~ 1.02[39]
Density of PEO (g/cm^3)	0.94 ~ 1.13[40]
Layer thickness of PA12 (nm)	5.2
Layer thickness of PEO (nm)	6.3
Grain size (nm)	25

4.4.4 Miscibility

In order to examine the miscibility between PS and PEBA, modulated DSC was used to determine the Tg of the blends at various compositions. Fig. 4.3a shows that the Tg of the PEBA remains almost constant (55.0 ~ 56.0°C) within the composition range examined, while the Tg of PS decreases more than 5°C from 98.9°C to 93.5°C when 5% and 10% of PEBA are added to the blends. At 20% of PEBA, the Tg of PS increases to 96.8°C and at 40%, it returns to the same value as the pure PS and remains unchanged afterwards. It was not possible to detect the Tg of the PEO in the PEBA at its low concentrations (e.g. 5% and 10%). It should be noted that the PEBA is a copolymer of 45% PA12 and 55% PEO adding to the difficulty in sensitivity due to concentration issues even when using modulated DSC. Note that although the PEBA copolymer consists of PEO blocks and PA12 blocks, only one Tg at -55.5°C was detected which is considered to represent the glass transition of the PEO block [25] since the Tg of PA12 homopolymer is much higher (36°C [41]). This single Tg result could be attributed to the fact that the PA12 chain in the copolymer is short making the Tg too weak to be detected in DSC.

Nevertheless, the decrease of the Tg of the PS phase clearly demonstrates that certain partial miscibility between PS and PEBA is achieved at low PEBA concentrations (≤ 20%). The PS

phase in these blends is thus actually a “PS-rich phase” with a small amount of PEBA. Using the Fox equation [42]:

$$\omega_1 = \frac{T_{g1}(T_{g2} - T'_g)}{T'_g(T_{g2} - T_{g1})}$$

where ω1 is the weight fraction of the PEBA in the PS-rich phase; T_{g1}, T_{g2} and T'_g are the glass transition temperatures of the neat PEBA, neat PS and the PS-rich phase respectively. The amount of PEBA in the PS-rich phase can be calculated to be 2.1%, 2.1% and 0.8% for the blends of PS/PEBA 95/5, 90/10 and 80/20 respectively. Despite the evidence of partial miscibility, the term “PS phase” will be used throughout the following discussion.

Clearly from the discussion above, some interactions appear to be occurring between the PS and the PEO block in PEBA. Yilmaz et al. studied the miscibility of PS/PEO in solution by examining different miscibility parameters derived from the Huggins equation[35]. They found that PS and PEO are immiscible over the entire composition range studied at 30°C. Ting et al. examined various solvent casting PS/PEO blends by standard DSC and FTIR and no significant interaction was detected [34]. However, these studies were carried out at PEO concentrations at or above 12.5%, while we observe that the partial miscibility between PS and PEBA happens at low concentrations of PEBA (typically ≤ 10%; the related PEO contents are only about half of the values). Besides, the miscibility between PEO and PS in the previous work was examined either directly in solution or on solvent casting films which are different from the current work where melt blending is used to prepare the samples. Kim and Burns showed that the partial miscibility between polycarbonate (PC) and poly(methyl methacrylate) (PMMA) after melt blending was higher than solvent casting as indicated from the Tgs of the components [42] perhaps owing to the casting conditions (e.g., solvent evaporation rate, casting temperature and solvents used) which can have a profound effect on the phase diagram of the two polymers [43]. In the solution state, Bank and coworkers reported that the compatibility between PS and Poly(vinyl methyl ether) (PVME), which may have similar interactions as PS/PEO, changed notably in different solvents [44]. To the best of our knowledge, very little work has been carried out on the phase behaviours of PS and PEO in the melt state. Galloway and Macosko prepared PS/PEO melt blends for continuity tests and the morphology results show that the two components are immiscible. They estimated the interfacial tension of the system as being very

low (1 mN/m), as in this study, but no detailed (partial) miscibility studies were performed. It is known that PS and poly(2,6-dimethyl-1,4-phenylene oxide) (PPO) are miscible over the whole composition range owing to the π-hydrogen bond between the electrodeficient methyl groups in PPO and π-orbitals in PS [45, 46]. Potentially, a similar π-hydrogen bonding, though probably much weaker, could be present between PS and PEO. This weak interaction results in only a partial miscibility at low concentrations of PEBA.

In order to evaluate the miscibility between PS and PEBA, the interaction between the PA12 and the PEO blocks should also be taken into account. In this context, Paul and coworkers developed a model to consider the contribution of the interaction between the components of a copolymer (A-B) to towards its miscibility with homopolymer (C) [47]. Using this approach, the binary interaction energy density b (proportional to the known chi parameter) for A-B and C can be estimated from the solubility parameter (δ). By taking δ_{PS} = 18.5 $MPa^{1/2}$ (average) [48], δ_{PEO} = 20.2 $MPa^{1/2}$ [48] and δ_{PA12} = 20.8 $MPa^{1/2}$ [49], $b_{PS,PEBA}$ is calculated to be 3.9 Mpa which is much larger than $b_{PS,PEO}$ (2.9 Mpa). Clearly, the presence of the PA12 in the PEBA copolymer makes it less miscible with PS as compared to PEO. This conclusion is in line with the high interfacial tension between PS and PA (Table 4.2). The trend also agrees well with the interfacial tension change between the two pairs, where $\gamma_{PS/PEO}$ = 1 mN/m and $\gamma_{PS/PEBA}$ = 1.6 mN/m. Although the latter interfacial tension is higher, it is not as high as would be expected based simply on a block copolymer composition argument. This is an indication that the PEO block in the PEBA chains orients preferentially towards the PS phase.

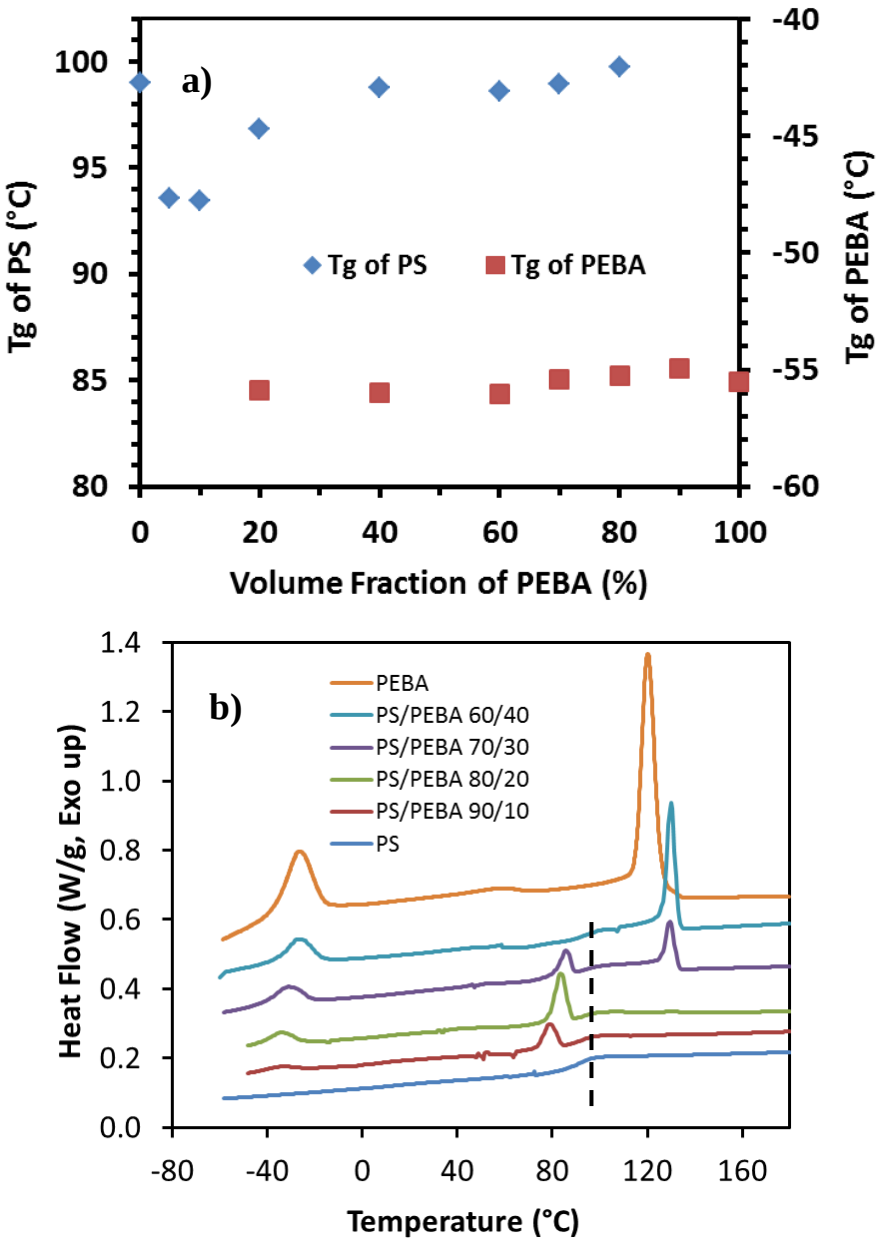

Figure 4.3: (a) The glass transition temperatures of PS and PEBA in the PS/PEBA blends; (b) crystallization behaviour of PEBA, PS and the PS/PEB blends during cooling. Dashed line indicates Tg of PS

Another very interesting feature is that the partial miscibility only happens at low PEBA compositions, which is different from the other reported partially miscible systems where the Tg of one phase changes gradually as the concentration of the other phase increases [50-52]. We consider that it could be owing to the PEBA molecular structure and the crystallization behaviours of PEBA in the PS/PEBA blends. Bhadane et al. studied blends of ethylene–

propylene–diene terpolymer (EPDM) and polypropylene (PP) and found that the blend demonstrates the morphology features of a partially miscible system [53]. However, the glass transition temperatures indicate the two polymers are completely immiscible and it was suggested that partial miscibility happens during melt blending but phase separation develops during cooling owing to crystallization of PP. In our system, as shown in Fig. 4.3b, multi-crystallization peaks were observed for PEBA. The one at around -35°C represents the crystallization of the PEO blocks while the others at higher temperatures result from PA. At low PEBA compositions (≤20%), the PA blocks crystallize at around 80°C, lower than the Tg of PS. At higher PEBA compositions (≥ 30%), the crystallization temperatures of the PA blocks shift to around 130°C. The phenomenon is known as retarded or fractionated crystallization and has been reported in many polymer blend and other confined systems; the effect normally results from the quantitative relationship between active heterogeneities and isolated domains of the minor phase [54, 55]. We assume that partial miscibility exists for all the PS/PEBA blends during melt blending. However, upon cooling, the different crystallization behaviours of PA in the blends lead to demixing. In the blends with higher PEBA compositions, phase separation between PS and PEO driven by the crystallization of PA happens since the crystallization temperature is much higher than the Tg of the PS phase and the chains can rearrange owing to a relatively high chain mobility for both PS and PEO in this case. For the blends at low PEBA compositions, the PS phase becomes glassy prior to the crystallization of PA. This has the effect of impeding phase separation since the PEO chains are fixed in the glassy PS.

4.4.5 Continuity and morphology

4.4.5.1 PEBA continuity determination by selective extraction

Selective solvent extraction was performed to quantify the continuity of the PEBA in different blends and the results are shown in Fig. 4.4. PEBA demonstrates a steep continuity development with volume fraction in both of the binary blends. The percolation threshold is estimated to be between 5-10% for both blends. Notably, the high interfacial tension LDPE/PEBA blend system shows about 50% of continuity at 20% PEBA and about 90% continuity at 25%. This high continuity at relatively low volume fraction is probably attributed to the high viscosity ratio (the viscosity of the dispersed phase to the viscosity of the matrix) of LDPE/PEBA which is about 1/6 under these processing conditions. Many models have been proposed to predict the co-continuous

region in immiscible polymer blends based on viscosity ratio [56-58]. Generally, though not always, the phase with the lower viscosity tends to form continuous structure since it minimizes the energy dissipation in the flow field [5]. Previous studies have also shows that a higher matrix viscosity is likely to result in higher continuity of the minor phase, especially in incompatible blends [9, 59]. Even higher continuity was observed in the PS/PEBA blends where about 40% continuity was obtained at only 10% PEBA. Further increasing the volume fraction of PEBA to 20% leads to almost 90% continuity. Since the viscosities of LDPE and PS are very close (1300 vs. 1180 Pa·s) under these processing conditions (200°C, 25 s^{-1}), the even higher continuity developed in the PS/PEBA blends can be explained by the lower interfacial tension between PS and PEBA (1.6 mN/m). As mentioned in the Introduction, low interfacial tension systems have been shown to result in stable fibrillar/extended structures of the minor phase even at very low concentrations [7, 53, 60]. The continuity development behaviour for the PS/PEBA blends thus shows the features of a Type I system (compatible binary blend). In these systems, the minor phase forms fibers at low concentrations and the continuity develops through a thread-thread coalescence mechanism [7]. This presumed fiber formation will be examined in more detail in the next section.

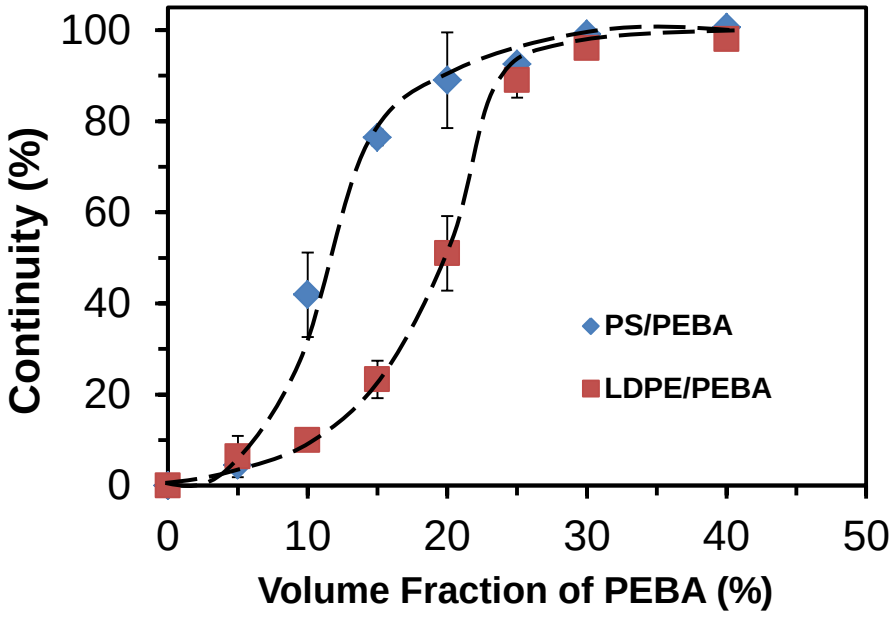

Figure 4.4: Continuity of PEBA in LDPE/PEBA and PS/PEBA blends.

4.4.5.2 Morphology of the blends

The morphology of the blends was characterized by SEM and the results are shown in Fig. 4.5. The apparent phase size in the PS/PEBA blends is much finer than the LDPE/PEBA blends. With 10% of PEBA, a clear droplet-matrix morphology is observed in the LDPE/PEBA blend. When the concentration increases to 20% and 30% the minor phase visually starts to form interconnected domains in LDPE/PEBA, indicating a significant increase in the continuity. The trend corresponds well with the continuity data shown in Fig. 4.4. The morphology in the PS/PEBA blends shows a similar transition. However, surprisingly, in the PS/PEBA 80/20 blend, although the PEBA phase appears as droplets, many of them seem to be connected to each other (from underneath or on the microtomed surface, see the circled spots). It is thus suspected that the PEBA domains are actually connected as "pearl necklace chains". The previous continuity data also support this assumption since approximately 90% of continuity was obtained for this sample.

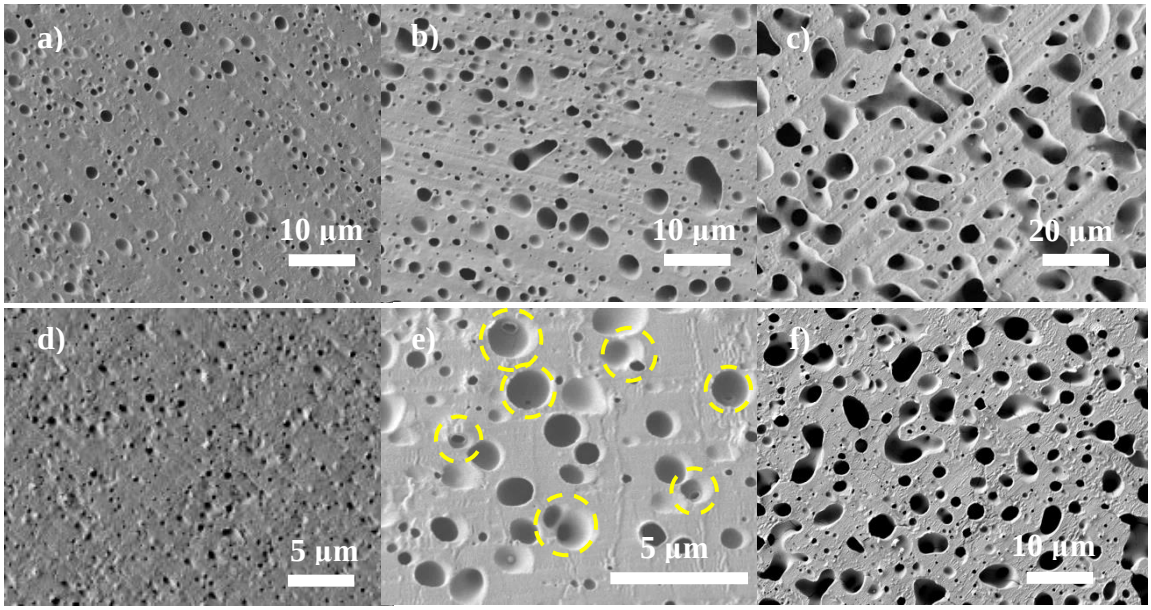

Figure 4.5: Morphology of the LDPE/PEBA and PS/PEBA blends with different volume fractions. LDPE/PEBA: (a) 90/10; (b) 80/20; (c) 70/30. PS/PEBA: (d) 90/10; (e) 80/20; (f) 70/30. PEBA was extracted. Circles indicate signs of connections between the PEBA domains.

In order to fully characterize the morphology of the minor PEBA phase in the different blends, a matrix dissolution technique was used as described in the Experimental part. The PS and LDPE were completely removed by THF and cyclohexane and the remaining PEBA was collected for SEM analysis. As shown in Fig.4.6, the PEBA presents as separated droplets in the LDPE/PEBA

(90/10) blend and when the concentration increases to 20%, a mix of droplets and elongated domains were observed. While in the case of PS/PEBA blends, the “pearl necklace chain” morphology of PEBA can be seen after removing the PS phase. Interestingly, this interconnected morphology is maintained even at very low concentration of PEBA (e.g., 5%) as would be expected in a Type 1 system. In order to clearly see the “pearl necklace chain” of PEBA, about 50 μg of the PEBA, after extracting PS from the PS/PEBA (95/5) blend, were diluted in 100 mL THF and ultrasonicated for 5 min to achieve good dispersion. After drying of the suspension on a copper plate under vacuum, SEM images were taken and are shown in Fig 4.6f where the morphology of a single chain is shown. The observed “pearl necklace chain” structure actually represents the classic capillary instability which is characterized by the development of sinusoidal distortions along a thread in a matrix [61, 62]. The phenomenon is controlled by a number of factors, including interfacial tension, viscosity, initial fiber diameter, distortion magnitude and temperature [8, 62]. In PS/PEBA blends, the thermodynamic and dynamic forces seem to be under a certain balance so that the capillary instability developed in mixing appears to be “frozen” and captured even at very low PEBA concentration.

The phase size of the PEBA was also quantitatively analyzed by image analysis (IA) and mercury intrusion porosimetry (MIP) after the extraction of the PEBA phase (Fig. 4.7). As the concentration of PEBA increases, the phase size increases in both LDPE/PEBA and PS/PEBA blends as also seen from the SEM images (Fig.5). Notably, with 5% and 10% of PEBA in PS, the Dn/Dv of the PEBA fibrillar phase are only 200/300 nm and 282/427 nm respectively, which can probably be attributed to the partial miscibility between the two polymers at low concentration and the Type I behavior. In the LDPE/PEBA system, the droplet phase size increases more notably from 690/1100 nm to 1034/2059 nm, representing the behavior of Type II system. It should be underlined that the phase size for LDPE/PEBA describes a droplet diameter below 20% and fiber diameters above that value. For PS/PEBA the phase size indicates a fiber diameter at all concentrations.

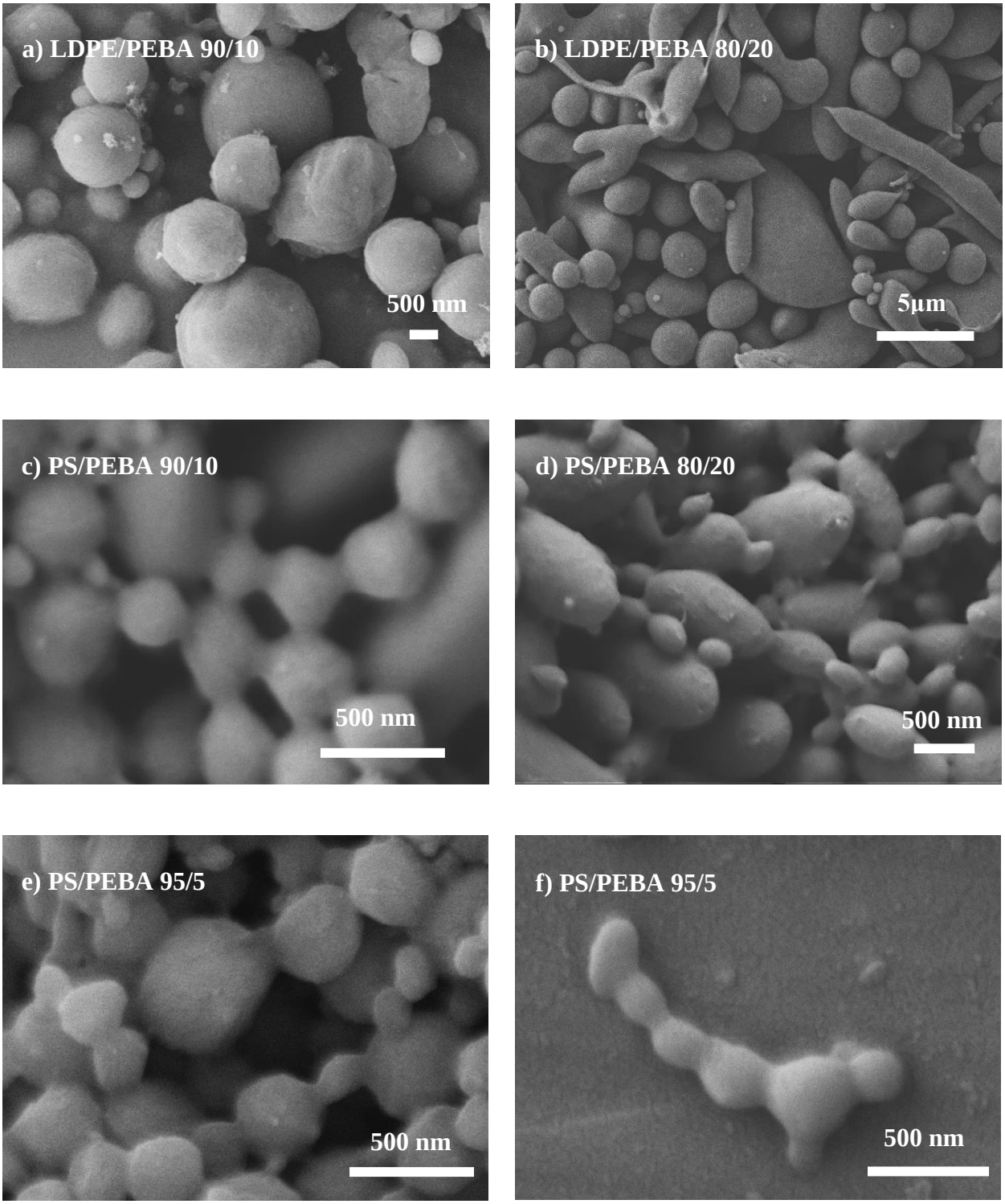

Figure 4.6: Morphology of the PEBA phase in the PS/PEBA and LDPE/PEBA blends with different compositions after LDPE and PS are selectively dissolved.

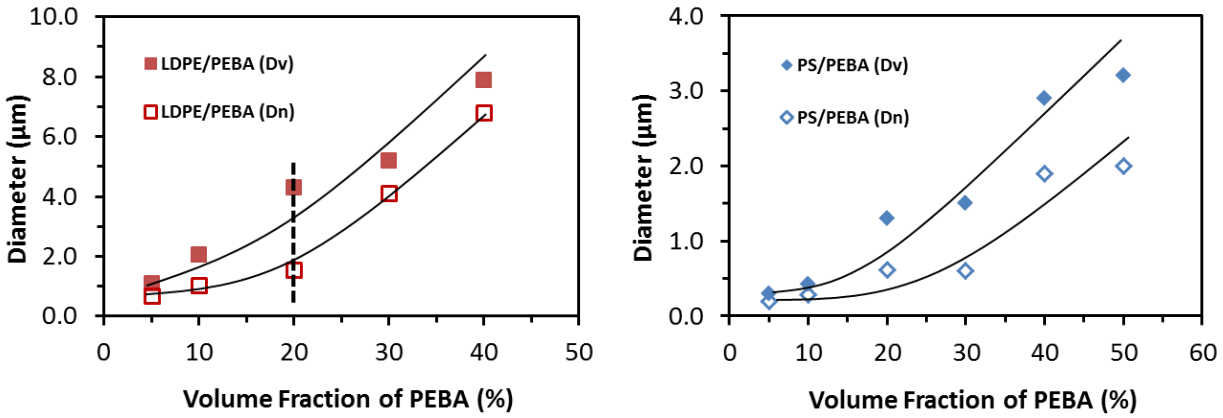

Figure 4.7: PEBA phase size in different blends obtained from IA (PEBA volume fraction ≤ 20%) and MIP (PEBA volume fraction > 20%). The dashed line for LDPE/PEBA system indicates the approximate concentration limit for droplets (left side) and fibers (right side). For PS/PEBA the phase size indicates a fiber diameter at all concentrations.

4.4.5.3 Frozen Capillary Instability

The LDPE/PEBA blend is a typical incompatible system (interfacial tension of 8.0 mN/m) and the continuity development follows the droplet-droplet coalescence mechanism as evidenced in Figs. 4.6a and b. However, the PS/PEBA blend, which has an intermediate-low interfacial tension (1.6 mN/m) as a result of low level partial miscibility, demonstrates some unique features, namely a pearl-necklace or frozen capillary instability type morphology as shown in Figure 6f. The two systems have very close viscosity ratio and storage/loss modulus (see Fig.1). Also, the two blends were processed under the same conditions. Therefore, the difference observed between PE/PEBA and PS/PEBA on morphology/continuity development should be mainly attributed to the difference in their interfacial tension. In order to understand the origin of this morphology it is important to recall that the formation of capillary instabilities is one of the principal mechanisms controlling dispersed phase morphology. The deformability of the dispersed phase can be expressed by the capillary number (Ca) as developed by Taylor [63, 64]. Upon exceeding a critical value, the dispersed phase can be deformed and finally breaks through the development of capillary instabilities. The stability of a deformed thread can be estimated by the time of breakup (t_b) from Tomotika's equation [62]:

$$t_b = \frac{2\eta_m R_0}{\Omega_m \sigma} \ln\left(\frac{0.82 R_0}{\alpha_0}\right)$$

where Ω_m is a tabulated function related to viscosity ratio, R_0 is the initial radius of the thread and α_0 is the initial distortion amplitude. Low interfacial tension compatible systems of interfacial tension less than 1 mN/m typically show a clear fibrillar/extended minor phase morphology even at low concentrations of 5% owing to the long breakup time; on the other hand high interfacial tension systems show a droplet morphology [7]. It appears in the case of PS/PEBA that an intermediate structure is also possible. The interfacial force is relatively low which allows the PEBA phase to be elongated by the external stress; but it is not low enough to make the deformed PEBA thread highly stable, and thus the sinusoidal distortion visually develops. These results indicate that there is a transition region of interfacial tension where the capillary breakup is sufficiently slow that it results in a dispersed phase morphology demonstrating frozen sinusoidal distortions. In such a case the continuity development PS/PEBA would take place by local coalescence at frozen instability crossover points. A schematic showing the continuity development in early stage of such a system is presented in Fig. 4.8. This model would explain the high continuity at low concentration and also the very low change in phase size up to about 15% concentration.

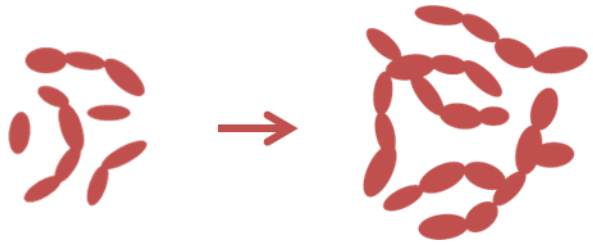

Figure 4.8: Schematic illustration of continuity development by frozen capillary instability in PS/PEBA up to 10% concentration.

4.4.6 Surface resistivity and charge dissipation mechanism

4.4.6.1 Influence of continuity on surface resistivity

The antistatic properties of the blends were evaluated by measuring the surface resistivity. After blending, the PEBA is expected to form a percolated 3D network within the matrix polymer to

dissipate the electrostatic charges and the morphology/continuity of the PEBA phase should have a crucial effect on the surface resistivity of the blends.

The surface resistivity was examined for different blends and the results were plotted as a function of PEBA concentration (Fig. 4.9). As the PEBA content increases, the surface resistivity decreases for both blends which can be attributed to the increase in the continuity of PEBA (Fig. 4.4). A notable decrease of the surface resistivity was observed when the volume fractions of the PEBA pass a critical concentration (c_{cri}) of about 5%. The value of c_{cri} is very close to the percolation threshold for continuity development shown in Fig. 4.4. The surface resistivities for the LDPE/PEBA and the PS/PEBA blends reach a plateau at 30% of the PEBA which also correlates to very high continuity levels of over 95% for both systems. The results for each individual blend system indicate a direct correlation between continuity and surface resistivity in the blends. However, when comparing different blends, the higher continuity of PEBA in PS at a given PEBA concentration did not translate into a lower surface resistivity when compared to PE/PEBA. In order to reach a surface resistivity below 10^{13} Ω/sq, 25% of the PEBA is needed in the PS/PEBA blends but only 20% in the case of the LDPE/PEBA blends. In fact the whole surface resisitivity curve for PS/PEBA is higher than that for LDPE/PEBA while the continuity curve shows an opposite behavior. These results suggest other factors, in addition to continuity, are also responsible for the resistivity of the blends.

Charge transport in a heterogeneous conductive system can be affected by the intrinsic conductivity of the conducting phase, continuity, volume fraction and the topological structure (tortuosity and constriction) [36, 65]. Wiedenmann et al. proposed the following equation to consider these factors [65]:

$$\frac{\sigma}{\sigma_0} = \frac{\varepsilon\beta}{\tau}$$

where σ and σ_0 are the measured conductivity and intrinsic conductivity of the conducting phase; ε is the volume fraction of the conducting phase; β is the constriction factor (the ratio of the minimum cross-section area over the maximum cross-section area along the conductive pathway); and τ is the tortuosity (the ratio of the real conductive pathway length over the shortest distance between the two points). In their system, they found that the tortuosity is nearly independent of the porosity and the constriction effect represents the dominant microstructure parameter

affecting the conductivity [65, 66]. Indeed, these factors need to be further studied in our system. Other factors to be considered, particularly in this study, are the partial miscibility between PS and PEBA and the special morphological features in the PS/PEBA blends at low concentrations of PEBA (≤ 20%). The former likely results in the presence of PS in the PEBA phase, which may reduce the chain mobility of PEO due to the specific interaction between PS and PEO [24] and thus the charge dissipation capacity. Meanwhile, matrix dissolution technique shows that the frozen-capillary instability morphologies in the PS/PEBA system possess very thin connecting filaments which can be significantly less than 100 nm (Fig. 4.6c-f). At such a scale (≤ 100 nm), the interactions between PS and PEBA at the interface may also limit the chain mobility of the PEO blocks [67, 68] and make the region less conductive locally as compared to the PEBA bulk.

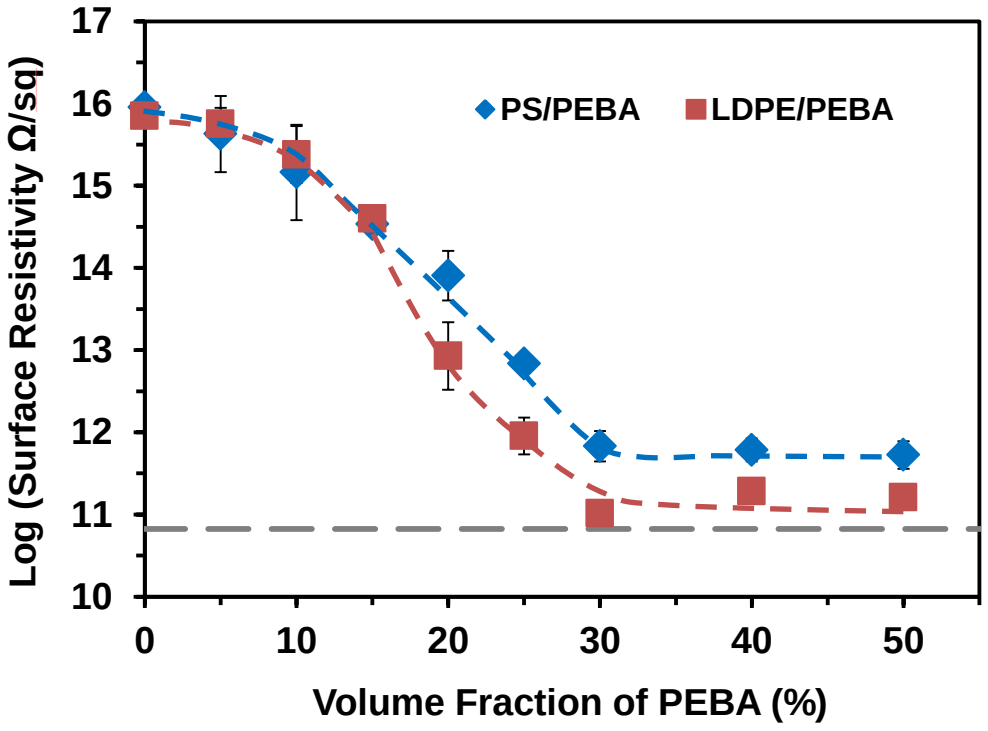

Figure 4.9: Surface resistivity in the LDPE/PEBA and PS/PEBA blends as a function of PEBA composition. The horizontal dashed line indicate the surface resistivity of pure PEBA.

4.4.6.2 Influence of water content and conceptual model for charge transport

The presence of water in PEBA copolymers plays a crucial role on their antistatic properties [19, 69]. In order to study this, the surface resistivities were examined as a function of water content

in the neat PEBA and for selected binary blends with LDPE and PS. The water contents (based on PEBA) in the samples were controlled by different conditioning times. As shown in Fig. 4.10, the log surface resistivity decreases linearly with increasing water content for all the samples examined. This behaviour corresponds to what was observed in salt doped polyelectrolytes where the conductivity increases with increasing salt concentration owing to the increase in the number of charge carriers [70, 71]. The results strongly indicate that water molecules serve as a medium for charge transportation in a certain form. The equilibrium water contents under the conditioning conditions are determined as ~ 2%. In the case of neat PEBA, limited points were collected for low water content due to its very fast water absorption rate. However, since its blends with LDPE and PS both show a linear dependence of log surface resistivity on water content, it would not be surprising that neat PEBA presents a similar behaviour.

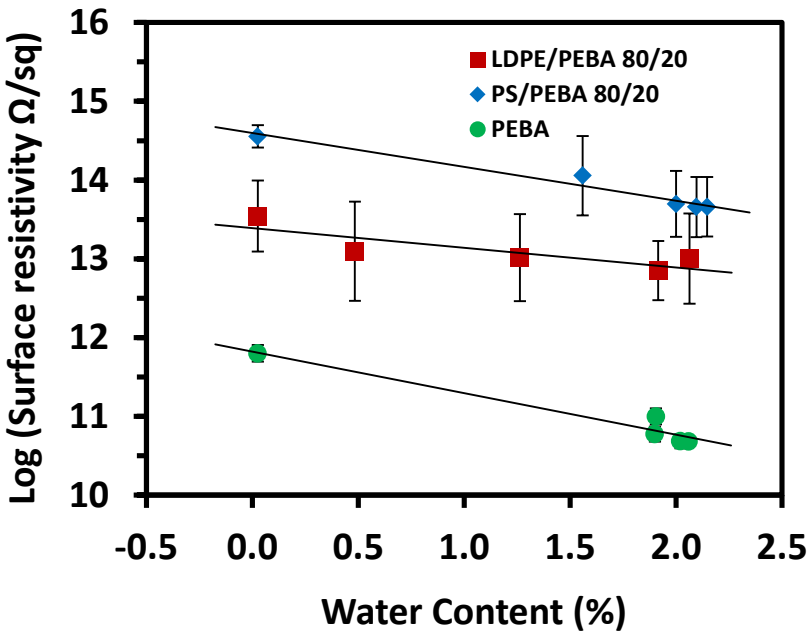

Figure 4.10: Effect of water content on surface resistivity for pure PEBA and its binary blends with LDPE and PS.

Although PEBA copolymers have been widely used in antistatic applications [15-17], the mechanism for charge transport in such copolymers is poorly understood. In similar copolymers consisting of PEO blocks, Lin and coworkers proposed a hydrogen bonding mechanism that dissipates charge after the polymer absorbs moisture [19, 69]. In that study, the H-bonds between the –CONH– group and water and between the $–OCH_2–$ group and water facilitate the ionization

of water molecules to generate protons that serve as the medium for charge transport. They further confirmed that the presence of hydrogen bonding between –the CONH– group and water molecules is important to obtain lower surface resistivity. However, they did not carry out studies on the solid-state microstructures of the copolymers, and therefore the microscopic charge transport pathway was not discussed. A considerable amount of research efforts have also been devoted to understand charge transport in lithium salt doped PEO based polymer electrolytes for their potential applications in batteries. It is generally believed that the ion transport is confined within the amorphous PEO domains where the ether oxygen coordinates with Li^+ [36, 72-74]. Owing to the segmental motion of the polymer chain, ion transport can be achieved by its migration between coordination sites. The conductivity strongly depends on the morphologies (e.g., lamellae, bicontinuous gyroid, cylinders and spheres) of the block copolymers used for electrolytes [75]. In lamella structures, Cheng and coworkers found that the in-plane conductivity can be 2000 times higher than that of through-plane due to the tortuosity effect [74].

Understanding the charge dissipative mechanism in PEBA copolymers is not only important to further control the antistatic properties of the current system, but is also necessary for the development of next generation IDPs. A conceptual charge dissipative mechanism for PEBA is proposed in Fig. 4.11. It is assumed that the PEBA absorbs water and H-bonds form between the water molecules and the ether and amide groups, which ionizes water in an equilibrium state. The produced protons can migrate between the ether groups through coordination. Since the PEO block in the PEBA copolymer is in a liquid state at room temperature, the strong chain mobility can assist the proton transport, imparting a charge dissipation capacity to the PEBA copolymer. As shown in Section 3.3, the PEBA shows a micro-phase separated lamellar morphology and the grain consists of two lamellae. The charge transport only happens in the PEO domains but is directed by the PA crystals (along the crystal growth direction). In the blends with PEBA, there are actually two modes of confinement at distinct length scales for the charge dissipation pathways: the confinement from the matrix which is typically at the micron scale and the confinement from the PA phase in the PEBA copolymer at the nano scale. After blending, if the phase size of PEBA is at the micron scale (e.g., in PE/PEBA blends), the confinement from the PA blocks can be statistically considered as the same for all samples. Thus virtually, only the tortuosity from the PEBA phase in the matrix needs to be considered. However, if the phase size of PEBA is at the same order as the grain size (< 100 nm), like some of the PEBA domains in the

PEBA/PS blends, the confinement from PA should also be considered which may lead to a much higher effective tortuosity for the PEBA phase in blends, since in this case, the PA crystal growth direction may not be along the elongated direction of the PEBA domain and thus may block the charge transport completely. This could be another possible reason, in addition to the interaction between PS and PEBA, why the surface resistivities of the PS/PEBA blends are higher than those of the LDPE/PEBA blends as shown in Fig. 4.9.

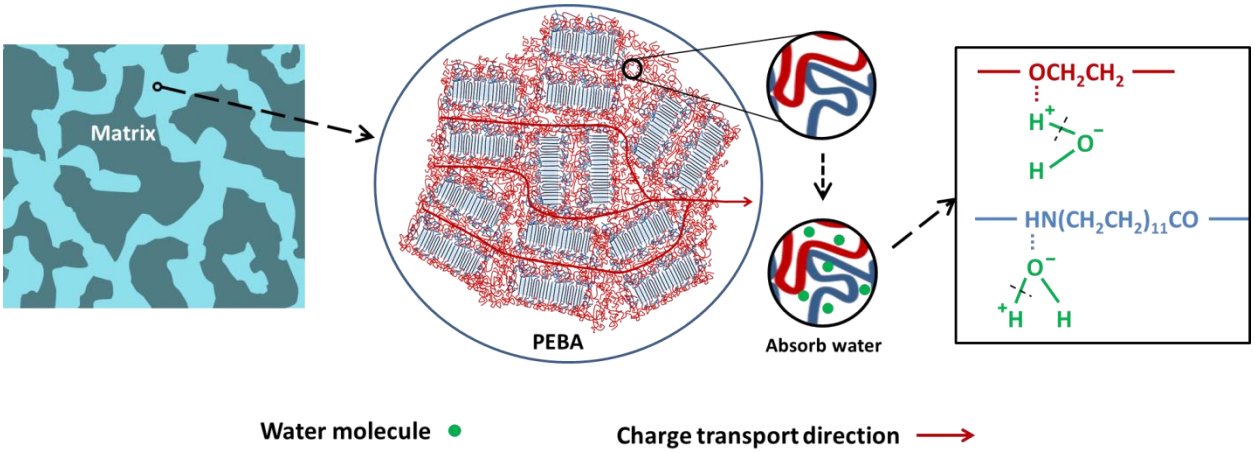

Figure 4.11: Schematic representation of the charge dissipation mechanism in the PEBA binary blend.

4.5 Conclusion

Binary blends of PEBA with LDPE and PS were studied by melt blending. The LDPE/PEBA blend is a highly incompatible system with an interfacial tension of 8.0 mN/m and the continuity develops through a droplet-droplet coalescence mechanism. The PS/PEBA system has an interfacial tension of 1.6 mN/m and a partial miscibility between the two components was observed at low concentrations of PEBA. A frozen capillary instability morphology was observed for the first time in PS/PEBA blends. It was shown that although the continuity develops at lower volume fractions in PS/PEBA than in LDPE/PEBA, surprisingly, the surface resistivity is higher for PS/PEBA over a wide range of PEBA compositions. This result was related to the partial miscibility of PS/PEBA and/or the significant constriction in the frozen capillary PEBA morphology when it is blended with PS, which reduces the charge transfer capacity of PEBA in the PS/PEBA blends. The log surface resistivity was found to decrease linearly as a function of

water content for both pure PEBA and the blends. A conceptual model for charge transport in the PEBA copolymer based on the migration of protons in the PEO domains is also proposed. The local phase size of PEBA in the blends could also be another important factor affecting charge dissipation.

4.6 Acknowledgment

The authors would like to acknowledge Arkema for funding this research. Jun Wang would like to thank the China Scholarship Council (CSC) for a scholarship. The authors would also like to thank Dr. Eric Gamache, Dr. Frederic Malet and Dr. Richard Chaigneau from Arkema for useful discussions. Prof. Frederic Sirois and Daniel Therriault from Ecole Polytechnique de Montreal are also acknowledged for providing the surface resistivity measurement fixtures.

4.7 References

1. Kobayashi T, Wood BA, Takemura A, and Ono H. Journal of Electrostatics 2006;64(6):377-385.
2. Rosner RB. Device and Materials Reliability, IEEE Transactions on 2001;1(1):9-16.
3. Malet FLG. Thermoplastic Poly(Ether-b-Amide) Elastomers: Synthesis. In: Fakirov S, editor. Handbook of Condensation Thermoplastic Elastomers: Wiley-VCH Verlag GmbH & Co. KGaA, 2006. pp. 241-262.
4. Eustache RP. Poly(Ether-b-Amide) Thermoplastic Elastomers: Structure, Properties, and Applications. In: Fakirov S, editor. Handbook of Condensation Thermoplastic Elastomers: Wiley-VCH Verlag GmbH & Co. KGaA, 2006. pp. 263-281.
5. Potschke P and Paul DR. Journal of Macromolecular Science-Polymer Reviews 2003;C43(1):87-141.
6. Favis BD. Factors Influencing the Morphology in Immiscible Polymer Blends in Melt Processing. In: Paul DR and Bucknall CB, editors. Polymer Blends: Formulation and Performance: Wiley-Interscience, 2000. pp. 501-537.
7. Li JM, Ma PL, and Favis BD. Macromolecules 2002;35(6):2005-2016.
8. Elemans PHM, Janssen JMH, and Meijer HEH. Journal of Rheology 1990;34(8):1311-1325.

9. Omonov TS, Harrats C, Moldenaers P, and Groeninckx G. Polymer 2007;48(20):5917-5927.

10. Vanoene H. Journal of Colloid and Interface Science 1972;40(3):448-467.

11. Bourry D and Favis BD. Journal of Polymer Science Part B: Polymer Physics 1998;36(11):1889-1899.

12. Sundararaj U and Macosko CW. Macromolecules 1995;28(8):2647-2657.

13. Ikkala OT, Laakso J, Väkiparta K, Virtanen E, Ruohonen H, Järvinen H, Taka T, Passiniemi P, Österholm JE, Cao Y, Andreatta A, Smith P, and Heeger AJ. Synthetic Metals 1995;69(1–3):97-100.

14. Cao Y, Smith P, and Heeger AJ. Synthetic Metals 1992;48(1):91-97.

15. Lacroix C. Antistatic styrene polymer composition, e.g. for production of TV or computer housings, contains polyamide-polyether block copolymer and special compatibilizer, e.g. styrene-maleic anhydride copolymer. Atofina (Aqor-C) Atofina (Aqor-C).

16. Greener J, Majumdar D, and Laney TM. Silver halide photographic film imaging element for antistatic protection, comprises a support containing a layer of polymeric antistatic material. Eastman Kodak Co (East-C) Eastman Kodak Co (East-C).

17. Havens MR. Antistatic film e.g. for packaging static-sensitive devices - has layer of polyetheramide block copolymer plus aromatic sulphonamide antistat and opt. also polyolefin layer. Grace & Co W R (Grac-C) Grace & Co-Conn W R (Grac-C).

18. Wang J, Bao L, Zhao H, and Lei J. Composites Science and Technology 2012;72(9):976-981.

19. Young M-Y and Lin J-J. Industrial & Engineering Chemistry Research 1998;37(11):4284-4289.

20. Wang G and Xue B. Journal of Applied Polymer Science 2010;118(4):2448-2453.

21. Fu Y, Wang J, Zhao G, Wang Y, and Chen S. Journal of Applied Polymer Science 2011;122(1):12-18.

22. Iwata T, Tsurumaki A, Tajima S, and Ohno H. Polymer 2014;55(10):2501-2504.

23. Dai L. Conducting Polymers. Intelligent Macromolecules for Smart Devices: Springer London, 2004. pp. 41-80.

24. Kobayashi T, Wood BA, and Takemura A. Journal of Applied Polymer Science 2012;123(2):1056-1067.

25. Bondar VI, Freeman BD, and Pinnau I. Journal of Polymer Science Part B: Polymer Physics 1999;37(17):2463-2475.

26. Reignier J and Favis BD. Macromolecules 2000;33(19):6998-7008.

27. Xing P, Bousmina M, Rodrigue D, and Kamal MR. Macromolecules 2000;33(21):8020-8034.

28. Saltikov S. The Determination of the Size Distribution of Particles in an Opaque Material from a Measurement of the Size Distribution of Their Sections. In: Elias H, editor. Stereology: Springer Berlin Heidelberg, 1967. pp. 163-173.

29. Li J and Favis BD. Polymer 2001;42(11):5047-5053.

30. Bousmina M, Ait-Kadi A, and Faisant JB. Journal of Rheology 1999;43(2):415-433.

31. Son Y. Polymer 2001;42(3):1287-1291.

32. Cho K, Hyun Kyoung J, Park CE, Kim J, and Kim KU. Polymer 1996;37(7):1117-1122.

33. Galloway JA and Macosko CW. Polymer Engineering and Science 2004;44(4):714-727.

34. Ting SP, Bulkin BJ, Pearce EM, and Kwei TK. Journal of Polymer Science: Polymer Chemistry Edition 1981;19(6):1451-1473.

35. Yilmaz E, Yilmaz O, and Caner H. European Polymer Journal 1996;32(8):927-933.

36. Bouchet R, Phan TNT, Beaudoin E, Devaux D, Davidson P, Bertin D, and Denoyel R. Macromolecules 2014;47(8):2659-2665.

37. Barbi V, Funari SS, Gehrke R, Scharnagl N, and Stribeck N. Macromolecules 2003;36(3):749-758.

38. Chintapalli M, Chen XC, Thelen JL, Teran AA, Wang X, Garetz BA, and Balsara NP. Macromolecules 2014;47(15):5424-5431.

39. Mark JE. 47. Nylon 12. Polymer Data Handbook (2nd Edition): Oxford University Press, 2009. pp. 302-306.

40. Pionteck J and Wypych G. 2. Types of Antistatic Agents. Handbook of Antistatics: ChemTec Publishing, 2007. pp. 17-31.

41. Xenopoulos A and Wunderlich B. Journal of Polymer Science Part B: Polymer Physics 1990;28(12):2271-2290.

42. Kim WN and Burns CM. Macromolecules 1987;20(8):1876-1882.

43. Saldanha JM and Kyu T. Macromolecules 1987;20(11):2840-2847.

44. Bank M, Leffingwell J, and Thies C. Macromolecules 1971;4(1):43-46.

45. Djordjevic MB and Porter RS. Polymer Engineering & Science 1983;23(12):650-657.

46. Ziaee S and Paul DR. Journal of Polymer Science Part B: Polymer Physics 1996;34(15):2641-2656.

47. Paul DR and Barlow JW. Polymer 1984;25(4):487-494.

48. Polymer Handbook, 3rd ed.: Wiley-Interscience, 1989.

49. Wohlfarth C. Solubility parameter of polyamide-12. In: Lechner MD and Arndt KF, editors. Polymer Solutions, vol. 6D2: Springer Berlin Heidelberg, 2010. pp. 1494-1496.

50. Fekete E, Földes E, and Pukánszky B. European Polymer Journal 2005;41(4):727-736.

51. Marin N and Favis BD. Polymer 2002;43(17):4723-4731.

52. López-Rodríguez N, López-Arraiza A, Meaurio E, and Sarasua JR. Polymer Engineering & Science 2006;46(9):1299-1308.

53. Bhadane PA, Champagne MF, Huneault MA, Tofan F, and Favis BD. Polymer 2006;47(8):2760-2771.

54. Groeninckx G, Vanneste M, and Everaert V. Crystallization, Morphological Structure, and Melting of Polymer Blends. In: Utracki LA, editor. Polymer Blends Handbook: Springer Netherlands, 2003. pp. 203-294.

55. Michell RM, Blaszczyk-Lezak I, Mijangos C, and Müller AJ. Polymer 2013;54(16):4059-4077.

56. Paul DR and Barlow JW. Journal of Macromolecular Science, Part C 1980;18(1):109-168.

57. Utracki LA. Journal of Rheology 1991;35(8):1615-1637.

58. Miles IS and Zurek A. Polymer Engineering & Science 1988;28(12):796-805.

59. Chuai CZ, Almdal K, and Lyngaae-Jørgensen J. Polymer 2003;44(2):481-493.

60. Veenstra H, van Lent BJJ, van Dam J, and de Boer AP. Polymer 1999;40(24):6661-6672.

61. Rayleigh L. Proceedings of the Royal Society of London 1879;29(196-199):71-97.

62. Tomotika S. On the Instability of a Cylindrical Thread of a Viscous Liquid Surrounded by Another Viscous Fluid, 1935.

63. Taylor GI. The Viscosity of a Fluid Containing Small Drops of Another Fluid, 1932.

64. Taylor GI. The Formation of Emulsions in Definable Fields of Flow, 1934.

65. Wiedenmann D, Keller L, Holzer L, Stojadinović J, Münch B, Suarez L, Fumey B, Hagendorfer H, Brönnimann R, Modregger P, Gorbar M, Vogt UF, Züttel A, Mantia FL, Wepf R, and Grobéty B. AIChE Journal 2013;59(5):1446-1457.

66. Holzer L, Wiedenmann D, Münch B, Keller L, Prestat M, Gasser P, Robertson I, and Grobéty B. Journal of Materials Science 2013;48(7):2934-2952.

67. Frank B, Gast AP, Russell TP, Brown HR, and Hawker C. Macromolecules 1996;29(20):6531-6534.

68. Buenviaje C, Ge S, Rafailovich M, Sokolov J, Drake JM, and Overney RM. Langmuir 1999;15(19):6446-6450.

69. Lin J-J, Young M-Y, Shau S-M, and Cheng IJ. Polymer 2000;41(7):2405-2417.

70. Zoppi RA, Fonseca CMNP, De Paoli M-A, and Nunes SP. Solid State Ionics 1996;91(1–2):123-130.

71. Manaresi P, Bignozzi MC, Pilati F, Munari A, Mastragostino M, Meneghello L, and Chiolle A. Polymer 1993;34(11):2422-2426.

72. Berthier C, Gorecki W, Minier M, Armand MB, Chabagno JM, and Rigaud P. Solid State Ionics 1983;11(1):91-95.

73. Druger SD, Ratner MA, and Nitzan A. Solid State Ionics 1983;9–10, Part 2(0):1115-1120.

74. Cheng S, Smith DM, and Li CY. Macromolecules 2014;47(12):3978-3986.

75. Villaluenga I, Chen XC, Devaux D, Hallinan DT, and Balsara NP. Macromolecules 2015;48(2):358-364.

CHAPTER 5 ARTICLE 2: ASSEMBLING CONDUCTIVE PEBA COPOLYMER AT THE CONTINUOUS INTERFACE IN TERNARY POLYMER SYSTEMS *

Jun Wang [a], Alejandra Reyna-Valencia [b], Basil D. Favis [a]

[a] *CREPEC, Department of Chemical Engineering, École Polytechnique de Montréal, Montréal, Québec, H3T 1J4, Canada*

[b] *Laboratoire d'étude des matériaux (LEM), Arkema-CERDATO, Serquigny, 27470, France*

5.1 Abstract

Two ternary blend systems of low-density polyethylene/poly(ether-block-amide)/polyethylene terephthalate (LDPE/PEBA/PET) and LDPE/PEBA/polyvinylidene fluoride (PVDF) are prepared by melt blending to thermodynamically assemble the ionic conductive copolymer PEBA at the continuous interface. For the LDPE/PEBA/PET system, a novel morphology transition from partial wetting to complete wetting is demonstrated as the PEBA composition increases. At low PEBA concentrations (e.g., 3%), the PEBA phase forms mostly discrete extended droplets at the LDPE/PET interface. As the concentration of PEBA increases, the PEBA domains at the interface form connected structures (at 5%) and finally transforms to a layer (≥ 10%) that completely segregates PET from LDPE. In the second ternary system, LDPE/PEBA/PVDF, complete wetting is observed with an intact PEBA layer (thickness of about 100 nm) observed at a concentration of 3% PEBA. Assembling the PEBA at the interface in this way results in the formation of conductive pathways with very low percolation thresholds and thus leads to a significant reduction in the resistivity as a function of PEBA concentration for both ternary systems as compared to binary blends with PEBA. The complete wetting morphology of LDPE/PEBA/PVDF shows a particularly sharp drop in resistivity. For antistatic applications requiring a surface resistivity lower than 10^{13} Ω/sq, 20% of PEBA is needed in the conventional binary blends; the value is reduced to 10% for LDPE/PEBA/PET, and as low as 1% for the LDPE/PEBA/PVDF system. Thermodynamic analysis indicates that LDPE/PEBA/PET is a weak

* Submitted to *Macromolecules*.

partial wetting system and the transition to a complete wetting morphology at higher PEBA concentration appears to be due to a competition between dewetting and coalescence of the PEBA phase at the interface. In the LDPE/PEBA/PVDF complete wetting system, a minimum concentration is also required to form a completely wet layer which depends on the spreading coefficient.

***Key words**: polymer blends, co-continuity, self-assembly, interface, weak partial wetting, complete wetting, resistivity, antistatic, morphology*

5.2 Introduction

The melt blending of conventional polymers with conducting components (including conducting polymers and inorganic fillers) to control the electrical properties of the final product has been of great interest over the past two decades. Significant research efforts have focused on reducing the percolation threshold of the conductive components in the system and to obtain tailored physical properties [1-8]. Levon et al. proposed a multiple percolation concept in conducting polymer blends [9]: if φ_B is the critical volume fraction for B to be percolated in A and A is percolated in a system with a critical volume fraction of φ_A, the critical volume fraction required for B to be percolated in the system will be reduced to $\varphi_A\varphi_B$. The concept is readily extrapolated to multiple percolated systems and its percolation threshold will be thus dramatically reduced.

Polymer blends which use electronically conducting polymers to tailor the electrical properties have been widely reported, in particular with polyaniline (PANI). Zilberman et al. examined the conductivity and morphology of binary and ternary blends involving PANI, polystyrene (PS) and polyamide (PA) [1]. With 10% of PANI in the ternary blends of PS/PA/PANI, a conductivity as high as ~10^{-4} S/cm can be obtained depending on the PA composition, much higher than those of the binary blends of PS/PANI (~10^{-14} S/cm) and PA/PANI (10^{-11} S/cm). Morphology analysis showed that PANI was preferentially located and percolated within the PA phase. Zhang et al. also obtained higher conductivities for the ternary blends of LDPE/ethylene-vinyl acetate (EVA)/PANI as compared to the binary blends of LDPE/PANI at the same concentrations of PANI, owning to the preferential localization of PANI in the EVA phase [10]. Ravati and Favis prepared a series of multi-phase PANI blends including ternary, quaternary and quinary blends [8].

As in other studies [1, 10], PANI was encapsulated by other polymers in the systems due to its high surface tension and polarity [8]. In that study, the percolation threshold of PANI was reduced to below 5% by utilizing a multi-percolated structure where PANI was situated as the innermost phase. In a following study, they developed a polymeric conductive material by depositing PANI on the surface of porous PE substrates through a layer-by-layer approach [11]. With this latter method, an ultra-low percolation threshold less than 0.19% was achieved, clearly showing the advantages of placing the conductive component at the interface. However, the LbL procedure involved in that study is relatively complicated as compared to direct melt blending. In addition to PANI, blends with ionic conductive polymers (typically polyethylene oxide based) have also been reported. Kobayashi and coworkers prepared ternary blends of PET/PEBA/ionomers through melt extrusion where PEBA is the conducting component [6, 12]. With 25% of PEBA in a PET matrix, the further addition of ionomer decreases the resistivity of the blends which was attributed to an increase of the surface area of PEBA and certain specific interactions between PEBA and the ionomer [12].

In ternary polymer blends comprised of two major phases A and C and a minor phase B located at the interface of A and C, two types of morphology can be obtained: partial wetting and complete wetting (Fig. 5.1). These morphologies can be predicted by Harkins' spreading theory [13-15]. The theory defines 3 spreading coefficients (λ) based on the interfacial tensions (γ) of different polymer pairs as shown in Fig. 5.1. If all the three spreading coefficients are negative, partial wetting tends to occur with three phase contact and the minor phase B arranges into droplets at the interface of A and C. If the interfacial tension between A and C (γ_{AC}) is high enough to make λ_{ABC} positive, the highly unfavoured A/C interface will be fully separated by a layer of phase B. The theory has been verified in a variety of polymer systems [8, 15-19]. Zhang et al. reported a PE/PS/poly(methyl methacrylate) (PMMA) blend system where the minor PS phase is present as a thin layer at the continuous PE/PMMA interface, demonstrating a complete wetting morphology [16]. They showed that with only 3% of PS, the continuity of PS can reach almost 70%.

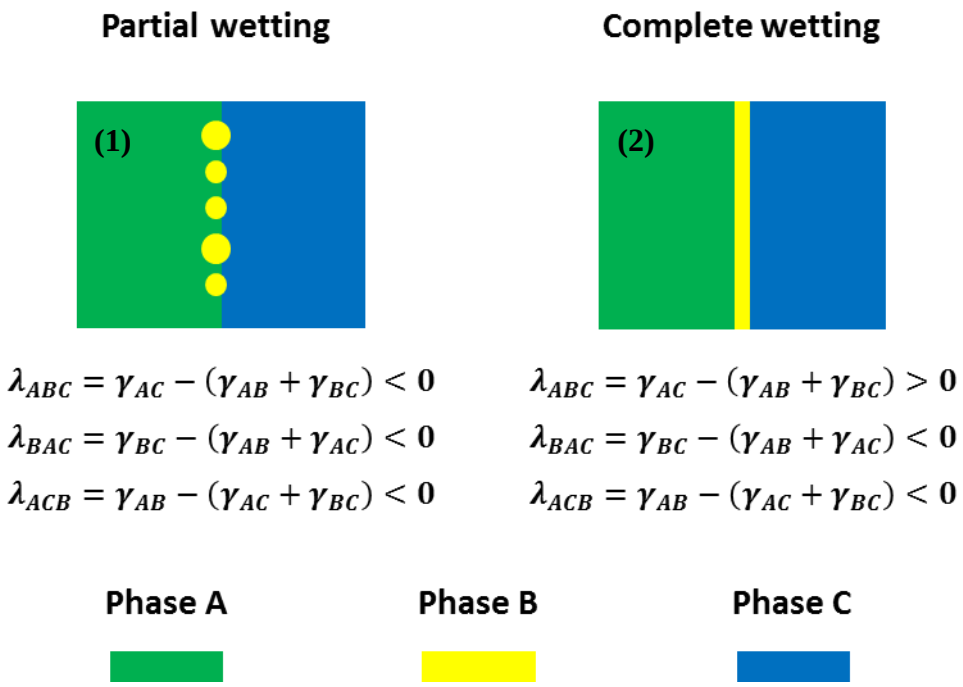

Figure 5.1: Partial and complete wetting morphologies in ternary blends of A/B/C predicted by Harkins' spreading theory (B: the minor phase at interface)

The localization of inorganic conductive fillers at the polymer interface has remained as a challenge [7, 20]. In this context, the finely percolated structures observed in the above-mentioned PE/PS/PMMA system provide an alternative approach [4, 5]. Although the localization of conductive inorganic fillers at the interface of polymer blends has been widely reported [2, 4, 5, 7, 20], to the best of our knowledge, no studies have been reported which assembles a polymeric conductive component at the interface of a continuous structure directly by melt blending.

Very little work has been published on the relationship between electrical properties and morphology in partially wet polymer systems. This could be due to the limited understanding of this particular morphology [15, 21, 22]. The classic work conducted by Torza and Mason presented partial wetting as a partial engulfing of one minor phase over another in a matrix phase [14]. Some recent work on the partially wet PE/PS/polypropylene (PP) system showed that the PS at the interface of the two major phases typically presents as isolated droplets [21]. Another study also showed in the polybutylene succinate/poly(lactic acid)/polycaprolactone (PBS/PLA/PCL) ternary system that partially wet PLA droplets form at the interface [22]. In that case, the partially wet morphology was maintained over a wide composition range and after annealing. Wilkinson et al. studied the partially wet ternary blends of PP/PA/poly[styrene-b-(ethylene-co-butylene)-b-

styrene] (SEBS) and showed that by replacing 25% of the SEBS with maleic-anhydride grafted SEBS (SEBS-g-MA) an acorn-type morphology formed where the PA phase was partially covered by the SEBS phase in the PP matrix [23]. The addition of SEBS-g-MA was believed to change the interfacial tensions between the phases and moved the system to the transition region between partial wetting and complete wetting (the spreading coefficient is close to zero). To date, it is still not clear how the microstructure of the phase at the interface (the intermediate phase) evolves during melt blending.

PEBA is a class of segmented block copolymers consisting of hard polyamide blocks and soft polyether blocks [24]. Depending on the polyamide/polyether ratio and the type of the blocks, a variety of physical properties can be obtained. When the polyether block is comprised of polyethylene oxide (PEO), an ionic conductive capacity is conferred to the copolymer [25-27]. The surface resistivity of neat PEBA without doping is typically higher than 10^6 Ω/sq and it is technically classified as a static dissipative material [12, 26, 28, 29]. However, "conductive" is used throughout the paper for the purpose of conciseness, and also because of the rapid development of PEO based polymer solid electrolytes, which are recognized as ionically conductive polymers [30-34]. The charge transportation mechanism in PEBA has been discussed in a previous paper [29].

In this work, for the first time, we aim to significantly reduce the percolation threshold of a conductive polymeric component (PEBA) by assembling it at the interface of two other continuous phases via complete or partial wetting directly through melt blending. The morphology development of the ternary blends and the microstructures of PEBA at the interface of the two systems will be compared and their effect on the resistivity of the blends will be systematically examined.

5.3 Materials and experimental

5.3.1 Materials

The PEBA used is a segmented copolymer with alternating polyethylene oxide (PEO) and polyamide 12 (PA12) blocks. The weight percentage of the PEO and PA12 is 55% and 45% respectively and the copolymer contains 10-20 blocks of each component [24]. The characteristics of the materials used in this work are summarized in Table 5.1. All the other

chemicals were purchased from Sigma-Aldrich. The polymers were dried at 60°C (PET at 90°C) under vacuum for 24 h before use.

Table 5.1: Characteristics of the polymers used

Polymer	Manufacturer	Mn/Mw (g/mol)	Tm/Tg (DSC)	Complex viscosity at 25 s^{-1} (Pa·s)	Surface resistivity (Ω/sq)/volume resistivity (Ω·cm)[d]
PEBA	Arkema	66,100/134,000[a]	Tm (PA) = 158°C Tm (PEO) = 9.8°C	210 (200 °C) 100 (250 °C)	6.0E+10/6.8E+8
LDPE	Total	–/135,000–140,000[b]	Tm = 111.0°C	1300 (200 °C) 759 (250 °C)	7.1E+15/4.7E+16
PET	DAK Americas	–	Tm = 243°C	806 (250 °C)	4.5E+16/1.1E+17
PVDF	Arkema	105,000/210,000[c]	Tm = 171°C	1460 (200 °C)	1.8E+15/1.0E+13

[a] GPC data; [b] from manufacture; [c] Ref. 35; [d] measured as described in Section 2.6.

5.3.2 Rheology

The rheological properties of the raw materials were examined on a MCR 301 rheometer (Anton Paar) with a parallel-plate configuration. A gap of 1 mm was used in all cases. Strain sweeps were first performed to determine the linear viscoelastic region. The thermal stability was evaluated in the oscillation mode with a frequency of 1 Hz at 200°C or 250°C for 20 min. The change of complex viscosity was found to be within 2% for all the materials at 200°C. At 250°C, the complex viscosities of PEBA and PET decreased by 17% and 11% respectively; the changes for LDPE and PS were within 1%. The frequency sweep was then performed for all the samples at a strain of 5-10%. N_2 was used all the time when applicable to minimize the degradation.

5.3.3 Interfacial tension measurement

The interfacial tensions of the various polymer pairs were determined by the breaking thread method using an Optiphot-2 microscope equipped with a hot stage. For each test, the polymer with the higher melting/glass transition temperature was used as the thread which was sandwiched by films of the other polymer. The temperature of the system was first increased slowly (at 5 °C/min) until the films were melted to reduce the residual stress and a higher heating

rate of 20–50°C/min was then applied to reach the designated temperature. Capillary instabilities gradually developed along the thread and the process was recorded by a camera connected to the microscope. The following formula was then used to calculate the interfacial tension:

$$\gamma = \frac{q\eta_m d_0}{\Omega_m}$$

where γ is the interfacial tension, q is the growth rate of the distortion, η_m is the matrix viscosity, d_0 is the initial thread diameter, and Ω_m is a tabulated function. N_2 was used to purge the system during the test. The final interfacial tension value reported is an average for 3–5 repeats of systems with well-developed capillary instabilities. More details concerning this technique are reported in previous publications [36].

5.3.4 Melt blending

All the blends were prepared by melt mixing in a Brabender internal mixer equipped with roller rotors for 9 min with the speed of 50 RPM under N_2 atmosphere. In all the formulations of ternary blends, the LDPE is the matrix and its volume fraction was fixed at 50%, while the volume fractions of the other component(s) changed accordingly as the concentration of PEBA was increased. The mixing chamber temperature was set at 255°C for blends with PET and at 200°C for the other samples. The real temperature of the melt was monitored to be 253 ± 1 °C and 200 ± 1°C after equilibrium was reached. In order to achieve a fill factor of 0.7, a total volume of 21 mL of material was added to the mixer. After blending, the samples were quickly taken from the mixer and immediately immersed in ice water to freeze-in the morphology for continuity and morphology analysis.

5.3.5 Morphology characterization, image analysis and selective extraction

The blend samples were cryogenically fractured in liquid nitrogen or microtomed using a Leica RM2165 microtome equipped with liquid nitrogen cooling system (LN21). The morphology was then characterized by scanning electron microscope (SEM). In order to improve the contrast, the PEBA phase was stained with 2 wt% phosphotungstic acid followed by washing with distilled

water to highlight the PEBA phase [37]. The samples were dried and coated with a gold layer by plasma sputtering on a Polaron SC502 sputter coater. The gold layer thickness was controlled to be about 1 nm by varying coating current and time. The SEM observations were conducted using a JEOL JSM 840 scanning electron microscope operated at 2–5 kV under the SB mode (detecting a mixture of secondary and backscattered electrons).

The image analysis was performed using a digitizing table from Wacom and SigmaScan v.5 software. The composition of PEBA located at the interface after blending was obtained based on the calculation of the area fraction it occupied on the SEM images. The thickness of the PEBA was estimated by the average length of the lines drawn across the PEBA domains which are almost perpendicular to the tangent line of the interface [22]. The interfacial area per volume or the perimeter per unit area (A_i) of the LDPE/PEBA interface LDPE/PEBA/PVDF were quantified based on the microtomed SEM images using the following equation [38].

$$A_i\left(\frac{\mu m^2}{\mu m^3}\right) = \frac{P(\mu m)}{A(\mu m^2)}$$

where *P* is the perimeter of the interface on a two-dimensional (2D) SEM image and *A* is the area of the image. At least 5 images from two different samples were analyzed. The average error in image analysis is estimated to be less than 15%.

In order to confirm PEBA is assembled at a continuous interface, selective extraction was performed. For example, in LDPE/PEBA/PET, if the PET/PEBA or the LDPE/PEBA is extracted and the structural integrity of the remaining LDPE and PET is maintained respectively, then both LDPE and PET are considered as continuous. LDPE, PEBA, PET and PVDF were extracted by boiling cyclohexane, formic acid (50°C), 1,1,1,3,3,3-hexafluoro-2-propanol (HFIP, room temperature) and dimethyl sulfoxide (70°C), respectively.

5.3.6 Resistivity measurement

In order to perform the resistivity tests, sheet samples were prepared by taking the sample directly from the internal mixer immediately after processing and quickly transferring it to a preheated mold (64 mm × 64 mm × 1mm). The assembly was then transferred to a hot press with a constant nitrogen flow for compression moulding. The temperature of the press was set at 180°C, 195°C and 260°C for LDPE/PEBA, LDPE/PEBA/PVDF and LDPE/PEBA/PET

respectively. The pressure of the press was increased to 150–200 psi slowly to minimize morphology change induced by the pressing process. A cold press was finally used to quickly cool down the sample to room temperature. The pressing conditions were optimized by a number of preliminary tests and the morphology was found to be well preserved after the molding process. Before the resistivity test, the samples were conditioned with 50% RH at room temperature for two weeks to ensure a constant water content. A Keithley electrometer (Model 6517B) with the 8009 Resistivity Test Fixture was used to determine the surface and volume resistivities of the samples by applying a DC voltage of 40 V and a bias time of 60 s. At least 4 tests were performed for each sample.

5.4 Results and discussion

5.4.1 Rheology

The complex viscosities of the neat polymers at the temperature corresponding to the processing temperature (200°C and 250°C) were examined and the results are shown in Fig. 5.2. At 50 RPM in the Brabender mixer, the shear rate is estimated to be around 25 s^{-1} [39]. Under these conditions, the viscosity of PEBA is much lower than that of the other polymers. The viscosities of the host polymers (components in addition to PEBA) are very close.

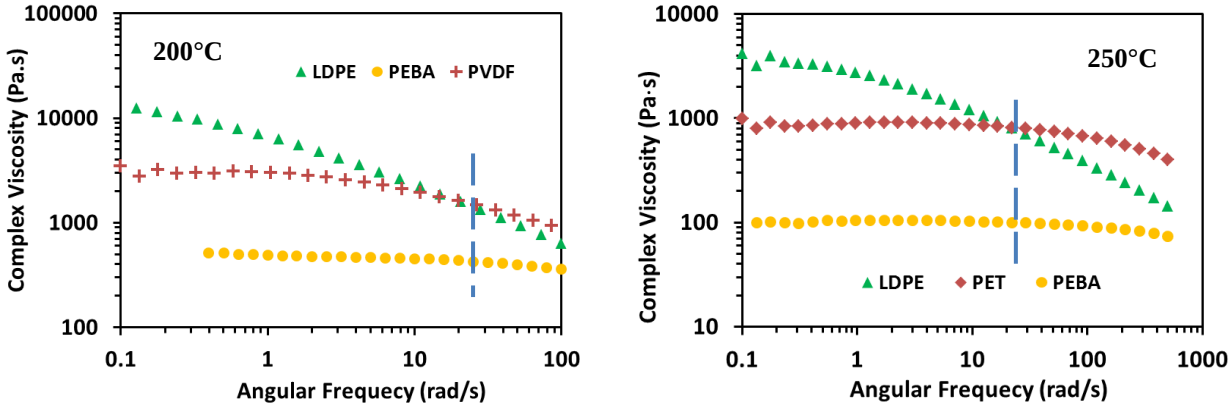

Figure 5.2: Complex viscosities of the neat polymers at 200 and 250°C. The dashed line indicates the processing shear rate of 25 s^{-1}.

5.4.2 Ternary blends

5.4.2.1 Interfacial tension and spreading predictions

The interfacial tensions among the different polymer pairs are listed in Table 5.2 and were measured directly by the breaking thread method. The spreading coefficients for the two ternary systems of LDPE/PEBA/PET and LDPE/PEBA/PVDF were then calculated and are also shown in the table. The spreading coefficient of LDPE/PEBA/PET ($\lambda_{PE/PEBA/PET}$) for example measures the tendency of the PEBA phase to spread over the PET phase in a PE matrix. The spreading of one phase over another is favoured by a high value of the spreading coefficient [14]. According to Harkin's theory (Fig. 5.1), in the LDPE/PET/PEBA blends (where PEBA is the minor phase), PEBA is expected to arrange into partially wet droplets at the interface of LDPE and PET due to the three negative spreading coefficients. The interfacial tensions $\gamma_{PE/PET}$ and $\gamma_{PE/PEBA}$ are very close (8.1 vs. 7.8 mN/m), leading to two comparable spreading coefficients for $\lambda_{PE/PEBA/PET}$ and $\lambda_{PE/PET/PEBA}$ (–1.5 vs. –2.1 mN/m). With a higher value of $\lambda_{PE/PEBA/PET}$, the tendency for PEBA to spread over PET is, however, slightly more favoured.

For the LDPE/PVDF/PEBA system, the theory predicts complete wetting with a positive $\lambda_{PE/PEBA/PVDF}$ = 1.2 mN/m, and PEBA should form a completely wet layer which completely separates PVDF from LDPE.

Table 5.2: Interfacial tensions, spreading coefficients and predicted morphologies (PEBA is the minor phase)

Ternary Blends	Interfacial tension (mN/m)	Spreading coefficient (mN/m)	Predicted Morphology
LDPE/PET/PEBA (250°C)	$\gamma_{PE/PET} = 8.1 \pm 0.9$ $\gamma_{PE/PEBA} = 7.8 \pm 0.9$ $\gamma_{PEBA/PET} = 1.8 \pm 0.2$	$\lambda_{PE/PET/PEBA} = -2.1 < 0$ $\lambda_{PET/PE/PEBA} = -14.1 < 0$ $\lambda_{PE/PEBA/PET} = -1.5 < 0$	Partial wetting: PEBA forms droplets at the LDPE/PET interface
LDPE/PVDF/PEBA (200°C)	$\gamma_{PE/PVDF} = 11.9$ [a] $\gamma_{PE/PEBA} = 8.0 \pm 1.4$ $\gamma_{PEBA/PVDF} = 2.7 \pm 0.3$	$\lambda_{PE/PVDF/PEBA} = -6.6 < 0$ $\lambda_{PVDF/PE/PEBA} = -17.2 < 0$ $\lambda_{PE/PEBA/PVDF} = 1.2 > 0$	Complete wetting: PEBA forms a layer which completely separates LDPE and PVDF

[a] From Ref. 8.

5.4.2.2 Interfacial tension and spreading predictions

Morphology evolution in the ternary blends

All the ternary systems are formulated as 50/X/Y (volume fraction) where LDPE is kept at a constant concentration of 50% and the composition of PEBA is increased with a corresponding decrease in the composition of the third phase. This strategy of formulation maintains a continuous structure for the LDPE, PET and LDPE, PVDF phases for up to 20% of PEBA in the systems and was confirmed by solvent extraction experiments.

Figs. 5.3a and b show the morphology of LDPE/PEBA/PET (50/3/47) at different magnifications and the white phase in the photos in the right column is PEBA which is stained by phosphotungstic acid. The 3% PEBA phase presents as partially wet discrete droplets at the interface, corresponding with the theoretical prediction from Harkins' spreading theory. However, the PEBA droplets seem not spherical but quite extended along the interface. This is different from a typical partial wetting system, such as PE/PS/PP where the PS droplets at the PE/PP interface appear very spherical [21]. This is probably because the interfacial tension between LDPE and PET is high in the LDPE/PEBA/PET system, and within a framework of partial wetting, the PEBA phases tend to spread to some level at the interface to reduce the highly unfavoured contact between LDPE and PET. In the PE/PP/PS system from the previous work, the interfacial tension between PE and PP is low compared to PE/PS or PP/PS, so the partially wet PS droplets tends to be more spherical to minimize the PS interaction with the PE/PP interface. The Neumann triangle approach can be used to quantitatively understand the shape of a partially wet droplet at the interface and that will be discussed in a later section. This tendency may also be considered by comparing the related corresponding spreading coefficient (λ): $\lambda_{PE/PEBA/PET}$ = −1.5 mN/m and $\lambda_{PE/PS/PP}$ = −6.5 mN/m. A larger λ is considered to favour spreading although other factors such as viscoelasticity may also play a role [14, 40, 41]. Thus, these results indicate that partially wet droplets can take different shapes at the interface depending on the relative interfacial tensions of the polymer pairs and the spreading coefficients [42]. More PEBA was observed at the interface as the concentration of PEBA was increased to 5% (Figs. 5.3c and d). Interestingly, the previously discrete PEBA domains observed at 3% of PEBA transform to a morphology with mixed PEBA layers and droplets as shown in Fig. 5.3d. Further increasing the concentration of PEBA to 10% and 15% leads to a complete PEBA layer formation at the interface. With composition variation, the morphology of the LDPE/PEBA/PET blend appears to

change from partial wetting (three-phase contact) (e.g., 3% PEBA) to complete wetting (two-phase contact) (e.g., 15% PEBA).

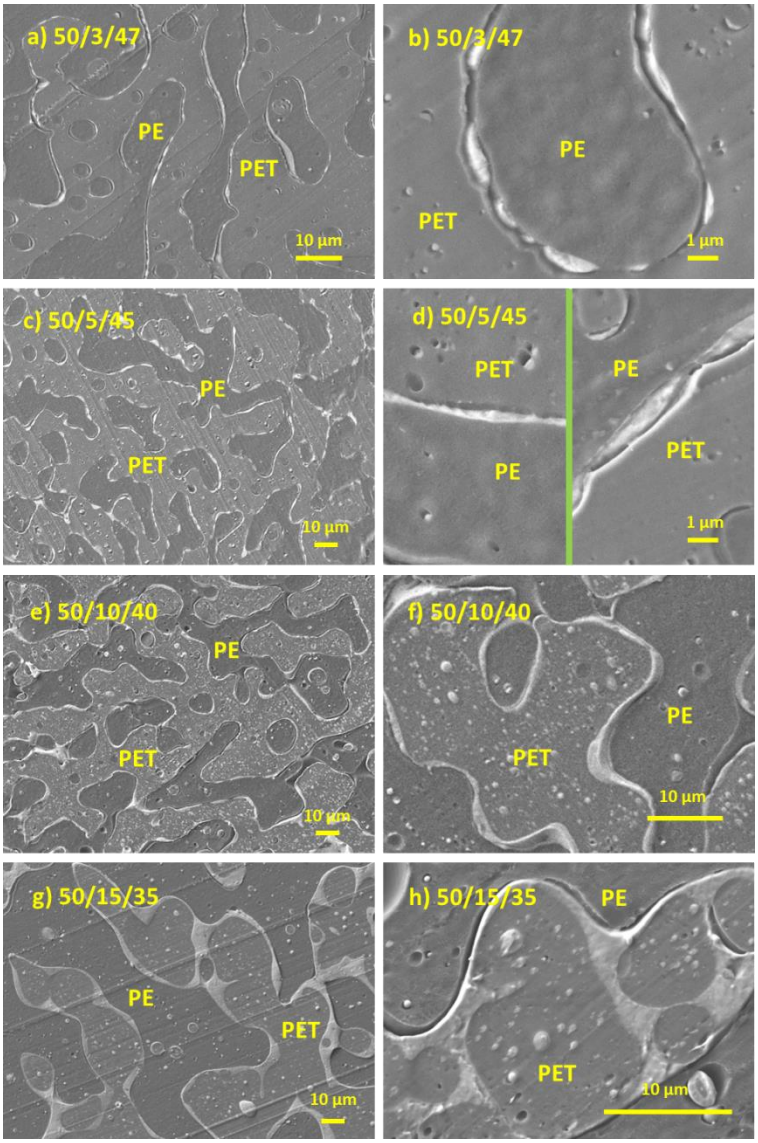

Figure 5.3: SEM images of cryo-microtomed LDPE/PEBA/PET blends with increasing PEBA composition. The right column shows the effect of phosphotungstic acid staining at a higher magnification (the white phase is PEBA). Photo (d) presents the observed two typical morphologies (layer and droplets) in different spots as separated by the line.

However, since microtomed images only reveal the information of the sample in 2D, cryo-fractured samples were also analyzed by SEM in order to observe the third dimension. Fig. 5.4

clearly confirms the above transition from partial wetting to complete wetting in the LDPE/PEBA/PET system as a function of composition. At 3%, PEBA forms separate discrete phases which display a weak partial wetting behavior at the interface. The extended PEBA domains have a thickness of around 280 nm perpendicular to the LDPE/PET interface and a dimension typically in the 1–3 µm range along the interface. Once the PEBA concentration is increased to 5%, percolated PEBA structures begin to dominate the morphology. At 10–15%, the PEBA forms a complete layer and fully separates the LDPE and PET phases. Note that a cursory estimation using image analysis shows that over 95% of the LDPE/PET interface is covered with 10% PEBA present in the system (Fig. 5.4c) (see Supporting Information Figs. 5.12 and 5.13). In this study, when the interface is covered by more than 95%, the observed morphology is considered as demonstrating complete wetting.

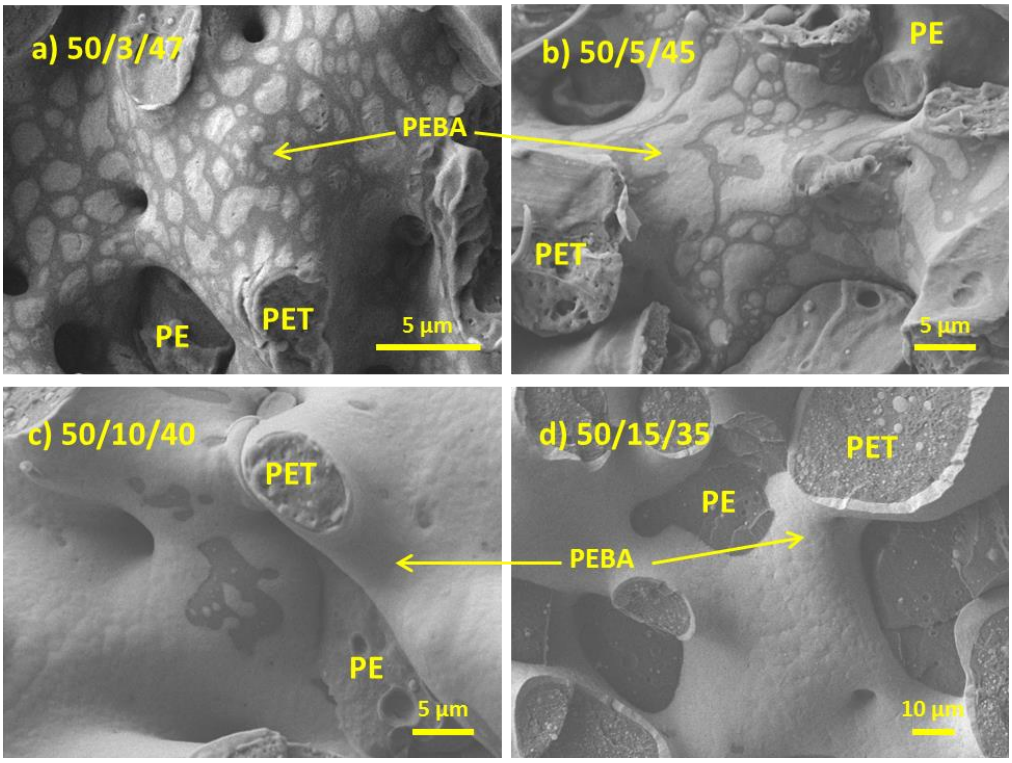

Figure 5.4: SEM images of cryo-fractured LDPE/PEBA/PET blends (the white domains are PEBA stained by phosphotungstic acid)

Unlike the weak partial wetting noted above, the LDPE/PEBA/PVDF system was predicted to demonstrate classic complete wetting. The spreading coefficient $\lambda_{PE/PEBA/PVDF}$ = 1.2 predicts a complete wetting morphology where PEBA should fully spread over PVDF and hence separate it from LDPE. Fig. 5.5 shows the morphology of the LDPE/PEBA/PVDF blends after cryo-fracture. In this case, it can be clearly seen that PEBA forms a thin complete layer at the interface of LDPE and PVDF at low PEBA concentrations. The integrity of the PEBA layer can be clearly identified at all concentrations down to 3% of PEBA at which point rupture did appear, but in only a very few spots (Figs. 5.5a and b). Observations of samples with lower PEBA concentrations become more difficult since it seems that the scale of the PEBA thickness approaches the contrast limit of the staining/SEM technique used to identify PEBA in this study.

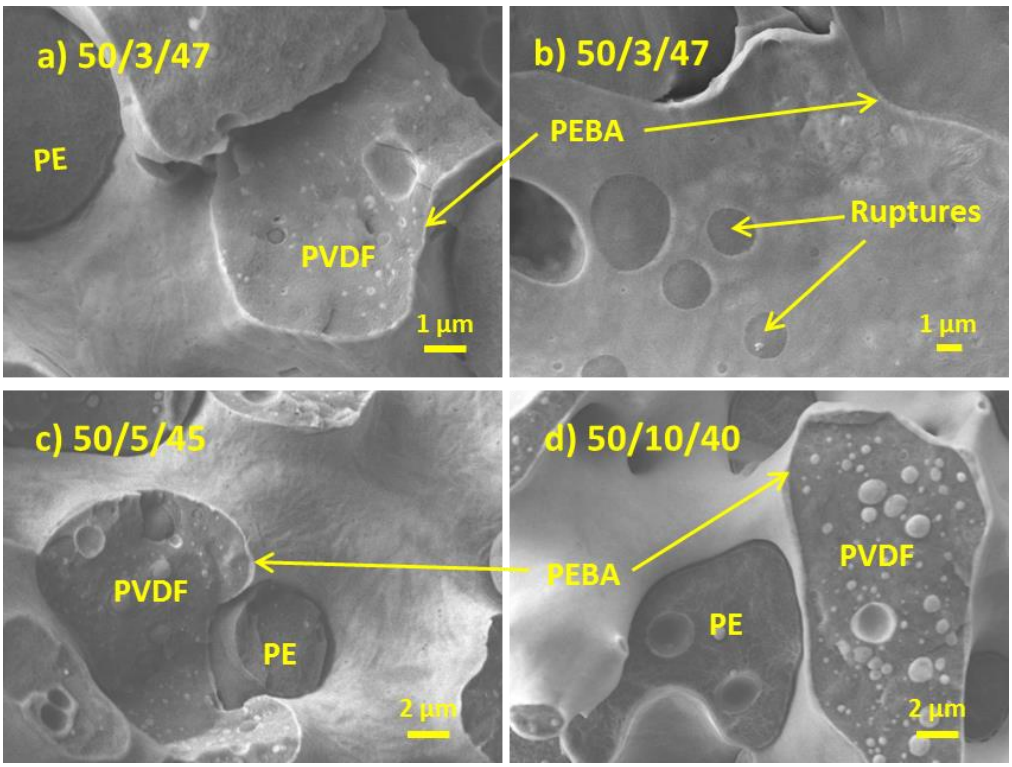

Figure 5.5: SEM images of cryo-fractured LDPE/PEBA/PVDF blends at different PEBA compositions (the white domains are PEBA stained by phosphotungstic acid).

As can be seen in Figs. 5.3–5.5, not all the PEBA is located at the interface for either LDPE/PEBA/PET or LDPE/PEBA/PVDF. A very small amount of PEBA domains (<5%) were

observed within the LDPE phases for both systems (Table 5.3). In the LDPE/PEBA/PET blends, the proportion of PEBA assembled at the interface decreases from 71% to 53% as the composition of PEBA increases from 5% to 10% (note that the amount of PEBA trapped within PET shows a significant corresponding increase to 43%) (Figs. 5.3b, d, f and Table 5.3), which corresponds to the region of transition from partial wetting to complete wetting. This is not surprising since the interface of LDPE and PET is saturated by PEBA at 10% and thus no strong thermodynamic forces are present to drive PEBA to the interface. The excess PEBA tends to go to the PET phase rather than LDPE probably owing to the much lower interfacial tension of PEBA/PET than LDPE/PEBA (Table 5.2). In the completely wet LDPE/PEBA/PVDF system, the fraction of PEBA at the interface is lower than that in LDPE/PEBA/PET until the transition from partial wetting to complete wetting in that latter system occurs. Around 40% of the PEBA was also found within the PVDF phase even in the system with a concentration of 3% PEBA (Fig. 5.5a and Table 5.3). Since the LDPE/PVDF interface is already saturated at 3% of PEBA, the same argument as above can be invoked. In fact, these results likely indicate that the complete wetting of the interface for LDPE/PEBA/PVDF takes place at values of PEBA less than 3%. It is interesting to note that a similar amount of PEBA is located at the interface (about 50%) when a complete PEBA layer forms in both systems.

Table 5.3: The distribution of PEBA and the interfacial area in the ternary blends

Blends		PEBA (%) in LDPE	PEBA (%) in PET or PVDF	**PEBA (%) at the interface**	Interfacial area ($\mu m^2/\mu m^3$)
LDPE/PEBA/PET	50/3/47	1.7	21	**77**	–
	50/5/45	1.8	27	**71**	
	50/10/40	4.3	43	**53**	
LDPE/PEBA/PVDF	50/3/47	3.3	44	**53**	0.20
	50/5/45	4.1	44	**51**	0.23
	50/10/40	2.8	46	**51**	0.21

The thicknesses of the PEBA phase estimated from the microtomed samples for LDPE/PEBA/PET and LDPE/PEBA/PVDF are shown in Fig. 5.6. In the case of the weak partially wet LDPE/PEBA/PET system, the domain thickness of PEBA increases dramatically from 284 nm to 2.5 µm with increasing PEBA composition from 3% to 15%. The transition from partial wetting to complete wetting happens at about 680 nm (with 10% PEBA). On the other hand, the PEBA phase thickness in the completely wet LDPE/PEBA/PVDF system is much lower than that for the weak partially wet system above and shows a more steady increment from 110 nm to 530 nm as PEBA concentration is increased. In this system, the PEBA layer thickness (L) can also be calculated by knowing the amount of PEBA at the interface (V) and the interfacial area (A_i): $L = V/A_i$ (Table 5.3). The calculated thicknesses correspond well with those directly measured from the SEM images as shown in Fig. 5.6. For example, at 3%, PEBA layer thicknesses of 102 nm (calculated) and 110 nm (measured) were obtained respectively. In this context, Reignier and Favis estimated in a PE/PS/PMMA system that the minimum thickness for PS to completely encapsulate PMMA is 40 nm, two times the radius of gyration of the PS [43].

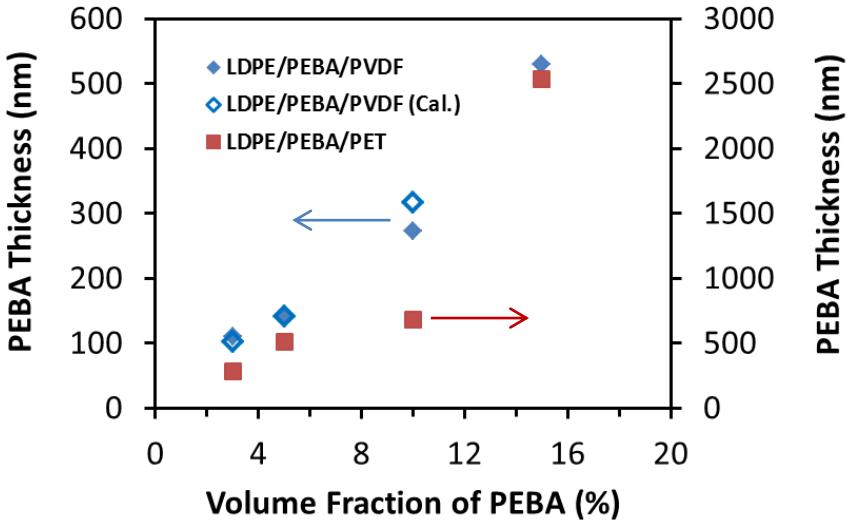

Figure 5.6: Domain thickness of PEBA at the interface in the ternary blends. Filled symbols: measured directly from SEM images; open symbols: calculated based on the amount of PEBA at the interface and the interfacial area.

5.4.2.3 Surface resistivity

Since the antistatic behavior of these blends was of principal interest, the surface resistivity of the blends was examined. This resistivity gives insight into the electrical percolation threshold in these blends. The volume resistivity was also examined and is shown in Supporting Information. The volume resistivity of the LDPE/PVDF sample is lower than that of the other blends at 0% PEBA due to the intrinsically lower PVDF volume resistivity as compared to other host polymers (see Table 5.1). In general, the trends of the volume resistivity of the different blends agree well with the surface resistivity curves, indicating a uniform structure from the surface to the bulk.

Fig. 5.7 shows three very different resisitivity behaviors for three blends: binary blend LDPE/PEBA; ternary LDPE/PEBA/PET and ternary LDPE/PEBA/PVDF. It should also be noted that the lower intrinsic surface resistivity of PVDF also contributes to reduce the resistivity of the blends and results in about a one-decade lower surface resistivity for LDPE/PVDF (50/50) as compared to the other blends before adding PEBA. However, the further significant decrease of surface resistivity for LDPE/PEBA/PVDF with increasing PEBA concentration is due to the introduction of PEBA (the amount of PVDF in the blends actually decreases as PEBA concentration increases).

A clear and very important reduction in percolation phenomena in Fig. 5.7 is observed as one progresses from the binary system to the weak partially wet ternary system with PET to the completely wet ternary system with PVDF. The results correspond well with the morphology development of PEBA in these systems (Figs. 5.3–5.5). It should be remembered that the morphology analysis showed that the weak partial wetting system of LDPE/PEBA/PET transitioned to a completely wet system at 10% PEBA. If one takes into account the one decade lower value in resistivity behavior observed at 0% PEBA for LDPE/PVDF, then the surface resistivity data at 10% PEBA in LDPE/PEBA/PET is comparable to the surface resistivity at 3% PEBA in LDPE/PEBA/PVDF (3.1×10^{13} *vs*. 1.2×10^{12} Ω/sq) where the complete PEBA layer is first observed microscopically in both cases. The intrinsic surface resistivity of PEBA used in this study is around 6×10^{10} Ω/sq making its blends of significant potential for antistatic applications. In this context, the surface resistivity of the material should be lower than 10^{13} Ω/sq [12]. To meet this requirement, at least 20% of PEBA is needed for the binary blends and 10% for the ternary blends of LDPE/PEBA/PET while only about 1% for the LDPE/PEBA/PVDF system.

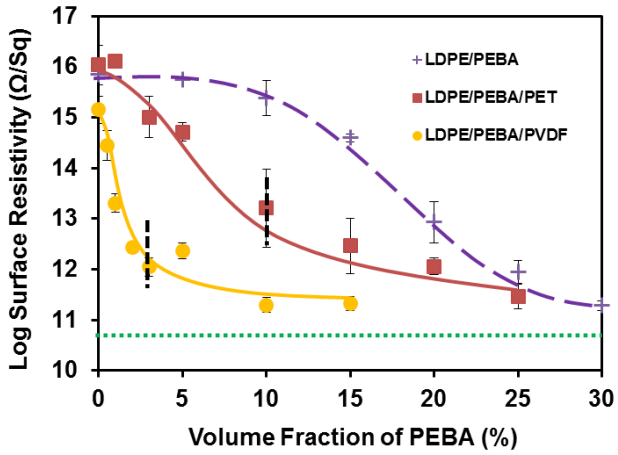

Figure 5.7: Surface resistivity of the binary and ternary blends. The dashed lines indicate the boundary of the two stages (steep reduction and gradual reduction) and the dotted line shows the surface resistivity of neat PEBA.

The decrease in the surface resistivity of the LDPE/PEBA/PET and LDPE/PEBA/PVDF blends may be divided into two stages, a region of steep reduction and a region of gradual reduction (dashed lines were drawn at the boundary of the two stages). The steep reduction of resistivity at lower concentrations (Stage I) of PEBA is indicative of the typical percolation phenomenon observed in many conductive systems where the conductive pathways are constructed at low concentrations [2, 7, 8]. In the LDPE/PEBA/PET system, the boundary between Stage I and Stage II (at about 10% as marked by dashed lines) for the surface resistivity coincides well with the transition from partial wetting to complete wetting (Fig. 5.4). A similar observation can be made in the completely wet LDPE/PEBA/PVDF system. The boundary between the two stages in surface resistivity lies at around 2–3%, providing further support for the inference that the PEBA layer in LDPE/PEBA/PVDF can fully cover the LDPE/PVDF interface only after its composition reaches this level.

The low level reduction in resisitivity with PEBA concentration in Stage II is due to other factors, such as the increasing composition of the conducting phase, and the reduction on constriction effect and tortuosity resulted from composition increment [30, 44]. In this context, Wiedenmann et al. proposed that the conductivity of a heterogeneous system is proportional to the intrinsic conductivity and volume fraction of the conducting phase, the constriction factor (the ratio of the minimum cross-section area over the maximum cross-section area along the conductive

pathway), and the reciprocal of the tortuosity (the ratio of the real conductive pathway length over the shortest distance between the two points) [44].

5.4.3 Transition from partial to complete wetting in LDPE/PEBA/PET

Following the work of Harkins and Feldman [13], Torza and Mason successfully demonstrated the use of spreading theory to predict the phase configurations in ternary immiscible liquid systems [14]. When two droplets are brought into contact in another phase, the engulfing of one droplet over the other is a combined process of penetration and spreading controlled by the size of the phases, the interfacial tensions and the spreading coefficients [14]. These arguments help one to understand the presence of PEBA partially wet droplets at the interface of LDPE and PET, but, it does not explain the observed transition from partial wetting to complete wetting at higher PEBA concentrations. It is well known that kinetic factors, such as viscosity and elasticity, can also affect the final morphology. Nemirovski et al. studied several immiscible ternary blends and argued that the spreading should be facilitated by a low engulfing-to-engulfed viscosity ratio [40]. Reignier et al. showed that the encapsulation of PS by PMMA observed in a PE/PS/PMMA system can only be explained by the interfacial free energy model when the elasticity contribution is considered [41]. These factors may be applicable when comparing blends comprised of different types of polymers with different viscoelasticities. However, in the present work, the transition from partial wetting to complete wetting happens in the same system and progresses only with increasing phase composition.

Static annealing was applied to selected samples to more clearly indicate the most stable morphology in the blend. Blends of LDPE/PEBA/PET with a composition of 50/3/47 and 50/15/35 demonstrate partial wetting and complete wetting morphologies respectively before annealing (Figs. 5.4a and d). After annealing, the general partial and complete wetting morphology features for those two samples are well preserved (Figs. 5.8a and b), indicating the stability of these morphological structures. The only distinction is that the PEBA domains in the LDPE/PEBA/PET blend with composition 50/3/47 look somewhat more roundish after annealing. The annealing of the complete wetting system of LDPE/PEBA/PVDF was also performed and the complete separation between LDPE and PVDF by PEBA is clearly shown after annealing (Figs. 5.8c and d).

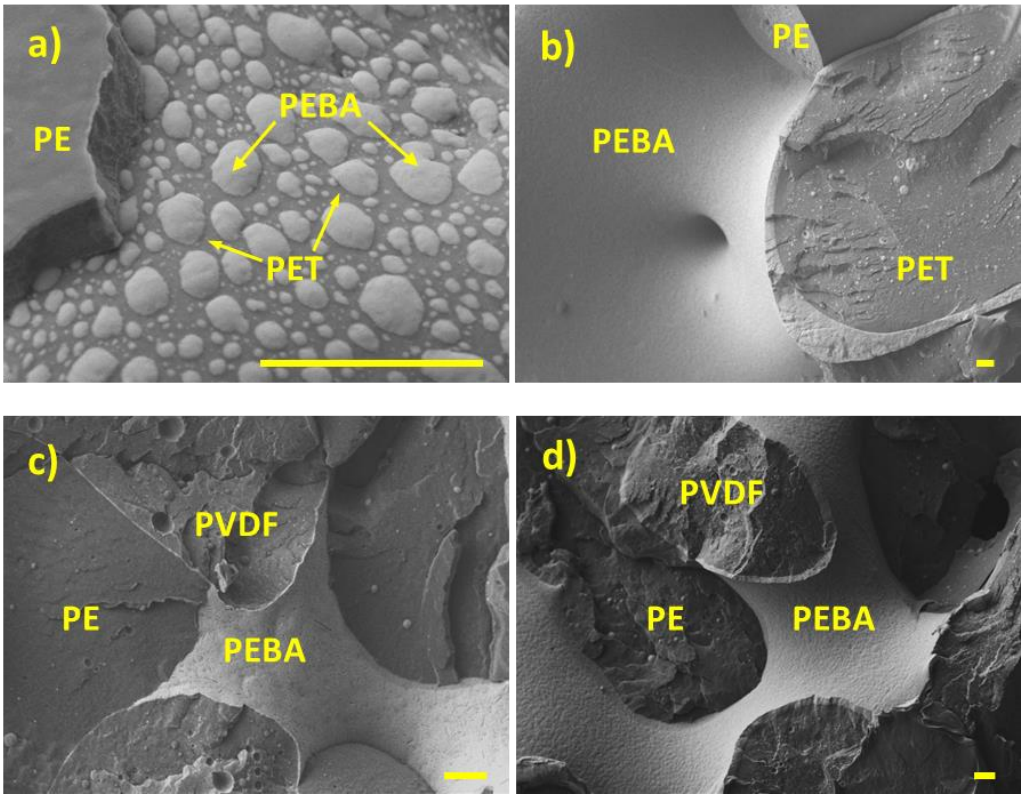

Figure 5.8: Morphology of the blends (PEBA is stained by phosphotungstic acid) after annealing for 10 min. (a) and (b): LDPE/PEBA/PET 50/3/47 and 50/10/40 at 260°C; (c) and (d): LDPE/PEBA/PVDF 50/3/47 and 50/10/40 at 200°C. Scale bar: 10 µm.

What then is the explanation for the transition from partial wetting to complete wetting with increasing PEBA concentration in LDPE/PEBA/PET?

In a partially wet ternary polymer blend system comprised of a minor phase with two other major phases, the minor phase will preferentially be located at the interface, arranging into discrete droplets. The shape of that droplet in equilibrium is defined by the interplay of the three interfacial tensions which can form the so-called Neumann triangle (Fig. 5.9) [45]. Applying the law of cosines, Eqn. (1) can be obtained:

$$cos\ \theta = \frac{{\gamma_{AC}}^2 - {\gamma_{AB}}^2 - {\gamma_{BC}}^2}{2\gamma_{AB}\gamma_{BC}} \quad (1)$$

where θ is the Neumann angle (contact angle), $\gamma_{AC,}$ γ_{AB} and γ_{BC} are the three interfacial tensions of the system (shown in Fig. 5.9). Thermodynamically, in order to have a transition from partial

wetting to complete wetting, cos θ has to approach 1 ($\theta \rightarrow 0$) which requires a high $\gamma_{AC,}$ a low γ_{AB} and a low γ_{BC}. For some systems, the right side of the formula gives a value even larger than 1, and Eqn. (1) is then equivalent to the Harkins' spreading theory expression for complete wetting (in Fig. 5.1 Case 2).

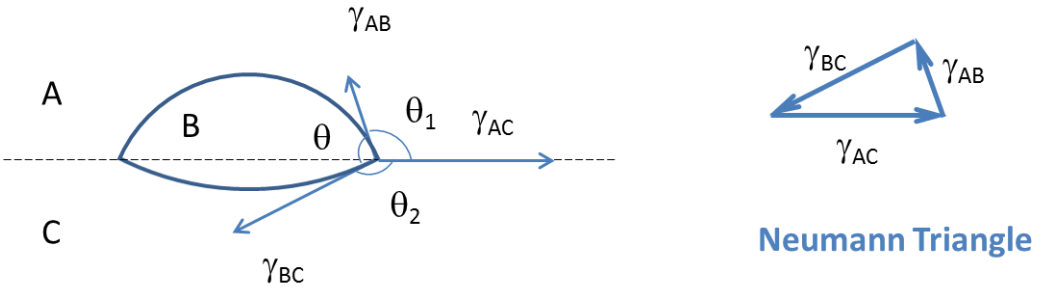

Figure 5.9: Schematic of the Neumann triangle: the equilibrium profile of a liquid B situated at the interface of liquids A and C.

When θ is small, such as in the present LDPE/PEBA/PET system where θ is estimated to be 1.5 (in radians) from Eqn. (1), the minor PEBA phase is driven to the interface and forms extended droplets during melt blending, partially covering the interface of LDPE and PET. Increasing the concentration of the PEBA phase results in an increased amount of the PEBA droplets at the interface and thus coalescence between the droplets can happen, leading to a larger domain size (thicker in the direction perpendicular to the interface and covering a larger area at the interface). This process advances and connected PEBA domains can develop. However, the connected structures are not stable and can disintegrate into smaller droplets due to the partial wetting nature of the system (dewetting). Thus, the final morphology of PEBA at the interface should be a balance of dewetting and coalescence. When the concentration of PEBA is increased, the coalescence effect will be clearly enhanced. As for the dewetting, to the best of our knowledge, no studies have been reported regarding a polymer film dewetting at the interface of two other polymers. However, the general trends may be inferred from the extensive work on the dewetting of thin films on solid substrates [46-50]. In this context, the dewetting speed (v) critically depends on the equilibrium contact angle θ_E (in radians, equivalent to θ in a three-liquid system as shown in Fig. 5.9):

$$v = \frac{\gamma {\theta_E}^3}{k\eta} \quad (2)$$

where γ and η are the surface tension and viscosity of the film phase, and k is a numerical dissipation factor [48, 49, 51]. Eqn. (2) indicates that strong partially wet systems with a high contact angle value and a high detwetting speed will be less susceptible to coalescence effects. In weak partially wet systems with small contact angles, coalescence will be able to counterbalance the slow dewetting speed and a transition to a coalescence-driven completely wet system could be expected. For ternary polymer blend systems, the surface tension in Eqn. (2) should be substituted by the interfacial tension which is typically one order of magnification lower. Eqn. (2) was also found to be applicable to systems with a polymer-polymer interface where the viscosity of the film is much lower than that of the substrate [51]. Note that the PEBA in our system has a much lower viscosity than the other polymers (Fig. 5.2). Thus, coalescence dominates over dewetting at a certain composition and gradually results in the full coverage of the partially wet interface. A conceptual model of this process is schematized in Fig. 5.10.

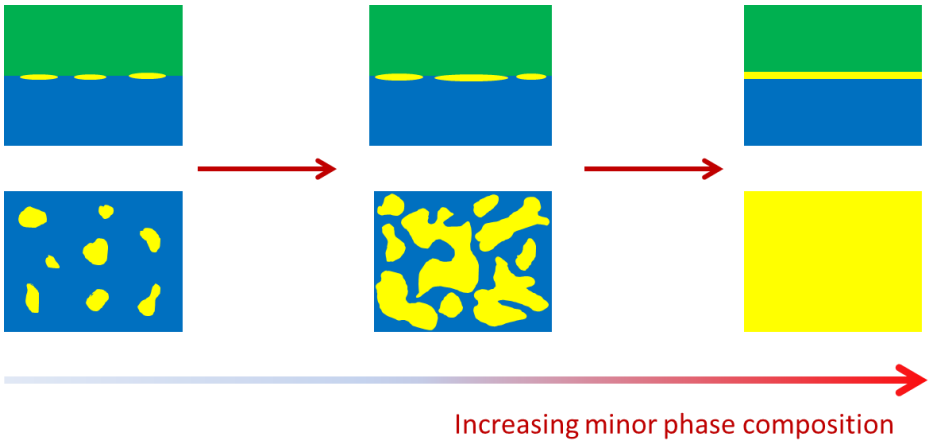

Figure 5.10: Schematic of the transition from partial wetting to complete wetting in weak partial wetting systems (Plane direction: perpendicular to the interface for top images and along the interface for lower images).

Some studies have shown that in certain systems the partial wetting morphology, characterized by isolated droplets at the interface, remains intact with composition variation [21, 22]. These systems may be referred to as strong partial wetting systems as compared to LDPE/PEBA/PET. An examination of Eqn. (2), can allow one to assume that the weak partial wetting system would be expected to have a contact angle $\theta < 1$ since if $\theta > 1$, the dewetting speed would be

significantly amplified with a power of 3 . In the LDPE/PEBA/PET system, θ is calculated to be 1.5 which agrees well with the in-situ measured value (see Supporting Information).

It is interesting that the coalescence driven completely wet LDPE/PEBA/PET (50/35/15) morphology is maintained after annealing (Fig. 5.8b). This can be explained since annealing affects both parameters, dewetting and coalescence. Clearly long annealing times would encourage dewetting, however those same long annealing times would also result in the well-known coarsening effect for the continuous LDPE and PET phases thus reducing their interfacial area. The PEBA is assembled at the interface of LDPE/PET, and therefore, decreasing the interfacial area would result in a coalescence of PEBA domains due to the conservation of volume. This coalescence effect appears to counterbalance the dewetting process and thus the integrity of the PEBA layer is maintained after annealing. The argument is supported by the observation of the ruptures of the PEBA layer in LDPE/PEBA/PET (50/35/15) at a lower annealing temperature (Fig. 5.11). In contrast to Fig. 5.8b, the coarsening effect in this case is not high enough to prevent the dewetting of the PEBA layer. The observation also further confirms the partial wetting nature of the LDPE/PEBA/PET system.

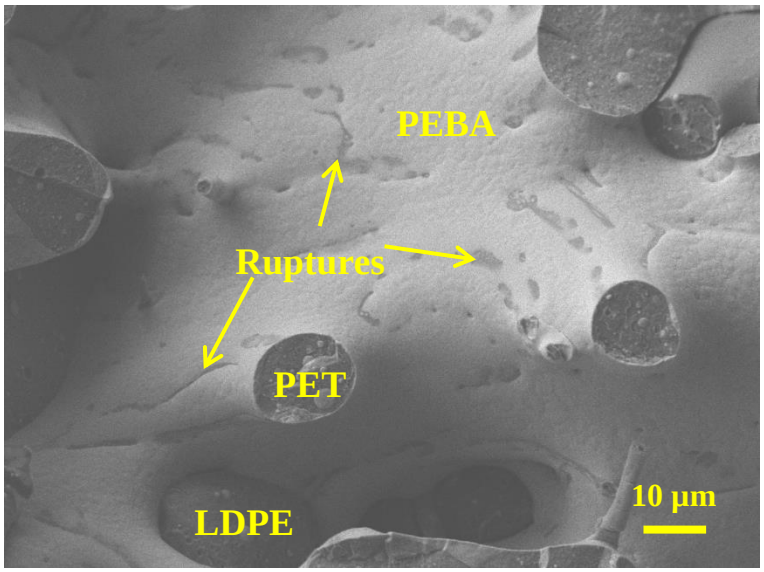

Figure 5.11: Morphology of cryo-fractured LDPE/PEBA/PET (50/35/15) annealed at 250°C for 10 min (PEBA is stained by phosphotungstic acid).

5.4.4 Minimum threshold concentration for complete wetting in LDPE/PEBA/PVDF

Another point for consideration would be to elucidate the relationship between the spreading coefficient and the minimum layer thickness of the intermediate phase in a completely wet ternary system. In the original work of Harkins and Feldman, a thick permanent sheet was observed for systems with low positive spreading coefficients, while a monomolecular layer seemed to form only with a high positive spreading coefficient [13]. Since then, very little work has been carried out. If one makes a comparison to the point of saturation of interfacial block copolymer modifiers at an A/B interface, typically areal densities of 0.1–0.2 molecule/nm^2 [21, 52] are observed. In the case of LDPE/PEBA/PVDF, the areal density of 3% PEBA at the LDPE/PVDF interface can be calculated to be 1.2 molecule/nm^2 (Mn of PEBA = 66100 g/mol [29]) which is about one order of magnification higher. Of course, in the case of the block copolymer interfacial modifier, significantly more interpenetration into the respective phases takes place.

As mentioned earlier, the thickness of the PEBA layer in the blend of LDPE/PEBA/PVDF (50/3/47) is estimated to be around 110 nm. At such a scale, the influence of Van Der Waals forces has to be considered which tend to thicken the film [47]. In a liquid-solid system, the free energy of the system can be thus written as [47]:

$$f = f_0 - \lambda S + \frac{A}{12\pi e^2} \quad (3)$$

where f_0 is a reference, λ is the spreading coefficient; S is the area covered by the liquid; A is the difference between the solid-liquid and liquid-liquid Hamaker constants; e is the film thickness. The last term on the right represents the contribution of van de Waals forces. Minimizing Eqn. (3) at constant volume of the film (constant $S{\cdot}e$) leads to:

$$e = a\left(\frac{3\gamma}{2\lambda}\right)^{\frac{1}{2}} \quad (4)$$

where a is a molecular length and γ is the surface free energy of the liquid phase. The result in this case is that the minimum layer thickness is expected to be inversely proportional to the square root of the spreading coefficient. This implies that the lower the spreading coefficient the higher the composition required to form a fully complete wetting layer. This conclusion would also support the notion that the minimum concentration to form a completely wet layer depends on the spreading coefficients. It is also evident from the above that a minimum concentration will be required in order to completely cover the interface. Indeed, further work would be required to explore the potentially important relationship between spreading coefficient, layer thickness and onset concentration in completely wet polymer blend systems.

The results in this work indicate that the boundary between partial wetting and complete wetting in ternary polymer blends is somewhat indistinct. For the weak partial wetting LDPE/PEBA/PET system, a transition from partial wetting to complete wetting is observed at high PEBA concentration, through a dewetting/coalescence model. The distinction of such a system with a complete wetting system strongly depends on the spreading coefficient. The present work indicates that even in completely wet systems, a compositional boundary (at very low PEBA concentrations) exists to form the completely wet structure and that this boundary is also determined by the magnitude of the positive spreading coefficient.

5.5 Conclusion

In this work it is shown that an ionic conductive polymeric component (PEBA) can be assembled at a continuous interface to form both weak partially wet (LDPE/PEBA/PET) and completely wet (LDPE/PEBA/PVDF) systems by melt blending. A novel morphological transition from partial wetting to complete wetting is demonstrated to be possible in the weak partial wetting LDPE/PEBA/PET, which is attributed to the dominant effect of coalescence over dewetting with increasing PEBA composition. It was shown that a minimum PEBA concentration is also required to form a fully wet interface in the complete wetting system of LDPE/PEBA/PVDF. Both of the ternary systems present a significant surface resistivity reduction as compared to the binary blends at the same PEBA composition due to the self-assembling of PEBA at the continuous interface. In particular, the completely wet LDPE/PEBA/PVDF blend demonstrates very effective percolation at low PEBA concentrations and a reduction of almost 3 orders of magnification in surface resistivity can be achieved with only 2% PEBA.

5.6 Acknowledgment

The authors would like to acknowledge Arkema for funding this research. Jun Wang would like to thank the China Scholarship Council (CSC) for a scholarship. The authors would also like to thank Dr. Eric Gamache and Ms. Laure Berdin Sguerra and Dr. Richard Chaigneau from Arkema for useful discussions. Prof. Daniel Therriault and Frederic Sirois from École Polytechnique de Montréal are also acknowledged for providing the resistivity measurement fixtures.

5.7 References

1. Zilberman, M.; Siegmann, A.; Narkis, M. *Polymers for Advanced Technologies* **2000,** 11, (1), 20-26.
2. Chen, J.; Shi, Y.-y.; Yang, J.-h.; Zhang, N.; Huang, T.; Chen, C.; Wang, Y.; Zhou, Z.-w. *Journal of Materials Chemistry* **2012,** 22, (42), 22398-22404.
3. Mao, C.; Zhu, Y.; Jiang, W. *ACS Applied Materials & Interfaces* **2012,** 4, (10), 5281-5286.
4. Cohen, E.; Zonder, L.; Ophir, A.; Kenig, S.; McCarthy, S.; Barry, C.; Mead, J. *Macromolecules* **2013,** 46, (5), 1851-1859.
5. Zhao, X. D.; Cao, J. P.; Zhao, J.; Hu, G. H.; Dang, Z. M. *Journal of Materials Chemistry A* **2014,** 2, (27), 10614-10622.
6. Kobayashi, T.; Wood, B. A.; Takemura, A.; Ono, H. *Polymer Engineering & Science* **2008,** 48, (11), 2247-2257.
7. Gubbels, F.; Jerome, R.; Vanlathem, E.; Deltour, R.; Blacher, S.; Brouers, F. *Chemistry of Materials* **1998,** 10, (5), 1227-1235.
8. Ravati, S.; Favis, B. D. *Polymer* **2010,** 51, (16), 3669-3684.
9. Levon, K.; Margolina, A.; Patashinsky, A. Z. *Macromolecules* **1993,** 26, (15), 4061-4063.
10. Zhang, Q.-H.; Wang, X.-H.; Chen, D.-J.; Jing, X.-B. *Journal of Polymer Science Part B: Polymer Physics* **2004,** 42, (20), 3750-3758.
11. Ravati, S.; Favis, B. D. *Polymer* **2011,** 52, (3), 718-731.
12. Kobayashi, T.; Wood, B. A.; Takemura, A.; Ono, H. *Journal of Electrostatics* **2006,** 64, (6), 377-385.

13. Harkins, W. D.; Feldman, A. *Journal of the American Chemical Society* **1922,** 44, (12), 2665-2685.

14. Torza, S.; Mason, S. G. *Journal of Colloid and Interface Science* **1970,** 33, (1), 67-83.

15. Hobbs, S. Y.; Dekkers, M. E. J.; Watkins, V. H. *Polymer* **1988,** 29, (9), 1598-1602.

16. Zhang, J. H.; Ravati, S.; Virgilio, N.; Favis, B. D. *Macromolecules* **2007,** 40, (25), 8817-8820.

17. Kolahchi, A. R.; Ajji, A.; Carreau, P. J. *Journal of Physical Chemistry B* **2014,** 118, (23), 6316-6323.

18. Zhang, K.; Mohanty, A. K.; Misra, M. *ACS Applied Materials & Interfaces* **2012,** 4, (6), 3091-3101.

19. Valera, T. S.; Morita, A. T.; Demarquette, N. R. *Macromolecules* **2006,** 39, (7), 2663-2675.

20. Göldel, A.; Marmur, A.; Kasaliwal, G. R.; Pötschke, P.; Heinrich, G. *Macromolecules* **2011,** 44, (15), 6094-6102.

21. Virgilio, N.; Marc-Aurèle, C.; Favis, B. D. *Macromolecules* **2009,** 42, (9), 3405-3416.

22. Ravati, S.; Favis, B. D. *Polymer* **2013,** 54, (25), 6739-6751.

23. Wilkinson, A. N.; Clemens, M. L.; Harding, V. M. *Polymer* **2004,** 45, (15), 5239-5249.

24. Malet, F. L. G., Thermoplastic Poly(Ether-b-Amide) Elastomers: Synthesis. In *Handbook of Condensation Thermoplastic Elastomers*, Fakirov, S., Ed. Wiley-VCH Verlag GmbH & Co. KGaA: 2006; pp 241-262.

25. Young, M.-Y.; Lin, J.-J. *Industrial & Engineering Chemistry Research* **1998,** 37, (11), 4284-4289.

26. Zoppi, R. A.; Fonseca, C. M. N. P.; De Paoli, M.-A.; Nunes, S. P. *Solid State Ionics* **1996,** 91, (1–2), 123-130.

27. Rosner, R. B. *Device and Materials Reliability, IEEE Transactions on* **2001,** 1, (1), 9-16.

28. Markarian, J. *Plastics, Additives and Compounding* **2008,** 10, (5), 22-25.

29. Wang, J.; Reyna-Valencia, A.; Favis, B. D. **2016**.

30. Bouchet, R.; Phan, T. N. T.; Beaudoin, E.; Devaux, D.; Davidson, P.; Bertin, D.; Denoyel, R. *Macromolecules* **2014,** 47, (8), 2659-2665.

31. Bouchet, R.; Maria, S.; Meziane, R.; Aboulaich, A.; Lienafa, L.; Bonnet, J.-P.; Phan, T. N. T.; Bertin, D.; Gigmes, D.; Devaux, D.; Denoyel, R.; Armand, M. *Nat Mater* **2013,** 12, (5), 452-457.

32. Gadjourova, Z.; Andreev, Y. G.; Tunstall, D. P.; Bruce, P. G. *Nature* **2001,** 412, (6846), 520-523.

33. Armand, M. *Advanced Materials* **1990,** 2, (6-7), 278-286.

34. Croce, F.; Appetecchi, G. B.; Persi, L.; Scrosati, B. *Nature* **1998,** 394, (6692), 456-458.

35. Zhang, H.; Lamnawar, K.; Maazouz, A. *Rheol. Acta* **2012,** 51, (8), 691-711.

36. Elemans, P. H. M.; Janssen, J. M. H.; Meijer, H. E. H. *Journal of Rheology* **1990,** 34, (8), 1311-1325.

37. Otterson, D. M.; Kim, B. H.; Lavengood, R. E. *J Mater Sci* **1991,** 26, (6), 1478-1484.

38. Dedecker, K.; Groeninckx, G. *Macromolecules* **1999,** 32, (8), 2472-2479.

39. Bousmina, M.; Ait-Kadi, A.; Faisant, J. B. *Journal of Rheology* **1999,** 43, (2), 415-433.

40. Nemirovski, N.; Siegmann, A.; Narkis, M. *Journal of Macromolecular Science, Part B* **1995,** 34, (4), 459-475.

41. Reignier, J.; Favis, B. D.; Heuzey, M.-C. *Polymer* **2003,** 44, (1), 49-59.

42. Virgilio, N.; Desjardins, P.; L'Espérance, G.; Favis, B. D. *Macromolecules* **2009,** 42, (19), 7518-7529.

43. Reignier, J.; Favis, B. D. *AIChE Journal* **2003,** 49, (4), 1014-1023.

44. Wiedenmann, D.; Keller, L.; Holzer, L.; Stojadinović, J.; Münch, B.; Suarez, L.; Fumey, B.; Hagendorfer, H.; Brönnimann, R.; Modregger, P.; Gorbar, M.; Vogt, U. F.; Züttel, A.; Mantia, F. L.; Wepf, R.; Grobéty, B. *AIChE Journal* **2013,** 59, (5), 1446-1457.

45. Wu, S., *Polymer interface and adhesion: Souheng Wu*. M. Dekker: New York, 1982.

46. Vrij, A.; Overbeek, J. T. G. *Journal of the American Chemical Society* **1968,** 90, (12), 3074-3078.

47. de Gennes, P. G. *Reviews of Modern Physics* **1985,** 57, (3), 827-863.

48. Wyart, F. B.; Daillant, J. *Canadian Journal of Physics* **1990,** 68, (9), 1084-1088.

49. Wyart, F. B.; Martin, P.; Redon, C. *Langmuir* **1993,** 9, (12), 3682-3690.

50. Sharma, A.; Reiter, G. *Journal of Colloid and Interface Science* **1996,** 178, (2), 383-399.

51. Wang, C.; Krausch, G.; Geoghegan, M. *Langmuir* **2001,** 17, (20), 6269-6274.

52. Adedeji, A.; Lyu, S.; Macosko, C. W. *Macromolecules* **2001,** 34, (25), 8663-8668.

5.8 Supporting Information

5.8.1 Interface coverage

The interface coverage by PEBA at the LDPE/PET interface in LDPE/PEBA/PET is estimated by the following equation:

$$Interface\ coverage\ (\%) = \frac{A_1}{A_0} \times 100$$

where A_0 is the area circled by the red line (area of LDPE/PET interface) and A_1 is the total area occupied by PEBA within the circled region (Fig. 5.12). Fig. 5.13 shows the evolution of the interface coverage as a function of PEBA composition in the LDPE/PEBA/PET blends. A_0 and A_1 were obtained by using a digitizing table from Wacom and SigmaScan v.5 software. In this method, the interface coverage in real three-dimensional space is approximated by its projection on the two-dimensional SEM image.

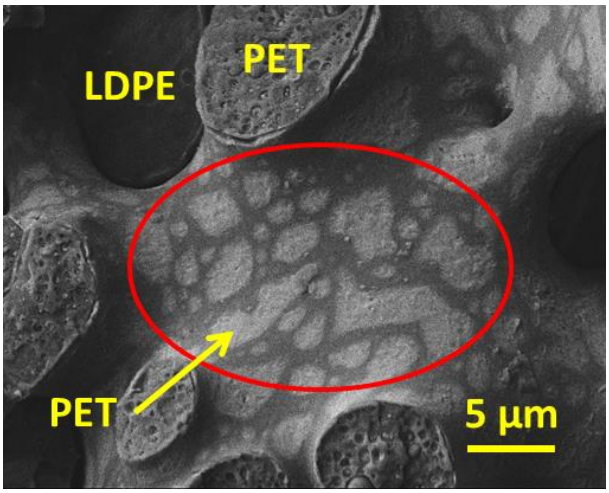

Figure 5.12: An example of an LDPE/PEBA/PET cryo-fractured sample for interface coverage calculation

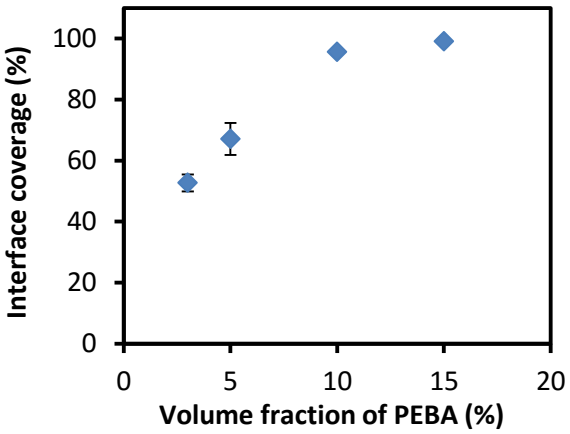

Figure 5.13: Interface coverage by PEBA at the LDPE/PET interface in LDPE/PEBA/PET blends

5.8.2 Volume resistivity of the blends

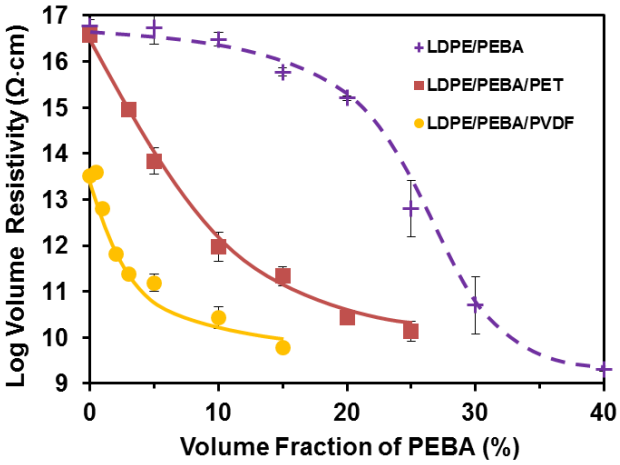

Figure 5.14: Volume resistivity of the blends.

Note that the initial lower volume resistivity for the LDPE/PEBA/PVDF system at 0% PEBA is due to the significant low volume resistivity of neat PVDF (10^{13} Ω·cm) as compared to other host polymers (10^{16} –10^{17} Ω·cm) (see Table 5.1 in the manuscript).

5.8.3 In-situ measurement of the Neumann angle for LDPE/PEBA/PET

The blend of LDPE/PEBA/PET (50/3/47) processed in Brabender internal mixer was subjected to annealing at 260°C for 10 min. The sample was cryo-microtomed and stained by phosphotungstic acid. The SEM images were then taken after gold coating. In order to determine the Neumann angle θ, the LDPE/PEBA and PET/PEBA interfaces were first fitted by complete circles (Fig. 5.15) [1-2]. The symmetrical axis of the two circles is defined by their centers (O1 and O2). The two centers are joined to the line of 3-phase contact respectively by the segments PO1 and PO2. The sum of the formed angles α and β mathematically equals the Neumann angle θ (defined by the tangent lines at P of the two circles) as shown in Fig. 5.15. The Neumann angle was then averaged based on 7 measurements: θ = 86° ± 8° = 1.5 ± 0.1 (in radians). The result corresponds very well with that obtained by Eqn. (1) from the interfacial tension values in the manuscript.

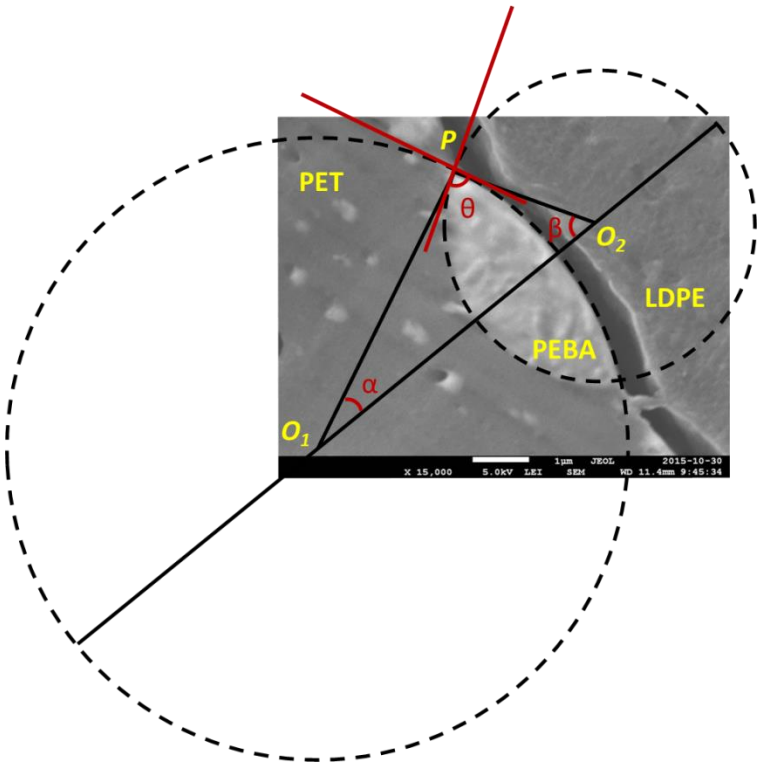

Figure 5.15: Geometrical parameters of the LDPE/PEBA/PET (50/3/47) blend for determining the Neumann angle θ.

5.8.4 References

(1) Torza, S.; Mason, S. G., Three-phase interactions in shear and electrical fields. *J. Colloid Interface Sci.* **1970,** *33* (1), 67-83.

(2) Virgilio, N.; Desjardins, P.; L'Espérance, G.; Favis, B. D., In Situ Measure of Interfacial Tensions in Ternary and Quaternary Immiscible Polymer Blends Demonstrating Partial Wetting. *Macromolecules* **2009,** *42* (19), 7518-7529.

CHAPTER 6 ARTICLE 3: CONTROLLING THE HIERARCHICAL STRUCTURING OF CONDUCTIVE PEBA IN TERNARY AND QUATERNARY BLENDS*

Jun Wang [a], Alejandra Reyna-Valencia [b], Richard Chaigneau [b], Basil D. Favis [a]

[a] *CREPEC, Department of Chemical Engineering, École Polytechnique de Montréal, Montréal, Québec, H3T 1J4, Canada*

[b] *Laboratoire d'étude des matériaux (LEM), Arkema-CERDATO, Serquigny, 27470, France*

6.1 Abstract

There is an advantage, when preparing conductive systems, to use less expensive commodity polymer phases as carriers of the conductive polymer. However, when the conductive polymer is blended with polyolefins and/or polystyrene as a ternary blend, it has a tendency to form the core or inside phase due to its high interfacial tension with the other components. This can limit its capacity to reduce resistivity as compared to situating it at the interface. In this work starting with a ternary low-density polyethylene/polystyrene/poly(ether-block-amide) (LDPE/PS/PEBA) blend, we will examine the influence of the conductive PEBA concentration on its morphology when it exists as a core phase and its effect on resistivity. Then, the hierarchical structuring of the PEBA phase will be modified through two strategies: by the addition of a fourth phase (quaternary blend) and by the addition of a copolymer interfacial modifier. Each of these approaches will be shown to be capable of allowing the PEBA to form a percolated structure confined between two other continuous phases within systems of high commodity polymer content (70–90%). Meanwhile, the PEBA percolation threshold is dramatically decreased in these systems and significant reductions on surface resistivity (as high as 4 orders of magnitude) are obtained at low PEBA compositions

* Submitted to ACS Applied Materials & Interfaces.

Key words: *localization, multiphase, hierarchical structures, assembly, multiple percolation, surface resistivity, antistatic, morphology control, polymer blends, commodity polymer.*

6.2 Introduction

The world plastic market is dominated by the few commodity polymers with annual production of hundreds of millions of tons, including polyolefins, PS and polyvinylchloride (PVC). However, there is an increasing demand for commodity plastics with new functional properties (e.g., improved heat resistance, high mechanical strength, electrical properties) which are typically exhibited by expensive engineering polymers or non-polymeric materials [1]. Multiphase polymer blending, in particular, has been an approach of great interest to expand the applications for polymers by combining the properties of the different components [1-6].

The control of the morphology in multi-phase polymer systems is a key parameter to tailor the final properties of the product [3, 6-10]. In a ternary system consisting of two major phases A and B, and a minor phase C, the four possible morphological states are schematically shown in Fig. 6.1, which can be predicted by Harkins' spreading theory [11-13]. The theory defines three spreading coefficients based on interfacial tension. If one spreading coefficient is positive, complete wetting (two phase contact) is expected where C tends to be exclusively located within either A or B, or forms a layer fully separating the A/B interface (Fig. 6.1a–c). In the case of three negative spreading coefficients, phase C will preferentially arrange into droplets and partially wet (three phase contact) the A/B interface (Fig. 6.1d). Other factors such as composition, viscoelasticity and annealing have also been reported to have an effect on the final morphologies [10, 14-16].

Despite the wide interest and potential practical outcomes related to the morphology control of multiphase polymer blend systems, few studies have been published on the hierarchical structuring of phases in ternary or quaternary systems (i.e., controlling the phase location from within one phase to the interface; or conversion of the system from partial wetting to complete wetting). One possible approach to achieve that is to add a new component, either as a separate phase or an interfacial modifier. Studies on completely wet PE/PS/PMMA and PE/PS/PMMA/PVDF systems indicate that the PMMA core in the former can be transformed to layer structures at the interface of PS and PVDF, provided that the spreading coefficients of each

three-component system in the quaternary blend (4 sets in total) meet the complete wetting requirement in Harkins' theory [5, 17]. Interfacial modification was also shown to be another alternative to manipulate the type of the morphology by tailoring the interfacial tensions between the components. Horiuchi and coworkers reported that by adding maleated PS (PS–MA) to the ternary blend of PA/PS/polycarbonate (PC), the previously partial engulfing of PC by PS changed to a full encapsulation, indicating the morphology evolved from partial wetting to complete wetting [18]. Virgilio et al. showed that in a partially wet PE/PS/(polypropylene) PP ternary system, the minor PS phase formed droplets at the PE/PP interface or within PP [19]. After adding 1% (based on the volume of PS) of styrene-(ethylene-butylene) diblock copolymer (SEB), the PS droplets were found to be exclusively located at the HDPE/PP interface. Increasing the amount of SEB to 15%, the PS droplets were further pulled mostly to the PE phase. The morphology evolution was attributed to the reduction on the interfacial tension between PE and PS with the introduction of SEB.

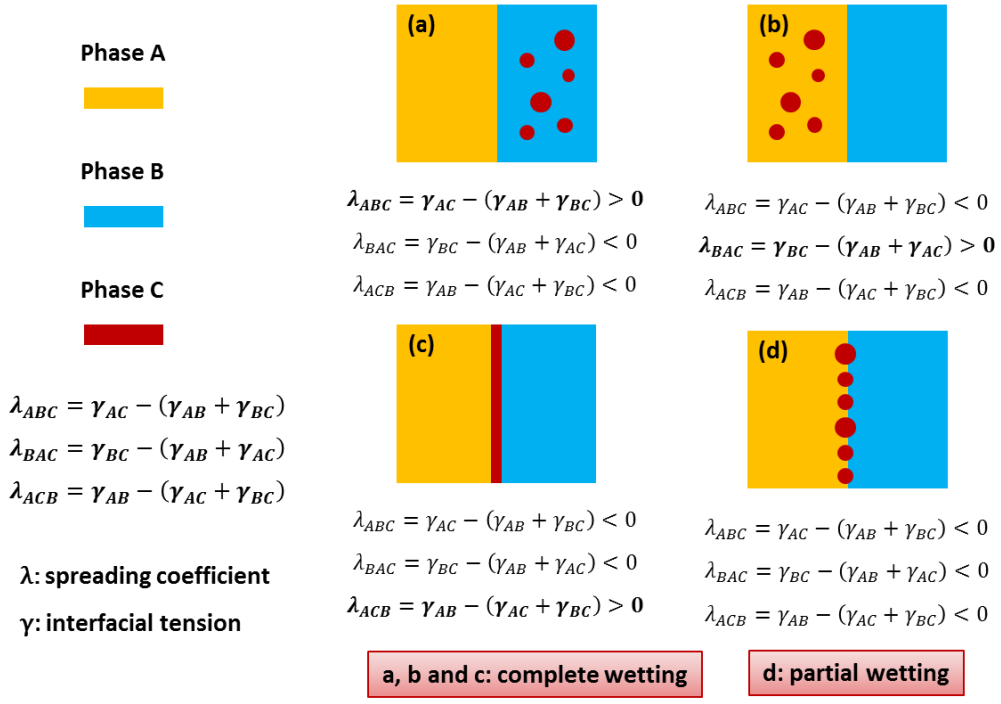

Figure 6.1: Possible morphologies in ternary blends of A/B/C predicted by Harkins' spreading theory (C is the minor phase).

The conductivity of a polymer blend is mostly determined by the morphology of the conductive phase as it is directly related to the development of the conductive pathways in the system. The percolation threshold in a heterophase system can be significantly reduced by increasing the number of phases to form multiple percolation structures (percolated structures within another percolated structure) [3, 5, 20]. For example, Zilberman et al. compared the conductivity between the ternary blends of polystyrene/polyamide/polyaniline (PS/PA/PANI) and the corresponding binary blends of PS/PANI and PA/PANI [3]. With 10% of PANI, the ternary blend shows a significantly higher conductivity due to the preferential localization of PANI within the PA phase. Ravati and Favis prepared multi-percolated systems comprised of up to five components with PANI always located in the core [5]. The percolation threshold was reduced to below 5% in the multiphase polymer blends. And with 5% of PANI, the conductivity was found to be significantly increased from 10^{-11} to about 10^{-6} S/cm as the number of components increases.

On the other hand, studies on conductive composite systems have indicated that the percolation threshold can be dramatically reduced by confining the conductive component at a continuous interface as compared to within one of the phases [2, 5, 21-22]. In the former case, the conductive particles have much more chance to collide in a confined space, which results in the formation of conductive pathways at low compositions.

PEBA is a class of block copolymers comprised of alternating polyamide (PA) and polyether blocks [23]. When polyethylene oxide (PEO) is presented as the polyether block, an ionically conductive property is imparted to the copolymer [24-26]. These polymers are of primary interests for antistatic applications [9, 27-28]. In a previous study, we demonstrated a reduction of almost 3 orders of magnification on surface resistivity with only 2% PEBA in the systems where PEBA is inherently assembled at the interface [10].

To date, few studies have been published on controlling the hierarchical structuring of a polymeric conductive phase in multiphase polymer blend systems and the influence of such a manipulation on conductivity/resistivity. In this study, we aim at controlling the localization of conductive PEBA in hierarchically structured and multi-percolated ternary and quaternary blends to significantly reduce the electrical percolation threshold for PEBA while maintaining a high content of LDPE and PS (70–90%). The LDPE/PS/PEBA blends will be first studied where PEBA is exclusively confined as the core phase within the PS. Then the addition of a fourth

polymeric component and also the influence of interfacial modification to localize PEBA at a continuous interface and its influence on surface resistivity will be examined.

6.3 Experimental

6.3.1 Materials

The PEBA copolymer is composed of alternating PEO and PA12 blocks. The weight percentage of the PA12 and PEO is 45% and 55% respectively with about 10–20 blocks of each component in the copolymer.29 The ethylene–acrylic ester–maleic anhydride (EAM) is a random terpolymer containing 6 wt% acrylic ester and 3.1 wt% maleic anhydride. Table 6.1 lists the main characteristics of the materials used in this study.. The other chemicals were supplied by Sigma-Aldrich. A vacuum oven was used to dry the polymers at 60°C (PET at 90°C) for 24 h before processing.

Table 6.1: Characteristics of the materials used*

Polymer	Manufacturer	Density at 25°C (g/cm^3) [a]	Tm/Tg [b]	Surface resistivity (Ω/sq) [c]
PEBA	Arkema	1.08	Tm = 158°C, 9.8°C	6.0E+10
PS	Americas Styrenics	1.04	Tg = 99°C	9.1E+15
LDPE	Total	0.92	Tm = 111°C	7.1E+15
PET	DAK Americas	1.35	Tm = 243°C	4.5E+16
PVDF	Arkema	1.75	Tm = 171°C	1.8E+15
EAM	Arkema	0.95	Tm = 107°C	1.8E+16

*PET: polyethylene terephthalate; PVDF: polyvinylidene fluoride

[a.] Determined by pressure-volume-temperature measurements; [b.] measured by differential scanning calorimetry (DSC) at 10°C/min; [c.] measured as described in Section 2.6.

6.3.2 Interfacial tension measurement

The interfacial tensions were determined by the breaking thread method on an Optiphot-2 microscope with a hot stage accessory. Threads were drawn from the melt with uniform diameters ranging from 20 to 40 μm. The threads were sandwiched within the counterpart polymer films prepared by compression mounding, and then the system was placed on the hot stage. The temperature was first increased slowly at 5°C/min to reduce the residual stress until

the films were melted and then was further increased to the designated temperature (the same as the processing temperature) at 20°C/min. The camera connected to the microscope recorded the development of capillary instabilities and images were analyzed by SigmaScan v.5 software for interfacial tension calculation using the following formula:

$$\gamma = \frac{q\eta_m D_0}{\Omega_m}$$

where γ is the interfacial tension, q is the growth rate of the distortion, η_m is the viscosity of the matrix, D_0 is the initial thread diameter, and Ω_m is a tabulated function. The system was purged by N_2 flow during the test. The final interfacial tension is averaged based on 3–5 repeats of systems with well-developed capillary instabilities. More information concerning this method can be found elsewhere.[30-31]

6.3.3 Melt blending

The blends were processed in a Brabender batch mixer (Plasti-Corder DDR501) for 9 min under a N_2 atmosphere. Roller blades were used and the mixing speed was set at 50 RPM. The processing temperature of the mixing chamber was set at 255°C for the blends with PET and at 200°C for the other samples. After a stabilization phase was achieved, the real temperature of the polymer melt was 253 ± 1°C and 200 ± 1°C respectively. With a fill factor of 0.7, 21 mL of material was added to the mixer for each blend. The materials of each blend were added to the mixer simultaneously except for the EAM modified LDPE/PS/PEBA system. In that case, 20% EAM (2% based on the final LDPE/PS/PEBA blend) was first mixed with PEBA at 200°C for 5 min. The mixture was then collected and blended with LDPE and PS using the above-mentioned procedure. After mixing, the samples were immediately taken from the blades and quenched in ice water to freeze-in the morphology. The continuity and morphology tests were then performed on these samples.

6.3.4 Morphology characterization and image analysis

The blends were cryogenically microtomed or fractured for morphology analysis. The microtoming was carried out on a Leica RM2165 microtome equipped with an LN21 cooling system. In order to increase the contrast between different phases, the PEBA phase was either extracted by formic acid (50°C), or stained with 2 wt% phosphotungstic acid for 30 min followed

by a distilled water surface wash.[32-33] A Polaron SC502 sputter coater was employed to coat the samples with a gold layer. . The thickness of the gold layer was controlled to be about 10 nm and 1 nm for the extracted and stained samples respectively by using a different coating current and time. The morphology was then characterized using a JEOL JSM 840 scanning electron microscope (SEM) with a voltage at 2–5 kV under the SB mode.

The SEM images were analyzed by a digitizing table from Wacom and SigmaScan v.5 software. The proportion of PEBA located within PS or at the LDPE/PS interface in the LDPE/PS/PEBA systems (unmodified or modified respectively) was obtained based on the calculation of the area fraction it occupied on the SEM images. The coverage of the PS/PET interface by PEBA in LDPE/PS/PEBA/PET is approximated by its projection on the two-dimensional SEM image as explained elsewhere.[10]

6.3.5 Selective extraction and continuity

The blend samples were cut into cubes of 5 × 5 × 5 mm for selective extraction. Formic acid (50°C) was used to selectively dissolve PEBA and LDPE (and PS in some cases) was removed by boiling cyclohexane. In these two cases, the solvent was refreshed until a constant weight was obtained after drying. A Soxhlet apparatus was used to selectively extract PS with cyclohexane and PET+PEBA with hexafluoro-2-propanol (temperature of the solvent in the extraction chamber is 40–50°C in both cases) for one week. The continuity (%) of the target phase is determined using the following formula:

$$\text{Continuity (\%)} = \frac{m_i - m_f}{m_0} \times 100\%$$

where m_i and m_f is the initial sample weight and the sample weight after the extraction respectively; m_0 is the weight of the target phase contained in the sample which is calculated based on the formulation.

6.3.6 Surface resistivity: preparation and measurement

The antistatic properties of the blends were evaluated by examining the surface resistivity. The blends were collected immediately after processing and put into a preheated copper mold with a

dimension of 64 mm × 64 mm × 1mm. Sheet samples were then prepared by compression moulding on a hot press. The press temperature was set to be 260°C for the LDPE/PS/PEBA/PET blends, 195°C for LDPE/PS/PEBA/PVDF, and 180°C for the other blends. In order to preserve the morphology, the pressure applied on the mold was gradually increased to 150–200 psi within a period of about 1 min. For the annealing of the LDPE/PS/PEBA blends modified with EAM, the pressure was released while maintaining the contact between the mold and the press, and the temperature was kept at 200°C for different periods of time. The pressed sample was then quickly cooled down to ambient temperature on a cold press. The sheet samples were conditioned with 50% RH at 21 ± 1 °C for 15 days to achieve a constant moisture content. The surface resistivity was measured as per the ASTM D257 Standard on a Keithley electrometer (Model 6517B) equipped with the 8009 Resistivity Test Fixture. A DC voltage of 40 V and a bias time of 60 s were applied.

6.4 Results and Discussion

6.4.1 Morphology of LDPE/PS/PEBA ternary blends

The LDPE/PS/PEBA blend with a volume fraction of 75/20/5 was prepared and the morphology was examined by SEM (Fig. 6.2). Based on the volume ratio, the three phases can be identified: the small holes result from the extraction of PEBA; the remaining dispersed phase is PS since it occupies 20% of the volume fraction in the blend; and finally the matrix is LDPE. Clearly, PEBA is located within the PS phase as the core in this system.

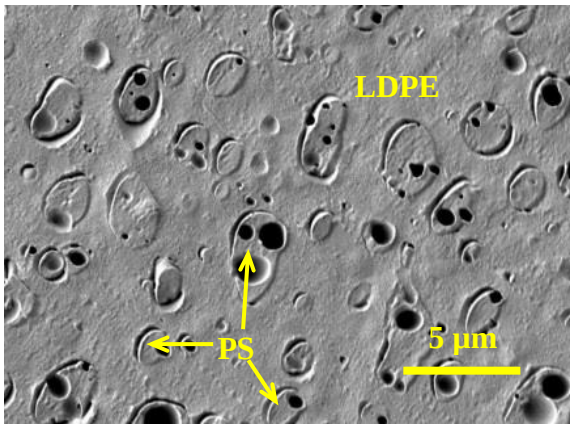

Figure 6.2: Morphology of LDPE/PS/PEBA with a volume fraction of 75/20/5 (PEBA extracted).

In order to develop percolated PEBA structures confined in a continuous PS phase, an LDPE/PS binary blend with volume fraction of 50/50 was firstly prepared to ensure a co-continuity for

LDPE and PS. Then the composition of LDPE is fixed at 50% and the composition of PS is gradually decreased while increasing the content of the third component PEBA (denoted as LDPE/PS/PEBA 50/X/Y). The continuity of PS in LDPE/PS (50/50) and LDPE/PS/PEBA (50/25/25) was determined to be 101% and 96% respectively. Thus, it can be inferred that the morphology of PEBA will develop within a continuous PS phase in the ternary LDPE/PS/PEBA blends with up to 25% PEBA, and a lower PEBA percolation threshold would be expected as compared to that in the binary blend due to the multiple percolation phenomenon [20]. The morphology evolution of the blends is reported in Fig. 6.3. As can be seen, virtually all the PEBA phase (>95%) is located in the PS phase and as the concentration of PEBA increases, the phase size becomes larger and more connected. Elongated PEBA domains start to appear with only 10% PEBA and a fully continuous morphology of PEBA was obtained at the volume fraction of 50/30/20 for the ternary blend with a PEBA continuity of 98%.

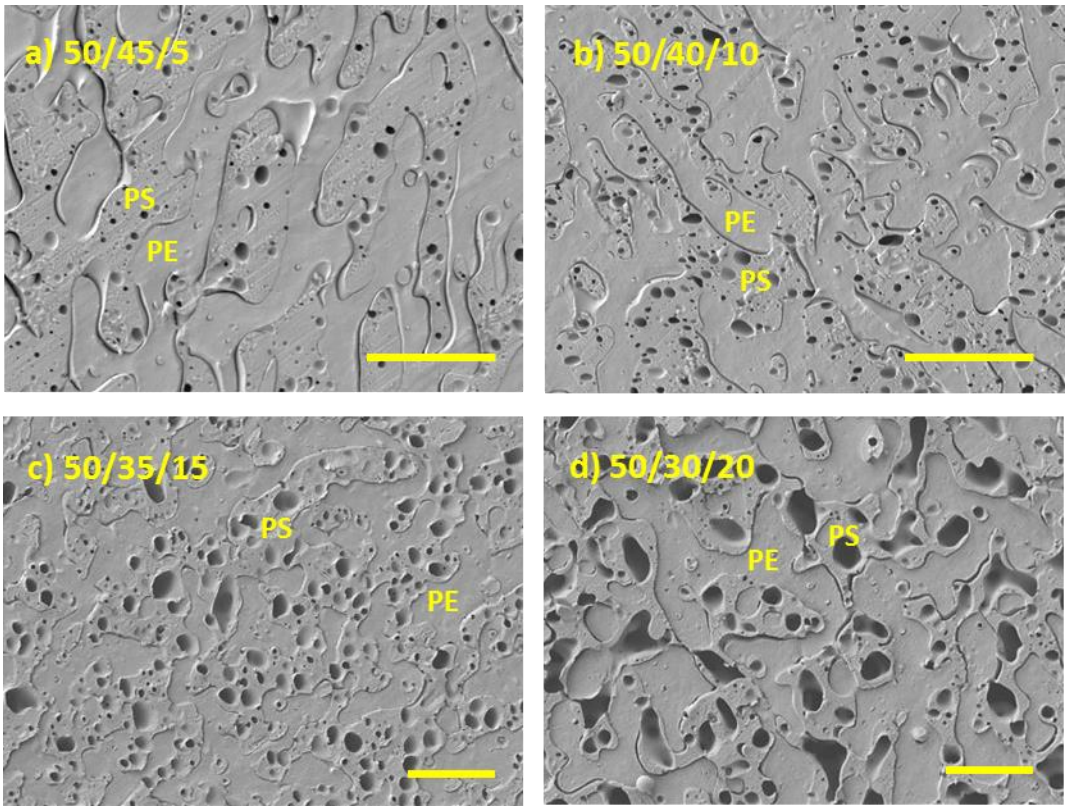

Figure 6.3: Morphology evolution in LDPE/PS/PEBA (50/X/Y) as the volume fraction of PEBA increases. Scale bar: 10 μm.

The interfacial tensions and the calculated spreading coefficients for LDPE/PS/PEBA are listed in Table 6.2. According to Harkins' spreading theory, a complete wetting morphology is predicted and PS tends to fully encapsulate PEBA, which agrees well with the morphology observation (Fig. 6.3).

Table 6.2: Interfacial tension and spreading coefficient for LDPE/PS/PEBA (200°C)

Interfacial tension (mN/m)	**Spreading coefficient (mN/m)**
$\gamma_{PE/PS} = 4.9 \pm 0.6$ [a]	$\lambda_{PE/PS/PEBA} = 1.5$
$\gamma_{PE/PEBA} = 8.0 \pm 1.4$ [b]	$\lambda_{PS/PE/PEBA} = -11.3$
$\gamma_{PS/PEBA} = 1.6 \pm 0.2$ [b]	$\lambda_{PE/PEBA/PS} = -4.7$

a: from Ref. [19].

b: from Ref. [34].

6.4.2 Structuring PEBA at the continuous interface in quaternary blends

In order to move the conductive PEBA to a continuous interface, a fourth phase is introduced to the LDPE/PS/PEBA system with the intent that that fourth phase forms continuous structures and is encapsulated by PEBA in the new quaternary blends. In order to achieve this, the multi-percolated features and hierarchical arrangement of LDPE, PS and PEBA should be preserved. All this requires a comprehensive examination on the interfacial tension and spreading coefficients of the system.

3.2.1 Spreading coefficients and morphology

PET and PVDF were selected and added to LDPE/PS/PEBA as the fourth component respectively based on their interfacial tensions with other polymers. Kolahchi et al. reported an interfacial tension of 4.2 mN/m for PS and PET. Combined with the other interfacial tensions determined in this study (Table 6.3) and according to Harkins' spreading theory, the PEBA phase is predicted to be situated between PS and PET where it would form a layer and fully separate PS and PET ($\lambda_{PS/PEBA/PET}$ = 0.1 mN/m). In the case of PVDF, a completely wet morphology with

PEBA being the intermediate phase between PS and PVDF is also predicted with a higher spreading coefficient $\lambda_{PS/PEBA/PET}$ = 0.5 mN/m. Previous work suggested that a high spreading coefficient facilitates the spreading of the intermediate phase at the interface in classic liquid systems (and systems of a liquid on the surface of a solid or another liquid) [11, 35]. However, this has rarely been studied in polymer blend systems.

Table 6.3: Interfacial tensions and spreading coefficients in LDPE/PS/PEBA/PET (250°C) and LDPE/PS/PEBA/PVDF (200°C)*

Polymer pairs	**Interfacial tension γ (mN/m)**	**Polymer pairs**	**Interfacial tension γ (mN/m)**
PS/PET	3.9 ± 0.6 (250°C)	PE/PEBA	7.8 (250°C)
PEBA/PS	2.3 ± 0.2 (250°C)	PE/PVDF	11.9 [b] (200°C)
PEBA/PET	1.8 ± 0.2 (250°C)	PS/PVDF	4.7 [b] (200°C)
PE/PS	4.0 [a] (250°C)	PEBA/PVDF	2.7 ± 0.3 (200°C)
PE/PET	8.1 ± 0.9 (250°C)		
Spreading coefficients			
LDPE/PS/PEBA/PET (250°C)		**LDPE/PS/PEBA/PVDF (200°C)**	
LDPE/PS/PEBA	LDPE/PS/PET	LDPE/PS/PEBA	LDPE/PS/PVDF
$\lambda_{PE/PS/PEBA}$ = 1.5	$\lambda_{PE/PS/PET}$ = 0.2	$\lambda_{PE/PS/PEBA}$ = 1.5	$\lambda_{PE/PS/PVDF}$ = 2.3
$\lambda_{PS/PE/PEBA}$ = –9.5	$\lambda_{PS/PE/PEBA}$ = –8.2	$\lambda_{PS/PE/PEBA}$ = –11.3	$\lambda_{PS/PE/PVDF}$ = –12.1
$\lambda_{PE/PEBA/PS}$ = –6.1	$\lambda_{PE/PEBA/PS}$ = –8.1	$\lambda_{PE/PEBA/PS}$ = –4.7	$\lambda_{PE/PVDF/PS}$ = –11.7
LDPE/PEBA/PET	PS/PEBA/PET	LDPE/PEBA/PVDF	PS/PEBA/PVDF
$\lambda_{PE/PEBA/PET}$ = –1.5	$\lambda_{PS/PEBA/PET}$ = –0.2	$\lambda_{PE/PEBA/PVDF}$ = 1.5	$\lambda_{PS/PEBA/PVDF}$ = 0.4
$\lambda_{PEBA/PE/PET}$ = –14.1	$\lambda_{PEBA/PS/PET}$ = –4.4	$\lambda_{PEBA/PE/PVDF}$ = –17.2	$\lambda_{PEBA/PS/PVDF}$ = –3.6
$\lambda_{PE/PET/PEBA}$ = –2.1	$\lambda_{PS/PET/PEBA}$ = –3.4	$\lambda_{PE/PEVDF/PEBA}$ = –6.6	$\lambda_{PS//PVDF/PEBA}$ = –6.1

* Some of the interfacial tensions used to calculate the spreading coefficients are presented in Table 2.

[a] Extrapolated based on Ref. [36]; [b] Obtained from Ref. [37].

Preliminary studies showed that the phase morphology and resistivity are both optimized when the composition of PS and PET are balanced (i.e., with a formulation of LDPE/PS/PEBA/PET 50/X/Y/X; see Supporting Information). The quaternary blends were thus prepared according to

this formulation rule with different concentrations of PEBA, which gives a combined content of LDPE and PS of over 70%.

It should be mentioned that the continuity of PS in either LDPE/PS/PEBA/PET (or LDPE/PS/PEBA/PVDF) blends examined in this study is over 98% as determined by the selective extraction of PS. The high levels of continuity for LDPE and PET (or PVDF) are also confirmed since their structures are self-supporting after extraction of the other phases. Thus, the morphology development for PS is expected to be confined at the continuous interface in the quaternary blends.

As shown in Figs. 6.4a and b (blends with 10% and 5% PEBA after microtoming), the quaternary system of LDPE/PS/PEBA/PET possesses multi-percolated structures which are hierarchically arranged in the order of LDPE/PS/PEBA/PET from outside to core. The PEBA phase is assembled at the interface of PS/PET and the completely wet layer of PEBA is clearly observed in the blend with 10% PEBA (Fig. 6.4a). However, at lower concentrations (e.g., 5% PEBA), the PEBA layer appears to be incomplete and some discontinuous regions are observed as indicated by the circles (Fig. 6.4b). In order to have a more comprehensive view of the morphology of PEBA, the cryo-fractured sample of 5% PEBA was characterized and is presented in Fig. 6.4c. The PEBA layer at the PS/PEBA interface in that case is not intact and many ruptures can be observed. The interface coverage is estimated to be approximately 75% for 5% PEBA. This value further decreases to about 50% with the sample containing 3% PEBA (Fig. 6.4d). Nevertheless, continuous PEBA structures appear to be well developed in these blends with very low PEBA compositions owing to the localization of PEBA at the interface in the LDPE/PS/PEBA/PET quaternary blend.

Interestingly, the morphology evolution of PEBA at the PS/PET interface shows a similar transition behaviour from partial wetting to complete wetting as observed in previous work on the LDPE/PEBA/PET system, which can be explained by the competition between dewetting and coalescence of the PEBA phase with increasing PEBA composition [10]. Thus, the interfacial tension between PS and PET was further determined with the same polymers used in this study and a value of 3.9 mN/m is obtained. The result is close to the value from literature we used previously, but it results in a negative $\lambda_{PS/PEBA/PET}$ (= – 0.2 mN/m). Therefore, a weak partial

wetting morphology is predicted ($\lambda_{PS/PEBA/PET}$ is close to 0) which corresponds with the morphology observation.

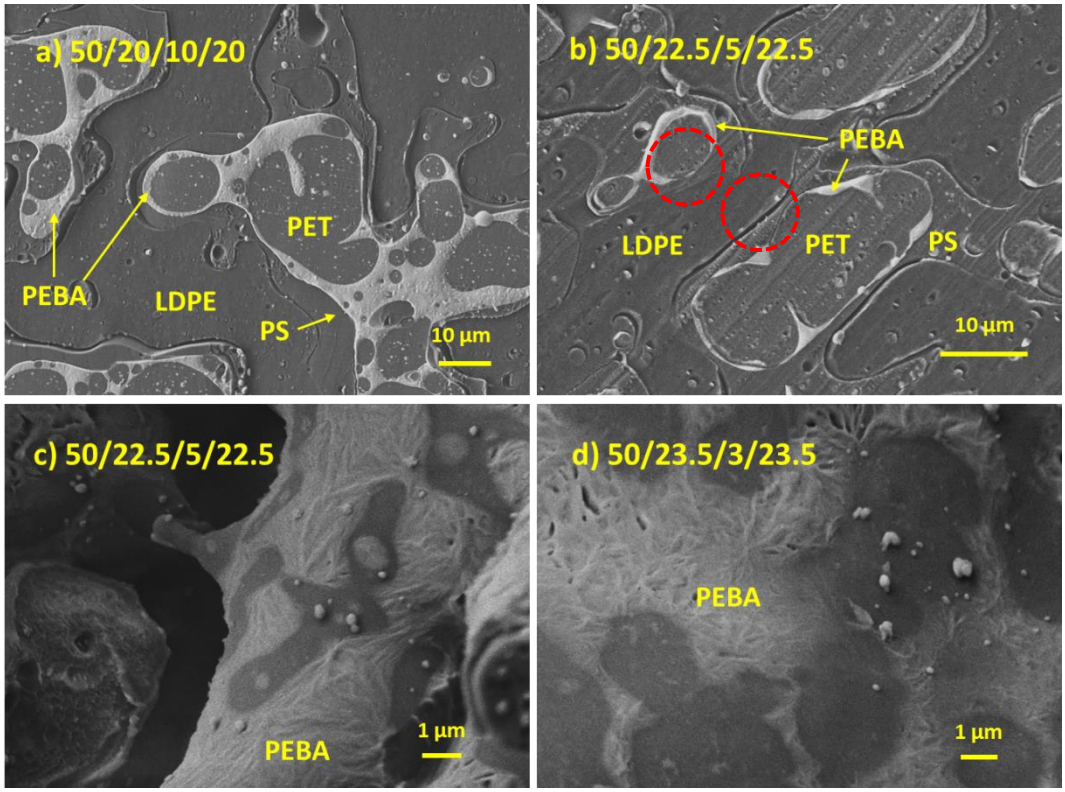

Figure 6.4: Morphology of the quaternary blends of LDPE/PS/PEBA/PET at different compositions (the white phase is PEBA stained by phosphotungstic acid). Cryo-microtomed samples: (a) 50/20/10/20 and (b) 50/22.5/5/22.5; cryo-fractured samples: (c) 50/22.5/5/22.5 and (d) 50/23.5/3/23.5.

The morphology of the cyro-microtomed LDPE/PS/PEBA/PVDF (50/20/10/20) quaternary blend is shown in Fig. 6.5a. The hierarchical ordering of LDPE/PS/PEBA/PET from outside to core is observed and PEBA forms intact layer structures situated at the PS/PVDF interface. Figs. 6.5b, c and d present the PEBA morphologies of cryo-fractured samples at low PEBA concentrations. Different from the previous quaternary system, the integrity of the PEBA layer appears to be maintained down to 3%, respecting the complete wetting prediction that PEBA fully separates PS and PVDF. We have demonstrated previously that a minimum concentration is also required to form a completely wet interface even in the complete wetting system [10]. However, at 3%, we approach the limit of the staining/SEM technique used to identify the PEBA phase. Thus, this

critical concentration may be more rigorously inferred from the resistivity results discussed below.

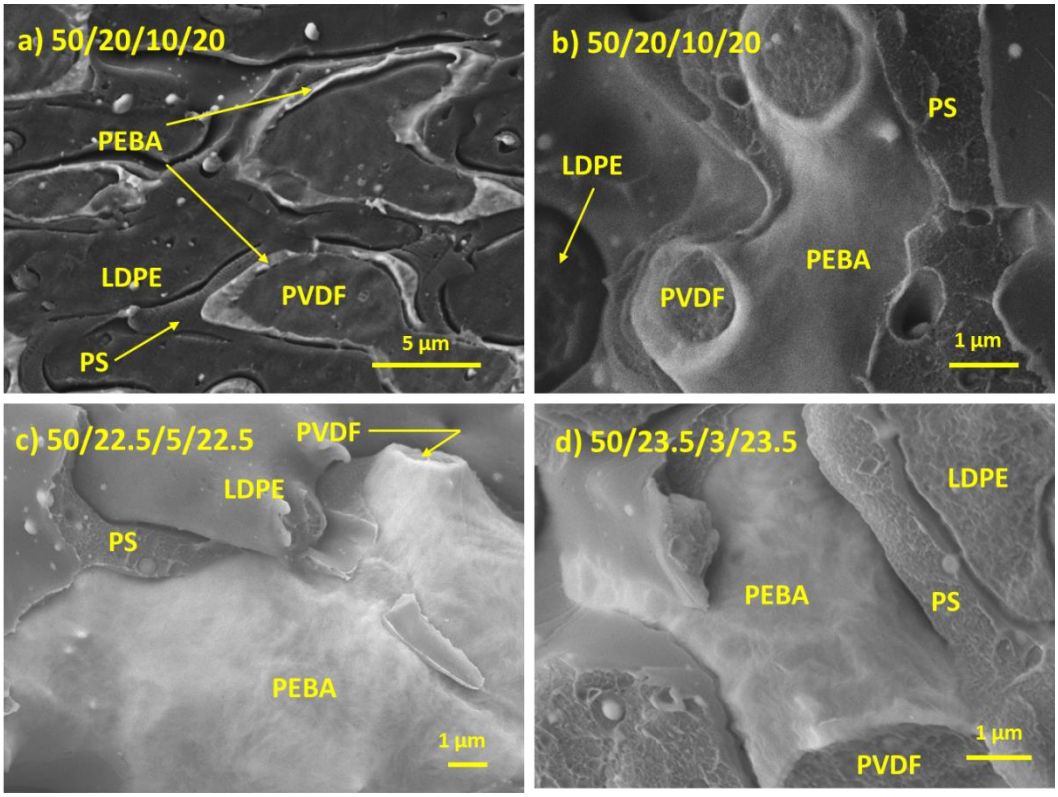

Figure 6.5: Morphology of the LDPE/PS/PEBA/PET quaternary blends at different compositions (the white phase is PEBA stained by phosphotungstic acid). Cryo-microtomed samples: (a) 50/20/10/20; cryo-fractured samples: (b) 50/20/10/20; (c) 50/22.5/5/22.5 and (d) 50/23.5/3/23.5.

In ternary blends, the complete/partial wetting morphology can be directly predicted by Harkins spreading theory (Fig. 6.1). However, in quaternary blends, it becomes more complicated since there are four sets of spreading coefficients corresponding to the four combinations of three-component systems out of the quaternary system (Table 4). Virgilio and Favis showed that the morphology and phase arrangement in a PE/PP/PS/PMMA quaternary system respect the tendency defined by all the four sets of ternary spreading coefficients [38]. Two three-phase contact lines formed in that quaternary blend due to the two partial wetting systems of PE/PP/PS and PP/PS/PMMA. The full compliance of all spreading coefficients is also demonstrated in LDPE/PS/PEBA/PVDF of the current study where the phase order is consistent with each

selected three-component system and only two-phase contact is observed at each interface. However, in LDPE/PS/PEBA/PET, an inherent conflict appears to exist if all the spreading coefficients need to be fulfilled. Partial wetting is predicted for LDPE/PEBA/PET, pointing to the existence of three phase contact lines (LDPE and PEBA should have contact on these lines), but the completely wet PS layer between LDPE and PEBA would exclude this scenario. This is confirmed in the morphology observation of Figs. 6.4a and b. The results imply that the morphology in quaternary blends is primarily determined by two of the four sets of spreading coefficients. For example, in the current LDPE/PS/PEBA/PET system, the morphology should mainly depend on the wettability of PS at the LDPE/PEBA interface and the wettability of PEBA at the PS/PET interface. These two tendencies can be fully predicted by the two sets of spreading coefficients related to the ternary systems of LDPE/PS/PEBA and PS/PEBA/PET. When there is a conflict, these two sets of spreading coefficients appear to dominate over the other two (LDPE/PS/PET and LDPE/PEBA/PET) as shown above. In other words, the morphology in a quaternary system does not necessarily respect all the four sets of spreading coefficients. In this context, Hobbs et al. showed that although both polycarbonate (PC) and poly(styrene-*co*-acrylonitrile) (SAN) are expected to completely segregate the PS from polybutylene terephthalate (PBT) due to the positive spreading coefficients (in the two ternary systems of PBT/PC/PS and PBT/SAN/PS respectively), in the PBT/PC/SAN/PS quaternary blend, neither PC nor SAN was found to fully engulf the PS phase [13]. Instead, PC and SAN form alternating domains surrounding PS within the PBT matrix. This could also be due to the dominating influence of partially wet PBT/PC/SAN and PC/SAN/PS over the completely wet PBT/PC/PS and PBT/SAN/PS.

6.4.3 Surface resistivity: ternary and quaternary blends

Fig. 6.6 reports the surface resistivity results of the LDPE/PS/PEBA ternary blends and the quaternary blends of LDPE/PS/PEBA/PET and LDPE/PS/PEBA/PVDF. The surface resistivities of the binary LDPE/PEBA blends and pure PEBA are also shown in the figure for comparison purposes. The resistivity in LDPE/PS/PEBA, where PEBA is the core phase, starts to decrease at 10% PEBA, followed by a significant reduction at 15%. The tendency is consistent with the morphology observation presented in Fig. 6.3. By confining PEBA within the PS phase in the ternary blend, lower surface resistivities, as compared to LDPE/PEBA, are obtained after the PEBA composition exceeds 10% indicating a lower percolation threshold. Fig. 6.6 also shows that a dramatic influence on percolation is observed when PEBA is localized at the continuous

interface in the two quaternary systems. With only 3% PEBA in LDPE/PS/PEBA/PET, the surface resistivity is reduced by two orders of magnitude from 1.5×10^{16} to 1.7×10^{14} Ω/sq. The reduction is not unexpected considering the connected structures developed at 3% PEBA (Fig. 6.4d). The resistivity further decreases to 3.6×10^{12} Ω/sq and starts to plateau afterwards as the PEBA composition is increased to 10% which points to the region of PEBA complete layer formation (Fig. 6.4). In the case of LDPE/PS/PEBA/PVDF where PEBA completely wets the PS/PVDF interface, a steep reduction of surface resistivity from 3.8×10^{15} to 1.8×10^{13} and 1.7×10^{12} is obtained with only 1% and 3% PEBA respectively, followed by a more gradual drop with a further increase in the PEBA composition (>3%). It also indicates that complete PEBA layers are developed at the PS/PVDF interface with about 3% PEBA [10].

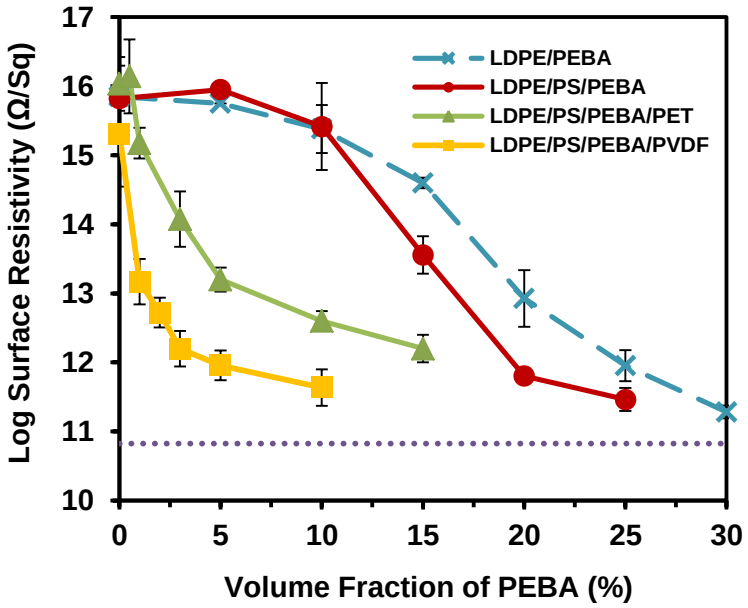

Figure 6.6: Surface resistivity of the binary, ternary blends and quaternary blends with PEBA. The horizontal dashed line shows the surface resistivity of pure PEBA.

By controlling the hierarchical structuring of PEBA in the blends, the percolation threshold is significantly reduced from the binary blend (PEBA is homogeneously distributed in the matrix) to the ternary blends of LDPE/PS/PEBA (PEBA is confined as the core phase within PS) to the quaternary blends of LDPE/PS/PEBA/PET and LDPE/PS/PEBA/PVDF (where PEBA forms connected structures/layers at the interface). The morphology evolution of these blends is schematically shown in Fig. 6.7. Confining PEBA at the interface in the quaternary blends results

in a 2–4 orders of magnitude decrease of surface resistivity as compared to that in the other blends, with the highest reduction achieved in the completely wet LDPE/PS/PEBA/PVDF system. For antistatic applications, the surface resistivity of the material needs to be reduced to below 10^{13} Ω/sq [39]. To meet this requirement, 20% PEBA is needed when it is directly blended with LDPE (binary blends) and about 15% for the ternary LDPE/PS/PEBA system. In the two quaternary blends (LDPE + PS > 70%), the amount of PEBA usage can be significantly reduced to 5% in the LDPE/PS/PEBA/PET system and as low as only about 1% in LDPE/PS/PEBA/PVDF.

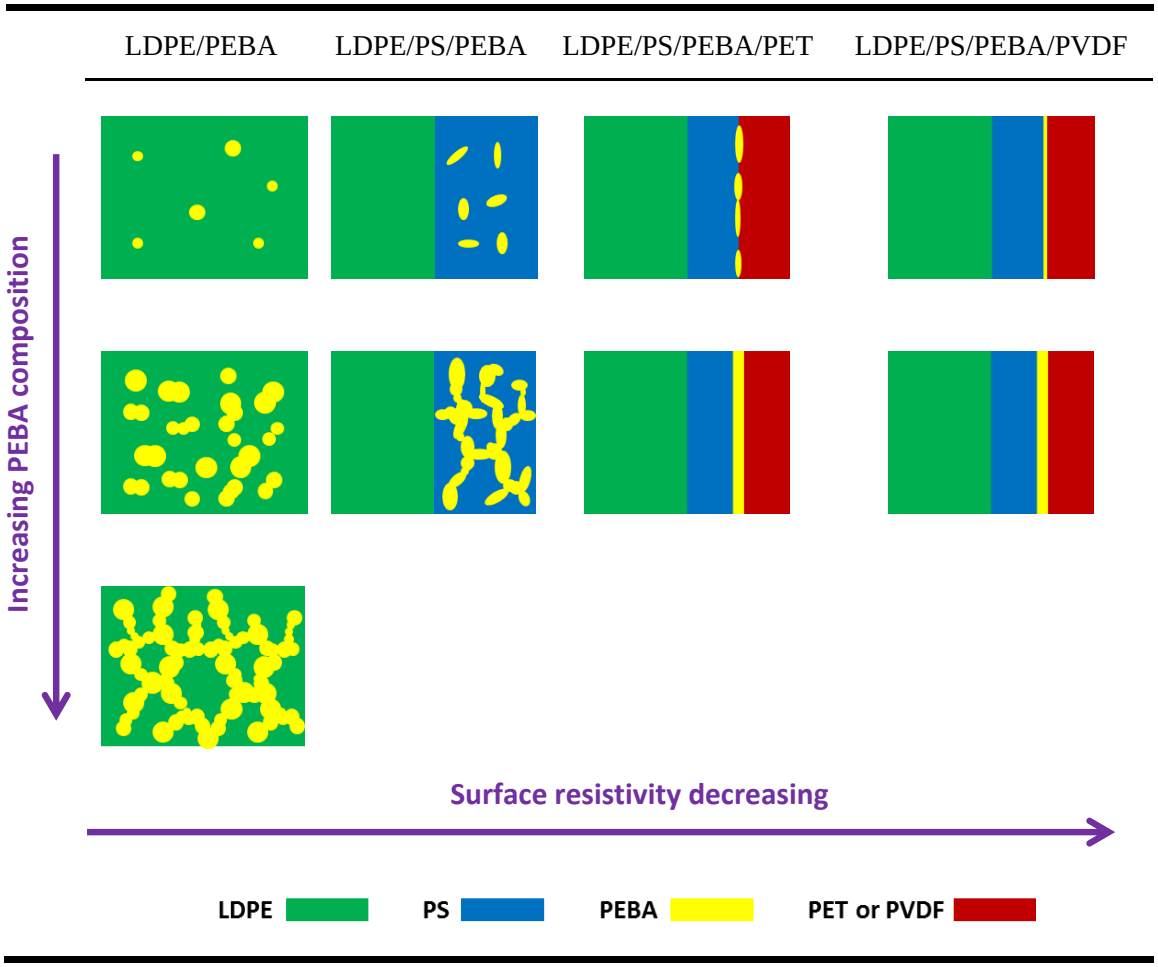

Figure 6.7: Schmatics of morphology and surface resistivity evolution in LDPE/PEBA, LDPE/PS/PEBA, LDPE/PS/PEBA/PET and LDPE/PS/PEBA/PVDF.

The surface resistivity of the LDPE/PS/PEBA/PET quaternary system is also lower than that of the previously reported LDPE/PEBA/PET ternary system at low PEBA concentrations (<10%) [10]. For example, with 3% of PEBA, the surface resistivity in the quaternary blend is 1.7×10^{14} Ω/sq while a value of 3.4×10^{15} Ω/sq is obtained for the ternary blend. The results are probably due to the higher levels of percolation in the quaternary blends and a higher spreading coefficient of $\lambda_{PS/PEBA/PET}$ than $\lambda_{PE/PEBA/PET}$ (–0.2 *vs.* –1.5 mN/m), which facilitates the formation of the conductive pathways of PEBA at the interface for the quaternary system. In the case of LDPE/PS/PEBA/PVDF, the obtained surface resistivity is comparable to that of the ternary LDPE/PEBA/PVDF blend (from previous work) despite the lower value of $\lambda_{PS/PEBA/PVDF}$ as compared to $\lambda_{PE/PEBA/PVDF}$ (0.4 *vs.* 1.2 mN/m) [10]. One possible explanation is the percolation threshold can be reduced by increasing the number of components in the multiphase system [5, 20]. The results indicate that the differences in spreading coefficient values may be compensated by increasing the number of phases and the subsequent higher levels of percolation.

6.4.4 Structuring PEBA at the continuous interface of a ternary blend by interfacial modification

In order to draw the PEBA phase out of the core phase and to the interface in LDPE/PS/PEBA, at even higher contents of LDPE and PS, one possible route is to add an interfacial modifier (compatibilizer). According to the interfacial tension and spreading coefficient values in Table 6.1, if $\gamma_{PE/PEBA}$ is reduced to below 3.3 mN/m, a positive $\lambda_{PE/PEBA/PS}$ may be obtained. A complete wetting morphology will thus be predicted, and PEBA will tend to spread at the interface of LDPE and PS. A random terpolymer of ethylene, acrylic ester and maleic anhydride (EAM) was used as the interfacial modifier for LDPE and PEBA. Figs. 6.8a and c present the morphology of LDPE/PS/PEBA (50/40/10) before and after modification with 2% EAM. Although more PEBA domains appear to be at the interface of LDPE and PS after interfacial modification (10% *vs.* 5%), they do not form the expected layer structures of PEBA. Rather, the morphological features of PEBA in those two cases are actually very similar. Annealing was further applied to show the thermodynamically stable morphology. After only 10 min annealing, the amount of PEBA located at the interface is increased from about 10% to 69% (Fig. 6.8d). And with 30 min annealing, almost 90% of PEBA self-assembles at the interface, arranging into closed-packed droplets and demonstrating a partial wetting morphology (Fig. 6.8e). For comparison, the blend

of LDPE/PS/PEBA without EAM was also annealed at 200°C for 30 min and Fig. 6.8b clearly shows that virtually all the PEBA remains within the PS phase after annealing.

The interfacial tensions in the EAM modified LDPE/PS/PEBA system were further estimated. PEBA was first premixed with EAM in the Brabender internal mixer at 200°C for 5 min, and was then used for interfacial determination by the breaking thread method. With the addition of EAM, the interfacial tension between PE and PEBA is reduced from 8.0 to 3.1 mN/m, probably due to the reaction between the maleic anhydride group in EAM and the amide group in PEBA which results in an EAM-PEBA copolymer [40-41]. At the same time, the interfacial tension between PS and PEBA is increased to 2.0 mN/m with the presence of EAM while the interfacial tension between LDPE and PS is assumed to remain unchanged. According to Harkins' spreading theory, a partial wetting morphology is predicted (three negative spreading coefficients) which corresponds to the observed morphology after annealing (Table 6.4 and Figs. 6.8d and e). Note that the possible reaction between PEBA and EAM should be mostly completed during the premixing step. A time sweep for the PEBA/EAM sample (with a volume ratio of 100/20) after premixing shows little change in complex viscosity for up to 40 min, indicating no further reaction proceeds (Data not shown).

Table 6.4: Interfacial tensions and spreading coefficients of the EAM modified LDPE/PS/PEBA (200°C)

Interfacial tension (mN/m)	**Spreading coefficient (mN/m)**
$\gamma_{PE/PS} = 4.9 \pm 0.6$	$\lambda_{PS/PE/PEBA} = -6.0 < 0$
$\gamma_{PE/PEBA} = 3.1 \pm 0.8$	$\lambda_{PE/PS/PEBA} = -3.8 < 0$
$\gamma_{PS/PEBA} = 2.0 \pm 0.3$	$\lambda_{PE/PEBA/PS} = -0.2 < 0$

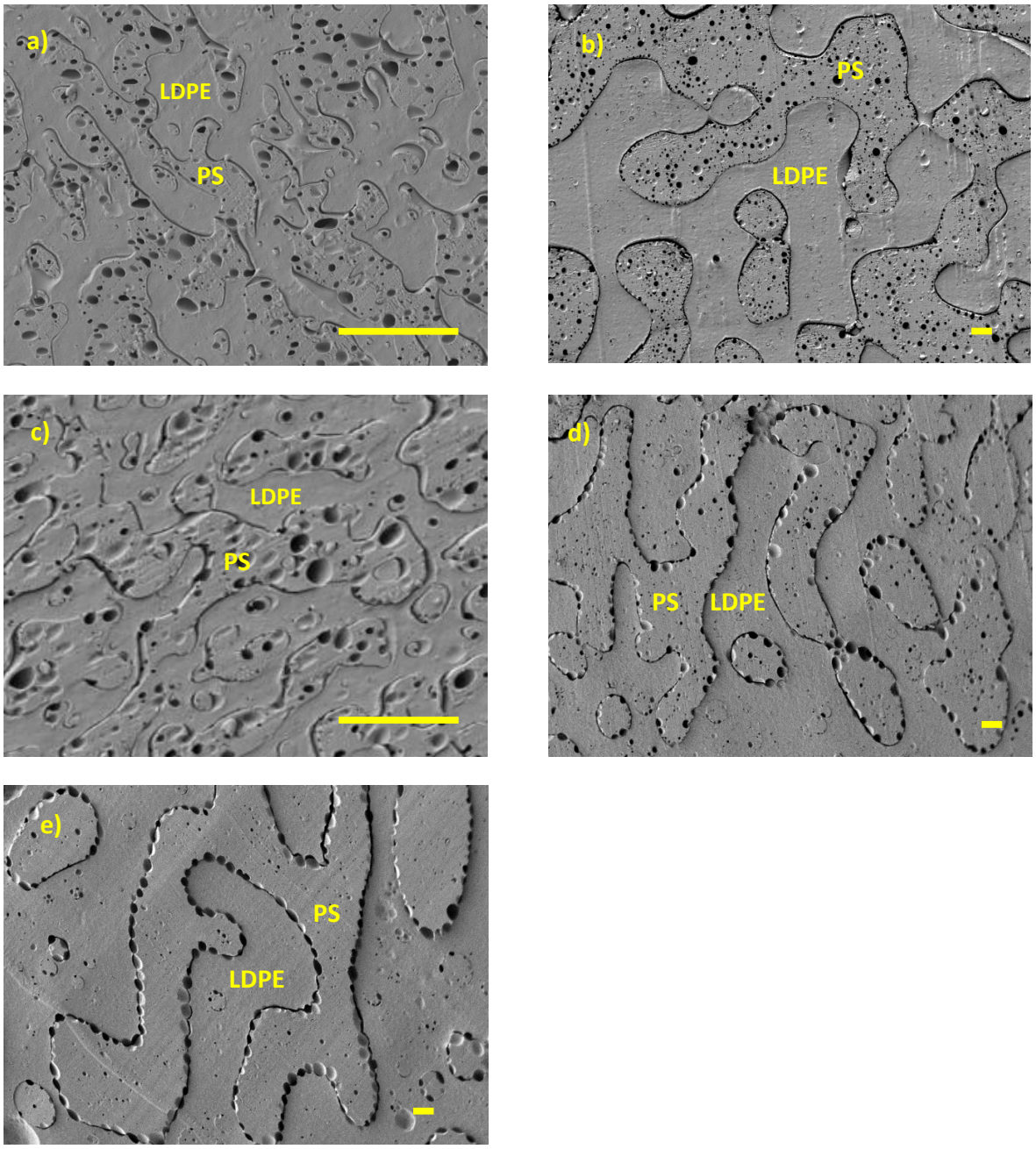

Figure 6.8: Morphology of the ternary LDPE/PS/PEBA (50/40/10) blends (microtomed surface and PEBA extracted). Without interfacial modification and annealed at 200°C for (a) 0 min and (b) 30 min. Modified with EAM and annealed at 200°C for (c) 0 min, (d) 10 min and (e) 30 min. Scale bar: 10 µm.

The surface resistivity of LDPE/PS/PEBA 50/40/10 with and without EAM interfacial modifier addition was determined as a function of annealing time and the results are reported in Fig. 6.9.

Little change was observed in the surface resistivity of the blend without EAM after up to 30 min annealing. This is expected since all the PEBA domains are still within the PS phase and remain discrete after annealing (Fig. 6.8b). However, after adding EAM, the surface resistivity of the sample significantly decreases from 5.6×10^{15} to 1.9×10^{13} Ω/sq with 30 min annealing, which is over two orders of magnitude lower than that of LDPE/PS/PEBA without modification. The results indicate the formation of PEBA conductive pathways at the LDPE/PS interface. To have a better view of the morphology, PEBA was stained by phosphotungstic acid and the sample was then examined by SEM. The PEBA phase appears as white after staining and the morphology features observed (Fig. 6.10a) are in good agreement with those in Fig. 6.8e. By zooming-in on the boundaries of the droplets, the distance between two adjacent droplets may be estimated. It should be noted that the microtomed plane likely tends to miss the equators of the droplets, leading to an overestimation of the closest distance. Virgilio et al. reported in a PE/PP/PS system compatibilized by a styrene-(ethylene-butylene) (SEB) diblock copolymer that the distance between two PS droplets at the PE/PP interface could be less than 50 nm [19]. In that study, the PS droplets appear to be separated by a thin film even though they are so close together that some deformation occurs. However, in the present system, a connection between two PEBA droplets was observed (Fig. 6.10b,). The cryo-fractured samples were also characterized to show the PEBA droplets in three-dimensional space (Figs. 6.10c, d and e). The close-packing of PEBA droplets at the continuous LDPE/PS interface can be seen in Figs. 6.10c and d. Surprisingly, many PEBA droplets are connected at the interface as shown in the high-magnification images (Fig. 6.10e). The formation of connected PEBA domains at the LDPE/PS interface explains the surface resistivity decrease observed in Fig. 6.9 for the compatibilized LDPE/PS/PEBA system after annealing.

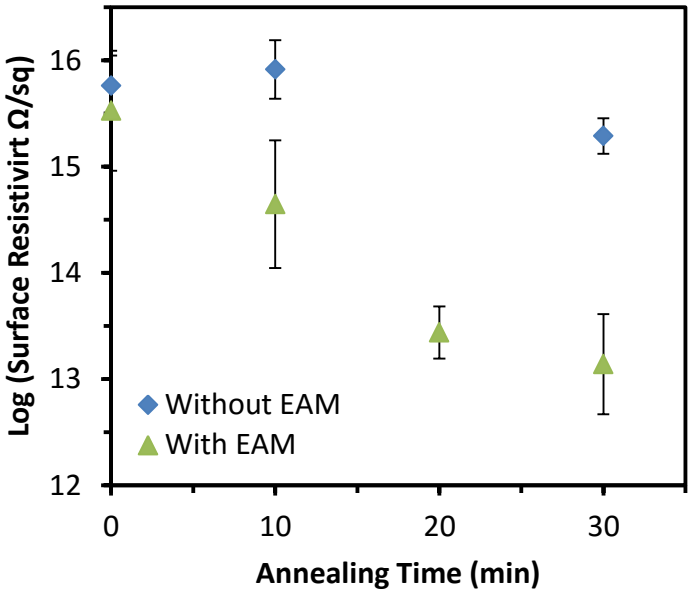

Figure 6.9: Surface resistivity of LDPE/PS/PEBA 50/40/10 with and without modification by EAM after annealing at 200°C for different periods of time.

The morphological difference between the PE/PP/PS blend from previous work [19] and the current LDPE/PS/PEBA system may be explained by the distribution of the compatibilizer and the spreading coefficients of the two systems. In the former case, the compatibilizer (SEB) should concentrate at the PE/PS interface [19] as schematically shown in Fig. 6.11a. Thus, the steric hindrance effect from the compatibilizer can suppress the coalescence between PS droplets since the frontiers of the two droplets are located at the PE side. In addition, the PE/PP/PS system demonstrates a strong partial wetting state with the estimated spreading coefficient $\lambda_{PE/PS/PP}$ between –3.2 and –5.1 mN/m [19], pointing to a strong tendency that PS forms discrete droplets at the PE/PP interface. In the EAM modified LDPE/PS/PEBA system, EAM modifies the LDPE/PEBA interface; however, the PEBA droplets are principally observed toward the PS phase and the coalescence between PEBA domains can likely occur on the PS side. The coalescence of PEBA will thus not be hindered by EAM since the EAM copolymers tend to

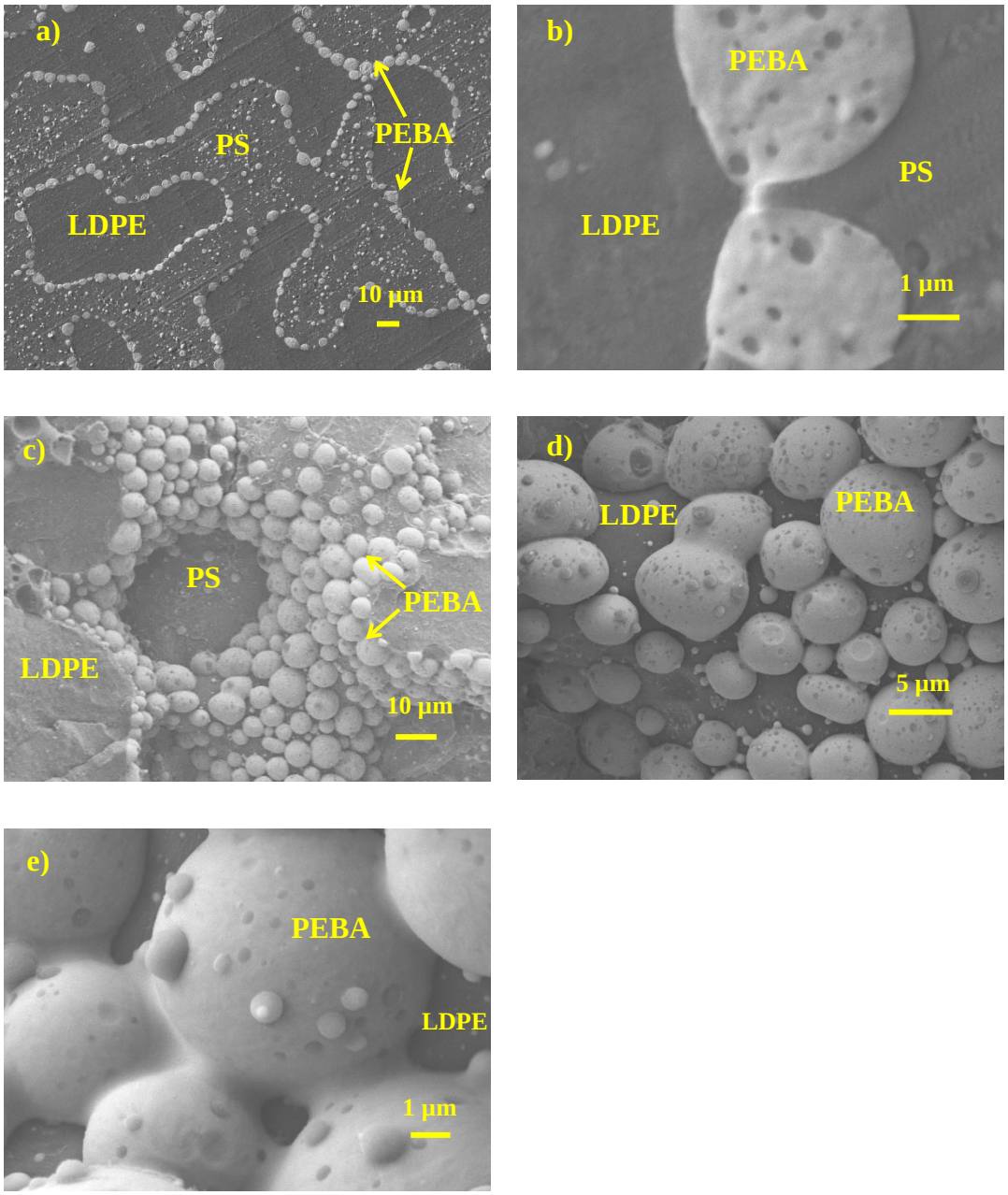

Figure 6.10: Detailed morphology of LDPE/PS/PEBA (50/40/10) with EAM after 30 min of annealing at 200°C (the white phase is PEBA which is stained by phosphotungstic acid). (a) and (b) are cryo-microtomed samples; (c)–(f) are cryo-fractured samples at different magnifications.

collect at the LDPE/PEBA interface (EAM is dominated by the ethylene component) (Fig. 6.11b). In addition to this effect, this is a weak partial wetting system ($\lambda_{PE/PEBA/PS}$ = –0.2 mN/m) where the competition between wetting and dewetting for the PEBA domains at the PE/PS interface is expected [10]. This would also tend to contribute to more PS coalescence and the observation of non-discrete droplets. Therefore, the spatially selective distribution of the copolymers and the difference in spreading coefficients are responsible for the morphology differences observed in the modified PE/PP/PS from the previous study and the modified LDPE/PS/PEBA systems studied here. The results also imply that in compatibilized partial wetting systems coalescence between partially wet droplets can occur when the droplets are mostly located at the unmodified phase side.

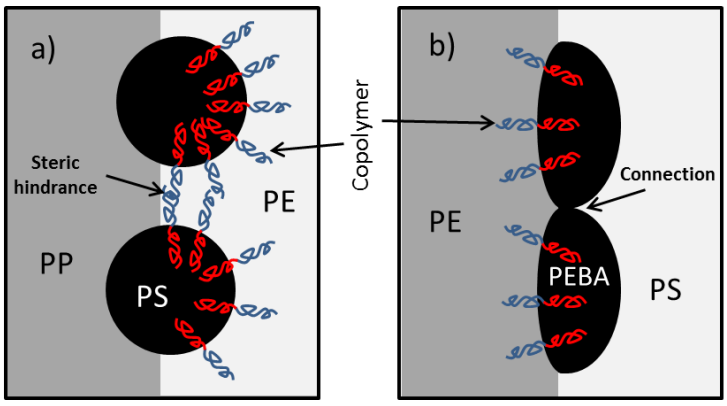

Figure 6.11: Schematic comparison of the morphology after annealing between the PE/PP/PS (modified with SEB) system from previous work (a) [19] and the PE/PS/PEBA (modified with EAM) system in this study (b).

It is also noted that some very small inclusions typically with a diameter of 100–300 nm are present in the PEBA droplets (Fig. 6.10b). They are likely to be PS since its interfacial tension with PEBA should be very low considering the very fine dimension of the domains. These inclusions may be captured by the PEBA phase during the coalescence between two adjacent PEBA droplets, which could be evidence for the argument that the collision between the PEBA droplets at LDPE/PS interface occurs on the PS side. However, it should be pointed out that

although the coalescence of liquid dispersed droplets within a matrix has been well studied [42-43], the mechanism is not well understood when the droplets coalesce at the interface of the other two phases (i.e., partial wetting system). More work will be needed to clearly address this question.

Another interesting point is the distinction between the morphologies of the EAM modified LDPE/PS/PEBA system before (most PEBA remains within PS, Fig.6.8c) and after (PEBA migrates to the interface, Fig. 6.8e) annealing. One possible explanation could be that LDPE/PS/PEBA is a compatibilized system. During melt mixing, the PEBA domains are readily deformed and disintegrated, creating new interfaces continuously. If the interfacial modifier does not have enough time to saturate the fresh interfaces in the dynamic mixing conditions, the compatibilized system would thermodynamically resemble, to some point, the original system without the interfacial modifier. This explains the morphological similarity between Fig. 6.8a and c. During annealing, the interfacial modifier has time to gradually saturate the interface. Thus, the PEBA droplets migrate to the interface of LDPE/PS progressively in the compatibilized system (Figs. 6.8d and e), resuming the equilibrium partial wetting morphology as predicted from Harkins' theory.

In this system with 90% LDPE and PS, PEBA was successfully localized to the LDPE/PS interface by using a small amount of EAM as an interfacial modifier. However, complete PEBA layer structures were not obtained and some annealing was required to complete the localization process . Future studies will identify a more effective interfacial modifier to generate completely wet PEBA layers at the interface.

6.5 Conclusion

In this study, we demonstrate two approaches to control the structuring and localization of the conductive PEBA in hierarchically ordered, multi-percolated ternary and quaternary polymer blend systems with high commodity polymer contents (volume fraction of LDPE and PS > 70%). When PET (or PVDF) is added to LDPE/PS/PEBA as the fourth phase, PEBA is moved from within the PS phase to the continuous interface of PS/PET (or PS/PVDF) in the quaternary blend of LDPE/PS/PEBA/PET (or LDPE/PS/PEBA/PVDF), which significantly decreases the percolation threshold for PEBA. The amount of PEBA required to obtain a surface resistivity of 10^{13} Ω/sq for antistatic applications is dramatically reduced to about 5% for LDPE/PS/PEBA/PET and only 1% for LDPE/PS/PEBA/PVDF. While only weak partial wetting

for PEBA is achieved in the LDPE/PS/PEBA/PET system, the superior performance of the LDPE/PS/PEBA/PVDF system is attributed to the formation of completely wet PEBA layers. In the second approach, the addition of a small amount of EAM to LDPE/PS/PEBA (50/40/10), combined with some annealing, also successfully draws PEBA to the LDPE/PS interface in the ternary LDPE/PS/PEBA system with an even higher commodity polymer content (LDPE+PS = 90%). A significant reduction in surface resistivity from 5.6×10^{15} to 1.9×10^{13} Ω/sq was also obtained. Further studies will aim at identifying a more effective interfacial modifier to achieve a completely wet PEBA layer at the LDPE/PS interface without the need for annealing.

6.6 Acknowledgment

The authors would like to thank Arkema for funding this research. Jun Wang would like to acknowledge the China Scholarship Council (CSC) for a scholarship. The authors would also like to thank Dr. Eric Gamache, Dr. Yves Deyrail and Dr. Damien Rauline from Arkema for useful discussions. Prof. Daniel Therriault and Frederic Sirois from École Polytechnique de Montréal are acknowledged for providing the resistivity measurement fixtures.

6.7 References

1. Pernot, H.; Baumert, M.; Court, F.; Leibler, L., Design and properties of co-continuous nanostructured polymers by reactive blending. *Nat Mater* **2002,** *1* (1), 54-58.

2. Gubbels, F.; Jerome, R.; Teyssie, P.; Vanlathem, E.; Deltour, R.; Calderone, A.; Parente, V.; Bredas, J. L., Selective Localization of Carbon Black in Immiscible Polymer Blends: A Useful Tool To Design Electrical Conductive Composites. *Macromolecules* **1994,** *27* (7), 1972-1974.

3. Zilberman, M.; Siegmann, A.; Narkis, M., Conductivity and structure of melt-processed polyaniline binary and ternary blends. *Polymers for Advanced Technologies* **2000,** *11* (1), 20-26.

4. Cohen, E.; Zonder, L.; Ophir, A.; Kenig, S.; McCarthy, S.; Barry, C.; Mead, J., Hierarchical Structures Composed of Confined Carbon Nanotubes in Cocontinuous Ternary Polymer Blends. *Macromolecules* **2013,** *46* (5), 1851-1859.

5. Ravati, S.; Favis, B. D., Low percolation threshold conductive device derived from a five-component polymer blend. *Polymer* **2010,** *51* (16), 3669-3684.

6. Zhang, K. Y.; Nagarajan, V.; Misra, M.; Mohanty, A. K., Supertoughened Renewable PLA Reactive Multiphase Blends System: Phase Morphology and Performance. *Acs Applied Materials & Interfaces* **2014,** *6* (15), 12436-12448.

7. Luzinov, I.; Xi, K.; Pagnoulle, C.; Huynh-Ba, G.; Jérôme, R., Composition effect on the core–shell morphology and mechanical properties of ternary polystyrene/styrene–butadiene rubber/polyethylene blends. *Polymer* **1999,** *40* (10), 2511-2520.

8. Favis, B. D., Factors Influencing the Morphology in Immiscible Polymer Blends in Melt Processing. In *Polymer Blends: Formulation and Performance*, Paul, D. R.; Bucknall, C. B., Eds. Wiley-Interscience: **2000**; Chapter 16, pp 501-537.

9. Kobayashi, T.; Wood, B. A.; Takemura, A.; Ono, H., Antistatic performance and morphological observation of ternary blends of poly(ethylene terephthalate), poly(ether esteramide), and ionomers. *Polymer Engineering & Science* **2008,** *48* (11), 2247-2257.

10. Wang, J.; Reyna-Valencia, A.; Favis, B. D., Assembling Conductive PEBA Copolymer at the Continuous Interface in Ternary Polymer Systems: Morphology and Resistivity (in preparation). **2016**.

11. Harkins, W. D.; Feldman, A., FILMS. THE SPREADING OF LIQUIDS AND THE SPREADING COEFFICIENT. *Journal of the American Chemical Society* **1922,** *44* (12), 2665-2685.

12. Torza, S.; Mason, S. G., Coalescence of Two Immiscible Liquid Drops. *Science* **1969,** *163* (3869), 813-814.

13. Hobbs, S. Y.; Dekkers, M. E. J.; Watkins, V. H., Effect of interfacial forces on polymer blend morphologies. *Polymer* **1988,** *29* (9), 1598-1602.

14. Valera, T. S.; Morita, A. T.; Demarquette, N. R., Study of Morphologies of PMMA/PP/PS Ternary Blends. *Macromolecules* **2006,** *39* (7), 2663-2675.

15. Nemirovski, N.; Siegmann, A.; Narkis, M., Morphology of ternary immiscible polymer blends. *Journal of Macromolecular Science, Part B* **1995,** *34* (4), 459-475.

16. Reignier, J.; Favis, B. D.; Heuzey, M. C., Factors influencing encapsulation behavior in composite droplet-type polymer blends. *Polymer* **2003,** *44* (1), 49-59.

17. Zhang, J.; Ravati, S.; Virgilio, N.; Favis, B. D., Ultralow Percolation Thresholds in Ternary Cocontinuous Polymer Blends. *Macromolecules* **2007,** *40* (25), 8817-8820.

18. Horiuchi, S.; Matchariyakul, N.; Yase, K.; Kitano, T., Morphology Development through an Interfacial Reaction in Ternary Immiscible Polymer Blends. *Macromolecules* **1997,** *30* (12), 3664-3670.

19. Virgilio, N.; Marc-Aurèle, C.; Favis, B. D., Novel Self-Assembling Close-Packed Droplet Array at the Interface in Ternary Polymer Blends. *Macromolecules* **2009,** *42* (9), 3405-3416.

20. Levon, K.; Margolina, A.; Patashinsky, A. Z., Multiple percolation in conducting polymer blends. *Macromolecules* **1993,** *26* (15), 4061-4063.

21. Ravati, S.; Favis, B. D., 3D porous polymeric conductive material prepared using LbL deposition. *Polymer* **2011,** *52* (3), 718-731.

22. Gubbels, F.; Jerome, R.; Vanlathem, E.; Deltour, R.; Blacher, S.; Brouers, F., Kinetic and Thermodynamic Control of the Selective Localization of Carbon Black at the Interface of Immiscible Polymer Blends. *Chemistry of Materials* **1998,** *10* (5), 1227-1235.

23. Malet, F. L. G., Thermoplastic Poly(Ether-b-Amide) Elastomers: Synthesis. In *Handbook of Condensation Thermoplastic Elastomers*, Fakirov, S., Ed. Wiley-VCH Verlag GmbH & Co. KGaA: **2006**, pp 241-262.

24. Rosner, R. B., Conductive materials for ESD applications: an overview. *Device and Materials Reliability, IEEE Transactions on* **2001,** *1* (1), 9-16.

25. Young, M.-Y.; Lin, J.-J., Electrostatic Dissipating Properties of Poly(oxyethylene)amine-Modified Polyamides. *Industrial & Engineering Chemistry Research* **1998,** *37* (11), 4284-4289.

26. Zoppi, R. A.; Fonseca, C. M. N. P.; De Paoli, M.-A.; Nunes, S. P., Solid electrolytes based on poly(amide 6-b-ethylene oxide). *Solid State Ionics* **1996,** *91* (1–2), 123-130.

27. Lacroix, C., Antistatic styrene polymer compositions. Google Patents: **2004**.

28. Greener, J.; Majumdar, D.; Laney, T. M., Photographic film with base containing polymeric antistatic material. Google Patents: **2001**.

29. Bondar, V. I.; Freeman, B. D.; Pinnau, I., Gas sorption and characterization of poly(ether-b-amide) segmented block copolymers. *Journal of Polymer Science Part B: Polymer Physics* **1999,** *37* (17), 2463-2475.

30. Elemans, P. H. M.; Janssen, J. M. H.; Meijer, H. E. H., The measurement of interfacial tension in polymer/polymer systems: The breaking thread method. *Journal of Rheology* **1990,** *34* (8), 1311-1325.

31. Xing, P.; Bousmina, M.; Rodrigue, D.; Kamal, M. R., Critical Experimental Comparison between Five Techniques for the Determination of Interfacial Tension in Polymer Blends: Model System of Polystyrene/Polyamide-6. *Macromolecules* **2000,** *33* (21), 8020-8034.

32. Otterson, D. M.; Kim, B. H.; Lavengood, R. E., The effect of compatibilizer level on the mechanical properties of a nylon 6/ABS polymer blend. *J Mater Sci* **1991,** *26* (6), 1478-1484.

33. Laura, D. M.; Keskkula, H.; Barlow, J. W.; Paul, D. R., Effect of glass fiber and maleated ethylene–propylene rubber content on tensile and impact properties of Nylon 6. *Polymer* **2000,** *41* (19), 7165-7174.

34. Wang, J.; Reyna-Valencia, A.; Favis, B. D., Continuity, morphology and surface resistivity in binary blends of poly(ether-block-amide) with polyethylene and polystyrene (in preparation). **2016**.

35. Torza, S.; Mason, S. G., Three-phase interactions in shear and electrical fields. *Journal of Colloid and Interface Science* **1970,** *33* (1), 67-83.

36. Carriere, C. J.; Biresaw, G.; Sammler, R. L., Temperature dependence of the interfacial tension of PS/PMMA, PS/PE, and PMMA/PE blends. *Rheologica Acta* **2000,** *39* (5), 476-482.

37. Dou, R.; Li, S.; Shao, Y.; Yin, B.; Yang, M., Insight into the formation of a continuous sheath structure for the PS phase in tri-continuous PVDF/PS/HDPE blends. *RSC Advances* **2016,** *6* (1), 439-447.

38. Virgilio, N.; Favis, B. D., Self-Assembly of Janus Composite Droplets at the Interface in Quaternary Immiscible Polymer Blends. *Macromolecules* **2011,** *44* (15), 5850-5856.

39. Kobayashi, T.; Wood, B. A.; Takemura, A.; Ono, H., Antistatic performance and morphological observation of ternary blends of poly(ethylene terephthalate), poly(ether esteramide), and Na-neutralized poly(ethylene-co-methacrylic acid) copolymers. *Journal of Electrostatics* **2006,** *64* (6), 377-385.

40. Jo, W. H.; Park, C. D.; Lee, M. S., Preparation of functionalized polystyrene by reactive extrusion and its blend with polyamide 6. *Polymer* **1996,** *37* (9), 1709-1714.

41. Balamurugan, G. P.; Maiti, S. N., Influence of microstructure and deformation behavior on toughening of reactively compatibilized polyamide 6 and poly(ethylene-co-butyl acrylate) blends. *European Polymer Journal* **2007,** *43* (5), 1786-1805.

42. Fortelný, I.; Zˇivný, A., Coalescence in molten quiescent polymer blends. *Polymer* **1995,** *36* (21), 4113-4118.

43. Yu, W.; Zhou, C.; Inoue, T., A coalescence mechanism for the coarsening behavior of polymer blends during a quiescent annealing process. I. Monodispersed particle system. *Journal of Polymer Science Part B: Polymer Physics* **2000,** *38* (18), 2378-2389.

6.8 Supporting Information

6.8.1 Effect of formulation on morphology and surface resistivity

The morphology of the quaternary LDPE/PS/PEBA/PET blends with volume fractions of 50/10/10/30, 50/20/10/20 and 50/30/10/10 are reported in Fig. 6.12. In all the blends, the phases follow the order of LDPE/PS/PEBA/PET and PEBA is at the interface of PS/PET. Note that Fig. 6.12b presents an image of LDPE/PS/PEBA/PET (50/10/10/30) at a higher magnification to clearly show the different phases.

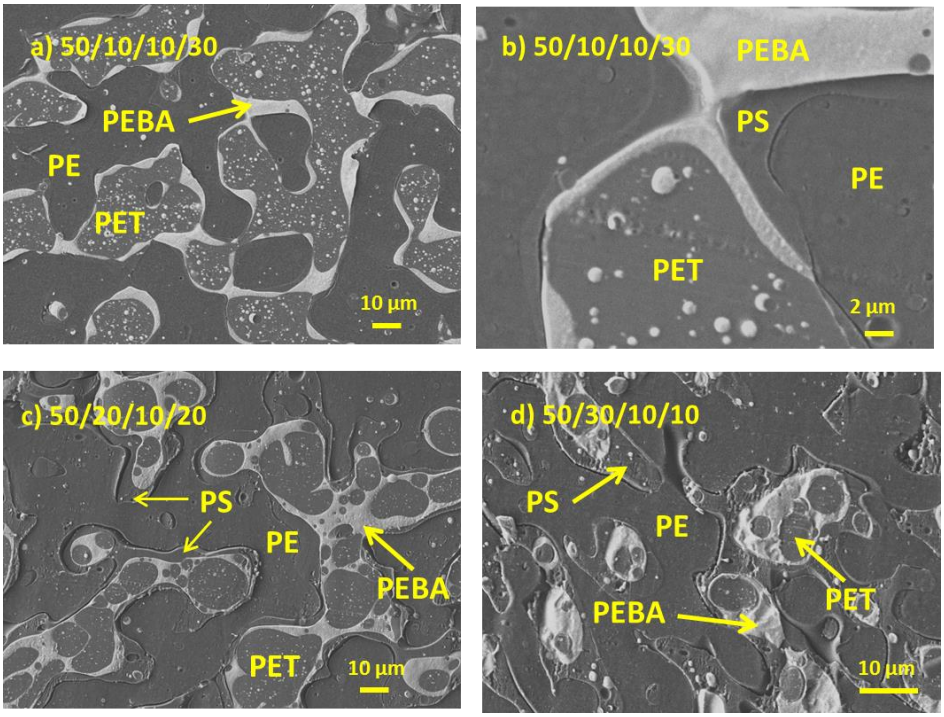

Figure 6.12: Morphology of the quaternary LDPE/PS/PEBA/PET blends with different formations characterized by SEM (the white phase is PEBA which is stained by phosphotungstic acid). (a) and (b): LDPE/PS/PEBA/PET (50/10/10/30) at low and high magnifications; (c): LDPE/PS/PEBA/PET (50/20/10/20); (d) LDPE/PS/PEBA/PET (50/30/10/10).

The image analysis was performed using a digitizing table from Wacom and SigmaScan v.5 software. The composition of PEBA located at the interface of PS/PET after blending was obtained based on the calculation of the area fraction it occupied on the images (Fig. 6.12); and the results are reported in Fig. 6.13. The amount of PEBA at the interface in LDPE/PS/PEBA/PET (50/10/10/30) is much less than in the other two blends (about 70% *vs.* 90%) and a considerable amount of PEBA is trapped in the PET phase. The surface resistivities of LDPE/PS/PEBA/PET (50/10/10/30) and LDPE/PS/PEBA/PET (50/20/10/20) are comparable but significantly lower than that of LDPE/PS/PEBA/PET (50/30/10/10) (Fig. 6.14), probably because in the latter case the PEBA and PET phases are not well percolated due to the limited volume fraction. Based on the morphology and surface resistivity results, the quaternary blend LDPE/PS/PEBA/PET (as well as LDPE/PS/PEBA/PVDF) is formulated with a volume fraction of 50/X/Y/X.

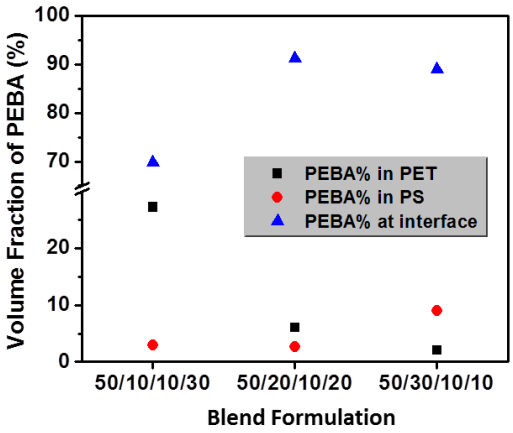

Figure 6.13: The proportions of PEBA in PS, PET and at the interface of PS/PET in the quaternary LDPE/PS/PEBA/PET blends (the small amount of PEBA in LDPE is neglected).

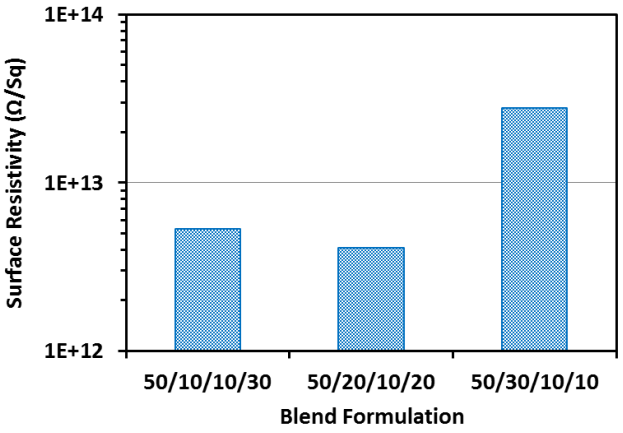

Figure 6.14: Surface resistivity of the LDPE/PS/PEBA/PET blends with volume fractions of 50/10/10/30, 50/20/10/20 and 50/30/10/10.

CHAPTER 7 GENERAL DISCUSSION

In this project, we studied the effect of morphology on resistivity in polymer blends with PEBA, aiming at achieving desirable surface resistivity with significantly less amount of PEBA. PEBA is a typical ionically conductive polymer with PEO blocks whose conductivity heavily depends on the chain mobility. Previous studies showed that the conductivity of ionically conductive polymers can be changed when blended with a miscible component due to the influence on the Tg of the conductive polymers. Therefore, we first prepared binary blends of LDPE/PEBA and PS/PEBA to identify the possible factors affecting the surface resistivity. LDPE and PS have significantly different interfacial tensions with PEBA (8.0 *vs*. 1.6 mN/m), and thus distinct morphology development and phase behaviors are expected in their blends with PEBA. Partial miscibility between PS and PEBA was confirmed by the shift of Tg for PS in the blends with low PEBA concentrations (< 20%). When comparing surface resistivity between samples with different formulations in the same system (either in LDPE/PEBA or in PS/PEBA), a higher continuity results in lower resistivity. However, although the PS/PEBA blends have higher continuities as compared to the LDPE/PEBA blends at the same PEBA concentrations (<30%), the resistivity of LDPE/PEBA is surprisingly lower than that of PS/PEBA. The results indicate that other factors also have important influence on the resistivity of the blends. We believe the partial miscibility between PS and PEBA (influence the PEO chain mobility) and/or the unique frozen capillary instability morphology (constriction effect) are the additional import factor(s) in our system to affect the surface resistivity. However, in this study we were not able to decouple these two factors and future work is needed to further examine their influence.

Compared to other factors, the continuity/percolation phenomenon is much easier to control, and therefore we then focus on obtaining systems with low percolation threshold for PEBA. Studies on localization of conductive fillers in polymer composite systems show that the electrical percolation threshold can be dramatically reduced if the filler is confined at the polymer interface. Thus we selected two systems LDPE/PEBA/PET (partial wetting) and LDPE/PEBA/PVDF (complete wetting) where PEBA is assembled at the interface of LDPE/PET and LDPE/PVDF respectively after blending. It was surprising that, although not as effective as the completely wet LDPE/PEBA/PVDF system, the partially wet LDPE/PEBA/PET system also demonstrates a significant reduction on percolation threshold for PEBA as compared to the binary blends. The true continuity was not determine in these blends since we found that solvent can penetrate

through the LDPE/PET interface and even discrete PEBA domains at the interface can be dissolved out. However, cryo-fractured images clearly show, for the first time, that partially wet PEBA phase can form connected structures at the interface (further transform to a complete wet layer at higher compositions) and these structures are stable at certain annealing conditions. The analysis on spreading coefficients indicates LDPE/PEBA/PET is a weak partial wetting system and the competition between dewetting and coalescence is responsible for the observed morphology. The findings suggest that weak partial wetting systems could be also interesting when designing devices requiring low percolation thresholds.

In a ternary partial wetting system, there are three interfaces. One point is not very clear in literature and has to be noted here is that the interface needs to be clearly indicated when talking about the wetting behaviours. In the same system, one may have weak partial wetting or strong partial wetting depending on the referred interface. For example, in the well-studied ternary PE/PP/PS system, different wetting behaviours can be obtained at different interfaces as determined by the related spreading coefficient (Table 7.1). In this dissertation, we have used a uniform notation. For example, $\lambda_{A/B/C}$ means the spreading coefficient which predicts the wetting behaviours of B at the interface A/C.

Table 7.1: Different wetting behaviours at different interfaces in the ternary PE/PP/PS blend

Interfaces	Corresponding Spreading Coefficient (mN/m)*	Wetting Behaviour
PS at PE/PP interface	$\lambda_{PE/PS/PP} = -6.5$	Strong partial wetting
PP at PE/PS interface	$\lambda_{PE/PP/PS} = -0.5$	Weak partial wetting
PE at PP/PS interface	$\lambda_{PP/PS/PE} = -3.3$	Strong partial wetting

* Data from Ref. [93].

In the last part of the project, we started with a ternary LDPE/PS/PEBA blend and demonstrate two approaches to control the hierarchical structuring of PEBA in multiphase systems particularly with high commodity polymer content (70–90%). In the first approach (adding a fourth phase), the key point is to identify a polymer phase that is fully encapsulated by PEBA and

that doesn't change the hierarchical ordering of LDPE, PS and PEBA. In the second interfacial modification approach, we successfully moved the PEBA to the interface of LDPE and PS, but completely wet PEBA layers were not obtained. This could be due to several reasons. Firstly, as PEBA is a copolymer of PA12 and PEO, it is thus inherently more difficult to find a proper interfacial modifier to have affinity with both blocks. Secondly, EAM is random terpolymer dominated by ethylene content (> 90 wt%). Thus, it is probably not as effective as the classic diblock or triblock copolymers in terms of compatibilization efficacy. Lastly, in mixing state, the interfacial modifier may not have enough time to saturate the interface. Actually, as shown in Fig. 7.1, studies have demonstrated that it is possible to convert the intermediate phase (Phase 3) from partially wet structures to completely wet layers by interfacial modification (change from partial wetting to complete wetting) (Fig. 7.1a). However, no studies have been able to draw a phase from within another phase to the interface and further completely wet the interface (change from complete wetting to another complete wetting) (Fig. 7.1b). In order for the interfacial modifier to come into play, it has to migrate to the interface of Phase 1/Phase 3. The difference in the two scenarios is that the interface between Phase 1 and Phase 3 inherently exists in Case *a* before adding the interfacial modifier, while in Case *b*, the interface has to be first created. Thus it will much more difficult for an interfacial modifier to effectively compatibilize the interface of Phase 1/Phase 3 in the latter. More work is definitely needed to demonstrate if Case *b* is achievable.

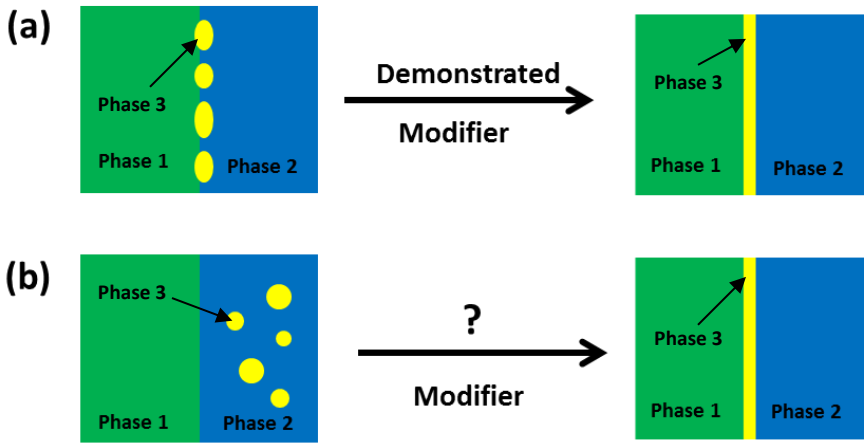

Figure 7.1: Two scenarios of effect of interfacial modification on phase localization in ternary polymer blends (Phase 3: the minor component). Case (a): change from partial wetting to complete wetting, has already demonstrated in literature. Case (b): change from complete wetting to another complete wetting, has not been reported.

CHAPTER 8 CONCLUSION AND RECOMMENDATIONS

8.1 Conclusion

In this project, the morphology and resistivity in a series of polymer blends containing an ionically conductive PEBA copolymer are systematically studied. Starting with binary blends, we first compared two systems with distinct interfacial tensions to investigate the PEBA continuity/morphology development and their influence on surface resistivity. It was shown that although continuity is a crucial parameter to determine the surface resistivity, other factors, such as miscibility and/or constriction effect, also play an important role. A frozen capillary instability morphology was observed in the PS/PEBA blends which is attributed to the intermediate-low interfacial tension (1.6 mN/m) and the partial miscibility. The charge dissipation mechanism in PEBA was also discussed. It was found that the log surface resistivity decreases linearly with increasing water content in both PEBA and the binary blends. A conceptual model to describe the charge dissipation in binary blends with PEBA is also presented.

Utilizing the multiple percolation phenomenon in multiphase polymer blends was found to be an effective approach to reduce the percolation threshold for PEBA. In this study, we cover all the possible morphological states in ternary polymer blend systems: LDPE/PEBA/PET (PEBA partially wets the LDPE/PET interface), LDPE/PEBA/PVDF (PEBA completely wets the LDPE/PVDF interface) and LDPE/PS/PEBA (PEBA is exclusively located within PS). Our results indicate that the lowest percolation threshold was obtained when PEBA forms a completely wet layer at the interface (*i.e.* the LDPE/PEBA/PVDF blends). The morphology development of PEBA confined at the interface was examined in both partially wet LDPE/PEBA/PET system and completely wet LDPE/PEBA/PVDF system. Thermodynamic analysis shows that LDPE/PEBA/PET is a weak partial wetting system and a novel morphological transition from partial wetting to complete wetting with increasing PEBA composition is demonstrated for the first time. In the LDPE/PEBA/PVDF complete wetting system, a minimum concentration is also required to form a completely wet layer which depends on the spreading coefficient. For antistatic applications requiring a surface resistivity lower than 10^{13} Ω/sq, 20–25% of PEBA is needed in the conventional binary blends and 15% for the ternary LDPE/PS/PEBA system. By assembling PEBAT at the continuous interface, the value is reduced to 10% for LDPE/PEBA/PET, and as low as 1% for the LDPE/PEBA/PVDF system.

Although PEBA is located within the PS phase in the LDPE/PS/PEBA system, which limits its ability to reduce the surface resistivity, blending PEBA with commodity polymers such as polyolefins and PS can present significant potential cost advantages. Therefore, we developed two approaches to localize PEBA at the interface of two other polymers in hierarchically ordered, multi-percolated ternary and quaternary polymer blend systems with high LDPE and PS contents (volume fraction: 70–90%). In the first approach, by adding PET (or PVDF) as the fourth phase to LDPE/PS/PEBA, PEBA is moved from within the PS phase to the continuous interface of PS/PET (or PS/PVDF) in the quaternary blend of LDPE/PS/PEBA/PET (or LDPE/PS/PEBA/PVDF), which significantly decreases the percolation threshold for PEBA. The amount of PEBA required to obtain a surface resistivity of 10^{13} Ω/sq for antistatic applications is dramatically reduced to about 5% for LDPE/PS/PEBA/PET and only 1% for LDPE/PS/PEBA/PVDF. The results indicate that the percolation threshold of PEBA can be further reduced by increasing the number of the components in multiphase systems and/or increasing the spreading coefficient. In the second approach, the addition of a small amount of EAM to LDPE/PS/PEBA (50/40/10), combined with some annealing, also successfully draws PEBA to the LDPE/PS interface in the ternary LDPE/PS/PEBA system with an even higher commodity polymer content (LDPE+PS = 90%). Although PEBA does not form completely wet layers, significant reduction in surface resistivity from 5.6×10^{15} to 1.9×10^{13} Ω/sq was obtained due to the connection between PEBA droplets at the LDPE/PS interface. Further studies will aim at obtaining complete PEBA layers at the LDPE/PS interface by using a more effective interfacial modifier.

8.2 Recommendations for future work

Based on the results obtained along the project, the following recommendations for further work are proposed:

1. Although we consider that the partial miscibility between PS and PEBA reduces the PEO chain mobility and thus reduces the ionic conductivity, we were not able to decouple this effect from the constriction influence in this study. Conductive AFM may be used to determine the conductivity of PEBA domains after blending with PS. The results can then be compared to the conductivity of pure PEBA to evaluate the partial miscibility influence.

2. It was found that before absorbing any moisture, dry PEBA still presents a low surface resistivity (~10^{12} Ω/sq), which is much lower than that of either PA12 or PEO homopolymer (10^{14} and 10^{15} Ω/sq respectively). Further study is needed to understand the charge dissipation mechanism in dry PEBA.
3. In the LDPE/PEBA/PVDF system, we show that a minimum concentration is also required to form a completely wet layer. In other words, there is minimum complete layer thickness which is expected to depend on the spreading coefficient. Based on the studies on the wettability of thin films on a solid surface, it would be interesting and feasible to develop a model to predict the minimum thickness/concentration to form a completely wet layer by knowing the spreading coefficient.
4. For the LDPE/PS/PEBA system, a more effective interfacial modifier than EAM may be used to move PEBA to the interface of LDPE/PS and form a completely wet layer. Possible candidates include PE-b-PEO and PE-b-PA12.
5. The intrinsic surface resistivity of the PEBA used in this study is relatively high (~ 10^{10} Ω/sq) which may be due to the lack of ions. To increase the conductivity of the PEBA, salts (e.g., lithium salt) or ionic liquid may be added to the blends or premixed with PEBA. Adding conductive fillers (e.g., carbon nanotube) can be another approach to increase the conductivity.
6. The PEBA blends in this study were processed in a batch mixer. For industrial applications, extrusion processing or/and injection molding are necessary. Although the thermodynamics won't change, some of the morphological features may be different. Considering the viscosity of PEBA is very low, one particular concern need to be examined would be the shear induced migration of PEBA to the surface of the final product.

BIBLIOGRAPHY

[1] R. B. Rosner, "Conductive materials for ESD applications: an overview," *Device and Materials Reliability, IEEE Transactions on*, vol. 1, pp. 9-16, 2001.

[2] M. A. Babinec, C. L. Mott, and D. C. Burdeaux, "Antistatic sheet material, package and method of making," ed: Google Patents, 1990.

[3] M. Kuang, S. Zhou, J. Lei, and Q. Li, "Low environmental sensitive antistatic material based on poly(vinyl chloride)/quaternary ammonium salt by blending with poly(ethylene oxide)," *Journal of Applied Polymer Science*, vol. 109, pp. 3887-3891, 2008.

[4] J. Markarian, "New developments in antistatic and conductive additives," *Plastics, Additives and Compounding*, vol. 10, pp. 22-25, 9// 2008.

[5] R. P. Eustache, "Poly(Ether-b-Amide) Thermoplastic Elastomers: Structure, Properties, and Applications," in *Handbook of Condensation Thermoplastic Elastomers*, S. Fakirov, Ed., ed: Wiley-VCH Verlag GmbH & Co. KGaA, 2006, pp. 263-281.

[6] T. Kobayashi, B. A. Wood, A. Takemura, and H. Ono, "Antistatic performance and morphological observation of ternary blends of poly(ethylene terephthalate), poly(ether esteramide), and ionomers," *Polymer Engineering & Science*, vol. 48, pp. 2247-2257, 2008.

[7] Y. Fu, J. Wang, G. Zhao, Y. Wang, and S. Chen, "Preparation and properties of poly(ether-ester-amide)/poly(acrylonitrile-co-butadiene-co-styrene) antistatic blends," *Journal of Applied Polymer Science*, vol. 122, pp. 12-18, 2011.

[8] M.-Y. Young and J.-J. Lin, "Electrostatic Dissipating Properties of Poly(oxyethylene)amine-Modified Polyamides," *Industrial & Engineering Chemistry Research*, vol. 37, pp. 4284-4289, 1998/11/01 1998.

[9] J.-J. Lin, M.-Y. Young, S.-M. Shau, and I. J. Cheng, "Preparation and electrostatic dissipating properties of poly(oxyalkylene)imide grafted polypropylene copolymers," *Polymer*, vol. 41, pp. 2405-2417, 3// 2000.

[10] S. Ravati and B. D. Favis, "Morphological states for a ternary polymer blend demonstrating complete wetting," *Polymer*, vol. 51, pp. 4547-4561, 9/17/ 2010.

[11] J. Zhang, S. Ravati, N. Virgilio, and B. D. Favis, "Ultralow Percolation Thresholds in Ternary Cocontinuous Polymer Blends," *Macromolecules,* vol. 40, pp. 8817-8820, 2007/12/01 2007.

[12] A. N. Wilkinson, M. L. Clemens, and V. M. Harding, "The effects of SEBS-g-maleic anhydride reaction on the morphology and properties of polypropylene/PA6/SEBS ternary blends," *Polymer,* vol. 45, pp. 5239-5249, 7/12/ 2004.

[13] S. Horiuchi, N. Matchariyakul, K. Yase, and T. Kitano, "Morphology Development through an Interfacial Reaction in Ternary Immiscible Polymer Blends," *Macromolecules,* vol. 30, pp. 3664-3670, 1997/06/01 1997.

[14] T. S. Valera, A. T. Morita, and N. R. Demarquette, "Study of Morphologies of PMMA/PP/PS Ternary Blends," *Macromolecules,* vol. 39, pp. 2663-2675, 2006/04/01 2006.

[15] S. Ravati and B. D. Favis, "Low percolation threshold conductive device derived from a five-component polymer blend," *Polymer,* vol. 51, pp. 3669-3684, 7/22/ 2010.

[16] M. Zilberman, A. Siegmann, and M. Narkis, "Conductivity and structure of melt-processed polyaniline binary and ternary blends," *Polymers for Advanced Technologies,* vol. 11, pp. 20-26, 2000.

[17] Q.-H. Zhang, X.-H. Wang, D.-J. Chen, and X.-B. Jing, "Electrically conductive, melt-processed ternary blends of polyaniline/dodecylbenzene sulfonic acid, ethylene/vinyl acetate, and low-density polyethylene," *Journal of Polymer Science Part B: Polymer Physics,* vol. 42, pp. 3750-3758, 2004.

[18] F. Gubbels, R. Jerome, P. Teyssie, E. Vanlathem, R. Deltour, A. Calderone, *et al.*, "Selective Localization of Carbon Black in Immiscible Polymer Blends: A Useful Tool To Design Electrical Conductive Composites," *Macromolecules,* vol. 27, pp. 1972-1974, 1994/03/01 1994.

[19] F. Gubbels, R. Jerome, E. Vanlathem, R. Deltour, S. Blacher, and F. Brouers, "Kinetic and Thermodynamic Control of the Selective Localization of Carbon Black at the Interface of Immiscible Polymer Blends," *Chemistry of Materials,* vol. 10, pp. 1227-1235, 1998/05/01 1998.

[20] M. H. Al-Saleh and U. Sundararaj, "An innovative method to reduce percolation threshold of carbon black filled immiscible polymer blends," *Composites Part A: Applied Science and Manufacturing,* vol. 39, pp. 284-293, 2// 2008.

[21] A.-C. Baudouin, J. Devaux, and C. Bailly, "Localization of carbon nanotubes at the interface in blends of polyamide and ethylene–acrylate copolymer," *Polymer,* vol. 51, pp. 1341-1354, 3/11/ 2010.

[22] J. Chen, Y.-y. Shi, J.-h. Yang, N. Zhang, T. Huang, C. Chen, *et al.,* "A simple strategy to achieve very low percolation threshold via the selective distribution of carbon nanotubes at the interface of polymer blends," *Journal of Materials Chemistry,* vol. 22, pp. 22398-22404, 2012.

[23] E. Cohen, L. Zonder, A. Ophir, S. Kenig, S. McCarthy, C. Barry, *et al.,* "Hierarchical Structures Composed of Confined Carbon Nanotubes in Cocontinuous Ternary Polymer Blends," *Macromolecules,* vol. 46, pp. 1851-1859, 2013/03/12 2013.

[24] W. D. Harkins and A. Feldman, "Films. Spreading of Liquids and the Spreading Coefficient," *Journal of the American Chemical Society,* vol. 44, pp. 2665-2685, 1922/12/01 1922.

[25] S. Torza and S. G. Mason, "Three-phase interactions in shear and electrical fields," *Journal of Colloid and Interface Science,* vol. 33, pp. 67-83, 1970/05/01 1970.

[26] X. D. Zhao, J. P. Cao, J. Zhao, G. H. Hu, and Z. M. Dang, "Advanced dielectric polymer nanocomposites by constructing a ternary continuous structure in polymer blends containing poly(methyl methacrylate) (PMMA) modified carbon nanotubes," *Journal of Materials Chemistry A,* vol. 2, pp. 10614-10622, 2014.

[27] J. Reignier and B. D. Favis, "Core–shell structure and segregation effects in composite droplet polymer blends," *AIChE Journal,* vol. 49, pp. 1014-1023, 2003.

[28] N. Virgilio, C. Marc-Aurèle, and B. D. Favis, "Novel Self-Assembling Close-Packed Droplet Array at the Interface in Ternary Polymer Blends," *Macromolecules,* vol. 42, pp. 3405-3416, 2009/05/12 2009.

[29] S. Ravati and B. D. Favis, "Interfacial coarsening of ternary polymer blends with partial and complete wetting structures," *Polymer,* vol. 54, pp. 6739-6751, 11/27/ 2013.

[30] W. D. Callister and D. G. Rethwisch, *Fundamentals of Materials Science and Engineering: An Integrated Approach, 4th Edition: An Integrated Approach*: Wiley, 2011.

[31] M. Armand, "Polymers with Ionic Conductivity," *Advanced Materials,* vol. 2, pp. 278-286, 1990.

[32] L. Dai, "Conducting Polymers," in *Intelligent Macromolecules for Smart Devices*, ed: Springer London, 2004, pp. 41-80.

[33] S. Bhadra, D. Khastgir, N. K. Singha, and J. H. Lee, "Progress in preparation, processing and applications of polyaniline," *Progress in Polymer Science,* vol. 34, pp. 783-810, 8// 2009.

[34] M. L. Clingerman, "Development and modelling of electrically conductive composite materials," 3035719 Ph.D., Michigan Technological University, Ann Arbor, 2001.

[35] H. Shirakawa, E. J. Louis, A. G. MacDiarmid, C. K. Chiang, and A. J. Heeger, "Synthesis of electrically conducting organic polymers: halogen derivatives of polyacetylene, (CH)," *Journal of the Chemical Society, Chemical Communications,* pp. 578-580, 1977.

[36] C. K. Chiang, C. R. Fincher, Y. W. Park, A. J. Heeger, H. Shirakawa, E. J. Louis, *et al.*, "Electrical Conductivity in Doped Polyacetylene," *Physical Review Letters,* vol. 39, pp. 1098-1101, 10/24/ 1977.

[37] J. R. Reynolds, C. K. Baker, C. A. Jolly, P. A. Poropatic, and J. P. Ruiz, "Electrically Conductive Polymers," in *Conductive Polymers and Plastics*, J. M. Margolis, Ed., ed Great Britain: Chapman and Hall, 1989.

[38] P. V. Wright, "Electrical conductivity in ionic complexes of poly(ethylene oxide)," *British Polymer Journal,* vol. 7, pp. 319-327, 1975.

[39] M. Watanabe, K. Sanui, N. Ogata, F. Inoue, T. Kobayashi, and Z. Ohtaki, "Ionic Conductivity and Mobility of Poly(propylene oxide) Networks Dissolving Alkali Metal Thiocyanates," *Polym J,* vol. 17, pp. 549-555, 04//print 1985.

[40] M. B. Armand, "POLYMER ELECTROLYTES," *Annual Review of Materials Science,* vol. 16, pp. 245-261, 1986.

[41] B. Scrosati and C. A. Vincent, "Polymer Electrolytes: The Key to Lithium Polymer Batteries," *MRS Bulletin,* vol. 25, pp. 28-30, 2000.

[42] N. Boden, S. A. Leng, and I. M. Ward, "Ionic conductivity and diffusivity in polyethylene oxode/electrolyte solutions as models for polymer electrolytes," *Solid State Ionics,* vol. 45, pp. 261-270, 1991/04/01 1991.

[43] S. Cheng, D. M. Smith, and C. Y. Li, "How Does Nanoscale Crystalline Structure Affect Ion Transport in Solid Polymer Electrolytes?," *Macromolecules,* vol. 47, pp. 3978-3986, 2014/06/24 2014.

[44] M. Watanabe, K. Sanui, N. Ogata, T. Kobayashi, and Z. Ohtaki, "Ionic conductivity and mobility in network polymers from poly(propylene oxide) containing lithium perchlorate," *Journal of Applied Physics,* vol. 57, pp. 123-128, 1985.

[45] R. Bouchet, T. N. T. Phan, E. Beaudoin, D. Devaux, P. Davidson, D. Bertin, *et al.*, "Charge Transport in Nanostructured PS–PEO–PS Triblock Copolymer Electrolytes," *Macromolecules,* vol. 47, pp. 2659-2665, 2014/04/22 2014.

[46] F. M. Gray, *Solid Polymer Electrolytes: Fundamentals and Technological Applications*: Wiley, 1991.

[47] A. J. Polak, "Ionically Conductive Polymers," in *Conductive Polymers and Plastics*, J. M. Margolis, Ed., ed Great Britain: Chapman and Hall, 1989.

[48] J.-H. Shin, W. A. Henderson, and S. Passerini, "Ionic liquids to the rescue? Overcoming the ionic conductivity limitations of polymer electrolytes," *Electrochemistry Communications,* vol. 5, pp. 1016-1020, 12// 2003.

[49] P. Aranda and E. Ruiz-Hitzky, "Poly(ethylene oxide)-silicate intercalation materials," *Chemistry of Materials,* vol. 4, pp. 1395-1403, 1992/11/01 1992.

[50] G. Inzelt, "Classification of Electrochemically Active Polymers," in *Conducting Polymers*, ed: Springer Berlin Heidelberg, 2012, pp. 7-82.

[51] A. R. Blythe and D. Bloor, *Electrical Properties of Polymers*: Cambridge University Press, 2005.

[52] T. Kobayashi, B. A. Wood, A. Takemura, and H. Ono, "Antistatic performance and morphological observation of ternary blends of poly(ethylene terephthalate), poly(ether esteramide), and Na-neutralized poly(ethylene-co-methacrylic acid) copolymers," *Journal of Electrostatics,* vol. 64, pp. 377-385, 6// 2006.

[53] J. K. W. Sandler, J. E. Kirk, I. A. Kinloch, M. S. P. Shaffer, and A. H. Windle, "Ultra-low electrical percolation threshold in carbon-nanotube-epoxy composites," *Polymer,* vol. 44, pp. 5893-5899, 9// 2003.

[54] R. Balint, N. J. Cassidy, and S. H. Cartmell, "Conductive polymers: Towards a smart biomaterial for tissue engineering," *Acta Biomaterialia,* vol. 10, pp. 2341-2353, 6// 2014.

[55] F. L. G. Malet, "Thermoplastic Poly(Ether-b-Amide) Elastomers: Synthesis," in *Handbook of Condensation Thermoplastic Elastomers*, S. Fakirov, Ed., ed: Wiley-VCH Verlag GmbH & Co. KGaA, 2006, pp. 241-262.

[56] J. P. Sheth, J. Xu, and G. L. Wilkes, "Solid state structure–property behavior of semicrystalline poly(ether-block-amide) PEBAX® thermoplastic elastomers," *Polymer,* vol. 44, pp. 743-756, // 2003.

[57] R. S. McLean and B. B. Sauer, "Nano-deformation of crystalline domains during tensile stretching studied by atomic force microscopy," *Journal of Polymer Science Part B: Polymer Physics,* vol. 37, pp. 859-866, 1999.

[58] B. B. Sauer, R. S. McLean, D. J. Brill, and D. J. Londono, "Morphology and orientation during the deformation of segmented elastomers studied with small-angle X-ray scattering and atomic force microscopy," *Journal of Polymer Science Part B: Polymer Physics,* vol. 40, pp. 1727-1740, 2002.

[59] V. Barbi, S. S. Funari, R. Gehrke, N. Scharnagl, and N. Stribeck, "SAXS and the Gas Transport in Polyether-block-polyamide Copolymer Membranes," *Macromolecules,* vol. 36, pp. 749-758, 2003/02/01 2003.

[60] M. Singh, O. Odusanya, G. M. Wilmes, H. B. Eitouni, E. D. Gomez, A. J. Patel, *et al.*, "Effect of Molecular Weight on the Mechanical and Electrical Properties of Block Copolymer Electrolytes," *Macromolecules,* vol. 40, pp. 4578-4585, 2007/06/01 2007.

[61] F. S. Bates and G. H. Fredrickson, "Block Copolymers—Designer Soft Materials," *Physics Today,* vol. 52, pp. 32-38, 1999.

[62] I. Villaluenga, X. C. Chen, D. Devaux, D. T. Hallinan, and N. P. Balsara, "Nanoparticle-Driven Assembly of Highly Conducting Hybrid Block Copolymer Electrolytes," *Macromolecules,* vol. 48, pp. 358-364, 2015/01/27 2015.

[63] J. Sax and J. M. Ottino, "Modeling of transport of small molecules in polymer blends: Application of effective medium theory," *Polymer Engineering & Science,* vol. 23, pp. 165-176, 1983.

[64] R. Yuan, A. A. Teran, I. Gurevitch, S. A. Mullin, N. S. Wanakule, and N. P. Balsara, "Ionic Conductivity of Low Molecular Weight Block Copolymer Electrolytes," *Macromolecules,* vol. 46, pp. 914-921, 2013/02/12 2013.

[65] F. Croce, G. B. Appetecchi, L. Persi, and B. Scrosati, "Nanocomposite polymer electrolytes for lithium batteries," *Nature,* vol. 394, pp. 456-458, 07/30/print 1998.

[66] D. Devaux, R. Bouchet, D. Glé, and R. Denoyel, "Mechanism of ion transport in PEO/LiTFSI complexes: Effect of temperature, molecular weight and end groups," *Solid State Ionics,* vol. 227, pp. 119-127, 10/29/ 2012.

[67] D. R. Paul and J. W. Barlow, "Polymer Blends," *Journal of Macromolecular Science, Part C,* vol. 18, pp. 109-168, 1980/01/01 1980.

[68] P. Potschke and D. R. Paul, "Formation of Co-continuous structures in melt-mixed immiscible polymer blends," *Journal of Macromolecular Science-Polymer Reviews,* vol. C43, pp. 87-141, 2003.

[69] B. D. Favis, " Factors Influencing the Morphology in Immiscible Polymer Blends in Melt Processing," in *Polymer Blends: Formulation and Performance,* D. R. Paul and C. B. Bucknall, Eds., ed: Wiley-Interscience, 2000, pp. 501-537.

[70] P. Pötschke and D. R. Paul, "Formation of Co-continuous Structures in Melt-Mixed Immiscible Polymer Blends," *Journal of Macromolecular Science, Part C,* vol. 43, pp. 87-141, 2003/01/04 2003.

[71] G. I. Taylor, *The Viscosity of a Fluid Containing Small Drops of Another Fluid* vol. 138, 1932.

[72] G. I. Taylor, *The Formation of Emulsions in Definable Fields of Flow* vol. 146, 1934.

[73] S. Tomotika, *On the Instability of a Cylindrical Thread of a Viscous Liquid Surrounded by Another Viscous Fluid* vol. 150, 1935.

[74] J. M. Li, P. L. Ma, and B. D. Favis, "The role of the blend interface type on morphology in cocontinuous polymer blends," *Macromolecules,* vol. 35, pp. 2005-2016, Mar 12 2002.

[75] P. A. Bhadane, M. F. Champagne, M. A. Huneault, F. Tofan, and B. D. Favis, "Continuity development in polymer blends of very low interfacial tension," *Polymer,* vol. 47, pp. 2760-2771, Apr 5 2006.

[76] H. Veenstra, B. J. J. van Lent, J. van Dam, and A. P. de Boer, "Co-continuous morphologies in polymer blends with SEBS block copolymers," *Polymer,* vol. 40, pp. 6661-6672, Nov 1999.

[77] U. Sundararaj and C. W. Macosko, "Drop Breakup and Coalescence in Polymer Blends: The Effects of Concentration and Compatibilization," *Macromolecules,* vol. 28, pp. 2647-2657, 1995/04/01 1995.

[78] I. Fortelný and J. Kovář, "Theory of coalescence in immiscible polymer blends," *Polymer Composites,* vol. 9, pp. 119-124, 1988.

[79] N. Tokita, "Analysis of Morphology Formation in Elastomer Blends," *Rubber Chemistry and Technology,* vol. 50, pp. 292-300, 1977.

[80] B. D. Favis and J. M. Willis, "Phase size/composition dependence in immiscible blends: Experimental and theoretical considerations," *Journal of Polymer Science Part B: Polymer Physics,* vol. 28, pp. 2259-2269, 1990.

[81] H. Veenstra, B. J. J. van Lent, J. van Dam, and A. Posthuma de Boer, "Co-continuous morphologies in polymer blends with SEBS block copolymers," *Polymer,* vol. 40, pp. 6661-6672, 11// 1999.

[82] P. H. M. Elemans, J. M. H. Janssen, and H. E. H. Meijer, "THE MEASUREMENT OF INTERFACIAL-TENSION IN POLYMER-POLYMER SYSTEMS - THE BREAKING THREAD METHOD," *Journal of Rheology,* vol. 34, pp. 1311-1325, Nov 1990.

[83] T. S. Omonov, C. Harrats, P. Moldenaers, and G. Groeninckx, "Phase continuity detection and phase inversion phenomena in immiscible polypropylene/polystyrene blends with different viscosity ratios," *Polymer,* vol. 48, pp. 5917-5927, 9/21/ 2007.

[84] H. Vanoene, "Modes of dispersion of viscoelastic fluids in flow," *Journal of Colloid and Interface Science,* vol. 40, pp. 448-467, 9// 1972.

[85] D. Bourry and B. D. Favis, "Cocontinuity and phase inversion in HDPE/PS blends: Influence of interfacial modification and elasticity," *Journal of Polymer Science Part B: Polymer Physics,* vol. 36, pp. 1889-1899, 1998.

[86] B. D. Favis and J. P. Chalifoux, "The effect of viscosity ratio on the morphology of polypropylene/polycarbonate blends during processing," *Polymer Engineering & Science,* vol. 27, pp. 1591-1600, 1987.

[87] R. GonzalezNunez, D. DeKee, and B. D. Favis, "The influence of coalescence on the morphology of the minor phase in melt-drawn polyamide-6/HDPE blends," *Polymer,* vol. 37, pp. 4689-4693, Oct 1996.

[88] S. Torza and S. G. Mason, "Coalescence of Two Immiscible Liquid Drops," *Science,* vol. 163, pp. 813-814, February 21, 1969 1969.

[89] S. Y. Hobbs, M. E. J. Dekkers, and V. H. Watkins, "Effect of interfacial forces on polymer blend morphologies," *Polymer,* vol. 29, pp. 1598-1602, 9// 1988.

[90] K. Zhang, A. K. Mohanty, and M. Misra, "Fully Biodegradable and Biorenewable Ternary Blends from Polylactide, Poly(3-hydroxybutyrate-co-hydroxyvalerate) and Poly(butylene succinate) with Balanced Properties," *ACS Applied Materials & Interfaces,* vol. 4, pp. 3091-3101, 2012/06/27 2012.

[91] J. Reignier, B. D. Favis, and M.-C. Heuzey, "Factors influencing encapsulation behavior in composite droplet-type polymer blends," *Polymer,* vol. 44, pp. 49-59, 1// 2003.

[92] H. Rastin, S. H. Jafari, M. R. Saeb, H. A. Khonakdar, U. Wagenknecht, and G. Heinrich, "On the reliability of existing theoretical models in anticipating type of morphology and domain size in HDPE/PA-6/EVOH ternary blends," *European Polymer Journal,* vol. 53, pp. 1-12, 4// 2014.

[93] N. Virgilio, P. Desjardins, G. L'Espérance, and B. D. Favis, "In Situ Measure of Interfacial Tensions in Ternary and Quaternary Immiscible Polymer Blends Demonstrating Partial Wetting," *Macromolecules,* vol. 42, pp. 7518-7529, 2009/10/13 2009.

[94] N. Virgilio and B. D. Favis, "Self-Assembly of Janus Composite Droplets at the Interface in Quaternary Immiscible Polymer Blends," *Macromolecules,* vol. 44, pp. 5850-5856, 2011/08/09 2011.

[95] H. F. Guo, S. Packirisamy, N. V. Gvozdic, and D. J. Meier, "Prediction and manipulation of the phase morphologies of multiphase polymer blends: 1. Ternary systems," *Polymer,* vol. 38, pp. 785-794, 2// 1997.

[96] H. F. Guo, N. V. Gvozdic, and D. J. Meier, "Prediction and manipulation of the phase morphologies of multiphase polymer blends: II. Quaternary systems," *Polymer,* vol. 38, pp. 4915-4923, // 1997.

[97] P. Le Corroller and B. D. Favis, "Effect of viscosity in ternary polymer blends displaying partial wetting phenomena," *Polymer,* vol. 52, pp. 3827-3834, 8/3/ 2011.

[98] N. Nemirovski, A. Siegmann, and M. Narkis, "Morphology of ternary immiscible polymer blends," *Journal of Macromolecular Science, Part B,* vol. 34, pp. 459-475, 1995/11/01 1995.

[99] M. Hemmati, H. Nazokdast, and H. Shariat Panahi, "Study on morphology of ternary polymer blends. I. Effects of melt viscosity and interfacial interaction," *Journal of Applied Polymer Science,* vol. 82, pp. 1129-1137, 2001.

[100] I. Luzinov, C. Pagnoulle, and R. Jérôme, "Ternary polymer blend with core–shell dispersed phases: effect of the core-forming polymer on phase morphology and mechanical properties," *Polymer,* vol. 41, pp. 7099-7109, 9// 2000.

[101] K. Levon, A. Margolina, and A. Z. Patashinsky, "Multiple percolation in conducting polymer blends," *Macromolecules*, vol. 26, pp. 4061-4063, 1993/07/01 1993.

[102] T. Kobayashi, B. A. Wood, and A. Takemura, "Crystallization, morphology, and electrical properties of bio-based poly(trimethylene terephthalate)/poly(ether esteramide)/ionomer blends," *Journal of Applied Polymer Science*, vol. 119, pp. 2714-2724, 2011.

[103] T. Kobayashi, B. A. Wood, and A. Takemura, "Morphology, dynamic mechanical, and electrical properties of bio-based poly(trimethylene terephthalate) blends, part 2: Poly(trimethylene terephthalate)/poly(ether esteramide)/polycarbonate blends," *Journal of Applied Polymer Science*, vol. 123, pp. 1056-1067, 2012.

[104] T. Kobayashi, B. A. Wood, G. S. Blackman, and A. Takemura, "Morphology, dynamic mechanical, and electrical properties of bio-based poly(trimethylene terephthalate) blends, part 1: Poly(trimethylene terephthalate)/poly(ether esteramide)/polyethylene glycol 400 bis(2-ethylhexanoate) blends," *Journal of Applied Polymer Science*, vol. 120, pp. 3519-3529, 2011.

[105] F. Fenouillot, P. Cassagnau, and J. C. Majesté, "Uneven distribution of nanoparticles in immiscible fluids: Morphology development in polymer blends," *Polymer*, vol. 50, pp. 1333-1350, 3/6/ 2009.

[106] E. Jalali Dil, "LOCALIZATION OF SOLID MICRO AND NANO-INCLUSIONS IN HETEROPHASE BIOPLASTIC BLENDS," PhD Thesis, Department of Chemical Engineering, École Polytechnique de Montréal, Montréal, Québec, Canada, 2015.

[107] A. Göldel, A. Marmur, G. R. Kasaliwal, P. Pötschke, and G. Heinrich, "Shape-Dependent Localization of Carbon Nanotubes and Carbon Black in an Immiscible Polymer Blend during Melt Mixing," *Macromolecules*, vol. 44, pp. 6094-6102, 2011/08/09 2011.

APPENDIX ARTICLE 4: HIERARCHICALLY POROUS POLYMERIC MATERIALS FROM TERNARY POLYMER BLENDS*

Jun Wang [a], Benoît H. Lessard [b], Milan Maric [b], Basil D. Favis [a]

[a] *CREPEC, Department of Chemical Engineering, École Polytechnique de Montréal, Montréal, Québec, H3T 1J4, Canada*

[b] *CREPEC, Department of Chemical Engineering, McGill University, Montréal, Québec, H3A 2B2, Canada*

A1 Abstract

Hierarchically porous polymers with controllable pore size were generated through a novel polymer blending strategy in an A/B/C-B-C ternary blend system. Polylactide/high-density polyethylene/poly(styrene-ethylene/butylene-styrene) triblock copolymer (PLA/HDPE/SEBS) was used as a model system to demonstrate this technique. During melt blending, the SEBS was driven into the HDPE phase owing to the presence of the PE block in the copolymer. With proper volume fractions of PLA/HDPE/SEBS (e.g., 50/25/25), a bi-modal, dual co-continuous morphology was obtained and hierarchically porous polymeric materials were further generated by selectively removing the PLA and SEBS phases. Annealing and compositional variation were further employed to control the pore size and it is shown that the length scales of the two co-continuous morphologies can be controlled independently.

Keywords*: hierarchically porous polymer, polymer blend, morphology control, annealing*

A2 Introduction

Hierarchical structures, defined as a structure containing elements on difference length scales, are commonly found in nature (e.g., bone and wood) [1]. In human society, these structures have also been constructed, ranging from macroscopic architectures (e.g., Eiffel Tower) to microscopic drug delivery devices (e.g., Multistage nanovectors) [2, 3]. Hierarchically porous materials have been of great interest recently owing to their potential applications in separation [4, 5], catalysis

* Published in *Polymer*: 2014, 55 (16): 3461–3467.

[6], energy storage and conversion [7], drug delivery and tissue engineering [8-11]. When used as scaffolds in tissue engineering, the primary pore size of the hierarchical system ranges from several to hundreds of microns to host different cells for growth [12]. The secondary or higher level of the hierarchical structures (length scale down to nanometer size) are constructed to mimic the extracellular matrix (ECM) features as well as to create the opportunity to introduce drugs, nutrients or nanoparticles, which can facilitate cell adhesion, proliferation and differentiation [9, 13, 14]. Although a few reports have been published for generating hierarchically porous materials for tissue engineering, the precise control over the pore size of the final structures, and in particular the independent control of the different length scales, is indeed challenging [8-10, 14-16].

A considerable amount of research effort has been devoted to generating porous polymeric materials. In this context, Svec and coworkers carried out an intensive study on generating porous polymer monoliths by utilizing phase separation during the polymerization process followed by removing the diluent [17]. The melt blending of immiscible polymers provides another interesting approach to produce porous polymeric materials which takes advantage of thermodynamically driven phase separation. At a certain composition range, the components can form the so-called co-continuous morphology during mixing which is characterized by each component being interconnected throughout the blend [18]. The morphology can then be frozen by quickly quenching the sample at low temperature and the subsequent selective extraction of one phase in the system results in a three dimensional (3D) porous polymer with full continuity. Using this strategy, it has been demonstrated that by controlling composition, interfacial properties and subsequent annealing conditions, the pore size can be tailored ranging from about 300 nm to hundreds of microns while the porosity varied from 30% to 95% without losing the structural integrity [18-20]. However, those results were obtained in a unimodal porous system. In this letter, we report a novel ternary polymer blending strategy to generate hierarchically porous, dual continuous polymeric materials with independent pore size control.

A3 Experimental

A3.1 Materials, characterization and blend preparation

The two homopolymers HDPE 3000 and PLA 3001D were supplied by Petromont and NatureWorks respectively. The triblock copolymer SEBS G1652, with a molecular weight of the

styrene block at 7,000 and the EB block at 37,500, was kindly provided by Kraton. All the materials were dried at 50°C under vacuum for 24 h before further processing.

The breaking thread method was used to determine the interfacial tension between HDPE and PLA on an Optiphot-2 microscope with a hot stage. The PLA thread was sandwiched the HDPE films and the temperature was increased to 200°C. The development of capillary instabilities was recorded and used to calculate the interfacial tension from the following equation:

$$\gamma = \frac{q\eta_m D_0}{\Omega_m}$$

where γ is the interfacial tension, q is the growth rate of the distortion, $\eta_m$is the viscosity of matrix (HDPE) , D_0 is the initial thread diameter (PLA), and Ω_m is a tabulated function. More details about this method can be found in previous publications [19, 21].

The rheological tests were performed on a MCR 501 rheometer under nitrogen. A parallel-plate configuration was used with a gap of 1 mm. Stress sweeps were first performed to define the linear viscoelasticity region.

All the samples with different volume fractions were blended in a Brabender internal mixer with roller rotors at 200°C for 7 min with the rotor speed of 50 RPM under N_2. The volume of the mixer is 30 mL and a fill factor of 0.7 was used. After mixing, the samples were quickly taken from the blades and put into ice water to freeze-in the morphology. Subsequently, quiescent annealing of the blends was performed on a hot press with a constant N_2 flow.

A3.2 Selective extraction and continuity

Cyclohexane and 0.5 mol/L NaOH of MeOH/water (40/60, 60°C) solution were used to selectively remove SEBS and PLA phases respectively. Chloroform was used to extract both SEBS and PLA simultaneously as needed. To determine the continuity of SEBS and PLA, the samples after blending and quenching were cut into 1 cm^3 cubes and then subjected to selective extraction. The continuity of the phase X (SEBS or PLA) was calculated using the following equation:

$$\text{Continuity (\%) } of \text{ phase } X = \frac{m_i - m_f}{m_0^X} \times 100\%$$

where m_i and m_f is the weight of the sample before and after selective extraction of X, respectively. m_0^X is the weight of phase X contained in the sample before extraction.

A3.3 Morphology and pore size

The blends were cryogenically microtomed using a Leica RM2165 microtome equipped with an LN21 cooling system and the morphology was then characterized by atomic force microscope (AFM) and scanning electron microscope (SEM). Before SEM analysis, selective solvent extraction of different phases was performed; the samples were dried overnight at 60°C under vacuum for 24h and then coated with a gold layer by plasma sputtering. SEM observations were conducted using a JEOL JSM 840 scanning electron microscope operated at 2 kV. For the AFM analysis, the tapping mode was used on a Dimension 3100 scanning probe microscope equipped with a Nanoscope IIIa control module.

Nitrogen adsorption measurements were carried out on a Quantachrome Autosorb-1 (Boyntom Beach, FL) apparatus. The surface area is determined based on the Brunauer–Emmett–Teller (BET) theory.

The pore size and distribution of the extracted samples were examined by mercury intrusion porosimetry (MIP) (AutoPore IV 9500). The surface tension 0.485 N/m and contact angle 140° were used. The volume median diameter (the pore diameter at which half of the pore volume is filled with mercury) is used to characterize the pore size with the experimental error less than 10% obtained for all the samples. The detailed information for using MIP to characterize porous polymers has been reported previously [18].

A4 Results and discussion

A4.1 Interfacial tension and rheology

The interfacial tensions of different polymer pairs were examined and are listed in Table A1. The interfacial tension of PLA/PE was measured directly by the breaking thread method. The interfacial tensions of PE/PS, PLA/PS and PE/SEBS were obtained from the literature [18-20, 22, 23]. As the molecular structure of the SEBS used in this study is dominated by the central EB block and since the interfacial tensions of PLA/PS and PLA/PE are comparable, the interfacial tension of PLA/SEBS is estimated to be close to that of PLA/PE. A similar approximation was

used in a PP/PA/SEBS ternary system previously and the observed morphology of the blend showed good agreement as predicted [24]. With the above analysis, and according to Harkins theory [25], the SEBS is expected to be driven into the HDPE phase after the melt blending of PLA/HDPE/SEBS owing to the much lower HDPE/SEBS interfacial tension.

Table A1: Interfacial tensions between different polymers at 200°C (PE/SEBS at 195°C)

Polymer pairs	Interfacial tension γ (mN/m)
PLA/PE	5.0 ± 0.49
PE/PS	4.8 ± 0.35 [a]
PLA/PS	5.2 [b]
PE/SEBS	0.72 [c]
PLA/SEBS	$\approx \gamma_{PLA/PE}$

[a] From Ref.[22]. [b] Averaged from Ref. [18], [20] and [23]. [c] From Ref. [19].

It should be noted that the solubility parameters can also be used to roughly predict the miscibility between polymers. Although the values for many polymers are well documented, most of them are typically measured at low temperature [26]. Since the solubility parameter is sensitive to temperature, corrections need to be performed before comparison. Another point is that the determination of solubility parameter normally shows poor reproducibility which can be affected by many factors such as the set of solvents used. It is considered to be much less reliable to estimate the miscibility between polymers from solubility parameters as compared to interfacial tension.

The rheological properties of the polymers are shown in Fig. A1. It can be seen from the figure that the complex viscosities of PLA and HDPE used in this study are comparable and significantly lower than that of the SEBS; the viscosity of the HDPE/SEBS (50/50) blend lies in between the viscosities of HDPE and SEBS as expected. The elastic modulus follows a similar trend as the complex viscosity. It should also be noted that even at very low angular frequency, the SEBS and HDPE/SEBS blend still present a high elastic modulus, indicating the presence of a yield stress which has been reported previously [27]. The time sweep was also performed for a period of 60 min to examine the thermal degradation of the polymers and it was found that the

complex viscosities of HDPE and SEBS showed negligible changes at 220°C (Fig. S1 in the Supplementary Material). For the PLA, the complex viscosity decreased ~10% and ~20% at 200 and 220°C, respectively.

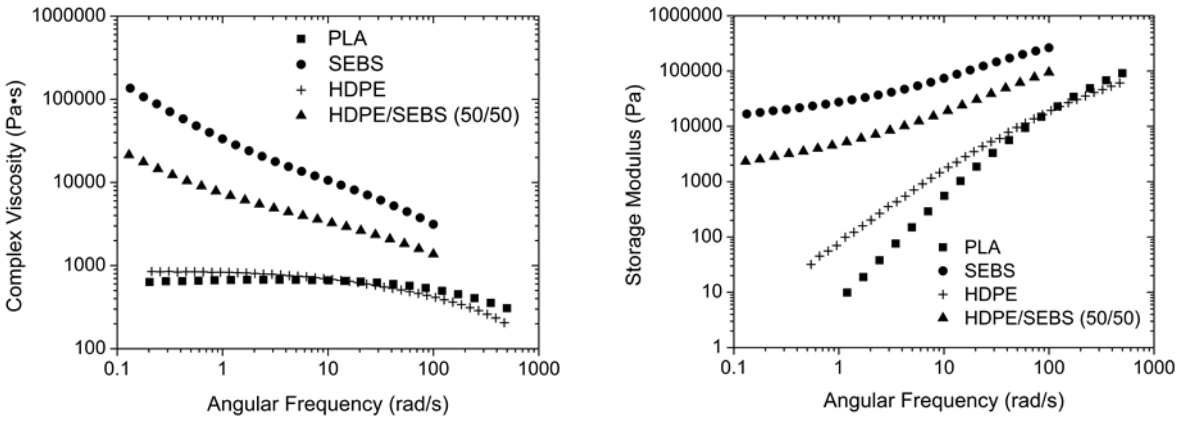

Figure A1: Complex viscosity and elastic modulus as a function of angular frequency at 200°C.

A4.2 Blend morphology and pore size

Fig. A2 (*a* ~ *c*) shows the morphology of the PLA/HDPE/SEBS ternary blends of different volume fractions after extracting SEBS with cyclohexane. As can be seen from the images, the SEBS phase was located in the HDPE phase as expected and gradually formed a finer, second, interpenetrated network within the interconnected HDPE phase as the SEBS concentration increased. The phase identification was further confirmed by removing the PLA phase in the blend with volume fraction 50/25/25 (Fig. A2 *d*). Meanwhile, the hierarchically porous materials were successfully generated and the pore sizes were determined by MIP (Fig. A2 *g*). The selective extraction of SEBS results in pores with a diameter of 438 nm and the removal of the PLA leads to larger pores of 3.3 μm. It should be mentioned that the sample PLA/HDPE/SEBS (50/25/25) without extraction was also examined and there was virtually no intrusion during the test. Also, for the sample after extracting both PLA and SEBS simultaneously, large fluctuations at the smaller pore size range (0.01 ~ 1 μm) were observed and the sample was deformed and compressed after the test. To overcome this problem, the pore sizes at two different length scales were determined separately by extracting only one phase at a time as shown in Fig. A2 *g*.

It is known that the MIP technique is mainly used to measure pore size and distribution in the macro and meso pore size range. For example, the MIP used in this work has the capacity to

determine the pore size from 10 nm to 300 μm. To determine if smaller micropores are present in the system, a nitrogen adsorption test was also performed and a surface area of 16 m^2/g was obtained from BET analysis for the sample of PLA/HDPE/SEBS 50/25/25 after extracting PLA and SEBS. The results, combined with SEM and AFM, confirm that no pores in the meso/micro range were created since such small pores would provide a much larger surface area.

The continuities of PLA and SEBS in the different ternary blends were also examined to demonstrate the interconnectivity of the PLA and SEBS phases (Table S1 in the Supplementary Material). Although all the three components used in our system are immiscible, there will be a region presenting a concentration gradient of the phases when crossing their interface, especially for the HDPE/SEBS interface which has a very low interfacial tension. So it is possible that a very small amount of SEBS (even PLA) remains at the interface after extraction. This will be determined in future work. In this study, however, when over 95% continuity is obtained, we consider the phase is fully continuous.

It is not surprising that the PLA phase maintains high continuity (> 97%) in all samples examined here since the volume fractions were all set at 50%. The continuity of SEBS is high even at low concentrations and reaches 88% continuity at 5% volume fraction. This is an exceptionally high level of continuity for such a low volume fraction of SEBS, especially considering that the viscosity ratio of SEBS/HDPE is around 10. However, it is not unreasonable if the following three factors are considered. Firstly, all the SEBS is confined to the HDPE phase which increases its effective concentration for continuity development. Approximately, it can be considered as doubled in the low concentration range. Secondly, PE/SEBS is a typical low interfacial tension system. In such a system, the dispersed phase forms highly stable fibers during melt blending and a higher continuity is expected due to a thread-thread coalescence mechanism [19, 27]. Li *et al*. reported a continuity of about 25% at an SEBS volume fraction of 15% in HDPE/SEBS blends [19], and Veenstra *et al*. obtained 10% continuity with 10% SEBS in PP/SEBS blends [27]. Additionally, in low interfacial tension systems, it has been shown that the viscosity ratio, under the range examined in the study (0.2 ~ 5), has little effect on continuity [28]. Lastly and most importantly, before extracting SEBS, PLA was first removed in our system which introduces interconnected pores into the samples. This step significantly increases the surface area of the sample and from the nitrogen adsorption results (data not shown), there is an over 100 times increase in the surface area as compared to a solid sample. The continuities cited above were

typically determined on a solid sample where only the SEBS connecting to the outer surface can be dissolved out. But in the present case, not only those connecting to the outer surface can be extracted, but also the SEBS connecting to the high amount of surface of the continuous pores that resulted from the previous removal of PLA. The above factors combine to result in an exceptional high continuity of SEBS at low concentration.

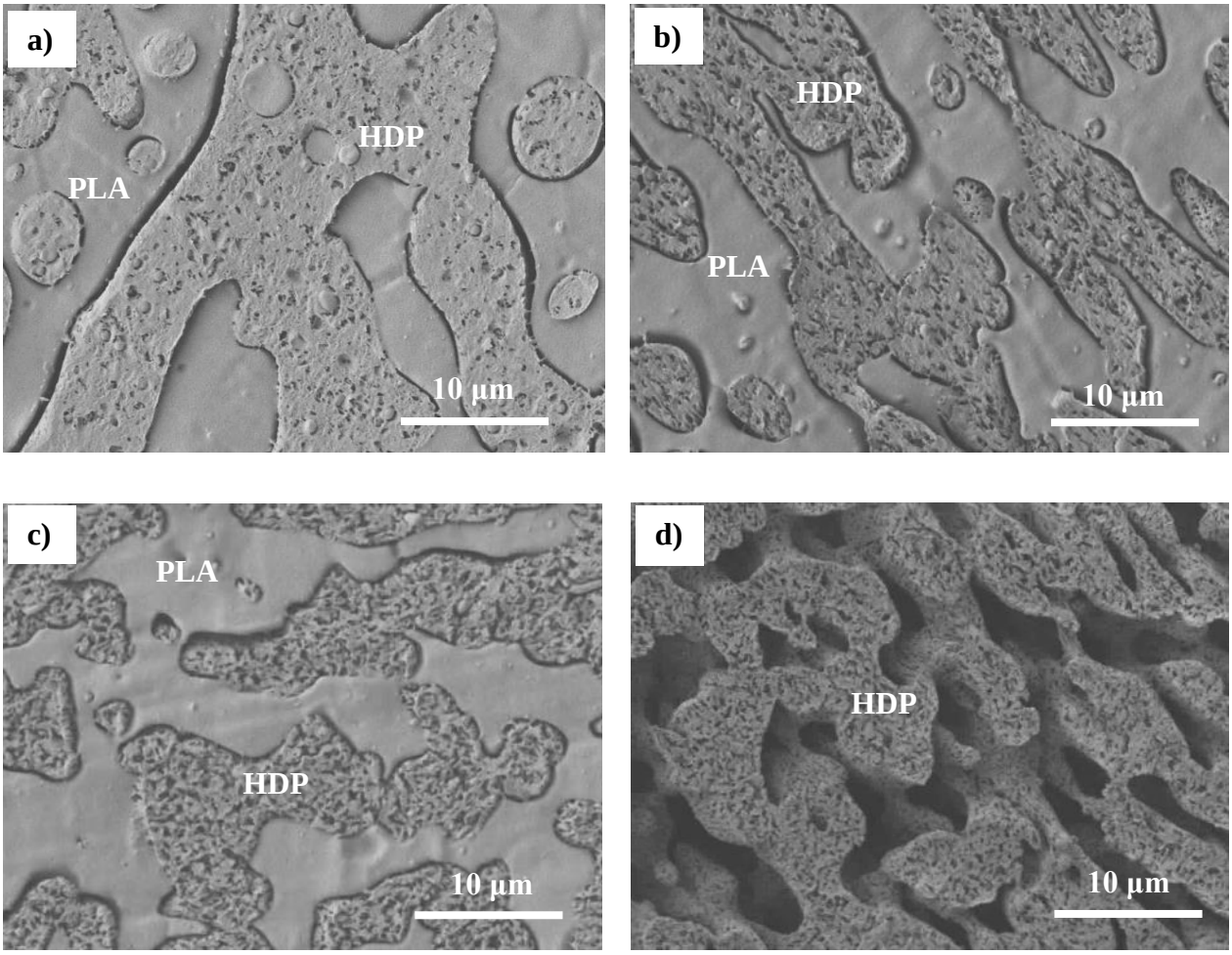

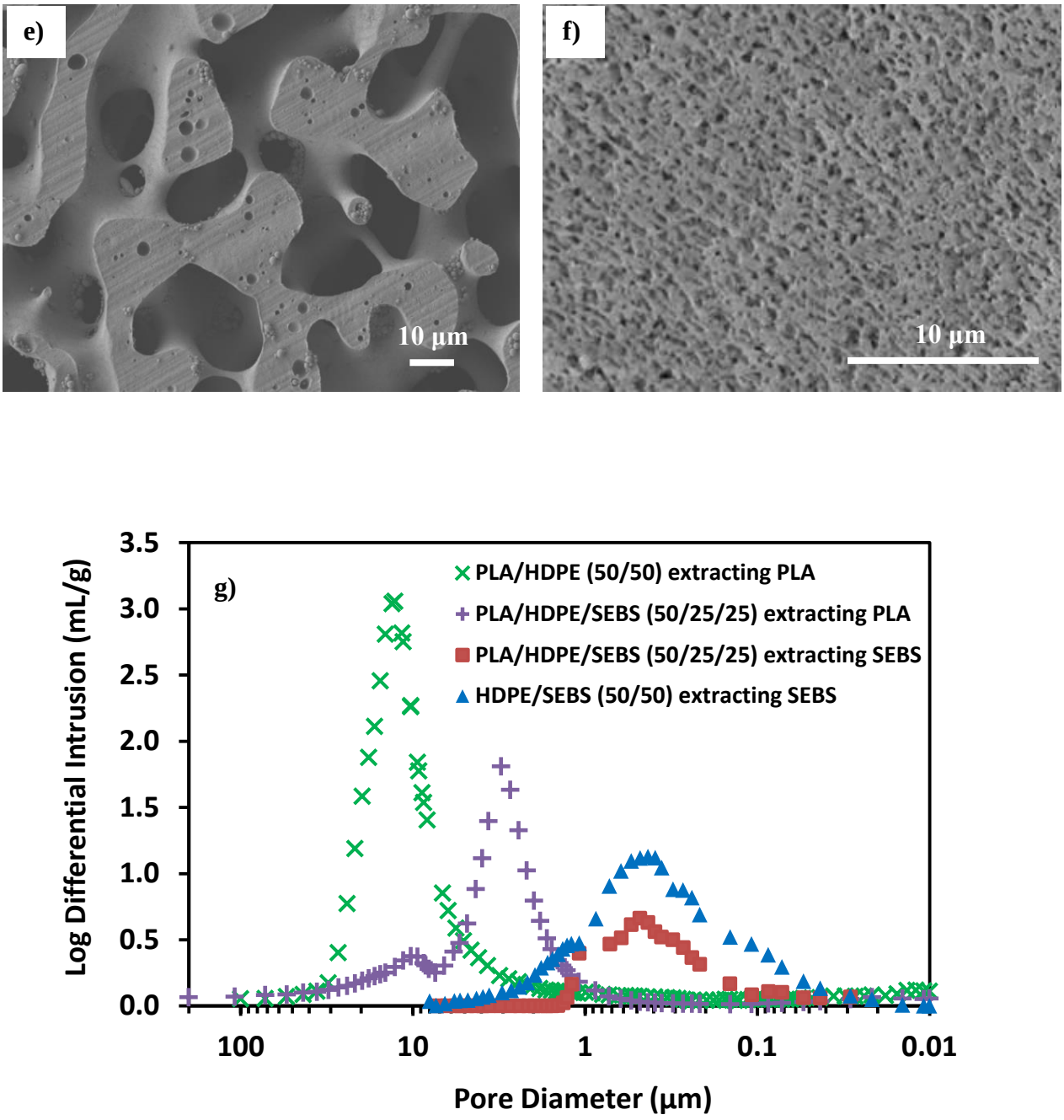

Figure A2: SEM and MIP results: a) ~ c): PLA/HDPE/SEBS (50/45/5, 50/35/15, 50/25/25, SEBS extracted by cyclohexane); d) PLA/HDPE/SEBS (50/25/25, PLA and SEBS extracted by chloroform); e) PLA/HDPE (50/50, PLA extracted by chloroform); f) HDPE/SEBS (50/50, SEBS extracted by cyclohexane); g) Mercury Intrusion Porosimetry (MIP) results.

The pore sizes of the porous materials resulting from the ternary blend of PLA/HDPE/SEBS (50/25/25) were compared to those of the binary systems HDPE/PLA (50/50) and HDPE/SEBS (50/50) (Fig. A2: *d* ~ *g*). The size of the submicron scale pores resulting from the removal of the SEBS from the ternary system was found to be similar to that of the binary blend of HDPE/SEBS (438 *vs*. 392 nm), while the size of the larger pores by removing the PLA are much smaller in the ternary system as compared to the binary blend of HDPE/PLA (3.3 *vs.* 12.0 μm). This difference is significant and can be explained from two possible viewpoints. The addition of SEBS creates a very low interfacial tension system with HDPE and thus very fine microstructures. This results in a cascade-type effect where the finely dispersed HDPE imposes a finer structure on the PLA even though the HDPE/PLA interfacial tension remains high. A similar effect has already been reported for multiple phase systems where the compatibilization of one of the pairs results in significantly reduced phase sizes for the other components [29]. Another possible explanation for the phase size difference may be related to the high viscosity of the SEBS phase. It has been shown previously in binary co-continuous polymer blends that increasing the viscosity of either phase can reduce the coalescence, leading to a smaller phase size [30]. Compared to the HDPE in HDPE/PLA, the HDPE/SEBS "blend phase" in the ternary blend has a much higher viscosity (Fig. A1) which suppresses the coalescence of PLA during blending and thus results in a smaller PLA phase. In any case either, or both of the above explanations in combination, would tend to result in a reduced PLA phase size.

The microstructures of the blends were further examined by AFM under the tapping mode. In the ternary blend of PLA/HDPE/SEBS (50/25/25), as can be seen from Fig. A3 *a*, three phases can be observed; and according to the previous SEM results, the larger bright phase is the PLA phase while the two smaller phases are HDPE and SEBS. By further zooming in (Fig. A3 *b* and *c*), the HDPE and SEBS phase can be identified respectively since the SEBS block copolymer has a typical microphase-separated morphology. The characteristic morphology of SEBS was further confirmed by observing the pure SEBS (Fig. A3 *d*). It should be mentioned that it is difficult to use AFM for phase identification in polymer blends and the quality of the images mainly depends on the quality of microtoming and the properties of the polymers. In the present case, the samples were cryo-microtomed at about − 140°C and a number of tests were performed for each sample. However, since HDPE has a glass transition temperature below − 120°C, it is very difficult to

avoid some cutting effects (e.g., Fig. A3 b and c). Nevertheless, the main features of the images can be identified without difficulty.

A number of nano-droplets with diameter 30~300 nm are also observed (Fig. A3 *b* and *c*), and they seem to be only located within the SEBS phase. This kind of subinclusion phenomenon was also observed in other polymer blend systems, but the mechanism for their formation remains poorly understood [31, 32]. In the present case, the nano-droplet inclusions are considered to be PLA since their smooth curvature and distinct interface between the inclusions and the surrounding SEBS indicates a high interfacial tension. They are probably entrapped in the SEBS phase owing to the high viscosity of SEBS during processing. Further evidence to confirm that the nano-droplets are PLA is that such inclusions were not observed in the binary blend of HDPE/SEBS, but are observed in the PLA/SEBS blend (Fig. A3 *e* and *f*).

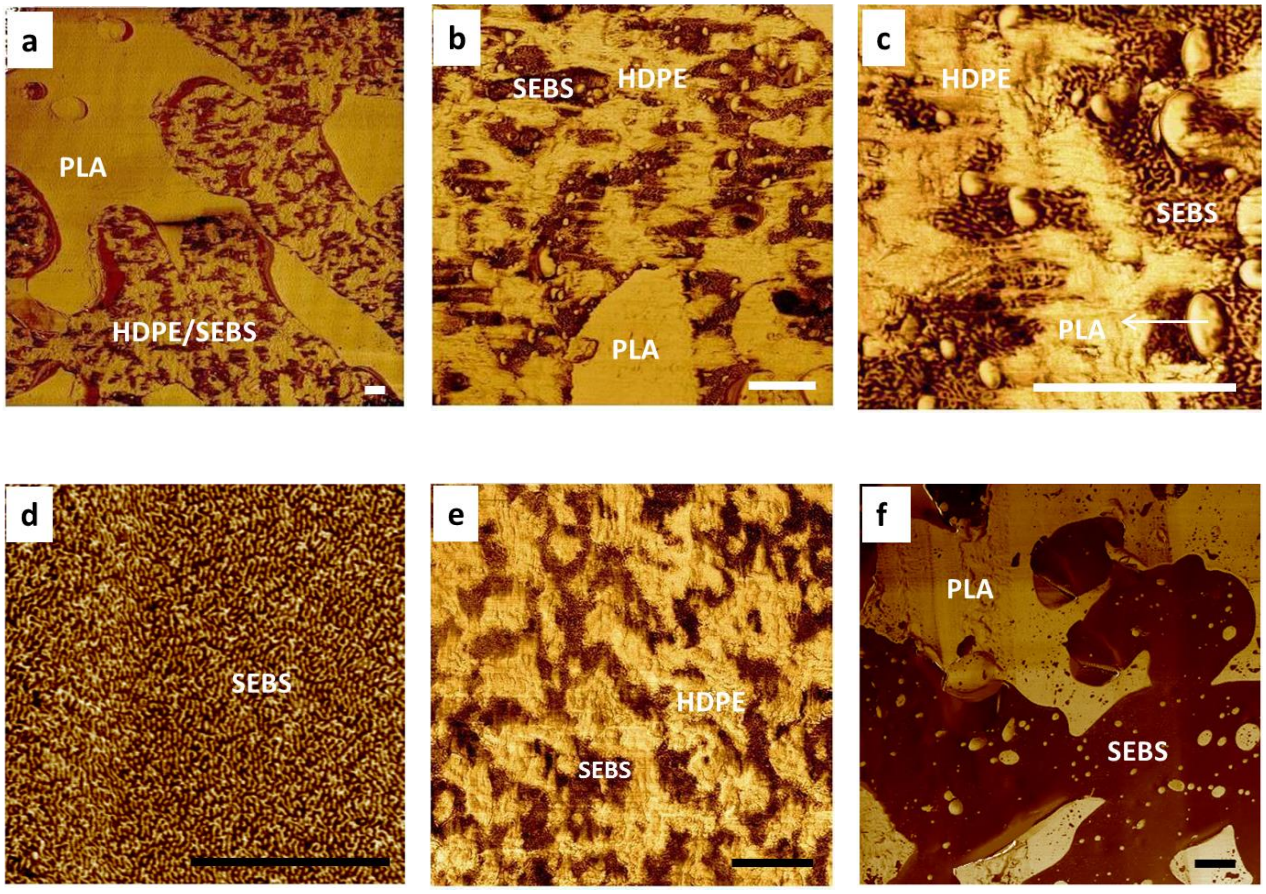

Figure A3: AFM phase images: a, b, c) HDPE/PLA/SEBS (25/50/25) at different magnifications; d) pure SEBS; e) HDPE/SEBS (50/50); f) PLA/SEBS (50/50). Scale bar: 1μm.

It is worthy to stress that SEBS preserves its microphase-separated morphology after melt blending (Fig. A3 *c vs. d*). Since copolymers with degradable blocks have been synthesized and used to generate meso-porous unimodal polymeric materials [33], the present systems also provide a novel promising avenue to fabricate hierarchically macro-meso porous materials providing the C block in the C-B-C copolymer can be designed to be removed from the system.

A4.3 Control of the pore size by annealing

In the case of an application field such as tissue engineering, the optimal pore size of the scaffold to host the cell growth ranges from several to hundreds of microns depending on cell type [12]. In order to examine the potential of the current system to achieve larger pore sizes, annealing was undertaken. This strategy has been successfully used for unimodal porous polymers generated from single co-continuous polymer blends. It has been shown that the pore size can be controlled over two orders of magnitude from submicron to hundreds of microns [18, 20, 30, 34, 35] by varying annealing temperature and time. Fig. A4 shows the pore size evolution for the ternary PLA/HDPE/SEBS (50/25/25) blend annealed at 200°C for a period of 60 min (also see Fig. S2 in the Supplementary Material). The pore sizes of the continuous PLA and SEBS phases grew quickly during the first 10 min from 3.3 to 8.4 μm and from 438 to 702 nm respectively after which the growth rates gradually decreased and very limited pore size increments were observed during the last 30 min (11.4 to 12.4 μm for larger pores and 959 to 1080 nm for smaller pores). These results indicate that the coalescence of these continuous phases was supressed. In fact the results in Fig. A4 resemble the coarsening profile of a compatibilized co-continuous binary system [36]. Non-compatibilized co-continuous systems typically follow a linear profile for phase growth [30, 36]. The different coarsening profiles during annealing can be explained by the balance between a capillary pressure effect and capillary instability phenomena [36].

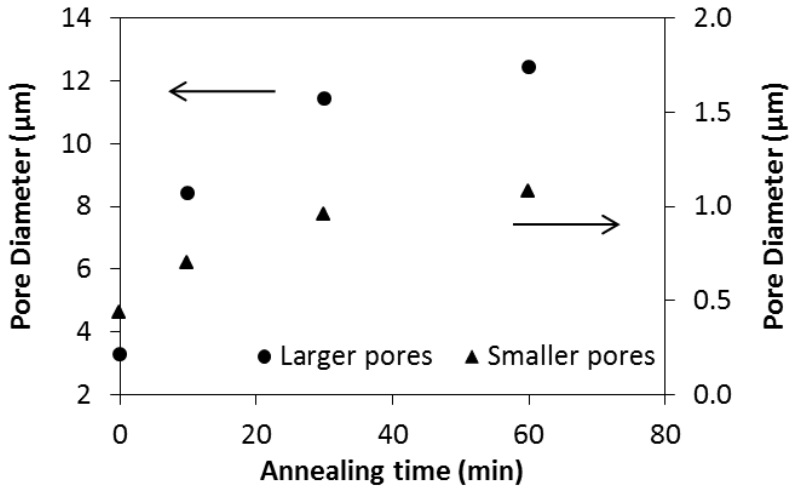

Figure A4: Pore size evolution for the ternary blend (PLA/HDPE/SEBS 50/25/25) annealed at 200°C for a period of 60 min (data obtained after extracting PLA and SEBS from the blends).

It is not unexpected that the HDPE/SEBS mixture presents a limited coalescence behavior. Similar phenomena have been reported previously in a polypropylene/SEBS system and the reason was attributed to be the low interfacial tension as well as the kinetic barrier provided by SEBS [37]. However, it is surprising that the growth rate of the PLA phase during annealing was also low. To understand this, an important factor to consider in the case of dual-continuous ternary polymer blends is the presence of two interfaces and the mutual effect of these interfaces on each other during the annealing process. For example, at the larger scale, the growth of the PLA phase, which is controlled by a capillary instability mechanism between PLA/HDPE, must be affected by the presence of SEBS and its effect on HDPE. In this way the very low interfacial tension between HDPE and SEBS has a cascade effect on the PLA/HDPE phase growth. Thus, although the PLA/HDPE system is a high interfacial tension, PLA phase growth shows a behavior that is similar to that of a partially compatibilized system.

Veenstra *et al*. reported a limited non-linear coarsening process for long time annealing in co-continuous polymer blends and they attributed the slow-down or even cessation of the phase growth to the high viscosity, more importantly, the yield stress originating from the physical cross-links of the SEBS copolymer phases [38, 39]. In this context, Elmendorp proposed an approximation to explain the effect of a yield stress on limiting the breakup of a polymer thread within another polymer matrix [40]. In that process, the breakup is driven by the pressure

difference along the distorted thread. The thread will not even break up for the systems where the pressure difference cannot overcome the yield stress. This is also a potential explanation for the non-linear coarsening behavior results in this work since both SEBS and the blend of HDPE/SEBS (50/50) show high viscosities and yield stresses at the low shear rates (Fig. A1) associated with annealing. In other studies, Macosko and co-workers also observed an initial linear growth followed by a slower coarsening rate in different binary blend systems of polyethylene/polystyrene, polypropylene/polystyrene and polystyrene/styrene-acrylonitrile [41, 42]. In their model, they consider that the excess interface free energy that drives the coarsening process is proportional to both interfacial area and interface curvature and the decrease in the coarsening rate is owing to the reduction of the interface curvature during annealing with respect to the viscous force.

The blend of PLA/HDPE/SEBS with a volume fraction of 50/40/10 was also examined using the annealing conditions of 220°C and 60 min. The smaller pore size in this ternary system remains the same at 1.3 μm while the larger pore size was doubled compared to the blend of 50/25/25 (30.9 *vs*. 16.5 μm) under the same conditions (Fig. A5: *a*, *b* and Fig. A6). Using the mutually dependent interfacial argument developed above, the reduction of the interfacial area between HDPE/SEBS with a decreasing amount of SEBS would be expected to reduce the "cascade effect" between the interfaces of different scales. This would lead to a higher coarsening rate of the PLA phase. It is less likely, but also possible, that the increased PLA coarsening could also be explained by the reduction in the yield stress and viscosity of the HDPE/SEBS system owing to the lower concentration of SEBS. By increasing the PLA phase to 60%, while maintaining the volume ratio of HDPE/SEBS (i.e., HDPE/PLA/SEBS 60/32/8), the larger pore diameter further increases to 70 μm without notably affecting the smaller pore size (increased to 1.38 μm) (Fig. A5: *c* and Fig. A6). This increment is mainly due to a composition effect. The above observation also indicates that the composition has a significant effect on the phase size for the high interfacial tension system, but has little influence in the case of low interfacial tension, which has been demonstrated previously [18, 19]. The continuity of the PLA and SEBS phases were also examined for all the ternary blends after annealing and was found to be 102 ~ 105%.

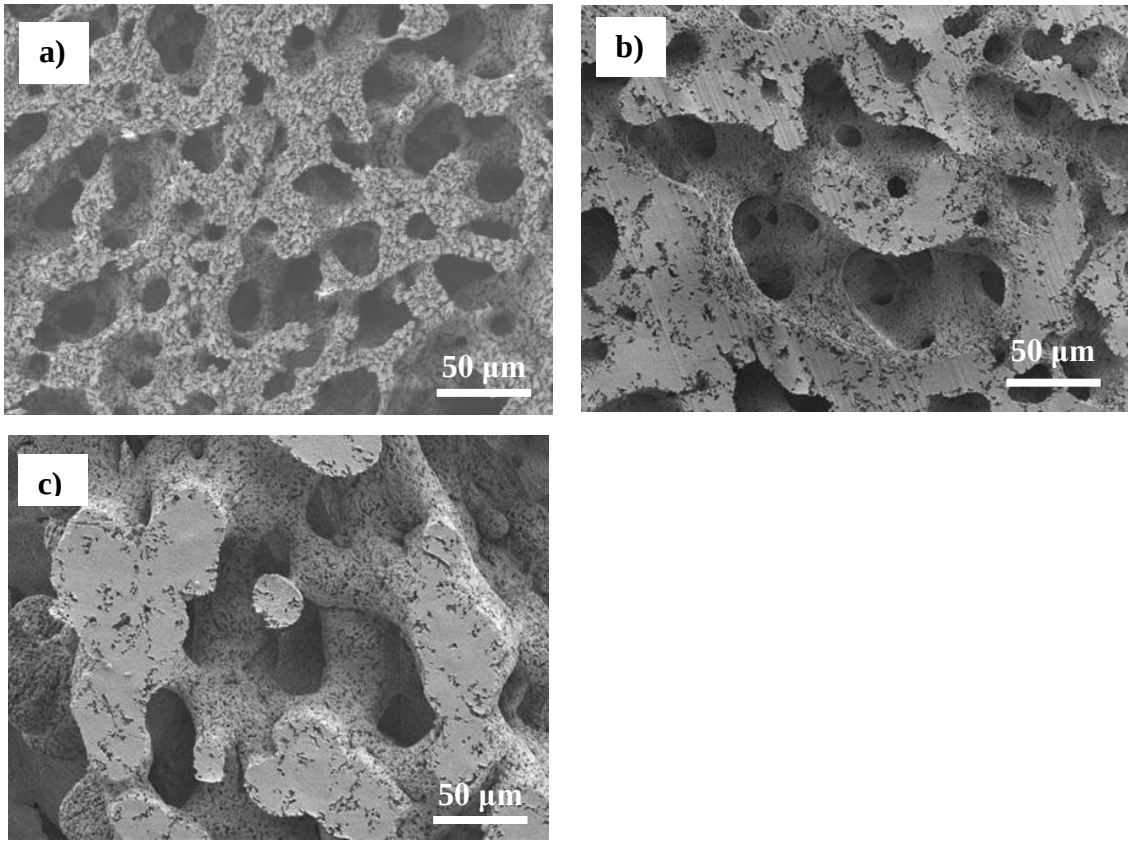

Figure A5: Morphology of the annealed (at 220°C for 60 min) ternary blends PLA/HDPE/SEBS with volume fractions: a) 50/25/25, b) 50/40/10, and c) 60/32/8.

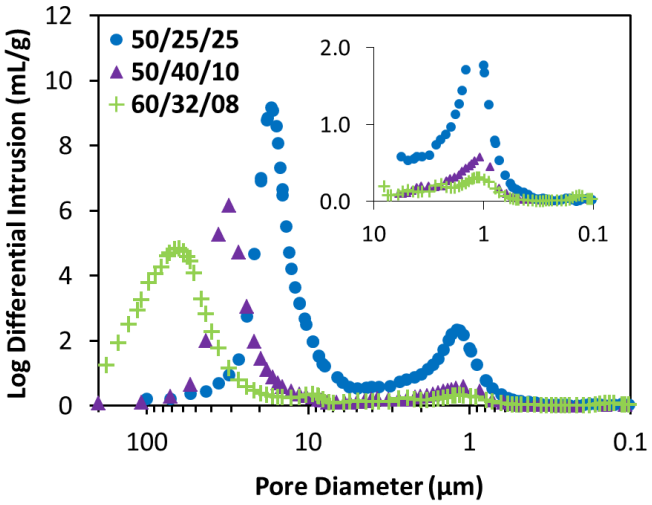

Figure A6: Pore size distribution (MIP results) of the blends PLA/HDPE/SEBS with different volume fractions after anealed at 220°C for 60 min (the smaller pore size region is further shown in the inserted image).

A5 Conclusion

We have demonstrated a novel approach to prepare dual-continuous hierarchically porous polymers with two distinct pore size scales from an A/B/C-B-C ternary polymer blend. PLA/HDPE/SEBS was used as a model system and after extraction of PLA and SEBS, hierarchically porous HDPE was generated with a large pore size scale of several microns and a smaller pore size of hundreds of nanometers. By varying the composition in annealing, the size of the larger pores can be tailored independently of the smaller ones. With the conditions used in this study, the smaller pores can be maintained constantly at around 1.3 μm while the larger pores can be controlled from 16.5 to 70 μm, a 4-fold difference, with the potential to increase even more at longer annealing times. This strategy provides a promising technique to fabricate fully interconnected dual-continuous porous materials of highly controlled microstructure.

A6 Acknowledgment

The authors would like to thank Sylvie St-Amour from FPInnovations for assistance with the MIP tests and Willard McLean and Yonghua Zhou from Kraton for providing the SEBS and the information on the polymer. Jun Wang would like to acknowledge the China Scholarship Council (CSC) for a scholarship. Benoît H. Lessard would like to thank the Natural Sciences and Engineering Research Council (NSERC) for a scholarship. The authors also express appreciation to the NSERC Strategic Network Program and the Network for Innovative Plastic Materials and Manufacturing Processes (NIPMMP) for supporting this work.

A7 References

[1] Bruck H. Implantable Biomedical Devices and Biologically Inspired Materials. In: Sharpe WN, Jr., editor. Springer Handbook of Experimental Solid Mechanics: Springer US, 2008. pp. 891-928.

[2] Lakes R. Nature 1993;361(6412):511-515.

[3] Godin B, Tasciotti E, Liu XW, Serda RE, and Ferrari M. Accounts of Chemical Research 2011;44(10):979-989.

[4] Wang D-W, Li F, Lu GQ, and Cheng H-M. Carbon 2008;46(12):1593-1599.

[5] Hasegawa G, Morisato K, Kanamori K, and Nakanishi K. Journal of Separation Science 2011;34(21):3004-3010.

[6] Lin Y-G, Hsu Y-K, Chen S-Y, Chen L-C, and Chen K-H. Journal of Materials Chemistry 2010;20(47):10611-10614.

[7] Li Y, Fu ZY, and Su BL. Advanced Functional Materials 2012;22(22):4634-4667.

[8] Yun H, Kim S, and Hyeon Y. Chemical Communications 2007;0(21):2139-2141.

[9] Roohani-Esfahani SI, Lu ZF, and Zreiqat H. Materials Letters 2011;65(17-18):2578-2581.

[10] Ko Y-G, Kawazoe N, Tateishi T, and Chen G. Journal of Biomedical Materials Research Part B: Applied Biomaterials 2010;93B(2):341-350.

[11] Li X, Wang X, Chen H, Jiang P, Dong X, and Shi J. Chemistry of Materials 2007;19(17):4322-4326.

[12] Yang SF, Leong KF, Du ZH, and Chua CK. Tissue Engineering 2001;7(6):679-689.

[13] García Cruz DM, Gomes M, Reis RL, Moratal D, Salmerón-Sánchez M, Gómez Ribelles JL, and Mano JF. Journal of Biomedical Materials Research Part A 2010;95A(4):1182-1193.

[14] George PA, Quinn K, and Cooper-White JJ. Biomaterials 2010;31(4):641-647.

[15] Singh R, Lee PD, Jones JR, Poologasundarampillai G, Post T, Lindley TC, and Dashwood RJ. Acta Biomaterialia 2010;6(12):4596-4604.

[16] Dorj B, Park J-H, and Kim H-W. Materials Letters 2012;73(0):119-122.

[17] Svec F and Frechet JMJ. Rigid Macroporous Organic Polymer Monoliths Prepared by Free Radical Polymerization. In: Svec F, Tennikova TB, and Zdenek D, editors. Monolithic Materials Preparation, Properties and Applications. Amsterdam: Elsevier, 2003. pp. 19-50.

[18] Sarazin P and Favis BD. Biomacromolecules 2003;4(6):1669-1679.

[19] Li JM, Ma PL, and Favis BD. Macromolecules 2002;35(6):2005-2016.

[20] Virgilio N, Sarazin P, and Favis BD. Biomaterials 2010;31(22):5719-5728.

[21] Elemans PHM, Janssen JMH, and Meijer HEH. Journal of Rheology 1990;34(8):1311-1325.

[22] Carriere CJ, Biresaw G, and Sammler RL. Rheologica Acta 2000;39(5):476-482.

[23] Biresaw G and Carriere CJ. Journal of Polymer Science Part B: Polymer Physics 2002;40(19):2248-2258.

[24] Wilkinson AN, Clemens ML, and Harding VM. Polymer 2004;45(15):5239-5249.

[25] Torza S and Mason SG. Journal of Colloid and Interface Science 1970;33(1):67-83.

[26] Grulke EA. Solubility Parameter Values. In: Brandrup J and Immergut EH, editors. Polymer handbook: Wiley, 1989. pp. VII/519-560.

[27] Veenstra H, van Lent BJJ, van Dam J, and de Boer AP. Polymer 1999;40(24):6661-6672.

[28] Bhadane PA, Champagne MF, Huneault MA, Tofan F, and Favis BD. Polymer 2006;47(8):2760-2771.

[29] Ravati S and Favis BD. Polymer 2010;51(16):3669-3684.

[30] Yuan ZH and Favis BD. AIChE Journal 2005;51(1):271-280.

[31] Pagnoulle C and Jerome R. Polymer 2001;42(5):1893-1906.

[32] Martin P, Maquet C, Legras R, Bailly C, Leemans L, van Gurp M, and van Duin M. Polymer 2004;45(10):3277-3284.

[33] Pitet LM, Amendt MA, and Hillmyer MA. Journal of the American Chemical Society 2010;132(24):8230-8231.

[34] Bramfeldt H, Sarazin P, and Vermette P. Journal of Biomedical Materials Research Part A 2009;91A(1):305-315.

[35] Yao DG, Zhang W, and Zhou JG. Biomacromolecules 2009;10(5):1282-1286.

[36] Yuan ZH and Favis BD. Journal of Polymer Science Part B-Polymer Physics 2006;44(4):711-721.

[37] Gergen WP, Lutz RG, and Davison S. Hydrogenated Block Copolymers in Thermoplastic Elastomer Interpenetrating Polymer Networks. In: Holden G, Legge NR, Quirk RP, and Schroeder HE, editors. Thermoplastic Elastomers: Hanser-Gardner Publications, 1996. pp. 297-329.

[38] Veenstra H, Van Dam J, and de Boer AP. Polymer 2000;41(8):3037-3045.

[39] Veenstra H, Van Dam J, and de Boer AP. Polymer 1999;40(5):1119-1130.

[40] Elmendorp JJ. Polymer Engineering & Science 1986;26(6):418-426.

[41] Pyun A, Bell JR, Won KH, Weon BM, Seol SK, Je JH, and Macosko CW. Macromolecules 2007;40(6):2029-2035.

[42] Lopez-Barron CR and Macosko CW. Soft Matter 2010;6(12):2637-2647.

A8 Supplementary Material

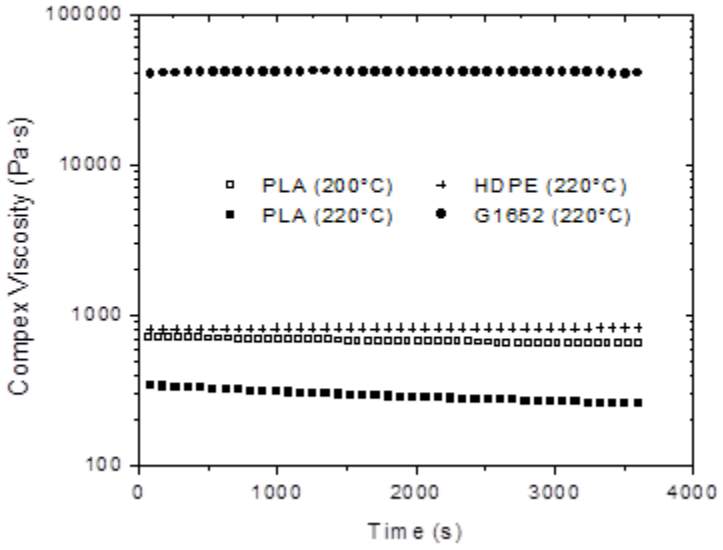

Figure A7: Time sweep measurements performed at 0.1 Hz

Table A2: Continuity of the ternary blends with different volume fractions.

Volume fraction of PLA/HDPE/SEBS	Continuity of PLA (%)	Continuity of G1652 (%)
50/45/5	> 97	88 ± 4.4
50/40/10		103 ± 1.1
50/35/15		98 ± 1.1
50/25/25		102 ± 0.3

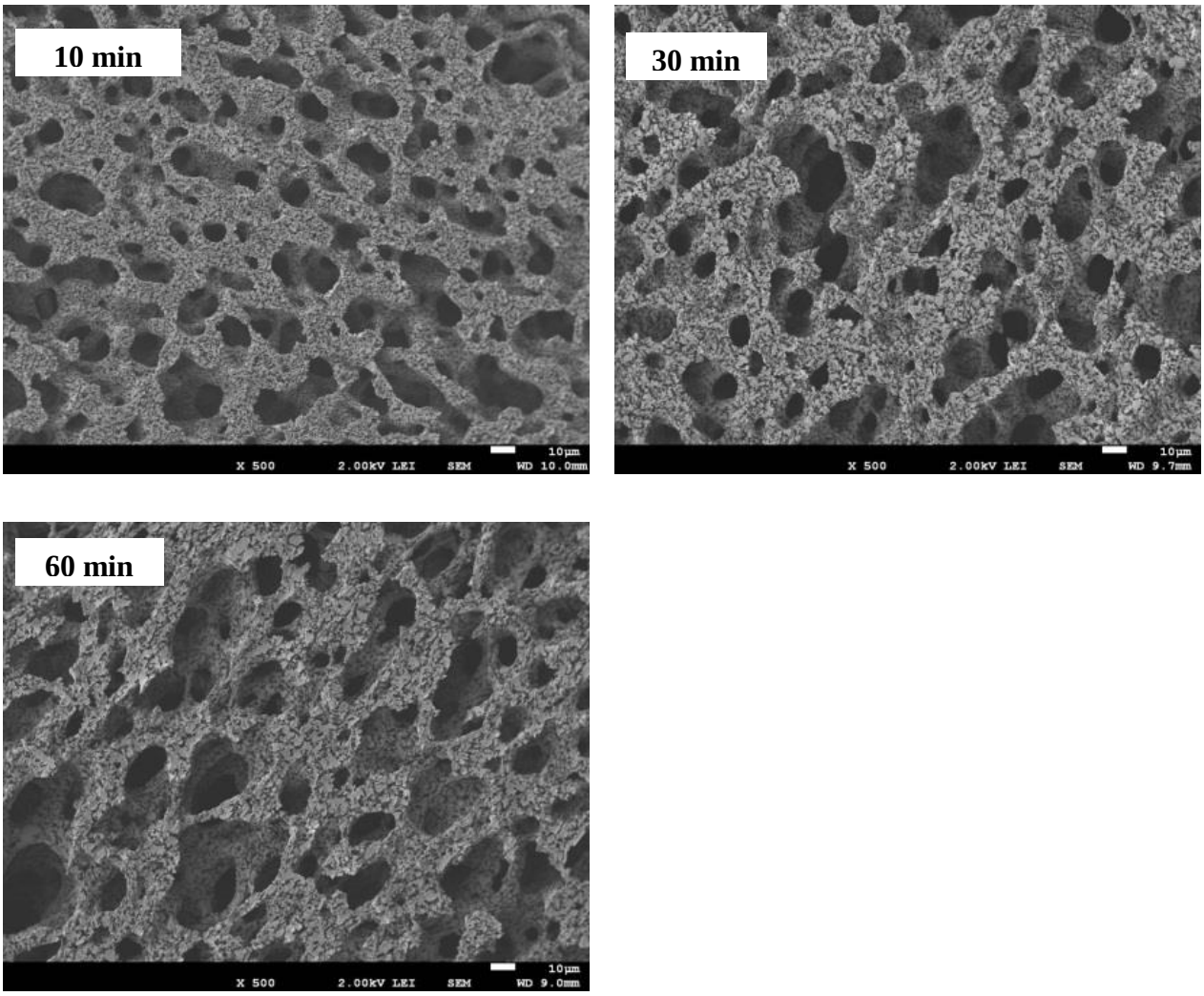

Figure A8: Morphology evolution of PLA/HDPE/SEBS 50/25/25 during annealing at 200°C (PLA and SEBS extracted).